Uncovering Mechanisms of VPS13A Neurodegeneration in Disease Models

by

Genesis Rodriguez

A dissertation submitted in partial fulfillment
of the requirements for the degree of
Doctor of Philosophy
(Neuroscience)
in the University of Michigan
2026

Doctoral Committee:

Associate Professor Sami J. Barmada, Co-Chair
Professor Henry L. Paulson, Co-Chair
Associate Professor Catherine Collins, Case Western Reserve University
Professor Emerita Roberta Fuller
Professor Emeritus Michael Uhler

Genesis Rodriguez

genesiro@umich.edu

ORCID iD: 0000-0001-5159-533X

© Genesis Rodriguez 2026

Dedication

Para mi mamá, mi papá y para todos los inmigrantes cuyo sacrificio y valentía siembran futuros que antes parecían imposibles.

Acknowledgements

This dissertation would not have been possible without the guidance and support of so many incredible people who believed in me and helped me grow, both personally and scientifically.

First and foremost, I am deeply grateful to my mentor, **Dr. Sami Barmada**. Thank you for taking me on during the uncertainty of the pandemic and for your patience, encouragement, and scientific guidance throughout this journey. Your trust in allowing me to build a new project in a rapidly evolving field has shaped me into the scientist I am today.

I also want to thank the individuals who donated tissue that made this work possible. My sincere appreciation goes to the **Advocacy for Neuroacanthocytosis Patients (NA Advocacy)**, the **Neuroacanthocytosis Advocacy USA, Inc.**, and all members of these communities for being so welcoming, collaborative, and supportive of VPS13A research.

I am grateful to my thesis committee, **Drs. Catherine Collins**, **Roberta Fuller**, **Henry Paulson**, and **Mike Uhler**, for their insights and feedback, which strengthened my work. Thank you as well to the **Todd**, **Paulson**, and **Parent labs** for sharing equipment and reagents, and to the **Department of Neurology**, the **Program in Biomedical Sciences**, the **Office of Graduate and Postdoctoral Studies**, the **Neuroscience Graduate Program**, and all associated staff for their support. A special thanks to **Dr. Audrey Seasholtz**, who has mentored me since before graduate school.

To all members of the Barmada lab, past and present, thank you. To **Elizabeth** for maintaining essential cell lines, **Xingli** for the thousands of rat neurons, and **Jake** for analyzing survival experiments and writing the code that made my work possible. To the graduate students who welcomed me, **Ahmed**, **Sumin**, and **Mike**, thank you for sharing your expertise and creating such a collaborative environment. A special thank you to **Nico**, my long-lost cousin, for encouraging me to use R and always lending a hand. To

my “Barm girls”, **Megan**, **Jojo**, and **Caroline**, thank you for your friendship, brilliance, and the countless hours of laughter and support. To **Emile**, thank you for being my cubicle buddy and modeling the rigor and passion I strive for. And to my students, **Anika**, **Amber**, **Sophie**, **Salam**, and my sister **Raquel**, thank you for helping me test hypotheses and allowing me to grow as a mentor.

I am also grateful to the mentors and programs that helped me reach this point, many of which support low-income and first-generation students. Thank you to the **Chican@ & Latin@ Studies program at UW–Madison**, especially **Rachelle Eilers**, for connecting me with a supportive community and leading me to **Dr. Avtar Roopra** and his lab, **Drs. Trina** and **Nadia**, who introduced me to neurobiology and prepared me for graduate school. I am also thankful for the **Ronald E. McNair Postbaccalaureate Achievement Program**, funded by TRIO, which provided early research training, summer fellowships, and conference opportunities. My gratitude extends to the **Postbaccalaureate Research Education Program (PREP)**, funded by NIGMS, and to **Drs. Ben Allen** and **Kate Barald**, as well as my cohort member **Anthony Garcia**, for their mentorship and support. Finally, thank you to **Dr. Geoffrey Murphy** and his lab, **Drs. Victor Cazares**, **Shannon Moore**, and **Tammy Stevenson**, whose passion for science continues to inspire me.

To all the friends I met during graduate school, especially **Ivette**, **Stephanie**, **Frankie**, **Samantha**, **Noah**, and **Vinodh**, thank you for the humor, memes, and adventures that made difficult days bearable. To my lifelong best friends, **Yeliza**, **Angeliesse**, and **Michelle**, thank you for never taking my long silences personally and for always showing up when I needed you. To all other friends from every stage of my life, thank you for your messages, encouragement, and belief in me. To my second family, **Connie**, **Hux**, **Aly**, **Trevor**, **Miles**, **Parker**, **AJ**, **Shannon**, **Caleb**, **Connor**, **Adelyn**, **Aubrey**, and everyone else, thank you for your visits, uplifting texts, and hundreds of smiling pictures that brightened even the toughest days.

To my extended family in the U.S. and Mexico, muchas gracias por siempre apoyarme y por esperarme con los brazos abiertos. To my **mom**, **dad**, **Raquel**, **Carlos**, and **Bella**, thank you for being the most supportive family I could have asked for. Gracias por nunca dudar de mí y por enseñarme a siempre preguntar e investigar; no lo hubiera

logrado sin su amor. To **Stokes**, thank you for teaching me patience, routine, and unconditional love; you are the best thing to come out of the pandemic, and I cannot wait for all the adventures ahead.

Finally, to my partner and the love of my life, **Aaron Huxford**, thank you for growing with me from our days as dorm neighbors at UW–Madison through our move to Ann Arbor, our life with Stokes, and all the challenges of graduate school. I could not have asked for a better person to stand by my side, and I cannot wait to see what our future holds.

Table of Contents

Dedication ..... **ii**

Acknowledgements ..... **iii**

List of Tables ..... **xi**

List of Figures ..... **xii**

Abstract ..... **xiii**

Chapter 1 Introduction **1**

1.1 Overview of VPS13A disease (chorea acanthocytosis) 1

1.2 Clinical characteristics of VPS13A disease 1

1.2.1 Chorea and other abnormal movements 1

1.2.2 Cognitive, behavioral, and psychiatric symptoms 2

1.2.3 Neuropathy 2

1.2.4 Epilepsy 2

1.2.5 Acanthocytes 2

1.2.6 Uncommon symptoms 3

1.2.7 Phenotypic variability 3

1.3 Neurodegeneration in VPS13A disease 3

1.4 Current treatments for VPS13A disease & advocacy organizations 5

1.5 VPS13A and the VPS13 protein family 6

1.5.1 VPS13A in humans 6

1.5.2 VPS13 paralogs in humans 7

1.5.3 VPS13 in yeast 7

1.6 Domains of VPS13 proteins 8

1.6.1 Repeating beta groove (RBG) domains 8

1.6.2 N-terminal chorein (chorein_N) domain 10

1.6.3 FFAT motif 10

1.6.4 VPS13 adaptor binding (VAB) domain 11

1.6.5 Small globular (SGD) and adenine phosphoribosyl-transferase (APT1) domains 11

1.6.6 C-terminal ATG2-like (ATG_C) domain 12

1.6.7 Pleckstrin homology (PH)-like domain 12

1.7 Proposed functions of VPS13A 13

1.7.1 Bulk transfer at organelle membrane contact sites (MCSs) 13

1.7.2 Mitochondrial health and dynamics 15

1.7.3 Cytoskeleton organization and actin dynamics 18

1.8 VPS13A and neurons 20

1.9 Summary and aims of dissertation 22

References 24

Chapter 2 VPS13A Loss Triggers Neurodegeneration in an HMGA1-Dependent Manner 50

Abstract 50

2.1 Introduction 52

2.2 Results 53

2.2.1 VPS13A disease patient-derived neurons display significant degeneration over time 53

2.2.2 VPS13A is necessary for neuronal survival 54

2.2.3 Loss of VPS13A has extensive pre- and post- translational effects 55

2.2.4 VPS13A interacts with the transcriptional regulator HMGA1 56

2.2.5 HMGA1 is upregulated in VPS13A disease models 57

2.2.6 HMGA1 upregulation is necessary and sufficient for neurodegeneration in VPS13A disease models 58

2.3 Discussion 59

2.4 Methods 62

2.4.1 Sex as a biological variable 62

2.4.2 HEK293T cell culture and transfection 62

2.4.3 CRISPR/Cas9 genome engineering 62

2.4.4 Primary rat neuron cell culture and transfection 63

2.4.5 iPSC-derived iNeuron culturing and maintenance 64

2.4.6 Human brain tissue samples 65

2.4.7 Immunohistochemistry and evaluation 65

2.4.8 Whole-genome sequencing of patient-derived iPSCs 66

2.4.9 RNA isolation for RT-PCR and RNA sequencing 67

2.4.10 Quantitative PCR (qRT-PCR) 67

2.4.11 Poly(A) mRNA sequencing 67

2.4.12 Western blot 69

2.4.13 Immunoprecipitation 70

2.4.14 Tandem-mass tag (TMT) isobaric labeling and mass spectrometry-based proteomics 71

2.4.15 Immunocytochemistry 74

2.4.16 Confocal microscopy 75

2.4.17 Longitudinal microscopy and survival analysis 75

2.4.18 Plasmids 76

2.4.19 Quantification and statistical analysis 77

2.4.20 Study approval 77

2.4.21 Resource availability 78

2.4.22 Reagents 78

2.5 Author contributions 89

2.6 Funding support 90

2.7 Acknowledgments 90

References 92

Figures 112

Supplemental figures 124

Chapter 3 VPS13A Loss Does Not Disrupt Selective Autophagy in HEK293T Cells 132

Abstract 132

3.1 Introduction 133

3.1.1 Macroautophagy 133

3.1.2 Selective autophagy 134

3.1.3 Mitophagy 134

3.1.4 Reticulophagy (ER-phagy) 136

3.1.5 VPS13 proteins and autophagy 137

3.2 Results 139

3.2.1 Loss of VPS13A does not lead to accumulation of autophagy markers in HEK293T cells 139

3.2.2 VPS13A deficiency does not alter ER-phagy or mitophagy flux in HEK293T cells 139

3.2.3 VPS13A deficiency does not result in broad changes to autophagy-associated protein abundance 140

3.3 Discussion 141

3.3.1 Limitations and future directions 142

References 144

Figures..... 165

Chapter 4 Discussion.....171

4.1 Establishing VPS13A disease relevant models..... 172

4.1.1 VPS13A disease patient-derived iNeurons and their limitations..... 172

4.1.2 Complementary VPS13A KO models..... 173

4.1.3 VPS13A KO HEK293T cells as a system for investigating mechanistic functions..... 174

4.2 ABCD1 and peroxisomal function..... 175

4.3 CRMP4 and cytoskeletal pathways in VPS13A disease..... 176

4.4 Carbonic anhydrase 8..... 179

4.5 HMGA1 and VPS13A..... 180

4.5.1 Identification of HMGA1 as a VPS13A-related protein..... 180

4.5.2 Molecular properties of HMGA1 and implications for transcriptional control..... 180

4.5.3 HMGA1 dysregulation across disease contexts..... 181

4.5.4 HMGA1 transcript variability and genetic background effects..... 182

4.5.5 HMGA1 protein accumulation and neuropathology..... 182

4.5.6 HMGA1-SP1 axis and transcriptional network remodeling..... 183

4.5.7 HMGA1 as a functional mediator of neurodegeneration..... 184

4.5.8 VPS13A-HMGA1 spatial organization and nuclear homeostasis..... 184

4.5.9 A working model for VPS13A–HMGA1 interactions..... 186

4.6 Conclusions..... 186

References..... 188

Figures..... 204

List of Tables

Table 2.1 Cell lines 78

Table 2.2 Chemical and peptides 79

Table 2.3 Antibodies 79

Table 2.4 Oligonucleotides 82

Table 2.5 Recombinant DNA 86

Table 2.6 Viruses and bacterial strains 87

Table 2.7 Software and algorithms 87

List of Figures

Figure 2.1 Human iNeurons derived from VPS13A disease patients show increased toxicity compared to familial controls. 112

Figure 2.2 VPS13A is necessary for neuronal survival. 114

Figure 2.3 VPS13A-deficient HEK293T cells demonstrate concordant changes at both the RNA and protein levels. 116

Figure 2.4 VPS13A interacts with HMGA1 in HEK293T cells. 118

Figure 2.5 HMGA1 is upregulated in VPS13A KO and VPS13A disease iNeurons compared to respective controls. 120

Figure 2.6 HMGA1 is both necessary and sufficient for neurotoxicity. 122

Supplemental Figure S2.1 Validation of VPS13A constructs using Sanger sequencing. 124

Supplemental Figure S2.2 ABCD1 and CRMP4 display elevated protein and RNA levels in VPS13A KO HEK293T cells. 126

Supplemental Figure S2.3 Enrichment for transcriptional regulators among VPS13A interacting proteins in HEK293T cells. 128

Supplemental Figure S2.4 Knockdown of HMGA1 is sufficient to rescue neurotoxicity in familial control iNeurons. 130

Figure 3.1 VPS13A KO HEK293T cells do not show significant differences in basal levels of autophagy markers. 165

Figure 3.2 VPS13A KO HEK293T cells do not show significant differences in ER-phagy or mitophagy. 167

Figure 3.3 VPS13A KO HEK293T cells do not show widespread alterations in ER-, mitochondrial-, or autophagy related proteins via global proteomic analysis. 169

Figure 4.1 Accumulation of HMGA1 protein in VPS13A-deficient cells 204

Abstract

Vacuolar protein sorting 13A (VPS13A) disease, formerly chorea acanthocytosis, is a rare autosomal-recessive neurodegenerative disorder characterized by heterogeneous clinical features, including chorea, cognitive and psychiatric symptoms, epilepsy, and acanthocytosis. Although limited neuropathological studies exist, they most often report neuroinflammation and neuronal death in basal ganglia structures, yet the molecular events that render these neurons vulnerable remain poorly understood. More than 70 pathogenic VPS13A mutations lead to an absence of the ~360-kDa VPS13A protein, a member of the conserved VPS13 family characterized by elongated hydrophobic cavities capable of transferring phospholipids across organelle membranes. Although VPS13 proteins localize to diverse organelle contact sites and are implicated in organelle homeostasis, the physiological role of VPS13A, and which pathways are directly disrupted in its absence, remains unclear.

This dissertation investigates VPS13A-dependent pathways essential for neuronal health. Chapter 1 reviews current literature on VPS13A disease, beginning with clinical and neuropathological features, followed by an overview of VPS13A structural domains and proposed functions of the protein. In Chapter 2, I show that VPS13A is essential for neuronal survival and that its loss leads to unexpected transcriptional dysregulation, including accumulation of the chromatin regulator HMGA1. I also demonstrate that elevated HMGA1 both necessary and sufficient for neurodegeneration in VPS13A-deficient models. In Chapter 3, I assess whether VPS13A is required for organelle selective autophagy pathways and find these pathways are not significantly altered in VPS13A knockout (V-KO) HEK293T cells, suggesting that previously reported autophagy defects may reflect secondary or cell-type-specific consequences. Chapter 4 summarizes these findings, discusses unresolved questions about VPS13A biology, and outlines future directions for investigating VPS13A function in disease-relevant neuronal systems.

Chapter 1 Introduction

1.1 Overview of VPS13A disease (chorea acanthocytosis)

Vacuolar protein sorting 13 homolog A (VPS13A) disease, historically called chorea acanthocytosis (ChAc, OMIM 200150), is a rare genetic neurodegenerative disorder characterized by a wide spectrum of progressive neurological, cognitive, and psychiatric symptoms[1,2]. Typically, VPS13A disease manifests in young adulthood (mean age of onset is ~30 years) and symptoms progress over the next decade or two often resulting in an early death (mean and life expectancy is ~11 years after onset)[3].

1.2 Clinical characteristics of VPS13A disease

The prevalence of VPS13A disease is estimated at approximately 1 in 1,000,000, though the disease is likely underreported or misdiagnosed due to its wide range of symptoms, symptom severity, and disease progression[4]. This broad clinical spectrum and rarity of the disease make early recognition and accurate diagnosis particularly challenging.

1.2.1 Chorea and other abnormal movements

The primary clinical feature is chorea, an involuntary irregular jerking of muscles, which appears in most, but not all, affected individuals[1,5–8]. Limb and trunk chorea typically emerges in early stages of the disease and may involve flinging movements of the limbs, shoulder shrugs, pelvic thrusts, violent spasms of the trunk and head, or sudden loss of muscle tone that can lead to falls and injuries[1,6]. Orofacial chorea is also very common, and involuntary movements of the face, mouth, tongue, and throat may cause repetitive lip and tongue biting, involuntary vocalizations (reported in ~2/3 of cases)[9], and difficulties with speech and swallowing[1,5,10–12]. These impairments can lead to secondary complications such as oral infections, severe malnutrition, choking, and reduced communication, which may eventually progress to mutism[1,6,8,9,11,13]. In roughly 1/3 of

individuals, chorea evolves into additional movement disorders including dystonia, tics, ataxia, bradykinesia, and in later disease stages, parkinsonism[1,2,7,8,11]. Altogether these reports highlight how varied and often progressive and disabling movement disorders are in VPS13A disease.

1.2.2 Cognitive, behavioral, and psychiatric symptoms

Cognitive decline is also common and may include executive dysfunction, memory and learning impairments, bradyphrenia, and dementia[1,2,14–16]. Behavioral and psychiatric symptoms affect approximately 2/3 of individuals and vary widely but can include apathy, depression, self-neglect, aggression, paranoia, hyperactivity, sexual disinhibition, obsessive-compulsive behaviors, emotional instability, psychosis, and suicidal ideation[1,2,14,16–20]. These cognitive and psychiatric manifestations can contribute substantially to disease burden and further complicate management.

1.2.3 Neuropathy

Almost all individuals with VPS13A disease experience diminished reflexes caused by axonal neuropathy[1]. Other neurological manifestations include primary myopathy, sensory loss, upper motor neuron involvement, and ocular abnormalities[1,6,12,21–25]. Furthermore, about half of affected individuals also experience muscle atrophy and weakness[1]. This combination of peripheral and central nervous system involvement reflects the multisystem nature of the disorder.

1.2.4 Epilepsy

Epilepsy affects approximately 45% of individuals and most often presents as generalized tonic-clonic seizures and temporal lobe foci, though nonconvulsive seizures also occur[1,8,10,26–31]. Epilepsy is typically one of the first reported symptoms and is difficult to manage because seizures can be life-threatening, are often unresponsive to anti-seizure medications, and can be triggered by certain psychiatric drugs, with some anticonvulsants worsening movement disorders[1–3,32]. Consequently, seizure management represents a major clinical challenge in VPS13A disease.

1.2.5 Acanthocytes

Acanthocytes, irregular, spiky-shaped red blood cells (RBCs; also called erythrocytes), are commonly associated with VPS13A disease; however, their abundance

varies widely among patients, can differ between samples from the same individual, and is completely absent in some cases[1,12,19,33–36]. Therefore, although acanthocytosis is often linked to the disorder, the presence of acanthocytes is not a reliable diagnostic marker on its own[1].

1.2.6 Uncommon symptoms

Mild cardiac involvement has been reported in some patients but remains poorly characterized[3,32,37]. More severe cardiac abnormalities, such as dilated cardiomyopathy, are extremely rare[38]. Additional uncommon symptoms that have been reported include an enlarged or abnormal spleen or liver[1,2,29,39], elevated liver enzymes[39], and sleep disturbances[1,12,40]. Together, these findings reinforce that while neurological symptoms are the most common, VPS13A disease is a multi-system disorder.

1.2.7 Phenotypic variability

Although certain clinical manifestations occur more frequently than others, no single symptom, or group of symptoms, has been reported in all diagnosed and suspected patients[1,3]. Phenotypic variability is extensive not only across the broader VPS13A disease population but also among individuals with the same biallelic pathogenic variants, including siblings and even monozygotic twins[1–3,16,28,41–45]. Furthermore, there have been no reports of heterozygous carriers (with a single affected allele) developing VPS13A disease related symptoms[1,15]. Overall, the clinical presentation of VPS13A disease is highly heterogeneous, with significant variability even among genetically identical individuals, underscoring the complexity of this disorder and the need for a personalized approach to diagnosis and care.

1.3 Neurodegeneration in VPS13A disease

Post-mortem examinations of brain tissue from individuals with VPS13A disease typically show marked atrophy of the caudate nucleus, with the head of the caudate nucleus being particularly susceptible, the putamen and globus pallidus[18,24,32,46], and occasionally, the substantia nigra[24,32]. Brain magnetic resonance imaging (MRI) and cranial tomography (CT) studies often mirror these findings, revealing bilateral atrophy in the same basal ganglia regions, with the caudate nucleus again being most vulnerable, along with moderate to severe anterior horn dilation of the lateral ventricles[18,23,31,45,47–50].

Functional imaging further supports these observations. ^{18}F-2-fluoro-2-deoxy-D-glucose positron emission tomography (^{18}F-FDG PET), which detects the radioactive tracer ^{18}F-FDG, a marker for glucose uptake, shows reduced glucose utilization in the caudate nucleus and putamen of individuals with VPS13A disease[27,28,41,44]. Likewise, ^{123}I-2β-carbomethoxy-3β-(4-iodophenyl)-*N*-(3-fluoropropyl) nortropane single photon emission computed tomography (^{123}I-FP-CIT SPECT), which uses the radioactive tracer ^{123}I-FP-CIT that binds to presynaptic dopamine transporters (DAT) in the striatum, typically shows reduced binding as well[28,41,44], substantiating the presence of striatal dysfunction.

Microscopic analyses of post-mortem brain tissue from individuals affected by VPS13A disease provide additional evidence of neurodegeneration in the basal ganglia. Findings range from unremarkable to near-complete neuronal loss, usually accompanied by a marked astrogliosis, particularly in the caudate nucleus and putamen[18,24,29,32,46,51]. Although considerable investigation is still needed, preliminary observations suggest that small and medium-sized neurons, largely corresponding to rich or medium spiny neurons (MSNs), the most abundant neuronal population in the caudate nucleus, may be especially vulnerable to neuronal death compared to large striatal neurons[46,52]. Some studies also report a dorsal–ventral pattern of neuron loss in the caudate nucleus and a caudal–rostral gradient in the putamen[46,53].

These findings are of particular interest because the caudate nuclei receive and integrate synaptic input from cortical and thalamic brain regions, transmit this information to other basal ganglia and thalamic nuclei for additional processing, and ultimately complete multiple distinct cortico-subcortical loops via projections back to the cortex[54–58]. These loops are essential for motor control, cognition, emotional regulation, and executive functions[55,58–61]. Consistent with this, caudate nucleus atrophy and dysfunction are also reported in several other neurological diseases, including Huntington's disease (HD)[62,63], Parkinson's disease (PD)[64,65], Alzheimer's disease (AD)[66–68], frontotemporal dementia (FTD)[69,70], and amyotrophic lateral sclerosis (ALS)[70,71], and in psychiatric conditions such as attention-deficit/hyperactivity disorder (ADHD)[72,73], obsessive-compulsive disorder (OCD)[74,75], schizophrenia[76–78], bipolar disorder[79–81], and depression[82,83].

Direct comparisons of post-mortem tissue from individuals with VPS13A disease and individuals with HD often show distinct patterns of selective vulnerability to neuronal loss and gliosis[46,51]. Although both conditions are characterized by neuronal loss in the striatum, HD typically shows more evenly spaced neuronal loss, whereas VPS13A disease often exhibits a dramatic increase in total astrocytes and glia and a much higher astroglia-to-neuron ratio, leaving very few surviving neurons[46,51].

Although striatal atrophy is a hallmark of VPS13A disease, longitudinal studies of morphological changes in affected individuals show no significant correlations between duration of illness, symptom severity, and striatal volume or shape[53]. Adding further complexity, several reports describe cortical and even global brain atrophy in some individuals[41,43,50,84]. Notably, gross pathological examinations have revealed varying degrees of hippocampal atrophy[24,29,32], and MRI and CT studies support these findings, showing a range of hippocampal volume loss, and in some cases, evidence of hippocampal sclerosis[8,10,11,26–30,32,41,44].

Together, these structural, functional, and microscopic findings show that VPS13A disease involves widespread but variable neurodegenerative changes, with the caudate nucleus and related basal ganglia circuits being particularly affected.

1.4 Current treatments for VPS13A disease & advocacy organizations

To date, there is no cure for VPS13A disease, and treatments are limited to supportive care on an individual basis based on presenting symptoms[1–3]. Symptom management typically requires multiple approaches often including medications such as dopamine antagonists or depletors to reduce choreic movements; botulinum toxin, benzodiazepines, and anticholinergic medications to manage dystonia; antidepressants or antipsychotics to target behavioral and psychiatric symptoms; and anti-epileptic drugs to mitigate seizures[1,8,15,85]. Deep brain stimulation of the globus pallidus pars interna is also reported to improve movement-related symptoms in some individuals[44,45,86].

Non-pharmacological interventions play an essential role as well. Mobility and adaptive devices, such as walkers, motorized chairs, mouthguards, home modifications, and assistive communication devices, often help reduce complications from neuropathy, myopathy, movement disorders, and cognitive impairment[1]. Physical, occupational,

speech/swallowing, and psychological therapies are also crucial for maintaining function and quality of life[1]. Nutritional assessments, weight monitoring, and potential gastrostomy tube placement can help ensure adequate nutrition and reduce the risk of aspiration associated with orofacial chorea[1]. Clinicians often recommend regular evaluation of cardiac, liver, and spleen function[1]. Access to family support, genetic counseling, family therapy, social services, nursing care, and patient advocacy groups is also strongly recommended to support patients and caregivers[1,3]. Together, these combined approaches aim to manage symptoms, prevent complications, and maintain daily functioning as much as possible.

Two related organizations provide vital support for patients, caregivers, related healthcare providers, and researchers in the neuroacanthocytosis community (which includes VPS13A disease and McLeod syndrome/XK disease):

1. **Advocacy for Neuroacanthocytosis Patients** (NA Advocacy; www.naadvocacy.org)-an international charity registered in the UK.
2. **Neuroacanthocytosis Advocacy USA, Inc.** (NA Advocacy USA; www.naadvocacyusa.org)-a registered non-profit in the US.

These sister organizations create a global community for affected individuals, their families, and caregivers, and advocate for research, help fund international collaborations among clinicians, pharmaceutical companies, and researchers. Their efforts include hosting regular virtual forums for Q&A, research updates, and engagement opportunities, distributing communication across social media, websites, and e-newsletters several times a year, and organizing an in-person international symposium every few years. Importantly, many aspects of the work described in this thesis, including the collaborations established with researchers in the VPS13A field, were made possible through the support and connections facilitated by these organizations. Overall, these resources play a critical part in advancing research and improving the support network available to individuals affected by VPS13A disease.

1.5 VPS13A and the VPS13 protein family

1.5.1 VPS13A in humans

The *vacuolar protein sorting 13A* (*VPS13A*) gene, previously called *CHAC*, spans approximately 250 kb on chromosome 9q21 and is organized into 73 exons[87–89]. *VPS13A* encodes multiple alternative splice variants, with the most abundant (main) transcript A consisting of exons 1–68 and 70–73 and encoding a large 3,174 amino acid protein[87,88]. *VPS13A* RNA and protein are expressed in all tissues including the brain[87–89].

VPS13A disease is caused by biallelic loss-of-function mutations resulting in undetectable levels of the approximately 360-kDa VPS13A protein[90]. Hundreds of known and likely pathogenic nonsense, frameshift, duplication, splice site, and insertion/deletion mutations are widely distributed throughout the entire *VPS13A* gene and are not limited to a particular region or domain [*VPS13A*[gene], ClinVar; https://www.ncbi.nlm.nih.gov/clinvar/?term=VPS13A[gene]][88–92].

VPS13A disease is inherited in an autosomal recessive manner, with both homozygous and compound heterozygous pathogenic mutations reported[1,3]. Notably, heterozygous carriers of pathogenic mutations have not been reported to develop any clinical or pathological of the disease[1–3]. Moreover, no clear genotype–phenotype correlations have been identified; even individuals carrying the same *VPS13A* mutations, including monozygotic twins, can present with markedly different clinical and neuropathological manifestations[13,21,28,41–44].

1.5.2 VPS13 paralogs in humans

VPS13A is a member of the highly conserved VPS13 protein family found in all eukaryotes[93]. Humans have four VPS13 paralogs, each associated with distinct neurological disorders, including Cohen syndrome (*VPS13B*, formerly *COH1*)[94–97], early-onset autosomal recessive Parkinson's disease (*VPS13C*)[98–101], dementia with Lewy bodies (*VPS13C*)[101,102], and hereditary spastic ataxia (*VPS13D*)[103–105]. Together, these findings underscore the importance of VPS13 proteins in neuronal function and but also highlight underlying functional differences between homologs.

1.5.3 VPS13 in yeast

Early studies first identified VPS13 in a *Saccharomyces cerevisiae* (yeast) mutant that is defective in sorting the vacuolar protease–carboxypeptidase Y (CPY) between the endosome and Golgi complex[106,107]. Subsequent studies found that the single Vps13

ortholog found in yeast is also required for sporulation[107–111], a stress-induced process during which diploid yeast cells undergo meiosis to produce four haploid nuclei that are then packaged into stress-resistant spores[112].

Eukaryotic cells contain a variety of membrane-bound organelles that compartmentalize distinct cellular functions[113]. Membrane contact sites (MCSs), dynamic regions where organelle membranes come into close proximity (typically about 10–30 nm) without fusing, are indispensable for a wide range of cellular processes such as the exchange of lipids, ions, and metabolites between organelles, the regulation of signaling pathways, metabolic activity, and organelle dynamics[113–116].

The formation and maintenance of MCSs are mediated by tethering protein complexes at specific contact sites[113,117]. One such protein complex in yeast, known as the endoplasmic reticulum-mitochondria encounter structure (ERMES) complex, tethers the endoplasmic reticulum (ER) and the outer mitochondrial membrane[118]. While ERMES mutants show dysregulated mitochondrial fission[119], loss of mitochondrial DNA (mtDNA) [120,121], and reduced ER-mitochondrial lipid exchange[118,122], they are still viable. However, not only are these deficits rescued by single amino acid substitutions in *VPS13*, but the combined loss of Vps13 and ERMES is lethal, suggesting that Vps13 and ERMES have overlapping functions[123–125]. This potential redundancy in function at membrane contact sites is further supported by the absence of the ERMES complex in metazoans[123].

Studies have also observed Vps13 at other MCSs including endosome-mitochondria[124], the nuclear envelope and vacuole (nuclear-vacuole junctions)[123–126], ER-peroxisomes[127], ER-endosomes[128,129], autophagosome-ER[130], ER-plasma membrane[131], mitochondria-vacuole[123,124,126]. In addition to localizing to MCSs, Vps13 also localizes to the membranes of single organelles such as the vacuole[123–125,128], endosomes[110,125,126,132], mitochondria[123,124,126], prospore membrane[110,111,124,131], the Golgi apparatus (Golgi)[133], and peroxisomes[126,127].

1.6 Domains of VPS13 proteins

1.6.1 Repeating beta groove (RBG) domains

VPS13 proteins are large, elongated, multi-domain proteins characterized by an extended region of repeating β-groove (RBG) domains (often called the extended chorein

domain) that make up the majority of their length[134–141]. Each RBG unit (~110–150 amino acids) typically consists of a five-stranded concave β-sheet accompanied by a sixth element, often a loop and/or a short helix, that curves back across the β-sheet groove (βββββ-loop)[139]. The convex (outer) surface of the RBG unit contains hydrophilic residues, whereas the concave (inner) surface is lined with hydrophobic residues, suggesting it is capable of binding lipids[138,139]. Because the sixth element crosses back over the groove, each RBG domain begins and ends on the same side of the β-sheet, allowing multiple RBG units to oligomerize end-to-end[138,139]. This organization results in the formation of an elongated rod-like structure with a continuous hydrophobic groove that acts as a tunnel or bridge capable of binding and transferring multiple phospholipids simultaneously along its length[136–142].

Further evidence supporting the model that VPS13 proteins serve as lipid transport bridges, facilitating the direct flow of phospholipids through the hydrophobic channel rather than shuttling them individually, comes from yeast studies showing that mutations converting hydrophobic residues lining the concave surface of the β-sheets to hydrophilic ones disrupt Vps13–dependent processes such as sporulation[134]. VPS13 homologs, both across and within species, often differ in their number of RBG repeats allowing them to span different distances between organelle membranes[139,140,143]. In humans, the VPS13A paralog is the shortest in sequence length and in RBG units, with 12 RBGs, and share the most sequence and structural homology with the yeast Vps13 ortholog, which contains 12 RBG repeats[139]. On the other hand, the human VPS13C (3,753 amino acids and 422 kDa) and VPS13D (4,388 amino acids and 492 kDa) paralogs have 15 RBG domains and VPS13B (4,011 amino acids and 448 kDa), which is the least homologous with VPS13A and yeast Vps13, has 13 RBGs[139].

Beyond the core RBG domain architecture (corresponding to RBG domains 2–11 in VPS13A), VPS13 proteins contain additional domains and recognition motifs that may contribute to their function, regulation, and subcellular localization[136–141]. Some of these domains are conserved across most VPS13 homologs and are referred to as canonical domains, whereas others, called non-canonical domains, vary among species and between the four human VPS13 paralogs[136–141]. Notably, there is considerable variability

in how VPS13 domains are defined and named across the literature, but a summary of these canonical and non-canonical domains is provided below.

1.6.2 N-terminal chorein (chorein_N) domain

The N-terminal region of all VPS13 proteins harbors a highly conserved chorein (chorein_N) domain, which is present in other evolutionarily conserved proteins, including the yeast autophagy-related protein ATG2 (ATG2A and ATG2B in humans)[135,139,144–152] and members of the bridge-like lipid transfer protein (BLTP) families 1–3. The BLTP family comprises BLTP1 (previously KIAA1109; Hob1 in yeast), BLTP2 (previously KIAA0100; Hob2 in yeast), BLTP3A (also known as UHRF1BP1), and BLTP3B (also known as SHIP164 or UHRF1BP1L)[138,153–157].

The chorein_N domain spans approximately 120 amino acids and adopts a wide scoop- or cup-like structure with a deep concave hydrophobic cavity capable of binding phospholipids[138–141,144,158]. Structurally, the chorein_N domain (corresponding to RBG1 in VPS13 proteins) exhibits strong homology with the core RBG2–11 domains found in VPS13 proteins[138,139]. However, its β-sheet is composed of four β-strands rather than the usual five and has a N-terminal amphipathic helix that is hypothesized to directly insert into organelle membranes, bind phospholipids, and directly funnel them into the core RBG repeats[138,139,141].

1.6.3 FFAT motif

Within their N-terminal regions, the human VPS13A and VPS13C paralogs contain a short seven amino acid long sequence containing two phenylalanines in a solvent exposed acidic tract, known as the FFAT motif[141,159–163]. This motif interacts with the major sperm protein (MSP) domain of vesicle-associated membrane protein (VAMP)-associated proteins (VAP), which are anchored to the ER membrane via a flexible linker peptide[141,159–163].

In the human VPS13A homolog, the FFAT motif is positioned on a large loop located at the seam of an RBG repeat[140,161], and *in vitro* studies show that this motif directly binds the human ER integral membrane protein–VAP-A[162,164]. Mutations that disrupt the FFAT motifs of VPS13A or VPS13C impair their recruitment to the ER membrane, underscoring the role of this motif for ER targeting[141,162]. VPS13D contains a

non-canonical phospho-FFAT motif that interacts with VAP proteins only when phosphorylated[165]. Although FFAT or phospho-FFAT motifs are found in three of the four human paralogs, their sequence position is not well conserved[140]. Moreover, despite lacking an FFAT or phospho-FFAT motif, both yeast Vps13 and human VPS13B still localize to the ER, indicating that additional regions within VPS13 proteins can mediate ER localization[140].

1.6.4 VPS13 adaptor binding (VAB) domain

VPS13 proteins contain a VPS13 adaptor-binding (VAB) domain, sometimes referred to as the SHR-BD or WD40-like domain, composed of six β-bladed repeats, each approximately 100 amino acids long, characterized by an asparagine residue at the N-terminus of each repeat[125,139]. Structural and computational modeling studies suggest that the VAB domain forms a flexible, arc-shaped structure at the C-terminal end of the elongated, rod-like bridge formed by the core RBG repeats[125,139]. This configuration allows the VAB domain to interact with adaptor proteins, aiding the recruitment of VPS13 to specific organelle membranes[125,136,140,166–168]. Although the VAB domain is broadly conserved among VPS13 homologs, sequence and structural variations of this domain alter the binding affinity of VPS13 homologs to different adaptor proteins and subcellular localization[125].

1.6.5 Small globular (SGD) and adenine phosphoribosyl-transferase (APT1) domains

The small globular domain (SGD) is located either at the C-terminus of the VAB domain in some VPS13 proteins[140]. In the yeast Vps13 and human VPS13A and VPS13C paralogs, the SGD (sometimes called a WWE-like domain) is inserted at RBG11[139,140,167,169,170]. Although this domain is not well characterized in VPS13 proteins, similar SGD domains bind proteins involved in ubiquitination and poly-ADP-ribosylation (PARylation)[171–173]. In contrast, the VPS13D paralog contains an SGD resembling a ricin β-type lectin domain which in other proteins helps bind carbohydrate-containing proteins[87,139,174]. VPS13B instead has an SGD that is described as a jelly roll fold, and unlike the other paralogs is located at the N-terminus of the VAB domain and currently does not have an identified function[140,175,176].

Downstream of the VAB domain and partially overlapping with the SGD in some prediction studies, VPS13 proteins have a C-terminal phospholipid–binding adenine phosphoribosyl-transferase like (APT1) domain, primarily composed of β-sheets[132,136,137,140,166,177]. This APT1 domain is also found in the ATG2 and BLTP2 proteins[148,177,178]. *In vitro* studies suggest that phospholipid binding by the APT1 domain, particularly to phosphatidylinositol 3-phosphate (PI3P), is regulated by the bivalent ions calcium and magnesium in the human VPS13 and ATG2 proteins, but not in yeast Vps13[177]. Additionally, human VPS13 paralogs also bind other phospholipids, including phosphatidylinositol 5-phosphate (PI5P), independent of these bivalent ions[177].

1.6.6 C-terminal ATG2-like (ATG_C) domain

VPS13 proteins contain a C-terminal region with strong sequence and structural homology to the C-terminus of ATG2 proteins, known as the ATG_C domain[132,143,147,152]. This domain is predicted to contain a few amphipathic helices that may enable these proteins to insert into some membranes and also contribute to their subcellular localization[147,151]. In yeast, this domain is required for early autophagosome formation and autophagic flux[179]. The ATG_C domain is critical for human ATG2A localization to lipid droplets and ER–mitochondrial MCSs[147,180]. The ATG_C domain in VPS13A is located downstream of the APT1 domain and helps the protein localize to lipid droplets and mitochondria[141,147]. Additional support for evolutionary conservation of this domain comes from studies that show both ATG2A and VPS13A interact with the autophagy related protein–ATG9A via this ATG_C domain[151,181].

1.6.7 Pleckstrin homology (PH)-like domain

The pleckstrin homology (PH)-like domain is located downstream of the ATG_C domain at the C-terminus of VPS13 proteins[182]. PH and PH-like domains are found in multiple membrane associated proteins and often interact with phosphoinositol (PI) phosphates, helping recruit these proteins to organelle membranes[183]. In yeast Vps13 and human VPS13B, the PH-like domain helps recruit these proteins to the Golgi where they aid in protein sorting in the trans-Golgi network[184]. In both yeast Vps13 and human VPS13A, PH-like domains directly interact with PI phosphates and Arf1 GTPase, a key regulator of protein trafficking of endo–lysosomal membranes[133]. Additionally, studies

suggest that the PH-like domain of VPS13A is required for its interaction with the plasma membrane lipid scramblase protein XK at ER–PM MCSs[163].

1.7 Proposed functions of VPS13A

1.7.1 Bulk transfer at organelle membrane contact sites (MCSs)

Structural and functional studies indicate that VPS13A localizes to organelle membranes via its N- and C- terminal domains, where it acts as a bridge to transport phospholipids between organelles[136–142]. VPS13A has been detected at multiple MCSs between organelles, including ER-mitochondria, ER-lipid droplets (LD), ER-plasma membrane, and ER-mitochondrial-endosome junctions[141,162,163,166,185–189]. Loss of VPS13A has been shown to alter organelle distribution and integrity to varying degrees[141,162,185], signaling its importance in maintaining inter-organelle communication, and overall cellular homeostasis.

Most eukaryotic cells contain thousands of different lipid species, distributed in a heterogeneous manner within the cell[190,191]. Instead, different organelles have characteristic lipid compositions which are necessary for their subcellular functions[192]. In eukaryotic cells, most lipids are made in the smooth ER, where enzymes synthesize them from lipid precursors often made in the cytoplasm or mitochondria[193,194]. After synthesis, lipids are often rapidly transported out of the ER either via vesicles that shuttle them across the cytoplasm to target organelles, or they are transported along bridge-like tethering proteins (BLTPs)[190–192,195]. ATG2 proteins are ~200 kDa rod-like BLTPs that tether the ER to phagophore membranes (also called isolation membranes) and transfer phospholipids needed for phagophore expansion, a process that eventually forms autophagosomes responsible for degrading and recycling cellular components[145,147,148,150,179–181,196].

As explained in previous sections, VPS13 proteins share multiple regions of homology with ATG2 proteins including the N-terminal chorein_N domain, RBG repeats, and the C-terminal APT1 and ATG_C domains[134,138–140,177,178]. In addition to the strong sequence and structural homology between these two proteins, *in vitro* studies also demonstrated that yeast Vps13 is required for the expansion and completion of the prospore membrane[93,110,111,125,131]. Furthermore, both VPS13 and ATG2 proteins interact

with the same protein, ATG9A[145,151,181]. Although human VPS13A has not been observed to participate in organelle membrane expansion to date, this possibility remains and is supported by *in vitro* studies that show VPS13A can bind phospholipids such as PI3P and PI5P[130–133,178,197]. Yeast VPS13 and ATG2 proteins bind various phospholipids as well, although there seem to be differences between all of these proteins when it comes to binding regulation[177]. Additionally, a clear connection between specific lipid related functions and clinical symptoms or neuropathology in VPS13A disease patients has not yet been established.

In a 2002 report of three affected families in the Arabian Peninsula, normal lipoprotein levels (pre-beta-lipoproteins and beta-lipoproteins) were reported in most individuals except for one, where high resolution electrophoresis revealed the absence of the pre-beta-lipoprotein band corresponding to very low-density lipoprotein (VLDL)[43]. VLDL is a major transporter of triglycerides and cholesterol from the liver to peripheral tissues–mostly adipose, skeletal, and cardiac[198]. Although this suggested that VLDL was absent in this affected individual, further investigation showed that this individual along with all others tested had normal Apolipoprotein A and B, cholesterol, and triglyceride levels[43].

A 2023 study of post-mortem brain tissue from four patients with VPS13A disease and 6 controls, compared levels of 593 lipid species[32,199]. They found no differences in overall lipid types but did observe some differences in individual sphingolipid and phospholipid subtypes in certain brain regions[32,199]. Specifically, levels of bis(monoacylglycerol)phosphate, sulfatide, lysophosphatidylserine, and phosphatidylcholine were elevated in either the caudate nucleus or putamen, but not the dorsolateral prefrontal cortex, in tissue from affected individuals[32,199]. Additionally, phosphatidylserine, monoacylglycerol, and N-acyl phosphatidylserine were elevated in the caudate nucleus, N-acyl serine was decreased in both the caudate nucleus and dorsal prefrontal cortex, and lysophosphatidylinositol was decreased in the dorsal prefrontal cortex of VPS13A disease tissue compared to controls[32,199].

Most recently, a 2025 study assessed lipid composition via mass spectrometry (lipidomics) in RBCs obtained from five individuals with VPS13A disease and 12 healthy controls[33,200]. Again, no significant differences were found in overall lipid types, but some

differences were found in individual phosphatidylethanolamine, ceramide, phosphatidylcholine, and sphingomyelin species[33,200].

Altogether, there are a few studies to suggest that VPS13A may participate in transporting phospholipids species, and potentially other lipid groups, between organelles, and that certain lipid species may be altered in VPS13A disease. Nevertheless, more evidence is needed not just to determine which lipid species changes contribute to specific neuropathology in VPS13A disease and which lipid species are directly transported by VPS13A, but also to define the precise subcellular localization where this transfer occurs and the factors that regulate it.

1.7.2 Mitochondrial health and dynamics

Mitochondria are highly dynamic, membrane-bound organelles found in eukaryotic cells, that have extensive functional and morphological diversity even within the same organism[201–203]. These organelles serve as a hub for cellular metabolism, contain their own DNA and protein translation machinery, and respond to different cell needs by rapidly changing their morphology (size, number, and localization)[202,203]. Many of the dynamic morphological changes to mitochondria are mediated by fission (division of one mitochondrion into two mitochondria) and fusion (union of two mitochondria into one mitochondrion)[204,205]. Mitochondrial dynamics are linked to several critical cellular processes including cell cycle regulation, apoptosis activation, cell migration, mitophagy, calcium signaling, production of reactive oxygen species (ROS), and protein transport, among others[201–205]. Therefore, a careful balance between fission and fusion events is needed to maintain cellular homeostasis[204,205]. Another key piece in the regulation of mitochondrial function is mitochondrial membrane potential ($\Delta\Psi_m$)[205]. Low $\Delta\Psi_m$ is associated with fission events that create one daughter mitochondrion with high $\Delta\Psi_m$ (which can go on to fuse with other healthy mitochondria), and one with low $\Delta\Psi_m$ that is more likely to be targeted for removal via mitophagy[205]. Because of these complex roles, it is not surprising that mitochondrial dysfunction is linked to a wide range of diseases– including metabolic and neurological disorders as well as various cancers[203]. However, pinpointing the exact mitochondrial functions that contribute to disease pathology can be extremely challenging.

In yeast, Vps13 localizes to mitochondria and to several mitochondria-associated MCSs, including ER-mitochondria, mitochondria-endosome, and mitochondria-vacuole regions[123–125]. Structural and *in vitro* studies suggest that Vps13 is recruited to specific organelle membranes by adaptor proteins that reside within the target organelle membrane[125,139]. One such adaptor is MCP1, an integral outer mitochondrial membrane (OMM) protein[125,126]. Structural analyses suggest that this Vps13-MCP1 interaction is mediated by the C-terminal domains of Vps13, specifically the VAB domain, which directly binds a putative PxP motif (a short amino acid sequence containing proline, followed by any amino acid, and then a proline) within MCP1[125,126,136].

Yeast also rely on protein complexes known as endoplasmic reticulum (ER)-mitochondria encounter structures (ERMES), which tether the ER and OMM[118]. Although loss of individual ERMES components is not lethal, these cells show reduced growth[206], altered mitochondrial distribution and morphology[206,207], loss of mitochondrial DNA (mtDNA)[120,121], slowed lipid transfer[118,122], and disturbed mitophagy[120,208]. However, these deficits can be rescued by single amino acid substitutions in Vps13, and combined loss of Vps13 and ERMES is lethal[123–126]. This suggests there is functional redundancy between these systems and supports a role for Vps13 in mitochondrial processes. Additionally, yeast Vps13 mutants show increased mitochondrial escape (transfer of mtDNA from the mitochondrion to the nucleus) as well as increased delivery of mitochondria to the vacuole for degradation[124].

Together, yeast studies link Vps13 to specific mitochondrial functions and show that Vps13 loss results in clear mitochondrial deficits. However, in higher eukaryotes, where both the ERMES complex and MCP1 are absent[143,164] evidence connecting VPS13A to mitochondrial function is more variable and relies primarily on localization data instead of well-defined functional mechanisms.

In vitro studies show that human VPS13A localizes to mitochondria as well as to ER-mitochondrial and mitochondrial-endosome MCSs, although the extent of this localization often varies depending on cell type[141,162,166,185]. As in yeast Vps13, mitochondrial targeting of human VPS13A is mediated by its C-terminal region, but unlike in yeast, several domains, including the APT1, ATG_C, and PH-like domains, seem to be involved[141,162,166]. Overexpression of VPS13A increases ER–mitochondria MCSs[141],

while loss of VPS13A results in reduced ER–mitochondrial[162] and mitochondrial–endosome MCSs[185]. Although additional studies across more cell types are needed to confirm this distribution, this data suggests that the Vps13 function of maintaining MCSs is conserved in human VPS13A.

Several studies report that VPS13A loss reduces the number of mitochondria as well as individual mitochondrial size[162,209,210], though some have observed the opposite effect[211]. Additional studies suggest that VPS13A loss may reduce the clearance of damaged mitochondria via mitophagy[162], increase phosphorylation of the serine 616 residue of dynamin-related protein-1 ($Drp1^{S616}$), which is associated with decreased fusion and increased fission[162], and result in $\Delta\Psi_m$ depolarization, which may induce apoptosis[212,213]. Together these findings point to a potential role, direct or indirect, for VPS13A in mitochondrial regulation.

Mitochondrial dysfunction has not yet been firmly demonstrated in VPS13A disease pathology. In a flow cytometry study of reticulocyte-enriched blood cell fractions, samples from individuals with VPS13A disease showed delayed mitochondrial clearance compared to healthy controls[214], but this has not been replicated in other patient-derived cell lines. Medium spiny neurons and motor neurons differentiated from induced pluripotent stem cells (iPSCs) derived from individuals with VPS13A disease (iMSNs and iMNs), exhibit fewer mitochondria and reduced mitochondrial length[211,212], consistent with findings in immortalized cell lines lacking VPS13A. However, these patient derived iMSNs and iMNs show significant $\Delta\Psi_m$ hyperpolarization (increased membrane potential) compared to controls[209,210], an effect opposite to the $\Delta\Psi_m$ depolarization in immortal cell lines where VPS13A has been silenced[212,213].

Overall, existing data, particularly from yeast studies, suggest that Vps13 proteins may participate in mitochondrial functions. However, in humans, beyond localization studies, only a limited number of findings link VPS13A to mitochondrial functions and even fewer demonstrate mitochondrial dysfunction in VPS13A disease. These observations are further complicated by various cell type specific differences which may influence VPS13A function and contribute to the wide clinical and neuropathological diversity associated with the disease. Therefore, additional studies are required to fully clarify these potential mechanisms.

1.7.3 Cytoskeleton organization and actin dynamics

The cytoskeleton is a complex and dynamic network of protein fibers that provides structural support, organizes cellular components, and enables cell movement and shape changes[215,216]. In eukaryotic cells, the cytoskeleton typically extends from the nucleus to the plasma membrane and consists of three major components, actin filaments, intermediate filaments, and microtubules[216].

Actin monomers (globular or G-actin), the most abundant cytoskeletal protein in most cells, polymerize to form actin filaments (filamentous or F-actin; also called microfilaments), which are long, thin, flexible fibers approximately 7 nm in diameter[217]. These filaments can then organize into bundles and three-dimensional networks and are often enriched beneath the plasma membrane[217]. The assembly and disassembly of F-actin filaments and higher-order structures are tightly regulated by several actin-binding proteins, and a careful ratio of G-actin to F-actin is essential for normal cellular functions[217]. While yeast have a single actin gene, *Act1*, humans express multiple isoforms encoded by six actin genes which are highly conserved but have slightly different functions and tissue-specific expression patterns[217]. Collectively, actin filaments help determine cell shape and support essential processes like migration, phagocytosis, and cell division[217].

Intermediate filaments, ~10 nm in diameter, are made up of various proteins whose expression highly depends on cell type[218]. Unlike actin filaments and microtubules, these filaments are absent in some eukaryotic organisms and cell types[218]. Over 50 different intermediate filament proteins have been identified and are broadly divided into six major groups (Type I–VI)[218]. Intermediate filaments are primarily structural components, strengthening epithelial tissues, forming part of the nuclear envelope, and stabilizing axons, instead of being involved in cell movement[218].

Microtubules are hollow rods, ~25 nm in diameter, composed primarily of α- and β-tubulin dimers, that undergo dynamic assembly and disassembly, much like actin filaments[219]. A third type of tubulin, γ-tubulin, is found at centrosomes and helps initiate microtubule polymerization[219]. Microtubules contribute to cell shape, intracellular transport, cell movement, and chromosome segregation during mitosis[219].

RBCs rely on a highly organized membrane-cytoskeletal network to withstand shear stress and maintain their biconcave shape[220,221]. Spectrin tetramers form long rods which connect end-to-end through short F-actin filaments to form a 2-dimensional lattice[222]. Junctional complexes form at spectrin-actin interactions and consist of proteins such as protein 4.1 and adducin, which anchor the lattice to the plasma membrane by interacting with transmembrane proteins like glycophorin C[222,223]. Additional membrane attachments occur at ankyrin complexes, where the middle region of spectrin rods binds ankyrin-1, which in turn associates with proteins including the integral plasma membrane protein band 3[224]. Together, junctional and ankyrin complexes vertically tether the spectrin-actin cytoskeletal network to the plasma membrane lipid bilayer, giving RBCs flexibility and strength[221,222]. Other proteins such as myosin IIA, a motor protein that forms bipolar filaments, also bind to the spectrin-actin network and generate contractile tension that provides membrane stiffness and helps shape the central dimple of the RBCs[225].

VPS13A is absent in RBCs from individuals with VPS13A disease[90]. Although acanthocytes are commonly associated with VPS13A disease, their prevalence varies significantly and does not correlate with clinical symptoms, neuropathology, or disease progression; therefore, they are not a reliable diagnostic marker on their own[1,12,19,33–36]. Nevertheless, changes in the membrane-cytoskeletal network have long been hypothesized to underlie acanthocytic erythrocytes.

Multiple studies indicate that VPS13A is involved in maintaining cytoskeletal organization and regulating actin polymerization. Endothelial cells treated with *VPS13A*-targeting siRNA show reduced F-actin and an increased G-actin to F-actin ratio[212,226], which is also seen in RBCs and platelets from individuals with VPS13A disease[212,213,227]. These changes are also associated with reduced cell stiffness[226], altered microtubule and intermediate filament structures[213], and abnormal cell morphology[212,213,227]. RBC membranes from affected individuals show reduced levels of β-adducin and β-actin, and C57BL/6J mice with a homozygous deletion of *VPS13A* (*VPS13A*$^{-/-}$) show similar reductions in their striatum[228]. Additionally, biochemical and immunocytochemical analyses show that both β-adducin and β-actin interact with overexpressed VPS13A in HEK293 cells[228]. In parallel, RBCs from patients show increased Lyn kinase driven tyrosine (Tyr)-phosphorylation of spectrin, adducin, and band 3[229], and Lyn kinase

inhibition in *VPS13A*$^{-/-}$ mice significantly reduces the number of acanthocytes, though not to WT levels[230]. Together, this data suggests that Lyn kinase mediated hyperphosphorylation of tyrosine residues on cytoskeleton-membrane network proteins weakens their interactions, thereby reducing RBC stability.

Consistent with a broader role for VPS13 proteins in cytoskeletal regulation, yeast *Vps13* mutants also display defects in actin organization. In yeast, actin is typically organized into long bundles of F-actin filaments called actin cables, which function as tracks for intracellular transport, or dynamic punctate actin cortical structures called actin patches, that are primarily involved in endocytosis. Yeast *Vps13* mutants display mislocalized actin patches with abnormal movements and impaired actin-dependent endocytosis[132,231]. Expression of VPS13 constructs in these yeast cells demonstrates that Vps13 binds actin[132], suggesting that VPS13 homologs across eukaryotic organisms may be involved in coordinating actin dynamics and cytoskeleton organization.

1.8 VPS13A and neurons

In mice, VPS13A is present in neurons as early as the embryonic stage and expression levels remain stable until adulthood[232]. In adult mice, VPS13A protein is widely expressed throughout the brain and is particularly enriched in the striatum, hippocampus, cerebellum, pons, and select cortical areas[232–234]. Whole brain fractionation analyses show that VPS13A is primarily found in microsomal fractions, which contain membranes derived from the ER, and potentially the Golgi, endosomes, and plasma membrane, as well as in synaptosomal fractions that contain intact presynaptic terminals[233]. Cell type specific analyses indicate that VPS13A is expressed in glutamatergic, GABAergic, and cholinergic neurons, but is rarely observed in glial cells[232]. At the cellular level, VPS13A is observed in the perinuclear reticular cytoplasm, particularly in striatal GABAergic MSNs[233], and neurites where it partially co-localizes with the ER and mitochondria depending on the study[232,233]. In differentiated PC12 dopaminergic cells, VPS13A is found at the distal end of neurites where it partially colocalizes with the synaptic vesicle protein synaptotagmin-I[234]. Fractionation experiments show that this colocalization occurs at dense-core vesicles which store dopamine, and overexpression of a C-terminal VPS13A

fragment increases K^+-induced dopamine release[234]. Together these observations suggest that VPS13A may contribute to exocytosis at dopaminergic terminals.

Stromal interaction molecule 1 (STIM1) is an ER transmembrane protein that acts as a Ca^{2+} sensor; when ER Ca^{2+} stores are depleted, STIM1 oligomerizes and translocates to ER–plasma membrane junctions, where it activates ORAI1 Ca^{2+} channels, allowing Ca^{2+} influx in a process known as store-operated Ca^{2+} entry (SOCE)[235]. Cortical neurons differentiated from iPSCs derived from individuals with VPS13A disease (iNeurons) exhibit significantly reduced ORAI1 and STIM1 transcript and protein levels, diminished SOCE, and increased apoptosis compared to control neurons[236]. Lithium treatment partially rescues these deficits, but its effects on ORAI1 and STIM1 RNA and protein levels are lost when serum and glucocorticoid inducible kinase 1 (SGK1) is inhibited, suggesting that lithium may be acting through the SGK1 pathway[236]. Additionally, treatment with 2-APB, an ORAI1 inhibitor, reduces lithium–mediated elevation of SOCE and anti-apoptotic effect, indicating that ORAI1-dependent Ca^{2+} entry is important for neuronal health[236]. Complementary work in the same iNeurons shows that Na^+/K^+-ATPase (Na^+/K^+ pump) capacity, a downstream target of SGK1, is significantly reduced, and that the resting membrane potential (V_m) is depolarized in patient derived iNeurons[237]. These deficits are improved with lithium treatment and again can be reversed with SGK1 inhibition[237]. Collectively, these findings suggest that SGK1-dependent regulation of SOCE and Na^+/K^+ pump function are impaired in VPS13A disease and contribute to deficits in neuronal excitability and reduced cell survival.

Studies suggest that loss of VPS13A results in synaptic dysfunction, particularly in striatal MSNs and cortical neurons. MSNs differentiated from iPSCs derived from individuals with VPS13A disease display enhanced neurite outgrowth and ramification, and elevated synaptic activity but similar synaptic density[238]. Additionally, patient derived iMSNs also show elevated Lyn kinase activity and increased G-actin to F-actin ratio, implicating the actin cytoskeleton and Lyn kinase[238]. Furthermore, treatment of patient derived iMSNs with the F-actin stabilizer phallacidin, or the Src kinase inhibitor PP2, significantly reduces synaptic activity to control levels, suggesting that iMSN hyperexcitability is mediated via Src kinase and actin-dependent mechanisms[238]. Mouse primary cortical and striatal neurons infected with VPS13A-targeting miR30-shRNA

(VPS13A-KD) also show increased dendritic branching, reduced levels of postsynaptic density protein 95 (PSD-95), and brain-derived neurotrophic factor (BDNF)[239]. Although this study found that VPS13A-KD does not result in neuronal loss in the cortex or striatum, they found that it does reduce levels of the neuron-derived chemokine CX3CL1 (also known as fractalkine, a neuronal regulator of microglia), and increase levels of gliosis[239]. These neurons also showed impaired induction of cortico-striatal long-term depression (LTD), which was partially rescued by BDNF and CX3CL1[239], indicating that VPS13A may be involved in synaptic plasticity and neuron-microglia communication.

VPS13A disease patient-derived midbrain and hindbrain iNeurons also show cytoskeletal deficits including dendritic microtubule fragmentation, proximal axonal degeneration, increased retrograde transport, and hyperpolarization[210]. Unlike other studies however, inhibition of Lyn kinase was ineffective in rescuing any of the phenotypes, strongly suggesting that VPS13A functions may be cell type specific[210].

Altogether there is evidence to suggest that VPS13A loss may disrupt Ca^{2+} signaling, actin regulation, synaptic plasticity, and neuronal morphology. Nevertheless, inconsistent findings hint at potential cell type specific differences that may further complicate an already complicated disease.

1.9 Summary and aims of dissertation

VPS13A disease is caused by loss-of-function mutations in the *VPS13A* gene, resulting in undetectable levels of the protein. VPS13A belongs to the evolutionarily conserved VPS13 family and shares strong homology with other BLTPs. Like its homologs, VPS13A is predicted to form an elongated, hydrophobic-lined, rod-shaped structure capable of transporting multiple phospholipids between lipid membranes. Although it has been linked to numerous cellular processes, its precise mechanistic roles, and the extent to which disruption of these functions contributes to disease pathology, remain unclear. As a result, current treatments only address associated symptoms and do not modify the underlying cause of disease. To this end, defining the physiological functions and regulatory mechanisms of VPS13A, and determining how loss of this protein leads to neurodegeneration, is essential for the development of effective disease-modifying therapies.

The overall goal of this dissertation is to elucidate the physiological functions of VPS13A and establish effective readouts to test whether their disruption contributes to disease. Throughout this dissertation, I utilize patient-derived cell lines, novel VPS13A knockout (V-KO) cells, and cells in which endogenous VPS13A has been fluorescently tagged. Chapter 2 examines the necessity of VPS13A in neuronal survival and identifies a previously unrecognized interactor, high-mobility group protein A1 (HMGA1), which may link VPS13A to transcriptional regulation. Chapter 2 also tests whether HMGA1 contributes to neuronal death in both patient-derived and V-KO neurons. Chapter 3 investigates the potential role of VPS13A in macroautophagy and in selective organelle autophagy. Finally, Chapter 4 concludes the dissertation, discusses limitations of this dissertation, and outlines future directions for advancing our understanding of VPS13A biology and its relevance to neurodegeneration in disease.

References

1. Peikert, K., Dobson-Stone, C., Rampoldi, L., Miltenberger-Miltenyi, G., Neiman, A., De Camilli, P., Hermann, A., Walker, R.H., Monaco, A.P., and Danek, A. (1993). VPS13A disease. In GeneReviews(®) (University of Washington, Seattle).

2. Walker, R.H., Peikert, K., Jung, H.H., Hermann, A., and Danek, A. (2023). Neuroacanthocytosis syndromes: The clinical perspective. Contact (Thousand Oaks.) *6*, 25152564231210340. https://doi.org/10.1177/25152564231210339.

3. Walker, R.H., Miranda, M., Jung, H.H., and Danek, A. (2019). Life expectancy and mortality in chorea-acanthocytosis and McLeod syndrome. Parkinsonism Relat. Disord. *60*, 158–161. https://doi.org/10.1016/j.parkreldis.2018.09.003.

4. Jung, H.H., Danek, A., and Walker, R.H. (2011). Neuroacanthocytosis syndromes. Orphanet J. Rare Dis. *6*, 68. https://doi.org/10.1186/1750-1172-6-68.

5. Yamamoto, T., Hirose, G., Shimazaki, K., Takado, S., Kosoegawa, H., and Saeki, M. (1982). Movement disorders of familial neuroacanthocytosis syndrome. Arch. Neurol. *39*, 298–301. https://doi.org/10.1001/archneur.1982.00510170040011.

6. Schneider, S.A., Lang, A.E., Moro, E., Bader, B., Danek, A., and Bhatia, K.P. (2010). Characteristic head drops and axial extension in advanced chorea-acanthocytosis: Axial Jerks in Chorea-Acanthocytosis. Mov. Disord. *25*, 1487–1491. https://doi.org/10.1002/mds.23052.

7. Termsarasab, P., and Frucht, S.J. (2018). The “stutter-step”: A peculiar gait feature in advanced Huntington’s disease and chorea-acanthocytosis: Stutter-step in HD and ChAc. Mov. Disord. Clin. Pract. *5*, 223–224. https://doi.org/10.1002/mdc3.12586.

8. Suzuki, F., Sato, N., Sugiyama, A., Iijima, K., Shigemoto, Y., Morimoto, E., Kimura, Y., Fujii, H., Takahashi, Y., Nakata, Y., et al. (2021). Chorea-acanthocytosis: Time-dependent changes of symptoms and imaging findings. J. Neuroradiol. *48*, 419–424. https://doi.org/10.1016/j.neurad.2019.11.006.

9. Saiki, S., Hirose, G., Sakai, K., Matsunari, I., Higashi, K., Saiki, M., Kataoka, S., Hori, A., and Shimazaki, K. (2004). Chorea-acanthocytosis associated with Tourettism. Mov. Disord. *19*, 833–836. https://doi.org/10.1002/mds.20050.

10. Wang, M., Li, H., Zhou, Q., Zhao, Q., Wang, M., Geng, Y., and Kang, H. (2024). Case report: Misdiagnosed orolingual dyskinesia as a consequence of seizures in a chorea-acanthocytosis patient with a novel VPS13A variation from a family with consanguineous marriage. Front. Neurol. *15*, 1352467. https://doi.org/10.3389/fneur.2024.1352467.

11. Bader, B., Walker, R.H., Vogel, M., Prosiegel, M., McIntosh, J., and Danek, A. (2010). Tongue protrusion and feeding dystonia: a hallmark of chorea-acanthocytosis: Letters to the Editor. Mov. Disord. *25*, 127–129. https://doi.org/10.1002/mds.22863.

12. Dulski, J., Sołtan, W., Schinwelski, M., Rudzińska, M., Wójcik-Pędziwiatr, M., Wictor, L., Schön, F., Puschmann, A., Klempíř, J., Tilley, L., et al. (2016). Clinical variability of neuroacanthocytosis syndromes-a series of six patients with long follow-up. Clin. Neurol. Neurosurg. *147*, 78–83. https://doi.org/10.1016/j.clineuro.2016.05.028.

13. Aasly, J., Skandsen, T., and Rø, M. (1999). Neuroacanthocytosis--the variability of presenting symptoms in two siblings. Acta Neurol. Scand. *100*, 322–325. https://doi.org/10.1111/j.1600-0404.1999.tb00404.x.

14. Lossos, A., Dobson-Stone, C., Monaco, A.P., Soffer, D., Rahamim, E., Newman, J.P., Mohiddin, S., Fananapazir, L., Lerer, I., Linetsky, E., et al. (2005). Early clinical heterogeneity in choreoacanthocytosis. Arch. Neurol. *62*, 611–614. https://doi.org/10.1001/archneur.62.4.611.

15. Walker, R.H. (2015). Management of neuroacanthocytosis syndromes. Tremor Other Hyperkinet. Mov. (N. Y.) *5*, 346. https://doi.org/10.7916/D8W66K48.

16. Hardie, R.J., Pullon, H.W., Harding, A.E., Owen, J.S., Pires, M., Daniels, G.L., Imai, Y., Misra, V.P., King, R.H., and Jacobs, J.M. (1991). Neuroacanthocytosis. A clinical, haematological and pathological study of 19 cases. Brain *114 (Pt 1A)*, 13–49.

17. Walker, R.H., Liu, Q., Ichiba, M., Muroya, S., Nakamura, M., Sano, A., Kennedy, C.A., and Sclar, G. (2006). Self-mutilation in chorea-acanthocytosis: Manifestation of movement disorder or psychopathology? Mov. Disord. *21*, 2268–2269. https://doi.org/10.1002/mds.21156.

18. Walterfang, M., Yucel, M., Walker, R., Evans, A., Bader, B., Ng, A., Danek, A., Mocellin, R., and Velakoulis, D. (2008). Adolescent obsessive compulsive disorder heralding chorea-acanthocytosis: Obsessive Compulsive Disorder Heralding ChAc. Mov. Disord. *23*, 422–425. https://doi.org/10.1002/mds.21725.

19. Sorrentino, G., De Renzo, A., Miniello, S., Nori, O., and Bonavita, V. (1999). Late appearance of acanthocytes during the course of chorea-acanthocytosis. J. Neurol. Sci. *163*, 175–178. https://doi.org/10.1016/s0022-510x(99)00005-2.

20. Elmgreen, S.B. (2019). Criminal behaviour associated with a novel mutation in the VPS13A-gene causing chorea-acanthocytosis. Case Rep. Psychiatry *2019*, 5947416. https://doi.org/10.1155/2019/5947416.

21. Vaisfeld, A., Bruno, G., Petracca, M., Bentivoglio, A.R., Servidei, S., Vita, M.G., Bove, F., Straccia, G., Dato, C., Di Iorio, G., et al. (2021). Neuroacanthocytosis syndromes in an Italian cohort: Clinical spectrum, high genetic variability and muscle involvement. Genes (Basel) *12*, 344. https://doi.org/10.3390/genes12030344.

22. Neutel, D., Miltenberger-Miltenyi, G., Silva, I., and de Carvalho, M. (2012). Chorea-acanthocytosis presenting as motor neuron disease: Corea-Acanthocytosis Presenting as MND. Muscle Nerve *45*, 293–295. https://doi.org/10.1002/mus.22269.

23. Gradstein, L., Danek, A., Grafman, J., and Fitzgibbon, E.J. (2005). Eye movements in chorea-acanthocytosis. Invest. Ophthalmol. Vis. Sci. *46*, 1979–1987. https://doi.org/10.1167/iovs.04-0539.

24. Miki, Y., Nishie, M., Ichiba, M., Nakamura, M., Mori, F., Ogawa, M., Kaimori, M., Sano, A., and Wakabayashi, K. (2010). Chorea-acanthocytosis with upper motor neuron degeneration and 3419_3420 delCA and 3970_3973 delAGTC VPS13A mutations. Acta Neuropathol. *119*, 271–273. https://doi.org/10.1007/s00401-009-0617-x.

25. Tamura, Y., Matsui, K., Yaguchi, H., Hashimoto, M., and Inoue, K. (2005). Nemaline rods in chorea-acanthocytosis. Muscle Nerve *31*, 516–519. https://doi.org/10.1002/mus.20243.

26. Al-Asmi, A., Jansen, A.C., Badhwar, A., Dubeau, F., Tampieri, D., Shustik, C., Mercho, S., Savard, G., Dobson-Stone, C., Monaco, A.P., et al. (2005). Familial temporal lobe epilepsy as a presenting feature of choreoacanthocytosis. Epilepsia *46*, 1256–1263. https://doi.org/10.1111/j.1528-1167.2005.65804.x.

27. Bader, B., Vollmar, C., Ackl, N., Ebert, A., la Fougère, C., Noachtar, S., and Danek, A. (2011). Bilateral temporal lobe epilepsy confirmed with intracranial EEG in chorea-acanthocytosis. Seizure *20*, 340–342. https://doi.org/10.1016/j.seizure.2010.12.007.

28. Weber, J., Frings, L., Rijntjes, M., Urbach, H., Fischer, J., Weiller, C., Meyer, P.T., and Klebe, S. (2018). Chorea-acanthocytosis presenting as autosomal recessive epilepsy in a family with a novel VPS13A mutation. Front. Neurol. *9*, 1168. https://doi.org/10.3389/fneur.2018.01168.

29. Mente, K., Kim, S.A., Grunseich, C., Hefti, M.M., Crary, J.F., Danek, A., Karp, B.I., and Walker, R.H. (2017). Hippocampal sclerosis and mesial temporal lobe epilepsy in chorea-acanthocytosis: a case with clinical, pathologic and genetic evaluation. Neuropathol. Appl. Neurobiol. *43*, 542–546. https://doi.org/10.1111/nan.12403.

30. Scheid, R., Bader, B., Ott, D.V., Merkenschlager, A., and Danek, A. (2009). Development of mesial temporal lobe epilepsy in chorea-acanthocytosis. Neurology *73*, 1419–1422. https://doi.org/10.1212/WNL.0b013e3181bd80d4.

31. Mitchell, S.D., Albin, R.L., Dauer, W.T., Goudreau, J.L., and Sidiropoulos, C. (2021). Heterozygous VPS13A and PARK2 mutations in a patient with parkinsonism and seizures. Case Rep. Neurol. *13*, 341–346. https://doi.org/10.1159/000515805.

32. Ditzel, R.M., Jr, Walker, R.H., Nirenberg, M.J., Tetlow, A.M., Farrell, K., Lind-Watson, K.J., Thorn, E.L., Dangoor, D.K., Gordon, R., De Sanctis, C., et al. (2023). An autopsy series of seven cases of VPS13A disease (chorea-acanthocytosis). Mov. Disord. *38*, 2163–2172. https://doi.org/10.1002/mds.29589.

33. Cloos, A.-S., Ghodsi, M., Stommen, A., Recktenwald, S.M., Kaestner, L., Danek, A., Spranger, A., Hermann, A., Peikert, K., and Tyteca, D. (2025). Red blood cell lipid distribution in the pathophysiology and laboratory evaluation of chorea-acanthocytosis and McLeod syndrome patients. Front. Physiol. *16*, 1543812. https://doi.org/10.3389/fphys.2025.1543812.

34. Reichel, F., Kräter, M., Peikert, K., Glaß, H., Rosendahl, P., Herbig, M., Rivera Prieto, A., Kihm, A., Bosman, G., Kaestner, L., et al. (2022). Changes in blood cell deformability in Chorea-Acanthocytosis and effects of treatment with dasatinib or lithium. Front. Physiol. *13*, 852946. https://doi.org/10.3389/fphys.2022.852946.

35. Bayreuther, C., Borg, M., Ferrero-Vacher, C., Chaussenot, A., and Lebrun, C. (2010). Choréo-acanthocytose sans acanthocytes. Rev. Neurol. (Paris) *166*, 100–103. https://doi.org/10.1016/j.neurol.2009.03.005.

36. Jin, S., Sun, Z., Fang, X., Chen, H., Yang, W., Wang, S., and Fan, J. (2024). A chorea-acanthocytosis patient with novel mutations in the VPS13A gene without acanthocyte. Neurol. Sci. *45*, 2057–2061. https://doi.org/10.1007/s10072-023-07174-0.

37. Quick, S., Heidrich, F.M., Winkler, M.-V., Winkler, A.H., Ibrahim, K., Linke, A., Speiser, U., Grabmaier, U., Buhmann, C., Marxreiter, F., et al. (2021). Cardiac manifestation is evident in chorea-acanthocytosis but different from McLeod syndrome. Parkinsonism Relat. Disord. *88*, 90–95. https://doi.org/10.1016/j.parkreldis.2021.05.015.

38. Kageyama, Y., Matsumoto, K., Ichikawa, K., Ueno, S.-I., Ichiba, M., Nakamura, M., and Sano, A. (2007). A new phenotype of chorea-acanthocytosis with dilated cardiomyopathy and myopathy. Mov. Disord. *22*, 1669–1670. https://doi.org/10.1002/mds.21556.

39. Paucar, M., Wincent, J., Rubin, C., Peikert, K., Kyhle, J., Hertegård, S., Möller, R., Beshara, S., and Svenningsson, P. (2024). Case report: Neuroacanthocytosis associated with novel variants in the VPS13A gene with concomitant nucleotide expansion for CANVAS and assessment with osmotic gradient ektacytometry. Front. Neurosci. *18*, 1409366. https://doi.org/10.3389/fnins.2024.1409366.

40. Dolenc-Grošelj, L., Jazbec, J., and Kobal, J. (2006). Sleep Features in Chorea-Acanthocytosis. In Neuroacanthocytosis Syndromes (Springer-Verlag), pp. 123–125. https://doi.org/10.1007/1-4020-2898-9_14.

41. Müller-Vahl, K.R., Berding, G., Emrich, H.M., and Peschel, T. (2007). Chorea-acanthocytosis in monozygotic twins: clinical findings and neuropathological changes as detected by diffusion tensor imaging, FDG-PET and (123)I-beta-CIT-SPECT. J. Neurol. *254*, 1081–1088. https://doi.org/10.1007/s00415-006-0492-5.

42. Oner O.G., and Varoglu A.O. (2025). Phenotypic variability in sisters with VPS13A disease (chorea-acanthocytosis). Ideggyogy. Sz. *78*, 69–72. https://doi.org/10.18071/isz.78.0069.

43. Bohlega, S., Al-Jishi, A., Dobson-Stone, C., Rampoldi, L., Saha, P., Murad, H., Kareem, A., Roberts, G., and Monaco, A.P. (2003). Chorea-acanthocytosis: clinical and genetic findings in three families from the Arabian peninsula. Mov. Disord. *18*, 403–407. https://doi.org/10.1002/mds.10361.

44. Niemelä, V., Salih, A., Solea, D., Lindvall, B., Weinberg, J., Miltenberger, G., Granberg, T., Tzovla, A., Nordin, L., Danfors, T., et al. (2020). Phenotypic variability in chorea-acanthocytosis associated with novel VPS13A mutations. Neurol. Genet. *6*, e426. https://doi.org/10.1212/NXG.0000000000000426.

45. Ouchkat, F., Regragui, W., Smaili, I., Naciri Darai, H., Bouslam, N., Rahmani, M., Melhaoui, A., Arkha, Y., El Fahime, E., and Bouhouche, A. (2020). Novel pathogenic VPS13A mutation in Moroccan family with Choreoacanthocytosis: a case report. BMC Med. Genet. *21*, 47. https://doi.org/10.1186/s12881-020-0983-8.

46. Ishida, C., Makifuchi, T., Saiki, S., Hirose, G., and Yamada, M. (2009). A neuropathological study of autosomal-dominant chorea-acanthocytosis with a mutation of VPS13A. Acta Neuropathol. *117*, 85–94. https://doi.org/10.1007/s00401-008-0403-1.

47. Chen, X., Zhang, P., Wang, L., and Zhang, Y. (2023). Novel heterozygous VPS13A pathogenic variants in chorea-neuroacanthocytosis: a case report. BMC Neurol. *23*, 350. https://doi.org/10.1186/s12883-023-03398-x.

48. Xiang, Y., Li, S., Liu, X., Li, J., Sun, Q., Chen, Y., Du, Y., and Wu, J. (2019). Neuroacanthocytosis: a case report of chorea-acanthocytosis. J. Integr. Neurosci. *18*, 197–201. https://doi.org/10.31083/j.jin.2019.02.165.

49. Shen, Y., Liu, X., Long, X., Han, C., Wan, F., Fan, W., Guo, X., Ma, K., Guo, S., Wang, L., et al. (2017). Novel VPS13A gene mutations identified in patients diagnosed with chorea-acanthocytosis (ChAc): Case presentation and literature review. Front. Aging Neurosci. *9*, 95. https://doi.org/10.3389/fnagi.2017.00095.

50. Henkel, K., Danek, A., Grafman, J., Butman, J., and Kassubek, J. (2006). Head of the caudate nucleus is most vulnerable in chorea-acanthocytosis: a voxel-based morphometry study. Mov. Disord. *21*, 1728–1731. https://doi.org/10.1002/mds.21046.

51. Liu, J., Heinsen, H., Grinberg, L.T., Alho, E., Amaro, E., Jr, Pasqualucci, C.A., Rüb, U., den Dunnen, W., Arzberger, T., Schmitz, C., et al. (2018). Subcortical neurodegeneration in chorea: Similarities and differences between chorea-acanthocytosis and Huntington's disease. Parkinsonism Relat. Disord. *49*, 54–59. https://doi.org/10.1016/j.parkreldis.2018.01.009.

52. Iwata, M., Fuse, S., Sakuta, M., and Toyokura, Y. (1984). Neuropathological study of chorea-acanthocytosis. Jpn. J. Med. *23*, 118–122. https://doi.org/10.2169/internalmedicine1962.23.118.

53. Walterfang, M., Looi, J.C.L., Styner, M., Walker, R.H., Danek, A., Niethammer, M., Evans, A., Kotschet, K., Rodrigues, G.R., Hughes, A., et al. (2011). Shape alterations in the striatum in chorea-acanthocytosis. Psychiatry Res. *192*, 29–36. https://doi.org/10.1016/j.pscychresns.2010.10.006.

54. Alegre-Cortés, J., Sáez, M., Montanari, R., and Reig, R. (2021). Medium spiny neurons activity reveals the discrete segregation of mouse dorsal striatum. Elife *10*. https://doi.org/10.7554/eLife.60580.

55. Driscoll, M.E., Bollu, P.C., and Tadi, P. (2025). Neuroanatomy, nucleus caudate. In StatPearls (StatPearls Publishing).

56. He, J., Kleyman, M., Chen, J., Alikaya, A., Rothenhoefer, K.M., Ozturk, B.E., Wirthlin, M., Bostan, A.C., Fish, K., Byrne, L.C., et al. (2021). Transcriptional and anatomical diversity of medium spiny neurons in the primate striatum. Curr. Biol. *31*, 5473-5486.e6. https://doi.org/10.1016/j.cub.2021.10.015.

57. Çırak, M., Yağmurlu, K., Kearns, K.N., Ribas, E.C., Urgun, K., Shaffrey, M.E., and Kalani, M.Y.S. (2020). The caudate nucleus: Its connections, surgical implications, and related complications. World Neurosurg. *139*, e428–e438. https://doi.org/10.1016/j.wneu.2020.04.027.

58. Graff-Radford, J., Williams, L., Jones, D.T., and Benarroch, E.E. (2017). Caudate nucleus as a component of networks controlling behavior. Neurology *89*, 2192–2197. https://doi.org/10.1212/WNL.0000000000004680.

59. Macfarlane, M.D., Looi, J.C.L., Walterfang, M., Spulber, G., Velakoulis, D., Styner, M., Crisby, M., Orndahl, E., Erkinjuntti, T., Waldemar, G., et al. (2015). Shape abnormalities of the caudate nucleus correlate with poorer gait and balance: results from a subset of the LADIS study. Am. J. Geriatr. Psychiatry *23*, 59-71.e1. https://doi.org/10.1016/j.jagp.2013.04.011.

60. Barkóczi, B., Nagypál, T., Nyujtó, D., Katona, X., Eördegh, G., Bodosi, B., Benedek, G., Braunitzer, G., and Nagy, A. (2017). Background activity and visual responsiveness of caudate nucleus neurons in halothane anesthetized and in awake, behaving cats. Neuroscience *356*, 182–192. https://doi.org/10.1016/j.neuroscience.2017.05.028.

61. Yanike, M., and Ferrera, V.P. (2014). Representation of outcome risk and action in the anterior caudate nucleus. J. Neurosci. *34*, 3279–3290. https://doi.org/10.1523/JNEUROSCI.3818-13.2014.

62. Agus, F., Crespo, D., Myers, R.H., and Labadorf, A. (2019). The caudate nucleus undergoes dramatic and unique transcriptional changes in human prodromal Huntington's disease brain. BMC Med. Genomics *12*, 137. https://doi.org/10.1186/s12920-019-0581-9.

63. Kasper, J., Eickhoff, S.B., Caspers, S., Peter, J., Dogan, I., Wolf, R.C., Reetz, K., Dukart, J., and Orth, M. (2023). Local synchronicity in dopamine-rich caudate nucleus influences Huntington's disease motor phenotype. Brain *146*, 3319–3330. https://doi.org/10.1093/brain/awad043.

64. Pasquini, J., Durcan, R., Wiblin, L., Gersel Stokholm, M., Rochester, L., Brooks, D.J., Burn, D., and Pavese, N. (2019). Clinical implications of early caudate dysfunction in Parkinson's disease. J. Neurol. Neurosurg. Psychiatry *90*, 1098–1104. https://doi.org/10.1136/jnnp-2018-320157.

65. Jia, X., Pan, Z., Chen, H., Wang, Z., Li, K., Wang, X., Wang, Z., Ma, H., Feng, T., and Yang, Q. (2020). Differential functional dysconnectivity of caudate nucleus subdivisions in Parkinson's disease. Aging (Albany NY) *12*, 16183–16194. https://doi.org/10.18632/aging.103628.

66. Barrett, E., Ivey, G., Cunningham, A., Coffman, G., Pemberton, T., Lee, C., Patra, P., Day, J.B., Lee, P.H.U., and Shim, J.W. (2024). Reduced GLP-1R availability in the caudate nucleus with Alzheimer's disease. Front. Aging Neurosci. *16*, 1350239. https://doi.org/10.3389/fnagi.2024.1350239.

67. Jiji, S., Smitha, K.A., Gupta, A.K., Pillai, V.P.M., and Jayasree, R.S. (2013). Segmentation and volumetric analysis of the caudate nucleus in Alzheimer's disease. Eur. J. Radiol. *82*, 1525–1530. https://doi.org/10.1016/j.ejrad.2013.03.012.

68. Udo, N., Hashimoto, N., Toyonaga, T., Isoyama, T., Oyanagi, Y., Narita, H., Shiga, T., Nakagawa, S., and Kusumi, I. (2020). Apathy in Alzheimer's disease correlates with the dopamine transporter level in the caudate nuclei. Dement. Geriatr. Cogn. Dis. Extra *10*, 86–93. https://doi.org/10.1159/000509278.

69. Josephs, K.A., Whitwell, J.L., Parisi, J.E., Petersen, R.C., Boeve, B.F., Jack, C.R., Jr, and Dickson, D.W. (2010). Caudate atrophy on MRI is a characteristic feature of FTLD-FUS: Caudate atrophy in FTLD-FUS. Eur. J. Neurol. 17, 969–975. https://doi.org/10.1111/j.1468-1331.2010.02975.x.

70. Masuda, M., Senda, J., Watanabe, H., Epifanio, B., Tanaka, Y., Imai, K., Riku, Y., Li, Y., Nakamura, R., Ito, M., et al. (2016). Involvement of the caudate nucleus head and its networks in sporadic amyotrophic lateral sclerosis-frontotemporal dementia continuum. Amyotroph. Lateral Scler. Frontotemporal Degener. *17*, 571–579. https://doi.org/10.1080/21678421.2016.1211151.

71. Machts, J., Loewe, K., Kaufmann, J., Jakubiczka, S., Abdulla, S., Petri, S., Dengler, R., Heinze, H.-J., Vielhaber, S., Schoenfeld, M.A., et al. (2015). Basal ganglia pathology in ALS is associated with neuropsychological deficits. Neurology *85*, 1301–1309. https://doi.org/10.1212/WNL.0000000000002017.

72. Dang, L.C., Samanez-Larkin, G.R., Young, J.S., Cowan, R.L., Kessler, R.M., and Zald, D.H. (2016). Caudate asymmetry is related to attentional impulsivity and an objective measure of ADHD-like attentional problems in healthy adults. Brain Struct. Funct. *221*, 277–286. https://doi.org/10.1007/s00429-014-0906-6.

73. Carrey, N., Bernier, D., Emms, M., Gunde, E., Sparkes, S., Macmaster, F.P., and Rusak, B. (2012). Smaller volumes of caudate nuclei in prepubertal children with ADHD: impact of age. J. Psychiatr. Res. 46, 1066–1072. https://doi.org/10.1016/j.jpsychires.2012.04.025.

74. Hansen, E.S., Hasselbalch, S., Law, I., and Bolwig, T.G. (2002). The caudate nucleus in obsessive-compulsive disorder. Reduced metabolism following treatment with paroxetine: a PET study. Int. J. Neuropsychopharmacol. *5*, 1–10. https://doi.org/10.1017/S1461145701002681.

75. Peng, Z., He, T., Ren, P., Jin, L., Yang, Q., Xu, C., Wen, R., Chen, J., Wei, Z., Verguts, T., et al. (2022). Imbalance between the caudate and putamen connectivity in obsessive-compulsive disorder. NeuroImage Clin. *35*, 103083. https://doi.org/10.1016/j.nicl.2022.103083.

76. Andreou, D., Jørgensen, K.N., Nerland, S., Calkova, T., Mørch-Johnsen, L., Smelror, R.E., Wortinger, L.A., Lundberg, M., Bohman, H., Myhre, A.M., et al. (2024). Caudate nucleus volume in medicated and unmedicated patients with early- and adult-onset schizophrenia. Sci. Rep. *14*, 22755. https://doi.org/10.1038/s41598-024-73322-x.

77. Mueller, S., Wang, D., Pan, R., Holt, D.J., and Liu, H. (2015). Abnormalities in hemispheric specialization of caudate nucleus connectivity in schizophrenia. JAMA Psychiatry *72*, 552–560. https://doi.org/10.1001/jamapsychiatry.2014.3176.

78. Hinkley, L.B.N., Haas, S.S., Cheung, S.W., Nagarajan, S.S., and Subramaniam, K. (2023). Reduced neural connectivity in the caudate anterior head predicts hallucination severity in schizophrenia. Schizophr. Res. *261*, 1–5. https://doi.org/10.1016/j.schres.2023.08.030.

79. Ong, D., Walterfang, M., Malhi, G.S., Styner, M., Velakoulis, D., and Pantelis, C. (2012). Size and shape of the caudate nucleus in individuals with bipolar affective disorder. Aust. N. Z. J. Psychiatry *46*, 340–351. https://doi.org/10.1177/0004867412440191.

80. Lippard, E.T.C., Weber, W., Welge, J., Adler, C.M., Fleck, D.E., Almeida, J., DelBello, M.P., and Strakowski, S.M. (2021). Variation in rostral anterior cingulate functional connectivity with amygdala and caudate during first manic episode distinguish bipolar young adults who do not remit following treatment. Bipolar Disord. *23*, 500–508. https://doi.org/10.1111/bdi.13025.

81. Hwang, J., Lyoo, I.K., Dager, S.R., Friedman, S.D., Oh, J.S., Lee, J.Y., Kim, S.J., Dunner, D.L., and Renshaw, P.F. (2006). Basal ganglia shape alterations in bipolar disorder. Am. J. Psychiatry *163*, 276–285. https://doi.org/10.1176/appi.ajp.163.2.276.

82. Butters, M.A., Aizenstein, H.J., Hayashi, K.M., Meltzer, C.C., Seaman, J., Reynolds, C.F., 3rd, Toga, A.W., Thompson, P.M., Becker, J.T., and IMAGe Research Group (2009). Three-dimensional surface mapping of the caudate nucleus in late-life depression. Am. J. Geriatr. Psychiatry *17*, 4–12. https://doi.org/10.1097/JGP.0b013e31816ff72b.

83. Zhang, J., Wu, X., Si, Y., Liu, Y., Wang, X., Geng, Y., Chang, Q., Jiang, X., and Zhang, H. (2024). Abnormal caudate nucleus activity in patients with depressive disorder: Meta-analysis of task-based functional magnetic resonance imaging studies with behavioral domain. Psychiatry Res. Neuroimaging *338*, 111769. https://doi.org/10.1016/j.pscychresns.2023.111769.

84. Alves, L.L., de Castro, P.L., Ferreira, A.B., de Campos, L. de A.N.B., da Fonseca, P.G.M., Torres, T.D., Gomes, M.P.D.S., Maiolo, V.C.A., and Bahia, P.R.V. (2025).

Neuroacanthocytosis: Case report and neuroimaging findings. Radiol. Case Rep. *20*, 667–669. https://doi.org/10.1016/j.radcr.2024.10.007.

85. Hermann, A., and Walker, R.H. (2015). Diagnosis and treatment of chorea syndromes. Curr. Neurol. Neurosci. Rep. *15*, 514. https://doi.org/10.1007/s11910-014-0514-0.

86. Xu, Y., Yu, J., Gao, Y., Su, Q., Xie, H., Liang, H., and Zheng, C. (2024). A case of chorea-acanthocytosis with significant improvement of symptoms at one year with deep brain stimulation: case report and literature review. Front. Neurol. *15*, 1377377. https://doi.org/10.3389/fneur.2024.1377377.

87. Velayos-Baeza, A., Vettori, A., Copley, R.R., Dobson-Stone, C., and Monaco, A.P. (2004). Analysis of the human VPS13 gene family. Genomics *84*, 536–549. https://doi.org/10.1016/j.ygeno.2004.04.012.

88. Rampoldi, L., Dobson-Stone, C., Rubio, J.P., Danek, A., Chalmers, R.M., Wood, N.W., Verellen, C., Ferrer, X., Malandrini, A., Fabrizi, G.M., et al. (2001). A conserved sorting-associated protein is mutant in chorea-acanthocytosis. Nat. Genet. *28*, 119–120. https://doi.org/10.1038/88821.

89. Ueno, S., Maruki, Y., Nakamura, M., Tomemori, Y., Kamae, K., Tanabe, H., Yamashita, Y., Matsuda, S., Kaneko, S., and Sano, A. (2001). The gene encoding a newly discovered protein, chorein, is mutated in chorea-acanthocytosis. Nat. Genet. *28*, 121–122. https://doi.org/10.1038/88825.

90. Dobson-Stone, C., Velayos-Baeza, A., Filippone, L.A., Westbury, S., Storch, A., Erdmann, T., Wroe, S.J., Leenders, K.L., Lang, A.E., Dotti, M.T., et al. (2004). Chorein detection for the diagnosis of chorea-acanthocytosis. Ann. Neurol. *56*, 299–302. https://doi.org/10.1002/ana.20200.

91. Dobson-Stone, C., Danek, A., Rampoldi, L., Hardie, R.J., Chalmers, R.M., Wood, N.W., Bohlega, S., Dotti, M.T., Federico, A., Shizuka, M., et al. (2002). Mutational spectrum of the CHAC gene in patients with chorea-acanthocytosis. Eur. J. Hum. Genet. *10*, 773–781. https://doi.org/10.1038/sj.ejhg.5200866.

92. Tomiyasu, A., Nakamura, M., Ichiba, M., Ueno, S., Saiki, S., Morimoto, M., Kobal, J., Kageyama, Y., Inui, T., Wakabayashi, K., et al. (2011). Novel pathogenic mutations and copy number variations in the VPS13A gene in patients with chorea-acanthocytosis. Am. J. Med. Genet. B Neuropsychiatr. Genet. *156B*, 620–631. https://doi.org/10.1002/ajmg.b.31206.

93. Park, J.-S., Halegoua, S., Kishida, S., and Neiman, A.M. (2015). A conserved function in phosphatidylinositol metabolism for mammalian Vps13 family proteins. PLoS One *10*, e0124836. https://doi.org/10.1371/journal.pone.0124836.

94. Cohen, M.M., Jr, Hall, B.D., Smith, D.W., Graham, C.B., and Lampert, K.J. (1973). A new syndrome with hypotonia, obesity, mental deficiency, and facial, oral, ocular, and limb anomalies. J. Pediatr. *83*, 280–284. https://doi.org/10.1016/s0022-3476(73)80493-7.

95. Kolehmainen, J., Black, G.C.M., Saarinen, A., Chandler, K., Clayton-Smith, J., Träskelin, A.-L., Perveen, R., Kivitie-Kallio, S., Norio, R., Warburg, M., et al. (2003). Cohen syndrome is caused by mutations in a novel gene, COH1, encoding a transmembrane protein with a presumed role in vesicle-mediated sorting and intracellular protein transport. Am. J. Hum. Genet. *72*, 1359–1369. https://doi.org/10.1086/375454.

96. Momtazmanesh, S., Rayzan, E., Shahkarami, S., Rohlfs, M., Klein, C., and Rezaei, N. (2020). A novel VPS13B mutation in Cohen syndrome: a case report and review of literature. BMC Med. Genet. *21*, 140. https://doi.org/10.1186/s12881-020-01075-1.

97. Zorn, M., Kühnisch, J., Bachmann, S., and Seifert, W. (2022). Disease relevance of rare VPS13B missense variants for neurodevelopmental Cohen syndrome. Sci. Rep. *12*, 9686. https://doi.org/10.1038/s41598-022-13717-w.

98. Monfrini, E., Spagnolo, F., Canesi, M., Seresini, A., Rini, A., Passarella, B., Percetti, M., Seia, M., Goldwurm, S., Cereda, V., et al. (2022). VPS13C-associated Parkinson's disease: Two novel cases and review of the literature. Parkinsonism Relat. Disord. *94*, 37–39. https://doi.org/10.1016/j.parkreldis.2021.11.031.

99. Lesage, S., Drouet, V., Majounie, E., Deramecourt, V., Jacoupy, M., Nicolas, A., Cormier-Dequaire, F., Hassoun, S.M., Pujol, C., Ciura, S., et al. (2016). Loss of VPS13C function in autosomal-recessive parkinsonism causes mitochondrial dysfunction and increases PINK1/Parkin-dependent mitophagy. Am. J. Hum. Genet. *98*, 500–513. https://doi.org/10.1016/j.ajhg.2016.01.014.

100. Darvish, H., Bravo, P., Tafakhori, A., Azcona, L.J., Ranji-Burachaloo, S., Johari, A.H., and Paisán-Ruiz, C. (2018). Identification of a large homozygous VPS13C deletion in a patient with early-onset Parkinsonism: LETTERS: NEW OBSERVATIONS. Mov. Disord. *33*, 1968–1970. https://doi.org/10.1002/mds.27516.

101. Smolders, S., Philtjens, S., Crosiers, D., Sieben, A., Hens, E., Heeman, B., Van Mossevelde, S., Pals, P., Asselbergh, B., Dos Santos Dias, R., et al. (2021). Contribution of rare homozygous and compound heterozygous VPS13C missense mutations to dementia with Lewy bodies and Parkinson's disease. Acta Neuropathol. Commun. *9*, 25. https://doi.org/10.1186/s40478-021-01121-w.

102. Kobayashi, R., Naruse, H., Koyama, S., Kawakatsu, S., Hayashi, H., Ishiura, H., Mitsui, J., Ohta, Y., Toda, T., Tsuji, S., et al. (2020). Familial dementia with Lewy bodies with VPS13C mutations. Parkinsonism Relat. Disord. *81*, 31–33. https://doi.org/10.1016/j.parkreldis.2020.10.008.

103. Seong, E., Insolera, R., Dulovic, M., Kamsteeg, E.-J., Trinh, J., Brüggemann, N., Sandford, E., Li, S., Ozel, A.B., Li, J.Z., et al. (2018). Mutations in VPS13D lead to a new recessive ataxia with spasticity and mitochondrial defects. Ann. Neurol. *83*, 1075–1088. https://doi.org/10.1002/ana.25220.

104. Gauthier, J., Meijer, I.A., Lessel, D., Mencacci, N.E., Krainc, D., Hempel, M., Tsiakas, K., Prokisch, H., Rossignol, E., Helm, M.H., et al. (2018). Recessive mutations in VPS13D cause childhood onset movement disorders. Ann. Neurol. *83*, 1089–1095. https://doi.org/10.1002/ana.25204.

105. Koh, K., Ishiura, H., Shimazaki, H., Tsutsumiuchi, M., Ichinose, Y., Nan, H., Hamada, S., Ohtsuka, T., Tsuji, S., and Takiyama, Y. (2020). VPS13D-related disorders presenting as a pure and complicated form of hereditary spastic paraplegia. Mol. Genet. Genomic Med. *8*, e1108. https://doi.org/10.1002/mgg3.1108.

106. Bankaitis, V.A., Johnson, L.M., and Emr, S.D. (1986). Isolation of yeast mutants defective in protein targeting to the vacuole. Proc. Natl. Acad. Sci. U. S. A. *83*, 9075–9079. https://doi.org/10.1073/pnas.83.23.9075.

107. Brickner, J.H., and Fuller, R.S. (1997). SOI1 encodes a novel, conserved protein that promotes TGN-endosomal cycling of Kex2p and other membrane proteins by modulating the function of two TGN localization signals. J. Cell Biol. *139*, 23–36. https://doi.org/10.1083/jcb.139.1.23.

108. Enyenihi, A.H., and Saunders, W.S. (2003). Large-scale functional genomic analysis of sporulation and meiosis in Saccharomyces cerevisiae. Genetics *163*, 47–54. https://doi.org/10.1093/genetics/163.1.47.

109. Nakanishi, H., Suda, Y., and Neiman, A.M. (2007). Erv14 family cargo receptors are necessary for ER exit during sporulation in Saccharomyces cerevisiae. J. Cell Sci. *120*, 908–916. https://doi.org/10.1242/jcs.03405.

110. Park, J.-S., and Neiman, A.M. (2012). VPS13 regulates membrane morphogenesis during sporulation in Saccharomyces cerevisiae. J. Cell Sci. *125*, 3004–3011. https://doi.org/10.1242/jcs.105114.

111. Park, J.-S., Okumura, Y., Tachikawa, H., and Neiman, A.M. (2013). SPO71 encodes a developmental stage-specific partner for Vps13 in Saccharomyces cerevisiae. Eukaryot. Cell *12*, 1530–1537. https://doi.org/10.1128/EC.00239-13.

112. Neiman, A.M. (2011). Sporulation in the budding yeast Saccharomyces cerevisiae. Genetics *189*, 737–765. https://doi.org/10.1534/genetics.111.127126.

113. Helle, S.C.J., Kanfer, G., Kolar, K., Lang, A., Michel, A.H., and Kornmann, B. (2013). Organization and function of membrane contact sites. Biochim. Biophys. Acta *1833*, 2526–2541. https://doi.org/10.1016/j.bbamcr.2013.01.028.

114. Henne, W.M., Liou, J., and Emr, S.D. (2015). Molecular mechanisms of inter-organelle ER-PM contact sites. Curr. Opin. Cell Biol. *35*, 123–130. https://doi.org/10.1016/j.ceb.2015.05.001.

115. Henne, W.M. (2016). Organelle remodeling at membrane contact sites. J. Struct. Biol. *196*, 15–19. https://doi.org/10.1016/j.jsb.2016.05.003.

116. Schrader, M., Godinho, L.F., Costello, J.L., and Islinger, M. (2015). The different facets of organelle interplay-an overview of organelle interactions. Front. Cell Dev. Biol. *3*, 56. https://doi.org/10.3389/fcell.2015.00056.

117. Olkkonen, V.M. (2015). OSBP-related protein family in lipid transport over membrane contact sites. Lipid Insights *8*, 1–9. https://doi.org/10.4137/LPI.S31726.

118. Kornmann, B., and Walter, P. (2010). ERMES-mediated ER-mitochondria contacts: molecular hubs for the regulation of mitochondrial biology. J. Cell Sci. *123*, 1389–1393. https://doi.org/10.1242/jcs.058636.

119. Murley, A., Lackner, L.L., Osman, C., West, M., Voeltz, G.K., Walter, P., and Nunnari, J. (2013). ER-associated mitochondrial division links the distribution of mitochondria and mitochondrial DNA in yeast. Elife *2*, e00422. https://doi.org/10.7554/eLife.00422.

120. Hobbs, A.E., Srinivasan, M., McCaffery, J.M., and Jensen, R.E. (2001). Mmm1p, a mitochondrial outer membrane protein, is connected to mitochondrial DNA (mtDNA) nucleoids and required for mtDNA stability. J. Cell Biol. *152*, 401–410. https://doi.org/10.1083/jcb.152.2.401.

121. Meeusen, S., and Nunnari, J. (2003). Evidence for a two membrane-spanning autonomous mitochondrial DNA replisome. J. Cell Biol. *163*, 503–510. https://doi.org/10.1083/jcb.200304040.

122. Nguyen, T.T., Lewandowska, A., Choi, J.-Y., Markgraf, D.F., Junker, M., Bilgin, M., Ejsing, C.S., Voelker, D.R., Rapoport, T.A., and Shaw, J.M. (2012). Gem1 and ERMES do not directly affect phosphatidylserine transport from ER to mitochondria or mitochondrial inheritance: Physiological roles of ERMES and Gem1 in yeast. Traffic *13*, 880–890. https://doi.org/10.1111/j.1600-0854.2012.01352.x.

123. Lang, A.B., John Peter, A.T., Walter, P., and Kornmann, B. (2015). ER-mitochondrial junctions can be bypassed by dominant mutations in the endosomal protein Vps13. J. Cell Biol. *210*, 883–890. https://doi.org/10.1083/jcb.201502105.

124. Park, J.-S., Thorsness, M.K., Policastro, R., McGoldrick, L.L., Hollingsworth, N.M., Thorsness, P.E., and Neiman, A.M. (2016). Yeast Vps13 promotes mitochondrial function and is localized at membrane contact sites. Mol. Biol. Cell *27*, 2435–2449. https://doi.org/10.1091/mbc.E16-02-0112.

125. Bean, B.D.M., Dziurdzik, S.K., Kolehmainen, K.L., Fowler, C.M.S., Kwong, W.K., Grad, L.I., Davey, M., Schluter, C., and Conibear, E. (2018). Competitive organelle-specific adaptors recruit Vps13 to membrane contact sites. J. Cell Biol. *217*, 3593–3607. https://doi.org/10.1083/jcb.201804111.

126. John Peter, A.T., Herrmann, B., Antunes, D., Rapaport, D., Dimmer, K.S., and Kornmann, B. (2017). Vps13-Mcp1 interact at vacuole-mitochondria interfaces and bypass ER-mitochondria contact sites. J. Cell Biol. *216*, 3219–3229. https://doi.org/10.1083/jcb.201610055.

127. Yuan, W., Akşit, A., de Boer, R., Krikken, A.M., and van der Klei, I.J. (2022). Yeast Vps13 is crucial for peroxisome expansion in cells with reduced peroxisome-ER contact sites. Front. Cell Dev. Biol. 10, 842285. https://doi.org/10.3389/fcell.2022.842285.

128. Chen, S., Mari, M., Parashar, S., Liu, D., Cui, Y., Reggiori, F., Novick, P.J., and Ferro-Novick, S. (2020). Vps13 is required for the packaging of the ER into autophagosomes during ER-phagy. Proc. Natl. Acad. Sci. U. S. A. *117*, 18530–18539. https://doi.org/10.1073/pnas.2008923117.

129. Suzuki, S.W., West, M., Zhang, Y., Fan, J.S., Roberts, R.T., Odorizzi, G., and Emr, S.D. (2024). A role for Vps13-mediated lipid transfer at the ER-endosome contact site in ESCRT-mediated sorting. J. Cell Biol. *223*, e202307094. https://doi.org/10.1083/jcb.202307094.

130. Dabrowski, R., Tulli, S., and Graef, M. (2023). Parallel phospholipid transfer by Vps13 and Atg2 determines autophagosome biogenesis dynamics. J. Cell Biol. *222*, e202211039. https://doi.org/10.1083/jcb.202211039.

131. Nakamura, T.S., Suda, Y., Muneshige, K., Fujieda, Y., Okumura, Y., Inoue, I., Tanaka, T., Takahashi, T., Nakanishi, H., Gao, X.-D., et al. (2021). Suppression of Vps13 adaptor protein mutants reveals a central role for PI4P in regulating prospore membrane extension. PLoS Genet. *17*, e1009727. https://doi.org/10.1371/journal.pgen.1009727.

132. Rzepnikowska, W., Flis, K., Kaminska, J., Grynberg, M., Urbanek, A., Ayscough, K.R., and Zoladek, T. (2017). Amino acid substitution equivalent to human chorea-

acanthocytosis I2771R in yeast Vps13 protein affects its binding to phosphatidylinositol 3-phosphate. Hum. Mol. Genet. *26*, 1497–1510. https://doi.org/10.1093/hmg/ddx054.

133. Kolakowski, D., Rzepnikowska, W., Kaniak-Golik, A., Zoladek, T., and Kaminska, J. (2021). The GTPase Arf1 is a determinant of yeast Vps13 localization to the Golgi apparatus. Int. J. Mol. Sci. *22*, 12274. https://doi.org/10.3390/ijms222212274.

134. Li, P., Lees, J.A., Lusk, C.P., and Reinisch, K.M. (2020). Cryo-EM reconstruction of a VPS13 fragment reveals a long groove to channel lipids between membranes. J. Cell Biol. *219*, e202001161. https://doi.org/10.1083/jcb.202001161.

135. Levine, T.P. (2019). Remote homology searches identify bacterial homologues of eukaryotic lipid transfer proteins, including Chorein-N domains in TamB and AsmA and Mdm31p. BMC Mol. Cell Biol. 20, 43. https://doi.org/10.1186/s12860-019-0226-z.

136. Adlakha, J., Hong, Z., Li, P., and Reinisch, K.M. (2022). Structural and biochemical insights into lipid transport by VPS13 proteins. J. Cell Biol. *221*, e202202030. https://doi.org/10.1083/jcb.202202030.

137. De, M., Oleskie, A.N., Ayyash, M., Dutta, S., Mancour, L., Abazeed, M.E., Brace, E.J., Skiniotis, G., and Fuller, R.S. (2017). The Vps13p-Cdc31p complex is directly required for TGN late endosome transport and TGN homotypic fusion. J. Cell Biol. *216*, 425–439. https://doi.org/10.1083/jcb.201606078.

138. Neuman, S.D., Levine, T.P., and Bashirullah, A. (2022). A novel superfamily of bridge-like lipid transfer proteins. Trends Cell Biol. *32*, 962–974. https://doi.org/10.1016/j.tcb.2022.03.011.

139. Levine, T.P. (2022). Sequence analysis and structural predictions of lipid transfer bridges in the repeating beta groove (RBG) superfamily reveal past and present domain variations affecting form, function and interactions of VPS13, ATG2, SHIP164, hobbit and tweek. Contact (Thousand Oaks.) *5*, 251525642211343. https://doi.org/10.1177/25152564221134328.

140. Dall'Armellina, F., Stagi, M., and Swan, L.E. (2023). In silico modeling human VPS13 proteins associated with donor and target membranes suggests lipid transfer mechanisms. Proteins *91*, 439–455. https://doi.org/10.1002/prot.26446.

141. Kumar, N., Leonzino, M., Hancock-Cerutti, W., Horenkamp, F.A., Li, P., Lees, J.A., Wheeler, H., Reinisch, K.M., and De Camilli, P. (2018). VPS13A and VPS13C are lipid transport proteins differentially localized at ER contact sites. J. Cell Biol. *217*, 3625–3639. https://doi.org/10.1083/jcb.201807019.

142. Pandey, T., Zhang, J., Wang, B., and Ma, D.K. (2023). Bridge-like lipid transfer proteins (BLTPs) in C. elegans: From genetics to structures and functions. Contact (Thousand Oaks.) *6*, 25152564231186490. https://doi.org/10.1177/25152564231186489.

143. Leterme, S., Bastien, O., Aiese Cigliano, R., Amato, A., and Michaud, M. (2023). Phylogenetic and structural analyses of VPS13 proteins in Archaeplastida reveal their complex evolutionary history in Viridiplantae. Contact (Thousand Oaks.) *6*, 25152564231211976. https://doi.org/10.1177/25152564231211976.

144. Lees, J.A., and Reinisch, K.M. (2020). Inter-organelle lipid transfer: a channel model for Vps13 and chorein-N motif proteins. Curr. Opin. Cell Biol. *65*, 66–71. https://doi.org/10.1016/j.ceb.2020.02.008.

145. Gómez-Sánchez, R., Rose, J., Guimarães, R., Mari, M., Papinski, D., Rieter, E., Geerts, W.J., Hardenberg, R., Kraft, C., Ungermann, C., et al. (2018). Atg9 establishes Atg2-dependent contact sites between the endoplasmic reticulum and phagophores. J. Cell Biol. *217*, 2743–2763. https://doi.org/10.1083/jcb.201710116.

146. McEwan, D.G., and Ryan, K.M. (2022). ATG2 and VPS13 proteins: molecular highways transporting lipids to drive membrane expansion and organelle communication. FEBS J. *289*, 7113–7127. https://doi.org/10.1111/febs.16280.

147. Tamura, N., Nishimura, T., Sakamaki, Y., Koyama-Honda, I., Yamamoto, H., and Mizushima, N. (2017). Differential requirement for ATG2A domains for localization to autophagic membranes and lipid droplets. FEBS Lett. *591*, 3819–3830. https://doi.org/10.1002/1873-3468.12901.

148. Valverde, D.P., Yu, S., Boggavarapu, V., Kumar, N., Lees, J.A., Walz, T., Reinisch, K.M., and Melia, T.J. (2019). ATG2 transports lipids to promote autophagosome biogenesis. J. Cell Biol. *218*, 1787–1798. https://doi.org/10.1083/jcb.201811139.

149. Ugur, B., Hancock-Cerutti, W., Leonzino, M., and De Camilli, P. (2020). Role of VPS13, a protein with similarity to ATG2, in physiology and disease. Curr. Opin. Genet. Dev. *65*, 61–68. https://doi.org/10.1016/j.gde.2020.05.027.

150. Osawa, T., Kotani, T., Kawaoka, T., Hirata, E., Suzuki, K., Nakatogawa, H., Ohsumi, Y., and Noda, N.N. (2019). Atg2 mediates direct lipid transfer between membranes for autophagosome formation. Nat. Struct. Mol. Biol. *26*, 281–288. https://doi.org/10.1038/s41594-019-0203-4.

151. van Vliet, A.R., Jefferies, H.B.J., Faull, P.A., Chadwick, J., Ibrahim, F., Skehel, M.J., and Tooze, S.A. (2024). Exploring the ATG9A interactome uncovers interaction with VPS13A. J. Cell Sci. *137*, jcs261081. https://doi.org/10.1242/jcs.261081.

152. Muñoz-Braceras, S., Calvo, R., and Escalante, R. (2015). TipC and the chorea-acanthocytosis protein VPS13A regulate autophagy in Dictyostelium and human HeLa cells. Autophagy *11*, 918–927. https://doi.org/10.1080/15548627.2015.1034413.

153. Hanna, M.G., Suen, P.H., Wu, Y., Reinisch, K.M., and De Camilli, P. (2022). SHIP164 is a chorein motif lipid transfer protein that controls endosome-Golgi membrane traffic. J. Cell Biol. *221*, e202111018. https://doi.org/10.1083/jcb.202111018.

154. Hanna, M.G., Rodriguez Cruz, H.O., Fujise, K., Wu, Y., Xu, C.S., Pang, S., Li, Z., Monetti, M., and De Camilli, P. (2025). BLTP3A is associated with membranes of the late endocytic pathway and is an effector of CASM. EMBO J. *44*, 6168–6195. https://doi.org/10.1038/s44318-025-00543-9.

155. Swan, L.E. (2025). VPS13 and bridge-like lipid transporters, mechanisms, and mysteries. Front. Neurosci. *19*, 1534061. https://doi.org/10.3389/fnins.2025.1534061.

156. Otto, G.P., Razi, M., Morvan, J., Stenner, F., and Tooze, S.A. (2010). A novel syntaxin 6-interacting protein, SHIP164, regulates syntaxin 6-dependent sorting from early endosomes. Traffic *11*, 688–705. https://doi.org/10.1111/j.1600-0854.2010.01049.x.

157. Banerjee, S., Daetwyler, S., Bai, X., Michaud, M., Jouhet, J., Binns, D., Madhugiri, S., Johnson, E., Wang, C.-W., Fiolka, R., et al. (2025). The Vps13-like protein BLTP2 regulates phosphatidylethanolamine levels to maintain plasma membrane fluidity and breast cancer aggressiveness. Nat. Cell Biol. *27*, 1125–1135. https://doi.org/10.1038/s41556-025-01672-3.

158. Melia, T.J., and Reinisch, K.M. (2022). A possible role for VPS13-family proteins in bulk lipid transfer, membrane expansion and organelle biogenesis. J. Cell Sci. *135*. https://doi.org/10.1242/jcs.259357.

159. Mikitova, V., and Levine, T.P. (2012). Analysis of the key elements of FFAT-like motifs identifies new proteins that potentially bind VAP on the ER, including two AKAPs and FAPP2. PLoS One *7*, e30455. https://doi.org/10.1371/journal.pone.0030455.

160. Slee, J.A., and Levine, T.P. (2019). Systematic prediction of FFAT motifs across eukaryote proteomes identifies nucleolar and eisosome proteins with the predicted capacity to form bridges to the endoplasmic reticulum. Contact (Thousand Oaks.) *2*, 1–21. https://doi.org/10.1177/2515256419883136.

161. Murphy, S.E., and Levine, T.P. (2016). VAP, a Versatile Access Point for the Endoplasmic Reticulum: Review and analysis of FFAT-like motifs in the VAPome.

Biochim. Biophys. Acta *1861*, 952–961. https://doi.org/10.1016/j.bbalip.2016.02.009.

162. Yeshaw, W.M., van der Zwaag, M., Pinto, F., Lahaye, L.L., Faber, A.I., Gómez-Sánchez, R., Dolga, A.M., Poland, C., Monaco, A.P., van IJzendoorn, S.C., et al. (2019). Human VPS13A is associated with multiple organelles and influences mitochondrial morphology and lipid droplet motility. Elife *8*, e43561. https://doi.org/10.7554/eLife.43561.

163. Guillén-Samander, A., Wu, Y., Pineda, S.S., García, F.J., Eisen, J.N., Leonzino, M., Ugur, B., Kellis, M., Heiman, M., and De Camilli, P. (2022). A partnership between the lipid scramblase XK and the lipid transfer protein VPS13A at the plasma membrane. Proc. Natl. Acad. Sci. U. S. A. *119*, e2205425119. https://doi.org/10.1073/pnas.2205425119.

164. Subra, M., Dezi, M., Bigay, J., Lacas-Gervais, S., Di Cicco, A., Araújo, A.R.D., Abélanet, S., Fleuriot, L., Debayle, D., Gautier, R., et al. (2023). VAP-A intrinsically disordered regions enable versatile tethering at membrane contact sites. Dev. Cell *58*, 121-138.e9. https://doi.org/10.1016/j.devcel.2022.12.010.

165. Guillén-Samander, A., Leonzino, M., Hanna, M.G., Tang, N., Shen, H., and De Camilli, P. (2021). VPS13D bridges the ER to mitochondria and peroxisomes via Miro. J. Cell Biol. *220*, e202010004. https://doi.org/10.1083/jcb.202010004.

166. Tornero-Écija, A., Zapata-Del-Baño, A., Antón-Esteban, L., Vincent, O., and Escalante, R. (2023). The association of lipid transfer protein VPS13A with endosomes is mediated by sorting nexin SNX5. Life Sci. Alliance *6*, e202201852. https://doi.org/10.26508/lsa.202201852.

167. Cai, S., Wu, Y., Guillén-Samander, A., Hancock-Cerutti, W., Liu, J., and De Camilli, P. (2022). In situ architecture of the lipid transport protein VPS13C at ER-lysosome membrane contacts. Proc. Natl. Acad. Sci. U. S. A. *119*, e2203769119. https://doi.org/10.1073/pnas.2203769119.

168. Dziurdzik, S.K., Bean, B.D.M., Davey, M., and Conibear, E. (2020). A VPS13D spastic ataxia mutation disrupts the conserved adaptor-binding site in yeast Vps13. Hum. Mol. Genet. *29*, 635–648. https://doi.org/10.1093/hmg/ddz318.

169. Dziurdzik, S.K., and Conibear, E. (2021). The Vps13 family of lipid transporters and its role at membrane contact sites. Int. J. Mol. Sci. *22*, 2905. https://doi.org/10.3390/ijms22062905.

170. Wang, X., Xu, P., Bentley-DeSousa, A., Hancock-Cerutti, W., Cai, S., Johnson, B.T., Tonelli, F., Shao, L., Talaia, G., Alessi, D.R., et al. (2025). The bridge-like lipid transport protein VPS13C/PARK23 mediates ER-lysosome contacts following

lysosome damage. Nat. Cell Biol. *27*, 776–789. https://doi.org/10.1038/s41556-025-01653-6.

171. Li, N., and Chen, J. (2014). ADP-ribosylation: activation, recognition, and removal. Mol. Cells *37*, 9–16. https://doi.org/10.14348/molcells.2014.2245.

172. Münzker, L., Kimani, S.W., Fowkes, M.M., Dong, A., Zheng, H., Li, Y., Dasovich, M., Zak, K.M., Leung, A.K.L., Elkins, J.M., et al. (2024). A ligand discovery toolbox for the WWE domain family of human E3 ligases. Commun. Biol. *7*, 901. https://doi.org/10.1038/s42003-024-06584-w.

173. Aravind, L. (2001). The WWE domain: a common interaction module in protein ubiquitination and ADP ribosylation. Trends Biochem. Sci. *26*, 273–275. https://doi.org/10.1016/s0968-0004(01)01787-x.

174. De Coninck, T., Gippert, G.P., Henrissat, B., Desmet, T., and Van Damme, E.J.M. (2024). Investigating diversity and similarity between CBM13 modules and ricin-B lectin domains using sequence similarity networks. BMC Genomics *25*, 643. https://doi.org/10.1186/s12864-024-10554-1.

175. Kumar, S., and Ruiz, N. (2023). Bacterial AsmA-like proteins: Bridging the gap in intermembrane phospholipid transport. Contact (Thousand Oaks.) *6*, 25152564231185932. https://doi.org/10.1177/25152564231185931.

176. Ugur, B., Schueder, F., Shin, J., Hanna, M.G., Wu, Y., Leonzino, M., Su, M., McAdow, A.R., Wilson, C., Postlethwait, J., et al. (2024). VPS13B is localized at the interface between Golgi cisternae and is a functional partner of FAM177A1. J. Cell Biol. *223*, e202311189. https://doi.org/10.1083/jcb.202311189.

177. Kolakowski, D., Kaminska, J., and Zoladek, T. (2020). The binding of the APT1 domains to phosphoinositides is regulated by metal ions in vitro. Biochim. Biophys. Acta Biomembr. *1862*, 183349. https://doi.org/10.1016/j.bbamem.2020.183349.

178. Kaminska, J., Rzepnikowska, W., Polak, A., Flis, K., Soczewka, P., Bala, K., Sienko, M., Grynberg, M., Kaliszewski, P., Urbanek, A., et al. (2016). Phosphatidylinositol-3-phosphate regulates response of cells to proteotoxic stress. Int. J. Biochem. Cell Biol. *79*, 494–504. https://doi.org/10.1016/j.biocel.2016.08.007.

179. Kotani, T., Kirisako, H., Koizumi, M., Ohsumi, Y., and Nakatogawa, H. (2018). The Atg2-Atg18 complex tethers pre-autophagosomal membranes to the endoplasmic reticulum for autophagosome formation. Proc. Natl. Acad. Sci. U. S. A. *115*, 10363–10368. https://doi.org/10.1073/pnas.1806727115.

180. Velikkakath, A.K.G., Nishimura, T., Oita, E., Ishihara, N., and Mizushima, N. (2012). Mammalian Atg2 proteins are essential for autophagosome formation and

important for regulation of size and distribution of lipid droplets. Mol. Biol. Cell *23*, 896–909. https://doi.org/10.1091/mbc.E11-09-0785.

181. van Vliet, A.R., Chiduza, G.N., Maslen, S.L., Pye, V.E., Joshi, D., De Tito, S., Jefferies, H.B.J., Christodoulou, E., Roustan, C., Punch, E., et al. (2022). ATG9A and ATG2A form a heteromeric complex essential for autophagosome formation. Mol. Cell *82*, 4324-4339.e8. https://doi.org/10.1016/j.molcel.2022.10.017.

182. Fidler, D.R., Murphy, S.E., Courtis, K., Antonoudiou, P., El-Tohamy, R., Ient, J., and Levine, T.P. (2016). Using HHsearch to tackle proteins of unknown function: A pilot study with PH domains. Traffic *17*, 1214–1226. https://doi.org/10.1111/tra.12432.

183. Achiriloaie, M., Barylko, B., and Albanesi, J.P. (1999). Essential role of the dynamin pleckstrin homology domain in receptor-mediated endocytosis. Mol. Cell. Biol. *19*, 1410–1415. https://doi.org/10.1128/MCB.19.2.1410.

184. Du, Y., Fan, X., Song, C., Chang, W., Xiong, J., Deng, L., and Ji, W.-K. (2024). Sec23IP recruits VPS13B/COH1 to ER exit site-Golgi interface for tubular ERGIC formation. J. Cell Biol. *223*. https://doi.org/10.1083/jcb.202402083.

185. Muñoz-Braceras, S., Tornero-Écija, A.R., Vincent, O., and Escalante, R. (2019). VPS13A is closely associated with mitochondria and is required for efficient lysosomal degradation. Dis. Model. Mech. *12*, dmm036681. https://doi.org/10.1242/dmm.036681.

186. Nishizawa, Y., Sakimoto, H., Nagata, O., Sasaki, N., Urata, Y., Arai, K., Hiwatashi, H., Yokoyama, I., Kishida, S., Sano, A., et al. (2025). Chorein deficiency promotes ferroptosis. FEBS Open Bio *15*, 58–68. https://doi.org/10.1002/2211-5463.13870.

187. Park, J.-S., Hu, Y., Hollingsworth, N.M., Miltenberger-Miltenyi, G., and Neiman, A.M. (2022). Interaction between VPS13A and the XK scramblase is important for VPS13A function in humans. J. Cell Sci. *135*, jcs260227. https://doi.org/10.1242/jcs.260227.

188. Park, J.-S., and Neiman, A.M. (2020). XK is a partner for VPS13A: a molecular link between Chorea-Acanthocytosis and McLeod Syndrome. Mol. Biol. Cell *31*, 2425–2436. https://doi.org/10.1091/mbc.E19-08-0439-T.

189. Ryoden, Y., Segawa, K., and Nagata, S. (2022). Requirement of Xk and Vps13a for the P2X7-mediated phospholipid scrambling and cell lysis in mouse T cells. Proc. Natl. Acad. Sci. U. S. A. *119*, e2119286119. https://doi.org/10.1073/pnas.2119286119.

190. Blom, T., Somerharju, P., and Ikonen, E. (2011). Synthesis and biosynthetic trafficking of membrane lipids. Cold Spring Harb. Perspect. Biol. *3*, a004713. https://doi.org/10.1101/cshperspect.a004713.

191. Cockcroft, S. (2021). Mammalian lipids: structure, synthesis and function. Essays Biochem. *65*, 813–845. https://doi.org/10.1042/EBC20200067.

192. Sarmento, M.J., Llorente, A., Petan, T., Khnykin, D., Popa, I., Nikolac Perkovic, M., Konjevod, M., and Jaganjac, M. (2023). The expanding organelle lipidomes: current knowledge and challenges. Cell. Mol. Life Sci. *80*, 237. https://doi.org/10.1007/s00018-023-04889-3.

193. Turk, S.M., Indovina, C.J., Miller, J.M., Overton, D.L., Runnebohm, A.M., Orchard, C.J., Tragesser-Tiña, M.E., Gosser, S.K., Doss, E.M., Richards, K.A., et al. (2023). Lipid biosynthesis perturbation impairs endoplasmic reticulum-associated degradation. J. Biol. Chem. *299*, 104939. https://doi.org/10.1016/j.jbc.2023.104939.

194. Jacquemyn, J., Cascalho, A., and Goodchild, R.E. (2017). The ins and outs of endoplasmic reticulum-controlled lipid biosynthesis. EMBO Rep. *18*, 1905–1921. https://doi.org/10.15252/embr.201643426.

195. Iglesias-Artola, J.M., Böhlig, K., Schuhmann, K., Cook, K.C., Lennartz, H.M., Schuhmacher, M., Barahtjan, P., Jiménez López, C., Šachl, R., Garikapati, V., et al. (2025). Quantitative imaging of lipid transport in mammalian cells. Nature *646*, 474–482. https://doi.org/10.1038/s41586-025-09432-x.

196. Otomo, T., and Maeda, S. (2019). ATG2A transfers lipids between membranes in vitro. Autophagy *15*, 2031–2032. https://doi.org/10.1080/15548627.2019.1659622.

197. Toulmay, A., Whittle, F.B., Yang, J., Bai, X., Diarra, J., Banerjee, S., Levine, T.P., Golden, A., and Prinz, W.A. (2022). Vps13-like proteins provide phosphatidylethanolamine for GPI anchor synthesis in the ER. J. Cell Biol. *221*, e202111095. https://doi.org/10.1083/jcb.202111095.

198. Juarez Casso, F.M., and Farzam, K. (2025). Biochemistry, very low density lipoprotein. In StatPearls (StatPearls Publishing).

199. Miltenberger-Miltenyi, G., Jones, A., Tetlow, A.M., Conceição, V.A., Crary, J.F., Ditzel, R.M., Jr, Farrell, K., Nandakumar, R., Barton, B., Karp, B.I., et al. (2023). Sphingolipid and phospholipid levels are altered in human brain in chorea-acanthocytosis. Mov. Disord. *38*, 1535–1541. https://doi.org/10.1002/mds.29445.

200. Peikert, K., Spranger, A., Miltenberger-Miltenyi, G., Glaß, H., Falkenburger, B., Klose, C., Tyteca, D., and Hermann, A. (2025). Phosphatidylethanolamines are the main lipid class altered in red blood cells from patients with VPS13A disease/chorea-acanthocytosis. Mov. Disord. *40*, 544–549. https://doi.org/10.1002/mds.30086.

201. Mosharov, E.V., Rosenberg, A.M., Monzel, A.S., Osto, C.A., Stiles, L., Rosoklija, G.B., Dwork, A.J., Bindra, S., Junker, A., Zhang, Y., et al. (2025). A human brain map of mitochondrial respiratory capacity and diversity. Nature *641*, 749–758. https://doi.org/10.1038/s41586-025-08740-6.

202. Osellame, L.D., Blacker, T.S., and Duchen, M.R. (2012). Cellular and molecular mechanisms of mitochondrial function. Best Pract. Res. Clin. Endocrinol. Metab. 26, 711–723. https://doi.org/10.1016/j.beem.2012.05.003.

203. Chen, W., Zhao, H., and Li, Y. (2023). Mitochondrial dynamics in health and disease: mechanisms and potential targets. Signal Transduct. Target. Ther. *8*, 333. https://doi.org/10.1038/s41392-023-01547-9.

204. Liesa, M., Palacín, M., and Zorzano, A. (2009). Mitochondrial dynamics in mammalian health and disease. Physiol. Rev. *89*, 799–845. https://doi.org/10.1152/physrev.00030.2008.

205. Twig, G., Elorza, A., Molina, A.J.A., Mohamed, H., Wikstrom, J.D., Walzer, G., Stiles, L., Haigh, S.E., Katz, S., Las, G., et al. (2008). Fission and selective fusion govern mitochondrial segregation and elimination by autophagy. EMBO J. *27*, 433–446. https://doi.org/10.1038/sj.emboj.7601963.

206. Hanekamp, T., Thorsness, M.K., Rebbapragada, I., Fisher, E.M., Seebart, C., Darland, M.R., Coxbill, J.A., Updike, D.L., and Thorsness, P.E. (2002). Maintenance of mitochondrial morphology is linked to maintenance of the mitochondrial genome in Saccharomyces cerevisiae. Genetics *162*, 1147–1156. https://doi.org/10.1093/genetics/162.3.1147.

207. Youngman, M.J., Hobbs, A.E.A., Burgess, S.M., Srinivasan, M., and Jensen, R.E. (2004). Mmm2p, a mitochondrial outer membrane protein required for yeast mitochondrial shape and maintenance of mtDNA nucleoids. J. Cell Biol. *164*, 677–688. https://doi.org/10.1083/jcb.200308012.

208. Böckler, S., and Westermann, B. (2014). Mitochondrial ER contacts are crucial for mitophagy in yeast. Dev. Cell *28*, 450–458. https://doi.org/10.1016/j.devcel.2014.01.012.

209. Glaß, H., Pal, A., Reinhardt, P., Sterneckert, J., Wegner, F., Storch, A., and Hermann, A. (2018). Defective mitochondrial and lysosomal trafficking in chorea-acanthocytosis is independent of Src-kinase signaling. Mol. Cell. Neurosci. *92*, 137–148. https://doi.org/10.1016/j.mcn.2018.08.002.

210. Glaß, H., Neumann, P., Pal, A., Reinhardt, P., Storch, A., Sterneckert, J., and Hermann, A. (2020). Combined dendritic and axonal deterioration are responsible for motoneuronopathy in patient-derived neuronal cell models of chorea-acanthocytosis. Int. J. Mol. Sci. *21*, 1797. https://doi.org/10.3390/ijms21051797.

211. Riccardi, V., Viscomi, C.F., Sandri, M., D'Alessandro, A., Dzieciatkowska, M., Stephenson, D., Federti, E., Hermann, A., Salviati, L., Siciliano, A., et al. (2025). Premature skeletal muscle aging in VPS13A deficiency relates to impaired autophagy. Acta Neuropathol. Commun. *13*, 83. https://doi.org/10.1186/s40478-025-01997-y.

212. Föller, M., Hermann, A., Gu, S., Alesutan, I., Qadri, S.M., Borst, O., Schmidt, E.-M., Schiele, F., vom Hagen, J.M., Saft, C., et al. (2012). Chorein-sensitive polymerization of cortical actin and suicidal cell death in chorea-acanthocytosis. FASEB J. *26*, 1526–1534. https://doi.org/10.1096/fj.11-198317.

213. Honisch, S., Yu, W., Liu, G., Alesutan, I., Towhid, S.T., Tsapara, A., Schleicher, S., Handgretinger, R., Stournaras, C., and Lang, F. (2015). Chorein addiction in VPS13A overexpressing rhabdomyosarcoma cells. Oncotarget *6*, 10309–10319. https://doi.org/10.18632/oncotarget.3582.

214. Lupo, F., Tibaldi, E., Matte, A., Sharma, A.K., Brunati, A.M., Alper, S.L., Zancanaro, C., Benati, D., Siciliano, A., Bertoldi, M., et al. (2016). A new molecular link between defective autophagy and erythroid abnormalities in chorea-acanthocytosis. Blood *128*, 2976–2987. https://doi.org/10.1182/blood-2016-07-727321.

215. Wickstead, B., and Gull, K. (2011). The evolution of the cytoskeleton. J. Cell Biol. *194*, 513–525. https://doi.org/10.1083/jcb.201102065.

216. Pollard, T.D., and Goldman, R.D. (2018). Overview of the cytoskeleton from an evolutionary perspective. Cold Spring Harb. Perspect. Biol. *10*, a030288. https://doi.org/10.1101/cshperspect.a030288.

217. Cooper, G.M. (2000). Structure and Organization of Actin Filaments. In The Cell: A Molecular Approach. 2nd edition (Sinauer Associates).

218. Cooper, G.M. (2000). Intermediate Filaments. In The Cell: A Molecular Approach. 2nd edition (Sinauer Associates).

219. Cooper, G.M. (2000). Microtubules. In The Cell: A Molecular Approach. 2nd edition (Sinauer Associates).

220. Lux, S.E., 4th (2016). Anatomy of the red cell membrane skeleton: unanswered questions. Blood *127*, 187–199. https://doi.org/10.1182/blood-2014-12-512772.

221. Himbert, S., and Rheinstädter, M.C. (2022). Structural and mechanical properties of the red blood cell's cytoplasmic membrane seen through the lens of biophysics. Front. Physiol. *13*, 953257. https://doi.org/10.3389/fphys.2022.953257.

222. Li, N., Chen, S., Xu, K., He, M.-T., Dong, M.-Q., Zhang, Q.C., and Gao, N. (2023). Structural basis of membrane skeleton organization in red blood cells. Cell *186*, 1912-1929.e18. https://doi.org/10.1016/j.cell.2023.03.017.

223. Salomao, M., Zhang, X., Yang, Y., Lee, S., Hartwig, J.H., Chasis, J.A., Mohandas, N., and An, X. (2008). Protein 4.1R-dependent multiprotein complex: new insights into the structural organization of the red blood cell membrane. Proc. Natl. Acad. Sci. U. S. A. *105*, 8026–8031. https://doi.org/10.1073/pnas.0803225105.

224. Grey, J.L., Kodippili, G.C., Simon, K., and Low, P.S. (2012). Identification of contact sites between ankyrin and band 3 in the human erythrocyte membrane. Biochemistry *51*, 6838–6846. https://doi.org/10.1021/bi300693k.

225. Smith, A.S., Nowak, R.B., Zhou, S., Giannetto, M., Gokhin, D.S., Papoin, J., Ghiran, I.C., Blanc, L., Wan, J., and Fowler, V.M. (2018). Myosin IIA interacts with the spectrin-actin membrane skeleton to control red blood cell membrane curvature and deformability. Proc. Natl. Acad. Sci. U. S. A. *115*, E4377–E4385. https://doi.org/10.1073/pnas.1718285115.

226. Alesutan, I., Seifert, J., Pakladok, T., Rheinlaender, J., Lebedeva, A., Towhid, S.T., Stournaras, C., Voelkl, J., Schäffer, T.E., and Lang, F. (2013). Chorein sensitivity of actin polymerization, cell shape and mechanical stiffness of vascular endothelial cells. Cell. Physiol. Biochem. *32*, 728–742. https://doi.org/10.1159/000354475.

227. Schmidt, E.-M., Schmid, E., Münzer, P., Hermann, A., Eyrich, A.-K., Russo, A., Walker, B., Gu, S., vom Hagen, J.M., Faggio, C., et al. (2013). Chorein sensitivity of cytoskeletal organization and degranulation of platelets. FASEB J. *27*, 2799–2806. https://doi.org/10.1096/fj.13-229286.

228. Shiokawa, N., Nakamura, M., Sameshima, M., Deguchi, A., Hayashi, T., Sasaki, N., and Sano, A. (2013). Chorein, the protein responsible for chorea-acanthocytosis, interacts with β-adducin and β-actin. Biochem. Biophys. Res. Commun. *441*, 96–101. https://doi.org/10.1016/j.bbrc.2013.10.011.

229. De Franceschi, L., Tomelleri, C., Matte, A., Brunati, A.M., Bovee-Geurts, P.H., Bertoldi, M., Lasonder, E., Tibaldi, E., Danek, A., Walker, R.H., et al. (2011). Erythrocyte membrane changes of chorea-acanthocytosis are the result of altered Lyn kinase activity. Blood *118*, 5652–5663. https://doi.org/10.1182/blood-2011-05-355339.

230. Peikert, K., Federti, E., Matte, A., Constantin, G., Pietronigro, E.C., Fabene, P.F., Defilippi, P., Turco, E., Del Gallo, F., Pucci, P., et al. (2021). Therapeutic targeting of Lyn kinase to treat chorea-acanthocytosis. Acta Neuropathol. Commun. *9*, 81. https://doi.org/10.1186/s40478-021-01181-y.

231. Soczewka, P., Kolakowski, D., Smaczynska-de Rooij, I., Rzepnikowska, W., Ayscough, K.R., Kaminska, J., and Zoladek, T. (2019). Yeast-model-based study identified myosin- and calcium-dependent calmodulin signalling as a potential target for drug intervention in chorea-acanthocytosis. Dis. Model. Mech. *12*, dmm036830. https://doi.org/10.1242/dmm.036830.

232. García-García, E., Chaparro-Cabanillas, N., Coll-Manzano, A., Carreras-Caballé, M., Giralt, A., Del Toro, D., Alberch, J., Masana, M., and Rodríguez, M.J. (2021). Unraveling the spatiotemporal distribution of VPS13A in the mouse brain. Int. J. Mol. Sci. *22*, 13018. https://doi.org/10.3390/ijms222313018.

233. Kurano, Y., Nakamura, M., Ichiba, M., Matsuda, M., Mizuno, E., Kato, M., Agemura, A., Izumo, S., and Sano, A. (2007). In vivo distribution and localization of chorein. Biochem. Biophys. Res. Commun. *353*, 431–435. https://doi.org/10.1016/j.bbrc.2006.12.059.

234. Hayashi, T., Kishida, M., Nishizawa, Y., Iijima, M., Koriyama, C., Nakamura, M., Sano, A., and Kishida, S. (2012). Subcellular localization and putative role of VPS13A/chorein in dopaminergic neuronal cells. Biochem. Biophys. Res. Commun. *419*, 511–516. https://doi.org/10.1016/j.bbrc.2012.02.047.

235. Silva-Rojas, R., Laporte, J., and Böhm, J. (2020). STIM1/ORAI1 loss-of-function and gain-of-function mutations inversely impact on SOCE and calcium homeostasis and cause multi-systemic mirror diseases. Front. Physiol. *11*, 604941. https://doi.org/10.3389/fphys.2020.604941.

236. Pelzl, L., Hauser, S., Elsir, B., Sukkar, B., Sahu, I., Singh, Y., Höflinger, P., Bissinger, R., Jemaà, M., Stournaras, C., et al. (2017). Lithium sensitive ORAI1 expression, store operated Ca2+ entry and suicidal death of neurons in chorea-Acanthocytosis. Sci. Rep. *7*, 6457. https://doi.org/10.1038/s41598-017-06451-1.

237. Hosseinzadeh, Z., Hauser, S., Singh, Y., Pelzl, L., Schuster, S., Sharma, Y., Höflinger, P., Zacharopoulou, N., Stournaras, C., Rathbun, D.L., et al. (2020). Decreased Na+/K+ ATPase expression and depolarized cell membrane in neurons differentiated from chorea-acanthocytosis patients. Sci. Rep. *10*, 8391. https://doi.org/10.1038/s41598-020-64845-0.

238. Stanslowsky, N., Reinhardt, P., Glass, H., Kalmbach, N., Naujock, M., Hensel, N., Lübben, V., Pal, A., Venneri, A., Lupo, F., et al. (2016). Neuronal dysfunction in iPSC-derived medium spiny neurons from chorea-acanthocytosis patients is reversed by Src kinase inhibition and F-actin stabilization. J. Neurosci. *36*, 12027–12043. https://doi.org/10.1523/JNEUROSCI.0456-16.2016.

239. García-García, E., Ramón-Lainez, A., Conde-Berriozabal, S., Del Toro, D., Escaramis, G., Giralt, A., Masana, M., Alberch, J., and Rodríguez, M.J. (2023).

VPS13A knockdown impairs corticostriatal synaptic plasticity and locomotor behavior in a new mouse model of chorea-acanthocytosis. Neurobiol. Dis. *187*, 106292. https://doi.org/10.1016/j.nbd.2023.106292.

Chapter 2 VPS13A Loss Triggers Neurodegeneration in an HMGA1-Dependent Manner[1]

Abstract

Loss-of-function mutations in the gene encoding vacuolar protein sorting factor 13A (VPS13A) underlie the rare autosomal-recessive neurodegenerative disorder termed VPS13A disease, formerly known as chorea acanthocytosis (ChAc). VPS13A loss results in progressive motor and cognitive symptoms, together with neuroinflammation and neuron loss centered in the basal ganglia, but the molecular mechanisms responsible for these manifestations remain obscure. Here, we utilize novel patient-derived cell lines, as well as VPS13A knockout (V-KO) neurons and immortalized cells, to demonstrate the necessity of VPS13A for neuronal survival. We observed pronounced differences in the proteome of V-KO cells, which in many cases mirrored changes at the RNA level, suggesting transcriptional dysregulation in response to VPS13A loss. Utilizing novel cell lines in which endogenous VPS13A is fused to the green fluorescent protein mNeonGreen (V-mNG), we identified high-mobility group protein A1 (HMGA1), a transcriptional regulator, as a candidate VPS13A interacting protein that accumulates upon VPS13A deletion. Notably, mimicking this phenomenon by HMGA1 overexpression reproduces neurotoxicity, while genetic reduction of HMGA1 extends neuronal survival in human neurons carrying VPS13A mutations, indicating that HMGA1 elevation is both necessary and sufficient for neurodegeneration in models of VPS13A disease. Collectively, these results reveal a previously unknown function for VPS13A in

[1] Adapted from:

Rodriguez G., Chen S.A., Rodriguez R., Salam A. T., Estor A.L., Sharma A., Turowski S.N., Qiao T., Waksmacki J., Li X., De Sanctis C., Thorn E.L., Walker R.H., Pinarbasi E., Tidball A., Crary J.F., Parent J., Fuller R.S., Tank E., Barmada S. **VPS13A loss triggers neurodegeneration in an HMGA1-dependent manner**. *Manuscript in preparation*.

transcriptional regulation and underscore the significance of this mechanism for maintaining neuronal survival in VPS13A disease.

2.1 Introduction

Vacuolar protein sorting 13 homolog A (VPS13A) disease, formerly known as chorea acanthocytosis (ChAc, OMIM 200150), is a rare autosomal recessive neurodegenerative disorder with an estimated prevalence of ~1 in 1,000,000 individuals[1–4]. VPS13A disease manifests with a wide range of motor, cognitive and behavioral symptoms[2–12], usually beginning in young adulthood with an average age of onset of 30 years[6–10]. Over 70 different homozygous or compound heterozygous mutations in the *VPS13A* gene, including insertions, deletions, and substitutions, lead to VPS13A disease; all of these mutations result in undetectable levels of the VPS13A protein or significant loss of function[13–18].

VPS13A belongs to the evolutionarily conserved VPS13 protein family[19], each of which features extended hydrophobic cavities capable of transporting phospholipids across organelle membranes[20–25]. Consistent with this, VPS13 family proteins are concentrated at organellar membranes and at contact sites between diverse organelles, including the endoplasmic reticulum[20,26,27], mitochondria[20,26–29], endosomes[21,27–31], peroxisomes[32–34], and lipid droplets[20,23,24,26,27,35,36], in addition to the plasma membrane[22,30,37,38], and nuclear envelope[22,37–39]. As with other members of the VPS13 family, VPS13A has been linked to autophagy[27,40–45], mitochondrial quality control[41–43,46–52], actin polymerization[42,46–48,50–55], and calcium homeostasis[26,53–58]. Notably, mutations in all four members of the VPS13A family (A–D) are associated with neurodegenerative disease: in addition to *VPS13A* mutations in VPS13A disease, *VPS13B* mutations are found in Cohen syndrome[59,60], *VPS13C* mutations have been identified in early and late-onset Parkinson's disease[61–63], and *VPS13D* mutations underlie spastic ataxia[64–66]. Despite the selective vulnerability of neurons to VPS13A loss, many previous investigations have focused on VPS13A solely in transformed cell lines. Whether VPS13A itself may have unique properties or functions in neurons remains unclear, potentially due to the lack of sensitive/selective antibodies, in addition to the large size of the gene (~250 kb) and protein (~360 kDa), all of which severely limit visualization, purification, and manipulation of the protein *in vitro* and *in vivo*.

Here, we utilize novel patient-derived cell lines, *VPS13A* knockout (V-KO) neurons, and human cell lines to demonstrate the necessity of *VPS13A* for neuronal survival. In

doing so, we uncover a previously unrecognized role for VPS13A in transcriptional regulation and highlight the significance of a novel candidate VPS13A interactor, HMGA1, for neurodegeneration in VPS13A disease models. Collectively, findings from these investigations may be pivotal for identifying new disease-modifying therapeutic targets and strategies in VPS13A disease.

2.2 Results

2.2.1 VPS13A disease patient-derived neurons display significant degeneration over time

We used whole-genome sequencing to confirm the location and character of the pathogenic mutation underlying VPS13A disease in two related siblings and their parents (**Fig. 2.1A**). In this pedigree, each parent carries one *VPS13A* allele harboring a single guanosine (G) deletion (∆G) (variation: NM_033305.3: c.6059>del, exon 46, (p.Pro2020fs); rs781242821) predicted to result in a shift in the *VPS13A* reading frame and nonsense-mediated RNA decay[8,16,18]. In keeping with the autosomal recessive nature of VPS13A disease, both affected children harbor two ∆G alleles. To study the impact of these mutations *in vitro*, we generated induced pluripotent stem cells (iPSCs) from one affected sibling (patient) and one unaffected parent (familial control). Reprogrammed iPSCs displayed a normal karyotype and successfully generated all three germ layers, confirming their pluripotency (data not shown). We then differentiated patient and familial control iPSCs into excitatory forebrain-like neurons (iNeurons) through the directed expression of master transcription factors Neurogenin 1 (Ngn1) and Neurogenin 2 (Ngn2), as previously described[67–71]. These cells expressed immunocytochemical markers of mature glutamatergic neurons, including vesicular glutamate transporter 1 (VGlut1) and synapsin-I (**Fig. 2.1B**). As expected, patient iNeurons displayed a complete loss of VPS13A protein by immunoblotting (**Fig. 2.1C**).

Given the neurodegeneration observed in post-mortem tissue from VPS13A disease patients[5,72–74], we predicted an elevated risk of death in patient iNeurons compared to familial controls. To assess this, we prospectively tracked thousands of individual neurons over 15 days (d) in culture using longitudinal fluorescence microscopy, a quantitative and sensitive method for monitoring neuronal fate *in vitro*[75–84]. We defined

time of death for each cell by retraction of neuronal processes, rounding of the soma, loss of fluorescence, or cellular blebbing as previously described (**Fig. 2.1D**)[82,83]. Although agnostic to the mechanism of cell death, these criteria are highly reproducible, amenable to automation, and as sensitive as conventional measures such as propidium iodide fluorescence[85]. We observed a significantly higher cumulative risk of death for patient iNeurons compared to familial controls (hazard ratio (HR)=2.03, ***p=3.18x10^{-10}, Cox proportional hazards analysis; **Fig. 2.1E**). These results suggest that loss of VPS13A in patient-derived iNeurons is associated with progressive degeneration compared to familial control iNeurons.

2.2.2 VPS13A is necessary for neuronal survival

Because patient-derived cell lines may harbor additional variants independent of *VPS13A* that could influence neuronal survival, we sought to confirm the results through targeted genetic reduction of *VPS13A* in otherwise healthy lines. First, we took advantage of a single-cell genome editing approach that we recently developed[86] to selectively knock out (KO) *VPS13A* in mature rat mixed primary cortical neurons. Neurons were transfected with vectors encoding single-guide (sg)RNAs targeting *VPS13A* (VPS13A-sgRNA) or a non-targeting control (NT-sgRNA), together with Cas9 nuclease and EGFP[86]. Forty-eight hours (h) after transfection, neurons were imaged by longitudinal fluorescence microscopy, and differences in the risk of death were determined by automated survival analysis (**Fig. 2.2A**)[75,81–84,86]. Neurons expressing VPS13A-sgRNA displayed a significantly elevated risk of death compared to those transfected with NT-sgRNA (HR=1.47, ***p<2x10^{-16}, Cox proportional hazards analysis; **Fig. 2.2B**), indicating that *VPS13A* KO is toxic to neurons.

We also validated the effect of VPS13A KO in human iNeurons. To eliminate endogenous VPS13A in healthy control iPSCs, we utilized a gene trap strategy in which the first coding exon of *VPS13A* was replaced by an open reading frame encoding a far-red fluorescent protein (iRFP), as well as a stop codon (TAA) and a strong polyadenylation signal (PAS) (**Fig. 2.2C**)[86,87]. The resulting VPS13A KO (V-KO) iPSCs as well as their isogenic controls (WT) were then differentiated into human iNeurons via induced expression of Ngn1/Ngn2, and complete loss of VPS13A in V-KO iNeurons was verified by immunoblotting (**Fig. 2.2D**). As before, neuronal maturity was confirmed by

immunostaining for VGlut1 and Synapsin-I (**Fig. 2.2E**). V-KO and WT iNeurons were then followed by longitudinal fluorescence microscopy for 15 d (**Fig. 2.2F**), and time of death for individual iNeurons was determined by survival analysis (**Fig. 2.2G**). Consistent with previous results in rat primary neurons (**Fig. 2.2A–B**) and in patient iNeurons (**Fig. 2.1D–E**), V-KO iNeurons exhibited a significantly greater risk of death compared to isogenic controls (HR=1.7035, ***p=3.74x10^{-7}, Cox proportional hazards analysis; **Fig. 2.2F**). Together these studies show that VPS13A is crucial for neuronal survival in both rat primary neurons and iNeurons.

2.2.3 Loss of VPS13A has extensive pre- and post- translational effects

To examine VPS13A disease mechanisms in a more tractable system free of toxicity, we generated a V-KO human embryonic kidney (HEK) 293T cell line using the same gene trap strategy (**Fig. 2.2C**). *VPS13A* loss in V-KO HEK293T cells was confirmed through Sanger sequencing (**Sup Fig. S2.1A**) and immunoblotting (**Fig. 2.3A**).

To begin to understand how loss of *VPS13A* could affect cellular survival, we took an unbiased approach and assessed the proteome of V-KO HEK293T cells by tandem mass tag mass spectrometry (TMT-MS). Over 100 proteins demonstrated significant differences in abundance ($p_{adj.}$<0.05, fold change (FC)>1.5) between V-KO and WT HEK293T cells, with the majority of proteins exhibiting reduced levels in V-KO cells (**Fig. 2.3B**). Unexpectedly, differentially expressed proteins were highly enriched for those involved in cell cycle regulation and DNA replication (**Fig. 2.3C**). Among the candidate proteins affected by V-KO were several associated with neurological and/or neurodegenerative disorders, including ABCD1[88,89] and CRMP4[90–93] (**Fig. 2.3B**), with ABCD1 demonstrating the largest FC of any protein upon loss of VPS13A (**Fig. 2.3D**). We subsequently confirmed ABCD1 and CRMP4 upregulation in V-KO cells by immunoblotting and immunocytochemistry (ICC; **Sup Fig. S2.2A–H**). Unexpectedly, we also observed a significant increase in the expression of *ABCD1* and *CRMP4* mRNA in V-KO cells compared to unedited controls (**Sup Fig. S2.2I–J**), suggesting that upregulation in V-KO cells occurs at the transcriptional level. These data raise the possibility that many of the noted differences in protein abundance by mass spectrometry may be driven by changes in transcription or genetic architecture, rather than protein stability or clearance.

To explore these questions, we examined global effects of *VPS13A* loss on gene expression through transcriptome-wide RNA sequencing (RNA-seq) of V-KO and WT HEK293T cells. In comparison to proteomic studies, we detected substantially more changes at the RNA level: >1,000 transcripts were significantly affected by V-KO ($p_{adj.}$<0.05, fold change (FC)>1.5; **Fig. 2.3E**), versus 136 proteins showing differential expression (**Fig. 2.3B**). Many of the transcripts displaying the most dramatic FC in V-KO cells were related to neuronal function and/or disease, including *SPARC*, *UNCX*, and *GABRA3* (**Fig. 2.3F**). Moreover, ~1/3 of proteins affected by V-KO (49 out of 136; $p=2.43x10^{-30}$, super exact test) displayed corresponding changes at the RNA level (**Fig. 2.3G**), suggesting transcriptional regulation in response to *VPS13A* loss. The overlapping set of 49 transcripts/proteins were enriched for components of the axon and growth cone (**Fig. 2.3H**), suggesting a preferential effect of *VPS13A* loss on neuronal structural factors. All except one of these factors displayed concordant expression changes at the RNA and protein levels, with 26/49 (53%) showing consistent upregulation of both RNA and protein, and 22/49 (45%) demonstrating downregulation of RNA/protein in V-KO compared to unmodified HEK293T cells (**Fig. 2.3I**). The 22 factors displaying concordant RNA/protein upregulation in V-KO cells were highly enriched for genes connected to neurological disorders, including axonal degeneration and neuropathy (**Fig. 2.3J**). Together, these data highlight a potential connection between VPS13A and the regulation of genes critical for neuronal structure and function.

2.2.4 VPS13A interacts with the transcriptional regulator HMGA1

Based on these data, we suspected that VPS13A loss may influence key transcription factors or other regulatory elements controlling gene expression. To test this, we sought to purify endogenous VPS13A and identify potential interacting proteins through unbiased mass spectrometry. Given that VPS13A is not an abundant protein, and immunoprecipitation is limited by the sensitivity and specificity of available VPS13A antibodies[20,31,94], we genetically labeled endogenous VPS13A in HEK293T cells using CRISPR/Cas9 genome engineering[87,95] (**Fig. 2.4A**). A cassette encoding the ultrabright fluorescent protein mNeonGreen (mNG) was inserted in-frame within *VPS13A* exon 35 (**Sup Fig. S2.1B**), providing an epitope tag as well as a means of visualizing native VPS13A by fluorescence microscopy (**Fig. 2.4B**). This location was chosen based on

homologous insertions of EGFP into the yeast homolog VPS13; unlike fusions at the N- or C-terminus, internal fusion of EGFP at this location preserves VPS13 functionality[20,26,94,96,97].

Following confirmation of correct mNG integration, candidate VPS13A interactors were identified via mNG immunoprecipitation (**Fig. 2.4C**) and TMT-MS. With this strategy, we successfully purified 211 proteins showing preferential association with VPS13A-mNG vs. mNG alone ($p<0.05$, fold change (FC)>1.5; **Fig. 2.4D**). Gene ontology (GO) analysis of these candidate interactors demonstrated enrichment (similarity≥0.8, signal≥0.01, strength≥0.01, FDR≤0.05) for proteins involved in chromosome organization, DNA repair, and cell cycle regulation (**Fig. 2.4E**). Furthermore, STRING network and UniProt keyword ontology categorized 52 of the 211 VPS13A interactors as functioning in 'transcription regulation' (n=52; KW-0805; **Sup Fig. S2.3A**). These data suggest that the widespread effects of VPS13A loss on the transcriptome may be driven by its interaction with factors involved in DNA packaging and gene expression.

To pursue this possibility and identify mechanisms responsible for transcriptional dysregulation upon *VPS13A* loss, we focused on the candidate interactors (**Fig. 2.4F**) that also demonstrated differential abundance upon VPS13A KO (**Fig. 2.3**). Only two candidates, carbonic anhydrase 8 (CA8) and high mobility group AT-hook 1 (HMGA1), fit these criteria. Of these two, only HMGA1 functions in transcriptional regulation[98–102] and displayed differential abundance at the protein but not RNA level, suggesting that its accumulation may be directly tied to loss of VPS13A, rather than indirectly mediated by compensatory or secondary effects in V-KO cells.

We next verified the interaction of VPS13A with HMGA1 in unmodified HEK293T cells by overexpressing HMGA1-GFP, followed by GFP immunoprecipitation and immunoblotting for VPS13A (**Fig. 2.4G**). We also verified HMGA1 upregulation in V-KO HEK923T cells by ICC and qRT-PCR (**Fig. 2.4H–J**), observing a significant increase at the protein level, with only a non-significant trend at the RNA level. These studies confirm the mass spectrometry results, indicating that HMGA1 not only physically interacts with VPS13A, but is also upregulated upon *VPS13A* loss.

2.2.5 HMGA1 is upregulated in VPS13A disease models

In light of the potential cell type-specific functions of VPS13A[37,103–107], and because we originally observed HMGA1 upregulation V-KO HEK293T cells, we next asked whether neurons displayed similar changes in HMGA1 upon loss of VPS13A. In accord with what we observed in V-KO HEK293T cells, we noted a significant increase in HMGA1 immunoreactivity by ICC in V-KO iNeurons compared to isogenic controls (**Fig. 2.5A–B**). Moreover, HMGA1 upregulation was post-translational in nature, as there was no significant difference in *HMGA1* RNA levels between V-KO and isogenic control (WT) iNeurons (**Sup Fig. S2.3B**). Furthermore, we observed an analogous upregulation of HMGA1 protein in patient iNeurons compared to familial controls (**Fig. 2.5C–D**), implying a consistent effect of *VPS13A* loss across cell lines. To verify this, we also explored downstream factors whose expression is regulated by HMGA1, including the transcription factor specificity protein 1 (SP1)[108–110]. Consistent with a functional upregulation of HMGA1 in cells lacking *VPS13A*, we noted significantly increased SP1 immunoreactivity in V-KO iNeurons compared to WT iNeurons (**Fig. 2.5E–F**), as well as in patient iNeurons compared to familial controls (**Fig. 2.5G–H**).

We also examined HMGA1 expression in post-mortem brain tissue from patients with VPS13A disease. Consistent with previous reports[5,72,73], VPS13A cases exhibited gliosis and neuronal loss in the basal ganglia (**Fig. 2.5I**). However, there was considerable variation among the three cases, mirrored by variability in HMGA1 staining. To investigate this further, gliosis (assessed via H&E staining) and HMGA1 intensity were semi-quantitatively evaluated by a neuropathologist blinded to the diagnosis (**Fig. 2.5J**). Although the small sample size precludes definitive conclusions, HMGA1 staining intensity appeared to correlate with severity of gliosis in these cases, implying HMGA1 upregulation with disease progression.

2.2.6 HMGA1 upregulation is necessary and sufficient for neurodegeneration in VPS13A disease models

To assess whether the observed changes in HMGA1 could be responsible for neurotoxicity in VPS13A disease, we first asked if HMGA1 upregulation alone is sufficient to recapitulate toxicity in otherwise healthy neurons. Rat primary neurons were transfected with a vector encoding mApple to mark the cell body and a vector encoding either EGFP-tagged HMGA1 (HMGA1-EGFP) or EGFP. As in **Fig. 2.2**, transfected

neurons were imaged at regular 24 h intervals over 7 d by longitudinal fluorescence microscopy (**Fig. 2.6A**). Automated survival analysis demonstrated a significantly higher risk of death for neurons expressing HMGA1-EGFP compared to those expressing EGFP (HR=1.32, ***$p<2x10^{-16}$, Cox proportional hazards analysis; **Fig. 2.6B**). Similar experiments were conducted in WT iNeurons co-transduced with lentiviruses encoding a red fluorescent protein (dsRedII), and either HMGA1-EGFP or EGFP (**Fig. 2.6C**). As with rodent primary neurons, iNeurons transduced with HMGA1-EGFP displayed a significantly higher risk of death compared to EGFP-expressing cells (HR=1.64, ***$p<2x10^{-16}$, Cox proportional hazards analysis; **Fig. 2.6D**). Together, these results show that HMGA1 upregulation is sufficient to drive neurodegeneration.

To test if HMGA1 upregulation is also necessary for the toxicity observed in VPS13A disease models, we transduced V-KO iNeurons with lentiviral constructs encoding non-targeting (NT) shRNA or shRNA against *HMGA1* (HMGA1-shRNA) and used longitudinal fluorescence microscopy to image neurons every 24 h for 13 d (**Fig. 2.6E**). In contrast to the toxic effect of HMGA1 when overexpressed, HMGA1-shRNA significantly extended the survival of V-KO iNeurons (HR=0.35 compared to NT-shRNA, $p=2x10^{-16}$, Cox proportional hazards analysis; **Fig. 2.6F**). These results were further validated in VPS13A disease patient-derived iNeurons, which were transduced with the same constructs before undergoing longitudinal fluorescence microscopy and survival analysis (**Fig. 2.6G**). As with V-KO iNeurons, patient iNeurons exhibited significantly longer survival upon HMGA1 knockdown (KD; HR=0.29, $p=2x10^{-16}$, Cox proportional hazards analysis; **Fig. 2.6H**). Familial control neurons treated with HMGA1-shRNA also displayed a reduced risk of death compared to NT-shRNA (**Sup. Fig. S2.4A–B**), consistent with the neurotoxic effects of *HMGA1* expression in rodent primary neurons and WT iNeurons (**Figs. 2.6A, C**). Taken together, these results show that HMGA1 is both necessary and sufficient for neurodegeneration in VPS13A disease models.

2.3 Discussion

At present, there is no cure for VPS13A disease, and treatments are limited to symptom management and supportive care[43,57,111,112]. This gap is largely driven by our incomplete understanding of VPS13A disease mechanisms, specifically how *VPS13A*

loss leads to age-dependent neurodegeneration. In this study, we establish a human neuron model of VPS13A disease and utilize this platform to clarify the contribution of a novel VPS13A-interacting protein, HMGA1, to neurotoxicity. Engineered cell lines in which endogenous *VPS13A* was deleted (V-KO) or was labeled with mNeonGreen (V-mNG) highlighted the physical interaction between VPS13A and HMGA1, and the pronounced upregulation of HMGA1 upon VPS13A loss. Notably, HMGA1 upregulation was both necessary and sufficient for cell death in V-KO human neurons and patient iPSC-derived neurons, implicating HMGA1 as a central node in the pathogenesis of VPS13A disease, and a potential target for therapy development.

We identified several proteins that displayed pronounced changes upon *VPS13A* loss in HEK293T cells, many of which are associated with neurological and/or neurodegenerative disorders. One of the most significantly affected proteins was ATP binding cassette subfamily D member 1 (ABCD1), also known as adrenoleukodystrophy protein (ADLP). Pathogenic ABCD1 mutations result in X-linked adrenoleukodystrophy (X-ALD), a metabolic disorder associated with progressive multifocal demyelination in the central nervous system (CNS) and/or peripheral adrenal insufficiency[88,113,114]. *VPS13A* deletion upregulated ABCD1 at both the protein and RNA levels, consistent with a transcriptional rather than a post-translational mechanism of action. We also uncovered consistent elevations in collapsin response mediator protein 4 (CRMP4) protein and RNA in V-KO cells. CRMP4 dysfunction has been directly implicated in cancer[115–117], schizophrenia[118,119], and autism spectrum disorder[118,120], in addition to neurodegenerative conditions such as amyotrophic lateral sclerosis (ALS)[90,121,122], Parkinson's disease (PD)[93,123,124], and Alzheimer's disease (AD)[93,125–127]. Whether or not the changes in CRMP4 noted in V-KO cells contribute to cytoskeletal abnormalities in erythrocytes and the observed phenomenon of acanthocytosis in VPS13A disease is unknown but could be explored in future studies.

The concordant changes in the RNA and protein levels of ABCD1 and CRMP4 in V-KO cells were not isolated events; indeed, meta-analysis of the proteomics and RNA-seq datasets showed that ~1/3 of proteins affected by V-KO displayed corresponding transcriptional increases or decreases, suggesting that at least some of the differences in protein abundance following V-KO occur at the RNA level. Consistent with these

findings, VPS13A localizes to the perinuclear space[22,35,37–39], and elimination of VPS13A leads to significant changes in several components of the nucleosome machinery involved in chromatin packaging, while many of the unique VPS13A interactors identified in this study participate in chromosome organization and transcriptional regulation. Although not considered a conventional transcription factor, HMGA1 can act as an 'architectural' transcription factor by binding to and altering chromatin structure[108,109,128–130]. HMGA1 has primarily been studied in the context of tumorigenesis[131–138], but emerging studies suggest a potential influence of HMGA1 on autophagy, protein clearance, and cellular senescence in neurodegenerative disease models[136–144]. Together with our data indicating the relevance of HMGA1 for neuronal survival, and a possible correlation between severity of neuropathological changes and HMGA1 expression, these observations suggest that HMGA1 may be pivotal for neuron loss and neuroinflammation in VPS13A disease patients. Additional investigations with more patient samples are required to confirm and extend these findings.

Not only did we observe elevations in HMGA1 in V-KO and VPS13A disease patient iPSC-derived neurons, but we also observed upregulation of downstream factors activated by HMGA1, including SP1. Abnormal SP1 levels and activity have also been observed in PD[145–147], AD[148–152], Huntington's disease[153,154], ALS[155,156], and prion disease[157], all of which are age-related neurodegenerative disorders. Although the precise contribution of SP1 to these conditions remains unknown, its relationship to HMGA1 and now VPS13A suggest that it may be part of the cascading downstream effects triggered by VPS13A loss that ultimately lead to neurodegeneration and clinical symptoms of disease. More focused studies incorporating patient samples and pharmacological SP1 inhibitors are required to address these possibilities.

Both HMGA1 and SP1 are associated with metastatic, aggressive cancers[131–138,158]. Their upregulation in models of VPS13A disease raises a fundamental question regarding the relationship between oncogenic transformation and neurodegenerative disease. While cell cycle progression typically leads to cell division and tissue growth, in post-mitotic cells such as neurons, re-entry into the cell cycle effectively triggers apoptosis and cellular senescence[159–161]. In support of this possibility, cell cycle represented the top gene ontology category among differentially expressed proteins in V-KO HEK293T cells

(**Fig. 2.3C**). Whether this mechanism contributes to neuronal dysfunction and death in VPS13A disease remains unknown, however, as do the factors that could stimulate cell cycle re-entry in affected neurons.

To our knowledge, this study provides the first indication that expression of HMGA1, SP1, or other transcriptional regulators may underlie neuron loss in VPS13A disease. In addition to establishing a potentially relevant disease mechanism, our observations highlight HMGA1 as a potential therapeutic target. We also introduce faithful models of VPS13A disease involving human neurons derived from VPS13A patients as well as iPSCs with targeted *VPS13A* deletions. These systems may be invaluable for exploring novel strategies for limiting cell cycle re-entry and/or cellular senescence as therapeutic candidates in VPS13A disease.

2.4 Methods

2.4.1 Sex as a biological variable

Our study examined both female and male humans and rats. Sex was not considered as a biological variable.

2.4.2 HEK293T cell culture and transfection

Human embryonic kidney (HEK) 293T cells (**Table 2.1. Cell lines**) were cultured in HEK media (1X DMEM, high glucose, pyruvate (DMEM; Gibco, 11995065) containing 1X GlutaMAX supplement (GlutaMAX; Gibco, 35050061), 100 units/mL penicillin-streptomycin (P/S; Gibco, 15140122), and 10% fetal bovine serum (FBS; Gibco, 10082147)) at 37°C in 5% CO_2. HEK293T cells were transfected using Lipofectamine 2000 (Invitrogen, 11668027) according to the manufacturer's instructions.

2.4.3 CRISPR/Cas9 genome engineering

2.4.3.1 Integration of mNeonGreen into the VPS13A locus

VPS13A mNeonGreen (V-mNG) HEK293T cells (**Table 2.1. Cell lines**) were created using a dual-nickase CRISPR/Cas9 strategy[87,95]. First, oligos complementary to the sequence flanking the region immediately upstream of *VPS13A* exon 35 (**Table 2.4. Oligonucleotides**) were annealed, digested, and ligated into the BbsI site of pX335-U6-Chimeric_BB-CBh-hSpCas9n(D10A)[95] (pX335 plasmid; Addgene, 42335; **Table 2.5.**

Recombinant DNA), which encodes Cas9n and chimeric single guide (sg)RNA. HEK293T cells were then transfected with 1.25 µg of each Cas9n-sgRNA vector pair, along with 2.5 µg of a homology-directed repair (HDR) cassette encoding the mNeonGreen (mNG) open reading frame flanked by 400 bp of sequence homologous to regions immediately upstream and downstream of the target region (VPS13A-mNG HDR plasmid; Eurofins Genomic Blue Heron (Blue Heron); **Table 2.5. Recombinant DNA**). After transfection, cells were split at a low density to allow transfected cells to establish individual colonies which were screened for cytoplasmic green fluorescence and transferred to a new dish. The screening process was repeated until 100% of the cells displayed cytoplasmic mNG signal, and correct integration of the mNG cassette into the VPS13A locus was confirmed via polymerase chain reaction (PCR) and Sanger sequencing using primers listed in **Table 2.4. Oligonucleotides**.

2.4.3.2 Integration of iRFP, stop codon, and poly(A) signal sequence into the VPS13A locus

V-KO HEK293T cells (**Table 2.1. Cell lines**) were created using a dual-nickase CRISPR/Cas9 strategy[87,95]. First, oligos complementary to the sequence flanking the region immediately upstream of VPS13A start codon (ATG) (**Table 2.4. Oligonucleotides**) were annealed, digested, and ligated into the BbsI site of the pX335 plasmid as described above. HEK293T cells were transfected with 1.25 µg of each Cas9n-sgRNA vector pair, along with 2.5 µg of a homology-directed repair cassette containing the near-infrared fluorescent protein (iRFP) encoding sequence, a stop codon (TAA), and a polyadenylation (poly(A)) stop signal sequence (PAS) flanked by 400 bp of sequence homologous to regions immediately upstream and downstream of the VPS13A start codon (V-KO-iRFP-STOP HDR plasmid; Blue Heron; **Table 2.5. Recombinant DNA**). After transfection, cells were screened until 100% of the cells displayed the iRFP signal and the correct integration of the cassette was confirmed as described above.

V-KO iNeuron cells were created using the same strategy used for HEK293T cells described above, but in 1021 iNeurons (**Table 2.1. Cell lines**).

2.4.4 Primary rat neuron cell culture and transfection

Cortices from embryonic day (E)19–20 Long-Evans rat embryos were dissected and dissociated, and primary neurons (**Table 2.1. Cell lines**) were plated at a density of $6x10^5$ cells/mL in Neurobasal complete media (NBC media; 500 mL Neurobasal Medium (NB media; Gibco, 21103049) containing 1X B27 supplement (B27; Gibco, 17504-044), GlutaMAX, and P/S) in 96-well plates. At *in vitro* day (DIV) 4, neurons were transfected with 50 ng of a control fluorescent plasmid to mark cell bodies and 150 ng of an experimental construct (**Table 2.5. Recombinant DNA**) using Lipofectamine 2000 as previously described[86]. Following transfection, cells were placed in warm NBC media or BrainPhys Imaging Optimized Medium (BrainPhys media; STEMCELL Technologies, 05796) and incubated at 37°C in 5% CO_2 until day (D) 1 of imaging for automated survival analysis as described below.

2.4.5 iPSC-derived iNeuron culturing and maintenance

iNeuron neural progenitors (NPs) were made from induced pluripotent stem cells (iPSCs) using the cell lines described in **Table 2.1. Cell lines**. In brief, iPSCs were washed in 1X PBS (PBS; Gibco, 14200-075) and dissociated in accutase (Sigma, A6964) for 5 m at 37°C. TeSR-E8 media (STEMCELL Technologies, 059910) was added, then cells were collected and centrifuged at 300xg for 5 m. After aspirating the media, pelleted cells were resuspended in 1 mL of fresh media containing ROCK inhibitor (ROCK-i; Cayman Chemical, 10005583), counted using a hemocytometer, plated at a density of $3.2x10^4$ cells/mL on a 60 mm vitronectin (Fisher, A14700)-coated plate in TeSR-E8 media+ROCK-i, and incubated at 37°C. Differentiation was induced with 2 µg/mL doxycycline (DOX; Sigma, D3447) for 48 h at 37°C. After 48 h, differentiating NPs were dissociated using accutase, frozen in TeSR-E8 media with 10% DMSO at the desired concentration, then stored in liquid nitrogen until needed.

When needed, frozen NPs were thawed and differentiated as described previously[86]. In short, at DIV0 NPs were thawed, plated on Poly-L-ornithine (Sigma, P3655) and laminin (Sigma, L2020)-coated plates in TeSR-E8 media containing 2µg/mL DOX and ROCK-i, and incubated at 37°C overnight (O/N).

On DIV1, the media was changed to N2 media (TeSR-E8 media containing 1X N2 supplement (N2; Gibco, 17502-048), 1X NEAA supplement (NEAA; Gibco, 11140-355050), 10 ng/mL human/mouse/rat BDNF recombinant protein (BDNF; Peprotech, 450-

02), 10 ng/mL human NT-3 recombinant protein (NT3; Peprotech, 450-03), 0.2 µg/mL laminin, and 2 µg/mL DOX).

On DIV2, the media was replaced with transition media (1:1 TeSR-E8 media and DMEM/F12 media (Gibco, 11320-033) containing N2, NEAA, 10 ng/mL BDNF, 10 ng/ml NT3, 0.2 µg/mL laminin, and 2 mg/mL DOX).

On DIV3, the media was changed to B27 media (Neurobasal–A Medium (Neurobasal–A media; Gibco, 12349-015) or BrainPhys media containing B27, GlutaMAX, 10 ng/mL BDNF, 10 ng/mL NT3, 0.2 µg/mL laminin, 1X CultureOne supplement (CultureOne; Gibco, A33202-01), and 2 mg/mL DOX). For survival experiments, DOX was omitted from DIV3 media onward.

On DIV6, most of the media was removed from the wells and iNeurons were transduced with concentrated virus (prepared by the University of Michigan Vector Core) to increase transduction efficiency. iNeurons were incubated at 37°C in 5% CO_2. The following day, on DIV7, iNeurons were topped off with fresh incubation media (Neurobasal A or Brain Phys media containing GlutaMAX, 10 ng/mL BDNF, 10 ng/mL NT3, and 2 mg/mL DOX). For survival experiments, DOX was omitted.

On DIV14 iNeurons were collected for RNA or protein harvesting, fixed with 4% paraformaldehyde for ICC, or imaged for D1 of survival analysis.

2.4.6 Human brain tissue samples

Post-mortem human brain tissue samples were obtained from patients with genetically confirmed VPS13A disease or without neurodegenerative disease who had enrolled and consented to brain donation. These samples were collected in accordance with ethical guidelines and with institutional review board (IRB) approval, ensuring the privacy and dignity of the donors while supporting ongoing neurological research, and were previously published in Ditzel et al. (2023)[5]. The samples, sex- and age-matched, were provided by the following centers: Mount Sinai Hospital, New York City, New York, USA; Rush University, Chicago, Illinois, USA; and University of Frankfurt am Main, Rostock, Germany; in collaboration with the Neuropathology Brain Bank & Research CoRE at Mount Sinai.

2.4.7 Immunohistochemistry and evaluation

Paraffin-embedded sections (6 µm-thick) from the basal ganglia of VPS13A patient cases (n=3) and a control case (n=1) were processed for chromogenic immunohistochemistry (IHC) using the Ventana Discovery Ultra platform (Ventana Medical Systems Inc., Roche Diagnostics) per the manufacture's instructions. Briefly, formalin-fixed sections were pretreated using cell conditioning antigen retrieval buffer (CC1; Tris, Borate, EDTA buffer pH 8.0–8.5; Roche Diagnostics, 950-224) to unmask epitopes. The sections were then incubated with the primary antibody HMGA1 (**Table 2.3. Antibodies**) diluted in Antibody Dilution Buffer (Roche Diagnostics, ADB250). Signal detection was performed using the ChromoMAP DAB Kit (Roche Diagnostics, 760-159), as per the manufacturer's protocol. Additional sections were stained with Hematoxylin & Eosin stain (H&E) to assess overall tissue architecture. Finally, all immunostained sections were mounted on glass slides, air-dried, and imaged by microscopy.

Whole-slide images were generated by the Mount Sinai Neuropathology Brain Bank & Research CoRE on an Apreio8 Versa scanner (Leica, Biosystems) equipped with a 20x objective. Slides were reviewed and high-quality light microscopy images were acquired by a neuropathologist, who was blinded to case identity, at the University of Michigan on an Olympus BX51 light microscope equipped with a UPlanSApo 60x oil objective with a numerical aperture of 1.35 and a working distance of 0.15 mm. Slides were assigned a semi-quantitative score of gliosis (based on H&E; scored 0–4) and HMGA1 intensity (based on IHC; scored 0–4) in the putamen, which was well-represented in all patients.

2.4.8 Whole-genome sequencing of patient-derived iPSCs

Whole-genome sequencing (WGS) was performed, and fastq files were generated. Cutadapt v2.3[162] was used to trim adapter sequences and low-quality bases, and read quality was assessed with FastQC v0.11.8[163,164]. Trimmed reads were then aligned to the human reference genome (GRCh38) using HISAT2[165], generating BAM files. The subsequent BAM files were sorted, marked for duplicates, and used for variant calling. Variants were called using HaplotypeCaller (GATK)[166]. Each VCF was then annotated using ANNOVAR[167] incorporating the refGene, cytoBand, and clinvar_20240917 databases. Variants located within Chr9: 70,000,000–88,000,000 were extracted and filtered for those predicted to disrupt coding sequences.

2.4.9 RNA isolation for RT-PCR and RNA sequencing

RNA was extracted using the Direct-zol RNA Miniprep Kit (Zymo, R2052) or using the TRIzol/phenol-chloroform method, which is as follows. RNA was harvested using TRIzol (Invitrogen, 15596026) followed by 1/5 vol chloroform (Sigma, 288306) added to TRIzol-lysate, 10 s vortexing at full speed, and centrifugation at full speed for 20 m at 4°C. After centrifugation, the aqueous layer was transferred to new tubes followed by 1/10 vol 3M sodium acetate (NaOAC; pH 5.2) and 1 vol isopropanol. Tubes were incubated O/N at -20°C for RNA precipitation. The following day, samples were centrifuged at full speed for 20m at 4°C and the supernatant was decanted. The RNA pellet was washed twice with 75% ethanol (EtOH), followed by two washes with 100% EtOH. The RNA pellet was then dried in a vacufuge at room temperature (RT) for 10m. RNA was resuspended in a resuspension mix consisting of: 1 µL of Baseline-ZERO DNase (BZD; LGC Biosearch Technologies, DB0715K), 1 µL RNase inhibitor, 5 µL BZBUFF (dnase buffer), and 43 µL of DNase/RNase free (UltraPure) water. After resuspension, RNA was purified using the Monarch RNA Cleanup Kit (New England Biolabs (NEB), T2040), as per the manufacturer's protocol.

2.4.10 Quantitative PCR (qRT-PCR)

Following RNA isolation, 1 µg of extracted RNA was used as a template for the synthesis of complementary DNA (cDNA), via reverse transcription, in a reaction volume of 20 µL using the High-Capacity cDNA Reverse Transcription Kit (Applied Biosystems, 4368814) following the manufacturer's instructions. Quantitative reverse transcription-PCR (qRT-PCR) reactions were then set up using PowerUp SYBR Green Master Mix (ThermoFisher, A25742), 1 µM of primers (**Table 2.4. Oligonucleotides**) and 1 µL of cDNA in technical triplicates. qRT-PCR reactions were run on a QuantStudio 6 real-time PCR system (Applied Biosystems) following the manufacturer's protocol. Relative gene expression was calculated using the Pfaffl mathematical model for relative transcript quantification (ΔΔCt method)[168] using GAPDH as the housekeeping gene. Values were plotted in GraphPad Prism v.10.4.1 (Prism) software.

2.4.11 Poly(A) mRNA sequencing

WT and V-KO HEK293T cell RNA was extracted using the TRIzol/phenol-chloroform method and purified as described above. After RNA isolation, RNA integrity was assessed on a TapeStation system (Agilent Technologies) using the Qubit RNA Broad Range Assay Kit (ThermoFisher, Q10210) following the manufacturer's protocol. Only samples with an RNA integrity number (RIN)≥8 were used to perform poly(A) enriched RNA-sequencing (RNA-seq). 1 µg of total RNA per sample was converted to mRNA via poly(A) purification using the NEBNext poly(A) mRNA Magnetic Isolation Module (NEB, E7490).

Following mRNA isolation, xGen Broad Range RNA library Prep Kit (Integrated DNA Technologies (IDT)) was used to construct the RNA libraries as per the manufacturer's instructions. Briefly, the mRNA was first fragmented followed by random priming and reverse transcription to incorporate an R1 Stubby Adaptor while generating first-strand cDNA. This was followed by an exonuclease 1 treatment and solid phase reversible immobilization (SPRI) cleanup step. After cleanup, Adaptase enzyme technology was used to simultaneously perform tailing and ligation of the cDNA (TLC) to incorporate an R2 Stubby Adapter to the 3' ends of the cDNA molecules, which was followed by another SPRI cleanup step. Normalase indexing PCR was then performed using xGen Normalase UDI primers (IDT), following the manufacturer's protocol. Briefly, Normalase UDI primers were added to each sample followed by PCR master mix. Samples were pulse-spun to collect contents, run on a thermal cycler for indexing PCR, and SPRI cleaned to create the final cDNA library which were checked for quality and quantity on a LabChip GX Touch Nucleic Acid Analyzer (Perkin Elmer) using the Quibit 1X dsDNA high sensitivity assay kit (ThermoFisher, Q33231). Samples were pooled and sequenced on an Illumina NovaSeq 6000 platform for 150 bp paired-end reads with an average depth of 100M reads/sample (at the University of Michigan Advanced Genomics Core).

2.4.11.1 <u>Mapping and alignment</u>

Reads were trimmed using Cutadapt v2.3[162]. FastQC v0.11.8[163,164] was used to ensure the quality of data. FastQ Screen[163] was used to screen for various types of contamination. Reads were mapped to the reference genome GRCm38 using STAR v2.7.8a[169] and assigned count estimates to genes with RSEM v1.3.3[170]. Alignment

options followed ENCODE standards for RNA–seq. MultiQC v1.7[171] was used to compile results and provide a detailed and comprehensive quality control report.

2.4.11.2 Differential expression analysis

Data were pre-filtered to remove genes with 0 counts in all samples. Differential gene expression analysis was performed using DESeq2 v1.34.0[172], using a negative binomial generalized linear model (thresholds: linear fold change (FC)>1.5 or <-1.5, Benjamini-Hochberg (FDR), $p_{adj.}$<0.05).

2.4.12 Western blot

Unless otherwise mentioned, cell lysates were prepared as follows: cells were collected in PBS and pelleted by centrifugation at 5,000xg for 5m at 4°C. Cell pellets were resuspended and lysed using a syringe in RIPA lysis and extraction buffer (RIPA; ThermoFisher, 89901) with cOmplete, Mini, EDTA-free Protease Inhibitor Cocktail (+PI cocktail; Millipore, 118361700021) on ice for 30m. Following lysis, samples were centrifuged at 15,000xg for 10m at 4°C. Supernatants were transferred to fresh tubes, and Bio-Rad Protein Assay (Bio-Rad, 5000006) was performed to estimate protein concentration. Samples were then diluted to equal volumes with RIPA+PI cocktail to a protein concentration of 25 µg per sample. Samples were reduced and denatured using 10X sample buffer (made of 10% sodium dodecyl sulfate (SDS; Fisher scientific, AAJ6760630), 20% glycerol, 0.0025% bromophenol blue, 100 mM EDTA (Sigma, E7889), 1M DTT (ThermoFisher, R0862), 20 mM Tris in deionized water (DI) water (pH 8.0)) and heated at 70°C for 5m.

Prepared samples were loaded onto an 8-10% SDS-PAGE gel with a 4% stacking gel and run at 85–110V for protein separation. Afterwards, protein transfer was performed at 110V for 1.5h at 4°C onto a methanol (MeOH)-activated 0.45 µm PVDF membrane (membrane; Millipore, IPVH09120). To ensure uniform loading, membranes were stained, imaged, and then washed using the Revert 700 Total Protein Stain Kit (Total Protein Stain; LiCOR BIO, 926-11010) on the Odyssey CLx System machine (LI-COR), as per the manufacturer's instructions. Following this, membranes were blocked at RT for 20m with blocking buffer. Depending on the antibody used, blocking buffer consisted of either 3% bovine serum albumin (BSA; Fisher, BP9703-10) or 4% non-fat dry milk

(NFDM), made in 1X Tris-buffered saline with 0.2% Tween-20 (TBST; Sigma, P9614). Membranes were then blotted with diluted primary antibody in corresponding blocking buffer (**Table 2.3. Antibodies**) on a rocker at 4°C O/N. The following day, blots were washed 3 times in wash buffer (made of 1X TBST) then incubated in secondary antibody diluted at 1:10,000 (**Table 2.3. Antibodies**) on a rocker for 1h at RT. After secondary antibody incubation, blots were washed 3 times, then developed using Pierce ECL Western Blotting Substrate (ThermoFisher, 32106) on a G Box Mini 6 imager (Syngene). Blots were stripped with Restore Western Blot Stripping Buffer (ThermoFisher, 21059), washed 3 times, and reprobed. Image Studio was used to quantify bands.

The following changes to the protocol detailed above were made when probing VPS13A. Cell pellets were resuspended and lysed using a syringe in a modified 2X Laemmli sample buffer (made of 2X Laemmli Sample Buffer (BIO-RAD, 1610737) containing 0.70 M Urea (Sigma, U1250-1KG) and 50 mM DTT). Samples were not heated. Prepared samples were loaded onto a 6% SDS-PAGE gel without a stacking gel. Protein transfer was performed using a modified transfer buffer (containing 10% MeOH instead of 20% MeOH) at 30V O/N at 4°C. The rest of the protocol was followed as above.

2.4.13 Immunoprecipitation

2.4.13.1 IP of HEK293T cells with mNeonGreen magnetic beads

Unless otherwise specified, immunoprecipitation (IP) using mNeonGreen (mNG) was performed as follows. Control (WT) and VPS13A-mNeonGreen (V-mNG) HEK293T cells were plated on 10-cm plates (1 plate per condition per replicate). The following day, control (WT) HEK293T cells were transfected O/N with 30 µg of control mNG plasmid (**Table 2.5. Recombinant DNA**) using 20 µL of Lipofectamine 2000 as per the manufacturer's protocol. After 48h, un-transfected WT (UT), mNG transfected WT (mNG), and V-mNG cells were collected with ice cold PBS and pelleted by centrifugation at 500xg for 4m at 4°C. Cell pellets were resuspended in ice cold IP lysis buffer (10 mM Tris/Cl pH 7.5, 150 mM NaCl, 0.5 mM EDTA, 0.5% NP-40 (ThermoFisher, 85124), and PI cocktail in Milli-Q water) on ice for 30m with extensive pipetting every 10m.

Following lysis, tubes were centrifuged at 20,000xg for 10m at 4°C. Supernatant was carefully transferred to new tubes, and protein concentration was estimated using

Bio-Rad protein assay. Each sample was subsequently diluted in ice cold IP lysis buffer to a total protein concentration of 500 µg in 200 µL. Following this, 300 µL of ice-cold IP dilution buffer (10 mM Tris/Cl pH 7.5 and 150 mM NaCl in MiliQ water) was added to each sample. At this point, 50 µL of each sample was saved as input for future analysis.

The remaining diluted lysate was added to 15–30 µL of equilibrated mNeonGreen Magnetic Beads (ChromoTek, ntma) which were prepared by washing 3 times in 500 µL ice-cold IP dilution buffer followed by magnetic separation of beads after each wash. Samples were placed on a tube rotator at 4°C O/N for protein binding. The following day on ice, mNG beads were magnetically separated, 50 µL of supernatant was saved for each sample for future analysis (flow), and the remaining flowthrough was discarded. mNG beads were then washed 3 times as detailed above. To elute bound proteins, beads were resuspended in 50 µL of modified 2X Laemmli sample buffer and boiled at 65°C for 5 min. mNG beads were then magnetically separated and discarded, leaving the remaining eluate. For each sample, eluate alongside a fixed volume of input and supernatant, was loaded onto an SDS-PAGE gel for western blot analysis as described earlier.

2.4.13.2 IP of HEK293T cells with GFP magnetic beads

GFP IP was performed like mNG IP described above, with the following changes. Control (WT) HEK293T cells were transfected with GFP or HMGA1–GFP constructs (**Table 2.5. Recombinant DNA**) as described earlier. After 48h, un-transfected (UT), GFP transfected (GFP), and HMGA1-GFP transfected WT cells (HMGA1-GFP) were collected, pelleted lysed and diluted to equal concentrations as described above. Following this, 50 µL of input was saved for each sample and the remaining lysate was added to 35 µL of equilibrated GFP Magnetic Beads (ChromoTek, gtma) prepared as previously described. Samples were placed on a tube rotator at 4°C O/N for binding. The following day, 50 µL of supernatant was saved per sample, GFP beads were washed, and bound proteins were eluted just as detailed above. Similarly, eluate, input and supernatant were loaded onto an SDS-PAGE gel for western blot analysis as described earlier.

2.4.14 Tandem-mass tag (TMT) isobaric labeling and mass spectrometry-based proteomics

2.4.14.1 Protein digestion and TMT labeling

Control (WT) and V-KO HEK293T cells were collected in ice-cold PBS and centrifuged at 1,000xg for 5m at 4°C. Cell pellets were resuspended in 150 µL of ice-cold RIPA+PI cocktail, syringe-lysed, centrifuged, and protein concentration was estimated as described earlier. Samples were diluted in RIPA to a total concentration of 1 µg/µL. 30 µL of diluted sample was used to validate V-KO via western blot analysis, and the remaining lysate was stored at -80°C until ready to proceed. Following V-KO verification, 75 µL (1µg/µL) of sample per replicate per condition were submitted to the University of Michigan Proteomics Resource Facility. There, samples were proteolyzed and labeled with TMT-sixplex™ Isobaric Label Reagent Set (TMT 6-plex; ThermoFisher, 90061) following the manufacturer's instructions. Briefly, upon reduction with 5 mM DTT for 30m at 45°C, and alkylation of cystines with 15 mM 2-chloroacetamide for 30m at RT, proteins were precipitated by adding 6 vol of ice-cold acetone and O/N incubation at -20°C. The following day, samples were spun down and precipitated pellets were allowed to air dry. After drying, pellets were resuspended in 100 mM TEAB and digested with trypsin/Lys-C mix (1:25 protease:protein; Promega) at 37°C with constant mixing using a thermomixer O/N (~16h). The next day, TMT 6-plex reagents were dissolved in 41 µL of anhydrous acetonitrile and samples were labeled by transferring the entire digest to TMT reagent vials and incubating at RT for 1h. Reactions were subsequently quenched using 8 µL of 5% hydroxyl amine followed by a 15m RT incubation. Labeled samples were then mixed and dried using a vacufuge. An offline fractionation of the combined sample (~200 µg) into 8 fractionations was performed using high pH reversed-phase peptide fractionation kit (Pierce, 84868) according to the manufacturers protocol. The following day, fractions were dried and reconstituted in 9 µL of 0.1% formic acid + 2% acetonitrile in preparation for liquid chromatography-mass spectrometry (LC-MS/MS) analysis.

To identify potential VPS13A interactors, TMT-labeling and mass-spectrometry proteomics of mNG immunoprecipitated samples was performed like the steps outlined above, with the following changes:

mNG transfected control (mNG) and V-mNG HEK293T cells were plated and transfected as described previously (4 10-cm plates per condition per replicate; for transfected cells 30 µg of DNA per 10-cm plate was used). For each replicate, plates of

the same condition were collected as described above and combined before being resuspended in 100 µL of ice-cold IP lysis buffer. Afterwards samples were lysed, centrifuged, and protein concentration was calculated as described previously. Samples were then diluted to equal protein concentrations and added to 40 µL of equilibrated mNG magnetic beads and bound O/N as described above. The following day, mNG beads were magnetically separated and washed three times as explained above. Unlike previously, after the third wash mNG beads were first resuspended in 200 µL of ice-cold IP dilution buffer. 20% of the resuspended beads for each sample were then magnetically separated, eluted in 50 µL of modified 2X sample buffer, and used to validate VPS13A and mNG protein precipitation via western blot analysis described before. The remaining 80% of resuspended beads for each sample were magnetically separated and stored without buffer at -80°C until ready to proceed. Following VPS13A and mNG protein verification, the remaining 80% of beads were submitted to the University of Michigan Proteomics Resource Facility. At the facility, the mNG beads were proteolyzed and labeled with TMT 6-plex as described above.

2.4.14.2 Liquid chromatography-mass spectrometry analysis (LC-multinotch MS3)

To obtain superior quantity accuracy, we employed multinotch-MS3[173] which minimizes the reporter ion ratio distortion resulting from fragmentation of co-isolated peptides during MS analysis. Orbitrap Fusion (ThermoScientific) and RSLC Ultimate 3000 nano-UPLC (Dionex) were used to acquire the data. 2 µL of the sample was resolved on a PepMap RSLC C18 column (75 µm i.d. x 50 cm; ThermoScientific) at the flow rate of 300 nL/min using a 0.1% formic acid + acetonitrile gradient system (2–22% acetonitrile in 150m; 22-32% acetonitrile in 40m; 20m wash at 90% followed by 50 min re-equilibration) and directly sprayed onto the mass spectrometer using EasySpray source (ThermoScientific). The mass spectrometer was set to collect one MS1 scan (Orbitrap; 120K resolution; AGC target 2x105; max IT 100 ms) followed by data-dependent, “Top Speed” (3s) MS2 scans (collision induced dissociation; ion trap; NCE 35; AGC 5x103; max IT 100 ms). For multinotch-MS3, the top 10 precursors from each MS2 were fragmented by HCD followed by Orbitrap analysis (NCE 55; 60K resolution; AGC 5x104; max IT 120 ms, 100-500 m/z scan range).

2.4.14.3 Data analysis

Proteome Discoverer v2.4 (ThermoFisher) was used for data analysis. MS2 spectra were searched against SwissProt human protein database (20353 entries; downloaded on 06/17/2020) using the following search parameters: MS1 and MS2 tolerance were set to 20 ppm and 0.5 Da, respectively; carbamidomethylation of cysteines (57.02146 Da) and TMT labeling of lysine and N-termini of peptides (229.16293 Da) were considered static modifications; oxidation of methionine (15.9949 Da) and deamidation of asparagine and glutamine (0.98401 Da) were considered variable. Identified proteins and peptides were filtered to retain only those that passed ≤1% FDR threshold. Quantitation was performed using high-quality MS3 spectra (average signal-to-noise ratio of 6 and<50% isolation interference).

2.4.15 Immunocytochemistry

Cells were plated on glass coverslips (Fisher Scientific, 1254) or 96-well black plates (Revvity, 6055302) and grown as described above. Cells were fixed with ice-cold 4% paraformaldehyde (PFA; Sigma, P6148) for 10m then rinsed with PBS. Cells were permeabilized at RT with 0.1% Triton X-100 (Bio-Rad, 161-0407) in PBS for 20m, followed by 10 mM glycine + PBS for 20m. Afterwards, cells were blocked for 1h at RT in blocking buffer (0.1% Triton-X-100, 2% fetal calf serum, and 3% BSA in MiliQ water) before O/N incubation at 4°C in primary antibodies diluted in blocking buffer (**Table 2.3. Antibodies**). The following day, cells were washed 3 times with PBS for 5m then incubated with secondary antibodies in blocking buffer for 1h at RT. After secondary incubation, cells were washed in Hoechst 33258 dye (Hoechst; Invitrogen, H3569) diluted at 1:5,000 in PBS for 10m at RT to mark the nucleus. After nuclei staining, cells were again washed 3 times. Cells in 96-well black plates were topped off with 150 µL of PBS and imaged as described below. Cells plated on glass coverslips were mounted on Superfrost Plus Microscope Slides (Fisher, 1255015) with Prolong Gold Antifade Mounting Reagent (Fisher, P10144) and allowed to dry O/N before imaging using confocal microscopy as described below. Images were analyzed by collecting measurements within cellular regions of interest (ROIs) using custom ImageJ/FIJI macros. Graphs were made using R.

2.4.16 Confocal microscopy

Confocal images were taken on a Nikon AXR NSPARC confocal system equipped with a 40x CFI 489 Apochromat LWD Lambda S objective with a working distance of 0.33 mm, and a 60x NA1.42 Oil/DIS 488 Plan-Apochromat Lambda D objective with a working distance of 1.5 mm.

2.4.17 Longitudinal microscopy and survival analysis

2.4.17.1 Semi-automated longitudinal fluorescent microscopy

For survival analysis experiments, neurons were plated, treated, and transfected/transduced as described above before day (D) 1 of imaging. Beginning on D1 of imaging, neurons were imaged every 24h for the duration of the experiment (see figure legends for experiment specific timelines). Neurons were imaged using a Nikon Eclipse Ti inverted microscope with PerfectFocus3a 20x objective lens and either an Andor iXon3 897 EMCCD or Andor Zyla 4.2 (+)sCMOS camera as previously described[77–79,81,82]. A Lambda CL Xenon lamp (Sutter) with 5 mm liquid light guide (Sutter) was used to illuminate samples, and custom scripts written in BeanShell for use in micromanager controlled all stage movements, shutters, and filters.

2.4.17.2 Automated survival analysis

For automated survival analysis of rat primary neurons, custom ImageJ/FIJI macros and Python scripts were used to identify neurons and draw cellular ROIs based upon size, morphology, and fluorescence intensity. Custom Python scripts were used to track ROIs over time, and cell death was marked by meeting a set of criteria that included loss of fluorescence, degeneration of neurite processes, and rounding of the soma as previously described[81–83].

2.4.17.3 Manual survival analysis

For manual survival analysis of iNeurons, image time series were processed by flat-field correction and image registration, then programmatically de-identified for blinded analysis. Time-series were then uploaded to a browser-based computer vision annotation tool (CVAT.ai) where a trained user manually annotated iNeuron time series using the point tracking mode. Briefly, individual fluorescent-positive cells were identified at D1, and

cell fate was tracked until the end of the time series. Cell death was identified by deformation of rounded somas into amorphous blebs, degeneration of neurite processes, and loss of fluorescence, and was recorded by marking tracks as “outside” (uncensored event) at the given time point. Live neurons at the final time point were not marked as “outside” (right-censored event).

For all automated and manual survival analyses, cox proportional hazards model was applied to the datasets in each experiment, stratifying by biological replicates, and the corresponding hazard plots and tables were generated in Visual Studio Code v1.100.2 (Microsoft) and R Studio v4.4.2 (**Table 2.7. Software and algorithms**).

2.4.18 Plasmids

Primers used for site-directed mutagenesis (SDM) and PCR amplifications were ordered from IDT (**Table 2.4. Oligonucleotides**). Plasmids for homology directed repair (HDR) and VPS13A KO were synthesized by Blue Heron (**Table 2.5. Recombinant DNA**). All plasmids were verified by Sanger sequencing prior to use.

pGW1-mNeonGreen (**mNG**) was synthesized by isolating the open reading frame of mNG from a VPS13A-mNG HDR plasmid previously obtained from Blue Heron and cloning it into an empty pGW1 plasmid. In short, mNG was cut and PCR amplified from VPS13A-mNG HDR using oligos described in **Table 2.4. Oligonucleotides** and PrimeSTAR GXL DNA polymerase (TaKaRa, R050A), then purified using the DNA clean & concentrator-5 (DNA C&C; Zymo Research, D4004). Purified mNG and pGW1 plasmid were double digested using KpnI-HF (NEB, R3142S) and AgeI-HF (NEB, R3552S). Digested plasmids were then cleaned using DNA C&C, ligated with T4 DNA ligase (NEB; M0202S), and transformed into TOP10 competent cells (Thermo Fisher). Clones were picked and Sanger sequenced using primers listed in **Table 2.4. Oligonucleotides**.

pSpCas9(BB)-2A-GFP_sgVPS13A (**VPS13A-sgRNA**) was generated by cloning guide sequences targeting VPS13A into the pSpCas9(BB)-2A-Puro (pX459) v2.0 plasmid (pX459 plsamid; Addgene, 62988). Briefly, pX459 was digested using BbsI-HF (NEB, R3539L), dephosphorylated using alkaline phosphatase (Thermo Fisher), and gel purified using Zymoclean Gel DNA Recovery Kit (Zymo Research, D4008). DNA oligos containing the guide sequences (**Table 2.4. Oligonucleotides**) were annealed and phosphorylated using T4 polynucleotide kinase (NEB, M0201S). Purified digested plasmids and annealed

oligos were ligated using Quick Ligase (NEB, M2200S) and transformed into Stbl3 competent cells (Thermo Fisher). Clones were picked and Sanger sequenced using primers noted in **Table 2.4. Oligonucleotides**.

To make **FUGW–HMGA1** (**HMGA1-GFP**), HMGA1 isolated from an untagged FUGW-HMGA1 (no GFP) plasmid previously obtained from GeneArt (Thermo Fisher), was cloned into FUGW–EGFP (Addgene, 14883). First, HMGA1 was cut and PCR amplified from the FUGW–HMGA1 (no GFP) plasmid using oligos described in **Table 2.4. Oligonucleotides** and Q5 Hot Start High-Fidelity 2X Master Mix (NEB, M0494S). DpnI (NEB, R0176S) treatment was used to isolate amplified HMGA1 which was then purified using DNA C&C. Purified HMGA1 and the FUGW-GFP plasmid were double digested using BamHI-HF (NEB, R3136S) and AgeI-HF (NEB, R3552S), and dephosphorylated using Quick CIP (NEB, M0525S). Digested plasmids were gel purified, ligated using Quick Ligase (NEB, M2200S), and then transformed into NEB 10-beta competent cells (NEB, C3019H). Clones were picked and whole plasmids were sequenced without primers using third generation sequencing (NGS generation 3) by Eurofins Scientific.

2.4.19 Quantification and statistical analysis

Statistical analysis and graphs were done using Prism, R, and Visual Studio Code software described in **Table 2.7. Software and algorithms**. Open-source R packages and customized R scripts used for specific experiments are detailed below.

All survival studies include biological replicates that were treated identically, but the experiments were performed at separate times. To combine data from biological replicates, we stratified the results based on experimental date. n indicates the number of cells analyzed. Statistical information, including mean and statistical significance value, is indicated in the figures or figure legends. At least three biological replicates were used per experiment. Data were considered statistically significant at *$p<0.05$, **$p<0.01$, and ***$p<0.001$.

2.4.20 Study approval

All vertebrate animal work was approved by the Committee on the Use and Care of Animals (UCUCA) at the University of Michigan, and all experiments were performed in accordance with UCUCA guidelines and designed to minimize animal use. Rats used

for primary neuron survival experiments were housed individually in chambers equipped with environmental enrichment and were cared for by the University of Michigan Unit for Laboratory Animal Medicine (Unit). All individuals involved in the care or long-term maintenance of rats were trained and approved by the Unit in accordance with the NIH-supported Guide for the Care and Use of Laboratory Animals. Personnel who handled the rats and administered euthanasia were properly trained in accordance with the University of Michigan Policy for Education and Training of Animal Care and Use Personnel. Euthanasia was consistent with the recommendations of the Guidelines on Euthanasia of the American Veterinary Medical Association. Brains from individual pups in each litter were pooled to maximize cell counts prior to plating and as a result, primary cortical neurons used for all studies included a mix of cells from both male and female pups.

2.4.21 Resource availability

2.4.21.1 Lead contact

Further information and requests for resources and reagents should be directed to and will be fulfilled by the lead contact, Sami Barmada (sbarmada@med.umich.edu).

2.4.21.2 Material availability

Plasmids and unique reagents generated in this manuscript are available by contacting the lead contact, Sami Barmada (sbarmada@med.umich.edu).

2.4.21.3 Data and code availability

RNA-seq and TMT labeling with LS MS/MS data have been deposited at GEO (accession number GSE126678) and are publicly available as of the date of publication. Accession numbers are listed in **Table 2.7. Software and algorithms**. Any additional information required to reanalyze the data reported in this paper is available from the lead contact upon request.

2.4.22 Reagents

Table 2.1 Cell lines

Cell Lines	Source	Identifier
Control (WT) HEK293T	ATCC	CRL-3216

Primary rat neurons	Charles River Laboratories	Long-Evans rat (Crl:LE)
VPS13A knockout (V-KO) HEK293T	This paper	NA
VPS13A mNeonGreen (V-mNG) HEK293T	This paper	NA
VPS13A disease patient (patient) iPSCs/NPs/iNeurons	This paper	ChAc1
Familial control (fam cntrl) iPSCs/NPs/iNeurons	This paper	ChAc4
1021 + hNgn1/2 control (WT) iPSCs/NPs/iNeurons	Weskamp et al., 202068	NA
VPS13A knockout 1021 + hNgn1/2 (V-KO) iPSCs/NPs/iNeurons	This paper	NA

Table 2.2 Chemical and peptides

Drug	**Source**	**Identifier**
Bafilomycin-A1 (BafA1)	Millipore Sigma	474787
Carbonyl cyanide m-chlorophenyl hydrazone (CCCP)	Cayman Chemical	25458
Torin1	Tocris	4247
Doxycycline hydrochloride (DOX)	Millipore Sigma	D3447
Dimethyl sulfoxide (DMSO)	Fisher Bioreagents	BP231-100
Lipofectamine 2000 transfection reagent	Invitrogen	11668027
mNeonGreen-Trap magnetic agarose	ChromoTek	ntma
GFP-Trap magnetic agarose	ChromoTek	gtma

Table 2.3 Antibodies

Antibody	**Application – Dilution**	**Source**	**Identifier**
Guinea pig polyclonal anti-VGlut1	ICC – 1:100	Millipore	AB5905; RRID: AB_2301751
Rabbit monoclonal anti-Synapsin-I	ICC – 1:100	Cell Signaling Technology	5297; RRID: AB_2616578

Chicken polyclonal anti-MAP2	ICC – 1:2,000	Novus Biologicals	NB300-213; RRID: AB_2138178
Human monoclonal anti-Actin	ICC – 1:100	Abcam	ab213251; RRID: ?
Rabbit polyclonal anti-VPS13A	WB – 1:1,000 in 4% Milk/TBST	Atlas Antibodies	HPA021662; RRID: AB_1858760
Rabbit polyclonal anti-alpha Tubulin	WB – 1:5,000 in 3% BSA/TBST	Abcam	ab18251; RRID: AB_2210057
Mouse monoclonal anti-GAPDH	WB – 1:1,000 in 3% BSA/TBST	Millipore	MAB374; RRID: AB_2107445
Rabbit polyclonal anti-β Actin	WB – 1:1,000 in 3% BSA/TBST	Cell Signaling Technology	4967; RRID: AB_330288
Mouse monoclonal anti-mNeonGreen	WB – 1:1,000 in 3% BSA/TBST	ChromoTek	32f6; RRID: AB_2827566
Rabbit polyclonal anti-GFP	WB – 1:1,000 in 3% BSA/TBST	Abcam	ab290; RRID: AB_303395
Mouse monoclonal anti-GFP	WB – 1:1,000 in 3% BSA/TBST	Invitrogen	MA5-15256; RRID: AB_1097928
Rabbit polyclonal anti-HMGA1	ICC – 1:250	Sigma-Aldrich	HPA065612; RRID: ?
Rabbit polyclonal anti-HGMA1	ICC – 1:500	Invitrogen	PA5-78007; RRID: AB_2735908
Rabbit monoclonal anti-HGMA1	IHC – 1:100	Invitrogen	MA5-35485; RRID: AB_2849386
Rabbit polyclonal anti-SP1	ICC – 1:100	Atlas Antibodies	HPA001853; RRID: AB_1080069
Rabbit polyclonal anti-TEX264	WB – 1:1,000 in 5% Milk/TBST	Novus Biologicals	NBP1-89866; RRID: AB_11009420
Rabbit monoclonal anti-Mfn2	WB – 1:1,000 in 5% Milk/TBST	Cell Signaling Technology	9482; RRID: AB_2716838
Rabbit polyclonal anti-ABCD1	WB – 1:1,000 in 3% BSA/TBST ICC – 1:100	Proteintech	50-172-6925
Rabbit polyclonal anti-CRMP4	WB – 1:1,000 in 5% Milk/TBST ICC – 1:1,000	Millipore	AB5454; RRID: AB_91876

Mouse monoclonal anti-Calnexin	ICC – 1:100	Invitrogen	MA3-027; RRID: AB_2069043
Goat polyclonal anti-chicken Alexa Flour 488	ICC – 1:100	Invitrogen	A-11039; RRID: AB_2534096
Donkey polyclonal anti-human Alexa Flour 488-AffiniPure	ICC – 1:100	Jackson ImmunoResearch Labs	709-545-149; RRID: AB_2340566
Goat polyclonal anti-guinea pig Alexa Flour 488	ICC – 1:250	Invitrogen	A-11073; RRID: AB_2534117
Donkey polyclonal anti-rabbit Alexa Flour Plus 488	ICC – 1:500	Invitrogen	A32790; RRID: AB_276283
Donkey polyclonal anti-mouse Alexa Flour Plus 488	ICC – 1:500	Invitrogen	A32766; RRID: AB_276282
Goat polyclonal anti-chicken Alexa Flour 568	ICC – 1:100	Invitrogen	A-11041; RRID: AB_2534098
Donkey polyclonal anti-goat Alexa Flour 568	ICC – 1:500	Invitrogen	A-11057; RRID: AB_2534104
Donkey polyclonal anti-rabbit Alexa Flour 568	ICC – 1:500	Invitrogen	A10042; RRID: AB_2534017
Donkey polyclonal anti-mouse Alexa Flour 568	ICC – 1:500	Invitrogen	A10037; RRID: AB_11180865
Goat polyclonal anti-chicken Alexa Flour 647	ICC – 1:500	Invitrogen	A-21449; RRID: AB_2535866
Goat polyclonal anti-human Alexa Flour 647	ICC – 1:250	Invitrogen	A21445; RRID: AB_2535862
Donkey polyclonal anti-goat Alexa Flour Plus 647	ICC – 1:500	Invitrogen	A32849; RRID: AB_2762840
Donkey polyclonal anti-rabbit Alexa Flour Plus 647	ICC – 1:500	Invitrogen	A32795; RRID: AB_2762835

Goat polyclonal anti-mouse Alexa Flour Plus 647	ICC – 1:500	Invitrogen	A32728; RRID: AB_2633277
Donkey polyclonal anti-mouse Alexa Flour 647	ICC – 1:500	Invitrogen	A31571; RRID: AB_162542
Rabbit polyclonal anti-goat peroxidase AffiniPure	WB – 1:10,000	Jackson ImmunoResearch Labs	305-035-003; RRID: AB_2339400

Table 2.4 Oligonucleotides

Primer Name	**Target**	**Target Sequence Location**	**Direction**	**Sequence (5' to 3')**
ABCD1 FW (p2704)	amplify ABCD1 mRNA	5' ABCD1	FW	AACATCCCGCGGATCACGA
ABCD1 RV (p2705)	amplify ABCD1 mRNA	5' ABCD1	RV	CTCCAGGGATCACCATCTTCC
CRMP4-all FW (p2708)	amplify CRMP4 all isoforms	5' CRMP4	FW	AGCCTGACTGAGGCCTATGA
CRMP4-all RV (p2709)	amplify CRMP4 all isoforms	5' CRMP4	RV	TCCTGCTTGACGCTGTCATT
VPS13A-KO sgRNA #1 SS RV (p1539)	sgRNA # 1 targeting VPS13A to insert V-KO-iRFP-stop HDR plasmid (sense strand)	5' UTR right before ATG start of VPS13A	RV	CACCGCCATGTTCCTCAGCCGTGGT
VPS13A-KO sgRNA #1 AS RV (p1540)	sgRNA # 1 targeting VPS13A to insert V-KO-iRFP-stop HDR plasmid (antisense strand)	5' UTR right before ATG start of VPS13A	RV	AAACACCACGGCTGAGGAACATGGC
VPS13A-KO sgRNA	sgRNA # 2 targeting VPS13A to insert V-KO-	within exon 1	FW	CACCGACGTGTTGAACCGGTTCTT

#2 SS FW (p1537)	iRFP-stop HDR plasmid (sense strand)			
VPS13A-KO sgRNA #2 AS FW (p1538)	sgRNA # 2 targeting VPS13A to insert V-KO-iRFP-stop HDR plasmid (antisense strand)	within exon 1	FW	AAACAAGAACCGGTTCAACACGTC
VPS13A 5' UTR FW (p1831)	Amplify/ sequence VPS13A and V-KO	5' UTR	FW	CGGAGCCGGTGAACCG
iRFP 3' FW (p2266)	sequence iRFP insertion in V-KO	3' end of iRFP	FW	GCAGATCGGCGTGATGGAAG
VPS13A downstream E1 RV (p1830)	amplify VPS13A	downstream of exon 1	RV	GGACTTGAACGCCAGAC
VPS13A-mNG 5' E35 FW (p1002)	Target genomic VPS13A exon 35 to insert mNG	within exon 35	FW	CTTAGTCAAGAAGATATAACAAC
VPS13A-mNG sgRNA #1 SS RV (p1184)	sgRNA # 1 targeting VPS13A to insert mNG (sense strand)	within exon 35	RV	CACCGGTCTTTTGTTACAGCAGGTG
VPS13A-mNG sgRNA #1 AS RV (p1185)	sgRNA # 1 targeting VPS13A to insert mNG (antisense strand)	within exon 35	RV	AAACCACCTGCTGTAACAAAAGACC
VPS13A-mNG sgRNA #2 SS FW (p1182)	sgRNA # 2 targeting VPS13A to insert mNG (sense strand)	within exon 35	FW	CACCGACTAATGCTTCACACCATTC

VPS13A-mNG sgRNA #2 AS FW (p1182)	sgRNA #2 targeting VPS13A to insert mNG (antisense strand)	within exon 35	FW	AAACGAATGGTGTGAAGCATTAGTC
5' mNG KpnI-Kozac FW (p2129)	Amplify mNG. Contains KpnI-HF recognition site + Kozak consensus sequence + ATG start + first 16 nucleotides of mNG	5' end of mNG in VPS13A-mNG HDR plasmid	FW	atccGGTACCgccaccatgGTGAGCAAGGGCGAGG
3' mNG AgeI RV (p2130)	Amplify mNG. Contains last 16 nucleotides of mNG + TAG stop + AgeI-HF recognition site	3' end of mNG in VPS13A-mNG HDR plasmid	RV	cagtaccggtCTACTTGTACAGCTCGTCC
VPS13A upstream E35 FW (p2258)	amplify/ sequence VPS13A and V-mNG	upstream of exon 35	FW	TGGTGTGGTAGAGGATTGAAACA
VPS13A-mNG upstream FW (p2283)	amplify/ sequence mNG insertion in V-mNG	upstream of exon 35	FW	ACAAGCTACTAAAGAGCACATGG
VPS13A E35 FW (p2291)	sequence VPS13A	within exon 35	FW	AACAAAAGACCAATACAGTGCC
VPS13A E35 RV (p2292)	sequence VPS13A	within exon 35	RV	TGCTGTAACAAAAGACCAATACA
mNG 3' FW (p2264)	sequence mNG insertion in V-mNG	3' end of mNeonGreen	FW	GAAGAACCAGCCGATGTACG

VPS13A-mNG downstream RV (p2284)	amplify/ sequence mNG insertion in V-mNG	downstream of exon 35	RV	GGAGCTACAGGGAAGTCAGGA
VPS13A downstream E35 RV (p2259)	amplify/ sequence VPS13A and V-mNG	downstream of exon 35	RV	AGAGATGTCTGAATGGAATTAGCTG
VPS13A E45 FW (p2256)	amplify VPS13A close to 3' end	within exon 45	FW	ACACAGAGAGTCTGGCGTTG
VPS13A E46 RV (p2257)	amplify VPS13A CDS close to 3' end	within exon 46	RV	CAGGTGAGGCAGTTCCCAAT
VPS13A-sgRNA sSS FW (p2579)	gN19 RNA guides to target VPS13A & insert into G700 (cas9)	VPS13A exon 3	FW	CACCGCTTCCAAAACAGCTTCAAC
VPS13A-sgRNA sAS RV (p2580)	gN19 RNA guides to target VPS13A & insert into G700 (cas9)	VPS13A exon 3	RV	AAACGTTGAAGCTGTTTTGGAAGC
pX335-U6 promoter FW (p0687)	Sequencing pSpcas9 (BB)-2A-Puro plasmids containing NT or VPS13A targeting guide RNAs	U6 promoter region	FW	ACTATCATATGCTTACCGTAAC
5' HMGA1 BamHI Kozac FW	Amplify HMGA1. Contains BamHI-HF recognition site + Kozak consensus sequence + ATG start + first 16 nucleotides of HMGA1	5' end of HMGA1 in untagged FUGW-HMGA1 plasmid	FW	ATGCGGATCCGCCACCATGAGTGAGT

3' HMGA1 AgeI RV	Amplifying HMGA1. Contains last 15 nucleotides of HMGA1 (excluding stop codon) + AgeI-HF recognition site	3' end of HMGA1 in untagged FUGW-HMGA1 plasmid	R	TACTACCGGTTGCTCCTCCTCCGAG
HMGA1a FW (p2808)	amplify HMGA1	5' HMGA1	FW	CGCTGGTAGGGAGTCAGAAGG
HMGA1a RV (p2809)	amplify HMGA1	5' HMGA1	RV	GTCTTGGCAGCACCCTTGTT

Table 2.5 Recombinant DNA

Plasmid	**Source**	**Identifier**
pGW1 (G0280)	Barmada S.J., et al. (2015)[78]	
pGW1-mApple (G130)	Barmada S.J., et al. (2015)[78]	
pGW1-iRFP (G344)	Gift from Lisa Sharkey, University of Michigan[174]	
pGW1-mNeonGreen (mNG; G1046)	This paper	
pX335-U6-Chimeric_BB-CBh-hSpCas9n (D10A) (pX335; G268)	Addgene; Cong L., et al. (2013)[95]	#42335 RRID: Addgene_42335
VPS13A-mNeonGreen HDR (G511)	Eurofins Genomic Blue Heron	
V-KO-iRFP-STOP HDR	Eurofins Genomic Blue Heron	
FUGW (EGFP; G1215)	Barmada S.J., et al. (2015)[78]	#14883 RRID: Addgene_14883
FUGW-HMGA1 (untagged, no GFP; G1461)	GeneArt Gene Synthesis, Thermo Fisher Scientific; This paper	
FUGW-HMGA1 (HMGA1-EGFP; G1489)	This paper	
pLV-Syn1-RGEDI-T2A-GFP (RGEDI)	VectorBuilder, Vector Design; Linsley J.W., et al. (2021)[175]	

pCAG-Lifeact-mRuby2 (Lifeact-mRuby2)	Gift from Asim Beg, University of Michigan; Parker S.S., et al. (2018)[176]	
pSpCas9(BB)-2A-GFP (pX459) (NT-sgRNA)	Addgene; Ran F.A., et al. (2013)[87]	#48138; RRID: Addgene_48138
pSpCas9(BB)-2A-GFP_sgVPS13A (VPS13A-sgRNA)	This paper	
GIPZ non-silencing lentiviral shRNA control (NT-shRNA)	Dharmacon	RHS4346
GIPZ HMGA1-targeting lentiviral shRNA (HMGA1-shRNA)	University of Michigan Vector Core; Dharmacon	Clone ID: V2LHS_195590; RHS4430-200175058

Table 2.6 Viruses and bacterial strains

Reagent	Source	Identifier
pLentilox-RSV2dsRed	University of Michigan Vector Core	

Table 2.7 Software and algorithms

Software/algorithm	Source	Identifier
Automated imaging and survival analysis	Flores B.N., et al. (2019)[77], Archbold H.C., et al. (2018)[84], Weskamp K., et al.(2019)[82], Malik A.M., et al.(2018)[83], McMillan M., et al. (2023)[86]	
ImageJ	Schindelin J., et al. (2012)[177], Fiji	RRID: SCR_002285
CVAT.ai	Facebook	
AdvaitaBio	Advaita Corporation	
GeneTools	Syngene	RRID: SCR_022505
GeneSys	Syngene	RRID: SCR_015770
Cutadapt v2.3	Martin M. (2011)[162]	RRID: SCR_011841
FastQC v0.11.8	Babraham Bioinformatics[164], Wingett S.W., et al. (2018)[163]	RRID: SCR_014583
STAR v2.7.8a	Dobin A., et al. (2013)[169]	RRID: SCR_004463
RSEM v1.3.3	Li B., et al. (2011)[170]	RRID: SCR_000262

MultiQC v1.7	Ewels P. (2016)[171]	RRID: SCR_014982
Proteome Discoverer v2.4	ThermoFisher	RRID: SCR_014477
SwissProt human protein database	Expasy: Swiss Bioinformatics Resource Portal	
DESeq2 v1.34.0	Bioconductor Love M.I., et al. (2014)[172]	RRID: SCR_015687
HISAT2	Kim D., et al. (2015)[165]	RRID: SCR_015530
HaplotypeCaller	Genome Analysis Toolkit (GTAK); DePristo M.A., et al. (2011)[166]	RRID: SCR_001876
ANNOVAR	Wang K., et al. (2010)[167]	RRID: SCR_012821
GraphPad Prism version 10.4.1 (Prism)	GraphPad Software	RRID: SCR_002798
R	The R Foundation	RRID: SCR_001905
R Studio version 4.4.2	postit	RRID: SCR_000432
Visual Studio Code version 1.100.2	Microsoft	RRID:SCR_026031
STRING-db version 12.0	Von Mering C., et al.(2003)[178], Franceschini A., et al. (2013)[179]	RRID: SCR_005223
R package – car version 3.1-3		RRID: SCR_022137
R package – cowplot version 1.2.0		RRID: SCR_018081
R package – ggbeeswarm version 0.7.2		RRID: SCR_026875
R package – ggpubr version 0.6.1		RRID: SCR_021139
R package – ggrepel version 0.9.6		RRID: SCR_017393
R package – ggsignif version 0.6.4		
R package – glue version 1.8.0		RRID: SCR_025249
R package – gridExtra version 2.3		
R package – magrittr version 2.0.3		

R package – patchwork version 1.3.1		
R package – SuperExactTest version 1.1.0	Wang M., et al. (2015)[180]	
R package – survival version 3.8-3		
R package – survminer version 0.5.0		
R package – tidyverse version 2.0.0		

2.5 Author contributions

Study design: GR and SJB

Whole-genome sequencing: AT, ST

Plasmid generation: GR, ET, SJB, GeneArt Gene Synthesis (ThermoFisher Scientific), Addgene, Dharmacon, University of Michigan Vector Core

Cloning: GR, ET, BF, (Assisted: RR, SC)

Virus generation: GR, University of Michigan Vector Core

qRT-PCR: GR

Western blot assays: GR, (Assisted: RR, AS, AE)

Immunocytochemistry: GR, (Assisted: RR, SC, SA)

Immunohistochemistry: JFC, RHW, CDS, EP

Confocal and automated microscopy: GR, (Assisted: RR, AE, SC, SA)

Light microscopy and IHC analysis: EP, JC, RW, CDS, ELT

TMT LS-MS/MS & proteomics analysis: GR, University of Michigan Advanced Genomics Core, University of Michigan Bioinformatics Core

RNAseq & analysis: GR, core, University of Michigan Advanced Genomics Core, University of Michigan Bioinformatics Core

Wrote code for image acquisition, neuronal survival analysis, and immunocytochemistry analysis: GR, JW

iPSC and HEK293T cell line creation: ET

Maintained iPSCs and differentiated them into neurons: GR, ET

Isolated and cultured primary neurons: XL
Conducted initial neuronal survival experiments: AT, TQ
Analyses: GR
Assembled figures, wrote, and edited the manuscript: GR and SJB

2.6 Funding support

This work was supported by the Weinbaum Lakritz family and the Weinbaum Lakritz Research Fund, the National Institutes of Health (R01NS097542, R01NS113943, and 1R56NS128110-01 to SJB; P30AG072931 to the University of Michigan Brain Bank and Alzheimer's Disease Research Center), the family of Angela Dobson and Lyndon Welch, the University of Michigan Rackham Merit Fellowship, the Society for Neuroscience: Neuroscience Scholars Program (NSP), the Robert Packard Center for ALS Research, the A. Alfred Taubman Medical Research Institute, and the Danto Family, Ann Arbor Active Against ALS. Contributions from the Icahn School of Medicine (JFC, CDS, RHW) were supported by a grant from NA Advocacy USA.

2.7 Acknowledgments

First and foremost, we thank all the individuals who graciously donated their skin cells used to make iPSCs, as well as the people who kindly donated post-mortem brain tissue used to conduct histological assays. We would like to thank the following centers (and doctors at these centers) for collecting the post-mortem brain tissue: Mount Sinai Hospital, New York City, New York, USA; Dr. Brandon Barton at Rush University, Chicago, Illinois, USA; and Dr. Kevin Peikert at the University of Frankfurt am Main, Rostock, Germany. We would like to thank the Neuropathology Brain Bank & Research CoRE, Icahn School of Medicine at Mount Sinai for processing the post-mortem brain tissue and conducting the histological staining. We are also extremely grateful to Dr. Henry Paulson and Dr. Peter Todd, as well as the members of their respective laboratories, in the Department of Neurology at the University of Michigan, for sharing antibodies and other reagents. Additionally, we thank: Tonya Kopas at the University of Michigan Vector Core for lentivirus preparation, and Venkatesha Basrur at the University of Michigan Proteomics Resource Facility for assisting in the relative quantitation of LC-MS/MS. Finally, we thank the University of Michigan Advanced Genomics Core for

assisting in next-generation RNA seq and Rebecca Tagett at the University of Michigan Bioinformatics Core who was critical for analyzing the next-generation RNA sequencing results.

References

1. Jung, H.H., Danek, A., and Walker, R.H. (2011). Neuroacanthocytosis syndromes. Orphanet J. Rare Dis. *6*, 68. https://doi.org/10.1186/1750-1172-6-68.

2. Peikert, K., Hermann, A., and Danek, A. (2022). XK-associated McLeod syndrome: Nonhematological manifestations and relation to VPS13A disease. Transfus. Med. Hemother. *49*, 4–12. https://doi.org/10.1159/000521417.

3. Peikert, K., Dobson-Stone, C., Rampoldi, L., Miltenberger-Miltenyi, G., Neiman, A., De Camilli, P., Hermann, A., Walker, R.H., Monaco, A.P., and Danek, A. (1993). VPS13A disease. In GeneReviews(®) (University of Washington, Seattle).

4. Walker, R.H., Peikert, K., Jung, H.H., Hermann, A., and Danek, A. (2023). Neuroacanthocytosis syndromes: The clinical perspective. Contact (Thousand Oaks.) *6*, 25152564231210340. https://doi.org/10.1177/25152564231210339.

5. Ditzel, R.M., Jr, Walker, R.H., Nirenberg, M.J., Tetlow, A.M., Farrell, K., Lind-Watson, K.J., Thorn, E.L., Dangoor, D.K., Gordon, R., De Sanctis, C., et al. (2023). An autopsy series of seven cases of VPS13A disease (chorea-acanthocytosis). Mov. Disord. *38*, 2163–2172. https://doi.org/10.1002/mds.29589.

6. Walker, R.H., Miranda, M., Jung, H.H., and Danek, A. (2019). Life expectancy and mortality in chorea-acanthocytosis and McLeod syndrome. Parkinsonism Relat. Disord. *60*, 158–161. https://doi.org/10.1016/j.parkreldis.2018.09.003.

7. Suzuki, F., Sato, N., Sugiyama, A., Iijima, K., Shigemoto, Y., Morimoto, E., Kimura, Y., Fujii, H., Takahashi, Y., Nakata, Y., et al. (2021). Chorea-acanthocytosis: Time-dependent changes of symptoms and imaging findings. J. Neuroradiol. *48*, 419–424. https://doi.org/10.1016/j.neurad.2019.11.006.

8. Lossos, A., Dobson-Stone, C., Monaco, A.P., Soffer, D., Rahamim, E., Newman, J.P., Mohiddin, S., Fananapazir, L., Lerer, I., Linetsky, E., et al. (2005). Early clinical heterogeneity in choreoacanthocytosis. Arch. Neurol. *62*, 611–614. https://doi.org/10.1001/archneur.62.4.611.

9. Vaisfeld, A., Bruno, G., Petracca, M., Bentivoglio, A.R., Servidei, S., Vita, M.G., Bove, F., Straccia, G., Dato, C., Di Iorio, G., et al. (2021). Neuroacanthocytosis syndromes in an Italian cohort: Clinical spectrum, high genetic variability and muscle involvement. Genes (Basel) *12*, 344. https://doi.org/10.3390/genes12030344.

10. Bohlega, S., Al-Jishi, A., Dobson-Stone, C., Rampoldi, L., Saha, P., Murad, H., Kareem, A., Roberts, G., and Monaco, A.P. (2003). Chorea-acanthocytosis: clinical and genetic findings in three families from the Arabian peninsula. Mov. Disord. *18*, 403–407. https://doi.org/10.1002/mds.10361.

11. Niemelä, V., Salih, A., Solea, D., Lindvall, B., Weinberg, J., Miltenberger, G., Granberg, T., Tzovla, A., Nordin, L., Danfors, T., et al. (2020). Phenotypic variability in chorea-acanthocytosis associated with novel VPS13A mutations. Neurol. Genet. *6*, e426. https://doi.org/10.1212/NXG.0000000000000426.

12. Yamamoto, T., Hirose, G., Shimazaki, K., Takado, S., Kosoegawa, H., and Saeki, M. (1982). Movement disorders of familial neuroacanthocytosis syndrome. Arch. Neurol. *39*, 298–301. https://doi.org/10.1001/archneur.1982.00510170040011.

13. Ueno, S., Maruki, Y., Nakamura, M., Tomemori, Y., Kamae, K., Tanabe, H., Yamashita, Y., Matsuda, S., Kaneko, S., and Sano, A. (2001). The gene encoding a newly discovered protein, chorein, is mutated in chorea-acanthocytosis. Nat. Genet. *28*, 121–122. https://doi.org/10.1038/88825.

14. Rampoldi, L., Dobson-Stone, C., Rubio, J.P., Danek, A., Chalmers, R.M., Wood, N.W., Verellen, C., Ferrer, X., Malandrini, A., Fabrizi, G.M., et al. (2001). A conserved sorting-associated protein is mutant in chorea-acanthocytosis. Nat. Genet. *28*, 119–120. https://doi.org/10.1038/88821.

15. Nishida, Y., Nakamura, M., Urata, Y., Kasamo, K., Hiwatashi, H., Yokoyama, I., Mizobuchi, M., Sakurai, K., Osaki, Y., Morita, Y., et al. (2019). Novel pathogenic VPS13A gene mutations in Japanese patients with chorea-acanthocytosis. Neurol. Genet. *5*, e332. https://doi.org/10.1212/NXG.0000000000000332.

16. Tomiyasu, A., Nakamura, M., Ichiba, M., Ueno, S., Saiki, S., Morimoto, M., Kobal, J., Kageyama, Y., Inui, T., Wakabayashi, K., et al. (2011). Novel pathogenic mutations and copy number variations in the VPS13A gene in patients with chorea-acanthocytosis. Am. J. Med. Genet. B Neuropsychiatr. Genet. *156B*, 620–631. https://doi.org/10.1002/ajmg.b.31206.

17. Dobson-Stone, C., Velayos-Baeza, A., Filippone, L.A., Westbury, S., Storch, A., Erdmann, T., Wroe, S.J., Leenders, K.L., Lang, A.E., Dotti, M.T., et al. (2004). Chorein detection for the diagnosis of chorea-acanthocytosis. Ann. Neurol. *56*, 299–302. https://doi.org/10.1002/ana.20200.

18. Dobson-Stone, C., Danek, A., Rampoldi, L., Hardie, R.J., Chalmers, R.M., Wood, N.W., Bohlega, S., Dotti, M.T., Federico, A., Shizuka, M., et al. (2002). Mutational spectrum of the CHAC gene in patients with chorea-acanthocytosis. Eur. J. Hum. Genet. *10*, 773–781. https://doi.org/10.1038/sj.ejhg.5200866.

19. Velayos-Baeza, A., Vettori, A., Copley, R.R., Dobson-Stone, C., and Monaco, A.P. (2004). Analysis of the human VPS13 gene family. Genomics *84*, 536–549. https://doi.org/10.1016/j.ygeno.2004.04.012.

20. Kumar, N., Leonzino, M., Hancock-Cerutti, W., Horenkamp, F.A., Li, P., Lees, J.A., Wheeler, H., Reinisch, K.M., and De Camilli, P. (2018). VPS13A and VPS13C are

lipid transport proteins differentially localized at ER contact sites. J. Cell Biol. *217*, 3625–3639. https://doi.org/10.1083/jcb.201807019.

21. De, M., Oleskie, A.N., Ayyash, M., Dutta, S., Mancour, L., Abazeed, M.E., Brace, E.J., Skiniotis, G., and Fuller, R.S. (2017). The Vps13p-Cdc31p complex is directly required for TGN late endosome transport and TGN homotypic fusion. J. Cell Biol. *216*, 425–439. https://doi.org/10.1083/jcb.201606078.

22. Muñoz-Braceras, S., Calvo, R., and Escalante, R. (2015). TipC and the chorea-acanthocytosis protein VPS13A regulate autophagy in Dictyostelium and human HeLa cells. Autophagy *11*, 918–927. https://doi.org/10.1080/15548627.2015.1034413.

23. Tamura, N., Nishimura, T., Sakamaki, Y., Koyama-Honda, I., Yamamoto, H., and Mizushima, N. (2017). Differential requirement for ATG2A domains for localization to autophagic membranes and lipid droplets. FEBS Lett. *591*, 3819–3830. https://doi.org/10.1002/1873-3468.12901.

24. Dall'Armellina, F., Stagi, M., and Swan, L.E. (2023). In silico modeling human VPS13 proteins associated with donor and target membranes suggests lipid transfer mechanisms. Proteins *91*, 439–455. https://doi.org/10.1002/prot.26446.

25. Li, P., Lees, J.A., Lusk, C.P., and Reinisch, K.M. (2020). Cryo-EM reconstruction of a VPS13 fragment reveals a long groove to channel lipids between membranes. J. Cell Biol. *219*, e202001161. https://doi.org/10.1083/jcb.202001161.

26. Yeshaw, W.M., van der Zwaag, M., Pinto, F., Lahaye, L.L., Faber, A.I., Gómez-Sánchez, R., Dolga, A.M., Poland, C., Monaco, A.P., van IJzendoorn, S.C., et al. (2019). Human VPS13A is associated with multiple organelles and influences mitochondrial morphology and lipid droplet motility. Elife *8*, e43561. https://doi.org/10.7554/eLife.43561.

27. Muñoz-Braceras, S., Tornero-Écija, A.R., Vincent, O., and Escalante, R. (2019). VPS13A is closely associated with mitochondria and is required for efficient lysosomal degradation. Dis. Model. Mech. *12*, dmm036681. https://doi.org/10.1242/dmm.036681.

28. Bean, B.D.M., Dziurdzik, S.K., Kolehmainen, K.L., Fowler, C.M.S., Kwong, W.K., Grad, L.I., Davey, M., Schluter, C., and Conibear, E. (2018). Competitive organelle-specific adaptors recruit Vps13 to membrane contact sites. J. Cell Biol. *217*, 3593–3607. https://doi.org/10.1083/jcb.201804111.

29. Tornero-Écija, A., Zapata-Del-Baño, A., Antón-Esteban, L., Vincent, O., and Escalante, R. (2023). The association of lipid transfer protein VPS13A with endosomes is mediated by sorting nexin SNX5. Life Sci. Alliance *6*, e202201852. https://doi.org/10.26508/lsa.202201852.

30. Park, J.-S., Okumura, Y., Tachikawa, H., and Neiman, A.M. (2013). SPO71 encodes a developmental stage-specific partner for Vps13 in Saccharomyces cerevisiae. Eukaryot. Cell *12*, 1530–1537. https://doi.org/10.1128/EC.00239-13.

31. Park, J.-S., Thorsness, M.K., Policastro, R., McGoldrick, L.L., Hollingsworth, N.M., Thorsness, P.E., and Neiman, A.M. (2016). Yeast Vps13 promotes mitochondrial function and is localized at membrane contact sites. Mol. Biol. Cell *27*, 2435–2449. https://doi.org/10.1091/mbc.E16-02-0112.

32. Nishizawa, Y., Sakimoto, H., Nagata, O., Sasaki, N., Urata, Y., Arai, K., Hiwatashi, H., Yokoyama, I., Kishida, S., Sano, A., et al. (2025). Chorein deficiency promotes ferroptosis. FEBS Open Bio *15*, 58–68. https://doi.org/10.1002/2211-5463.13870.

33. Yuan, W., Akşit, A., de Boer, R., Krikken, A.M., and van der Klei, I.J. (2022). Yeast Vps13 is crucial for peroxisome expansion in cells with reduced peroxisome-ER contact sites. Front. Cell Dev. Biol. *10*, 842285. https://doi.org/10.3389/fcell.2022.842285.

34. Federti, E., Matte, A., Riccardi, V., Peikert, K., Alper, S.L., Danek, A., Walker, R.H., Siciliano, A., Iatcenko, I., Hermann, A., et al. (2021). Adaptative up-regulation of PRX2 and PRX5 expression characterizes brain from a mouse model of chorea-acanthocytosis. Antioxidants (Basel) *11*, 76. https://doi.org/10.3390/antiox11010076.

35. Park, J.-S., and Neiman, A.M. (2020). XK is a partner for VPS13A: a molecular link between Chorea-Acanthocytosis and McLeod Syndrome. Mol. Biol. Cell 31, 2425–2436. https://doi.org/10.1091/mbc.E19-08-0439-T.

36. Chen, S., Roberts, M.A., Chen, C.-Y., Markmiller, S., Wei, H.-G., Yeo, G.W., Granneman, J.G., Olzmann, J.A., and Ferro-Novick, S. (2022). VPS13A and VPS13C influence lipid droplet abundance. Contact (Thousand Oaks.) *5*, 25152564221125612. https://doi.org/10.1177/25152564221125613.

37. García-García, E., Chaparro-Cabanillas, N., Coll-Manzano, A., Carreras-Caballé, M., Giralt, A., Del Toro, D., Alberch, J., Masana, M., and Rodríguez, M.J. (2021). Unraveling the spatiotemporal distribution of VPS13A in the mouse brain. Int. J. Mol. Sci. *22*, 13018. https://doi.org/10.3390/ijms222313018.

38. Hayashi, T., Kishida, M., Nishizawa, Y., Iijima, M., Koriyama, C., Nakamura, M., Sano, A., and Kishida, S. (2012). Subcellular localization and putative role of VPS13A/chorein in dopaminergic neuronal cells. Biochem. Biophys. Res. Commun. *419*, 511–516. https://doi.org/10.1016/j.bbrc.2012.02.047.

39. Kurano, Y., Nakamura, M., Ichiba, M., Matsuda, M., Mizuno, E., Kato, M., Agemura, A., Izumo, S., and Sano, A. (2007). In vivo distribution and localization

of chorein. Biochem. Biophys. Res. Commun. *353*, 431–435. https://doi.org/10.1016/j.bbrc.2006.12.059.

40. Lupo, F., Tibaldi, E., Matte, A., Sharma, A.K., Brunati, A.M., Alper, S.L., Zancanaro, C., Benati, D., Siciliano, A., Bertoldi, M., et al. (2016). A new molecular link between defective autophagy and erythroid abnormalities in chorea-acanthocytosis. Blood *128*, 2976–2987. https://doi.org/10.1182/blood-2016-07-727321.

41. Suzuki, S.W., West, M., Zhang, Y., Fan, J.S., Roberts, R.T., Odorizzi, G., and Emr, S.D. (2024). A role for Vps13-mediated lipid transfer at the ER-endosome contact site in ESCRT-mediated sorting. J. Cell Biol. *223*, e202307094. https://doi.org/10.1083/jcb.202307094.

42. Peikert, K., Federti, E., Matte, A., Constantin, G., Pietronigro, E.C., Fabene, P.F., Defilippi, P., Turco, E., Del Gallo, F., Pucci, P., et al. (2021). Therapeutic targeting of Lyn kinase to treat chorea-acanthocytosis. Acta Neuropathol. Commun. *9*, 81. https://doi.org/10.1186/s40478-021-01181-y.

43. Tornero-Écija, A.R., Navas, M.A., Muñoz-Braceras, S., Vincent, O., and Escalante, R. (2023). Effect of rapamycin on lysosomal accumulation in a CRISPR/Cas9-based cellular model of VPS13A deficiency. J. Cell. Mol. Med. *27*, 1557–1564. https://doi.org/10.1111/jcmm.17768.

44. Riccardi, V., Viscomi, C.F., Sandri, M., D'Alessandro, A., Dzieciatkowska, M., Stephenson, D., Federti, E., Hermann, A., Salviati, L., Siciliano, A., et al. (2025). Premature skeletal muscle aging in VPS13A deficiency relates to impaired autophagy. Acta Neuropathol. Commun. *13*, 83. https://doi.org/10.1186/s40478-025-01997-y.

45. van Vliet, A.R., Jefferies, H.B.J., Faull, P.A., Chadwick, J., Ibrahim, F., Skehel, M.J., and Tooze, S.A. (2024). Exploring the ATG9A interactome uncovers interaction with VPS13A. J. Cell Sci. *137*, jcs261081. https://doi.org/10.1242/jcs.261081.

46. Stanslowsky, N., Reinhardt, P., Glass, H., Kalmbach, N., Naujock, M., Hensel, N., Lübben, V., Pal, A., Venneri, A., Lupo, F., et al. (2016). Neuronal dysfunction in iPSC-derived medium spiny neurons from chorea-acanthocytosis patients is reversed by Src kinase inhibition and F-actin stabilization. J. Neurosci. *36*, 12027–12043. https://doi.org/10.1523/JNEUROSCI.0456-16.2016.

47. Honisch, S., Gu, S., Vom Hagen, J.M., Alkahtani, S., Al Kahtane, A.A., Tsapara, A., Hermann, A., Storch, A., Schöls, L., Lang, F., et al. (2015). Chorein sensitive arrangement of cytoskeletal architecture. Cell. Physiol. Biochem. *37*, 399–408. https://doi.org/10.1159/000430363.

48. Shiokawa, N., Nakamura, M., Sameshima, M., Deguchi, A., Hayashi, T., Sasaki, N., and Sano, A. (2013). Chorein, the protein responsible for chorea-acanthocytosis, interacts with β-adducin and β-actin. Biochem. Biophys. Res. Commun. *441*, 96–101. https://doi.org/10.1016/j.bbrc.2013.10.011.

49. Vonk, J.J., Yeshaw, W.M., Pinto, F., Faber, A.I.E., Lahaye, L.L., Kanon, B., van der Zwaag, M., Velayos-Baeza, A., Freire, R., van IJzendoorn, S.C., et al. (2017). Drosophila Vps13 is required for protein homeostasis in the brain. PLoS One *12*, e0170106. https://doi.org/10.1371/journal.pone.0170106.

50. Schmidt, E.-M., Schmid, E., Münzer, P., Hermann, A., Eyrich, A.-K., Russo, A., Walker, B., Gu, S., vom Hagen, J.M., Faggio, C., et al. (2013). Chorein sensitivity of cytoskeletal organization and degranulation of platelets. FASEB J. *27*, 2799–2806. https://doi.org/10.1096/fj.13-229286.

51. Föller, M., Hermann, A., Gu, S., Alesutan, I., Qadri, S.M., Borst, O., Schmidt, E.-M., Schiele, F., vom Hagen, J.M., Saft, C., et al. (2012). Chorein-sensitive polymerization of cortical actin and suicidal cell death in chorea-acanthocytosis. FASEB J. *26*, 1526–1534. https://doi.org/10.1096/fj.11-198317.

52. De Franceschi, L., Tomelleri, C., Matte, A., Brunati, A.M., Bovee-Geurts, P.H., Bertoldi, M., Lasonder, E., Tibaldi, E., Danek, A., Walker, R.H., et al. (2011). Erythrocyte membrane changes of chorea-acanthocytosis are the result of altered Lyn kinase activity. Blood *118*, 5652–5663. https://doi.org/10.1182/blood-2011-05-355339.

53. Yu, W., Honisch, S., Schmidt, S., Yan, J., Schmid, E., Alkahtani, S., AlKahtane, A.A., Alarifi, S., Stournaras, C., and Lang, F. (2016). Chorein sensitive Orai1 expression and store operated Ca2+ entry in rhabdomyosarcoma cells. Cell. Physiol. Biochem. *40*, 1141–1152. https://doi.org/10.1159/000453168.

54. Soczewka, P., Kolakowski, D., Smaczynska-de Rooij, I., Rzepnikowska, W., Ayscough, K.R., Kaminska, J., and Zoladek, T. (2019). Yeast-model-based study identified myosin- and calcium-dependent calmodulin signalling as a potential target for drug intervention in chorea-acanthocytosis. Dis. Model. Mech. *12*, dmm036830. https://doi.org/10.1242/dmm.036830.

55. Alesutan, I., Seifert, J., Pakladok, T., Rheinlaender, J., Lebedeva, A., Towhid, S.T., Stournaras, C., Voelkl, J., Schäffer, T.E., and Lang, F. (2013). Chorein sensitivity of actin polymerization, cell shape and mechanical stiffness of vascular endothelial cells. Cell. Physiol. Biochem. *32*, 728–742. https://doi.org/10.1159/000354475.

56. Kolakowski, D., Kaminska, J., and Zoladek, T. (2020). The binding of the APT1 domains to phosphoinositides is regulated by metal ions in vitro. Biochim. Biophys. Acta Biomembr. *1862*, 183349. https://doi.org/10.1016/j.bbamem.2020.183349.

57. Pelzl, L., Hauser, S., Elsir, B., Sukkar, B., Sahu, I., Singh, Y., Höflinger, P., Bissinger, R., Jemaà, M., Stournaras, C., et al. (2017). Lithium sensitive ORAI1 expression, store operated Ca2+ entry and suicidal death of neurons in chorea-Acanthocytosis. Sci. Rep. *7*, 6457. https://doi.org/10.1038/s41598-017-06451-1.

58. Honisch, S., Fehrenbacher, B., Lebedeva, A., Alesutan, I., Castor, T., Alkahtani, S., Alarifi, S., Schaller, M., Stournaras, C., and Lang, F. (2015). Chorein sensitive dopamine release from pheochromocytoma (PC12) cells. Neurosignals *23*, 1–10. https://doi.org/10.1159/000442599.

59. Kolehmainen, J., Black, G.C.M., Saarinen, A., Chandler, K., Clayton-Smith, J., Träskelin, A.-L., Perveen, R., Kivitie-Kallio, S., Norio, R., Warburg, M., et al. (2003). Cohen syndrome is caused by mutations in a novel gene, COH1, encoding a transmembrane protein with a presumed role in vesicle-mediated sorting and intracellular protein transport. Am. J. Hum. Genet. *72*, 1359–1369. https://doi.org/10.1086/375454.

60. Cohen, M.M., Jr, Hall, B.D., Smith, D.W., Graham, C.B., and Lampert, K.J. (1973). A new syndrome with hypotonia, obesity, mental deficiency, and facial, oral, ocular, and limb anomalies. J. Pediatr. *83*, 280–284. https://doi.org/10.1016/s0022-3476(73)80493-7.

61. Smolders, S., Philtjens, S., Crosiers, D., Sieben, A., Hens, E., Heeman, B., Van Mossevelde, S., Pals, P., Asselbergh, B., Dos Santos Dias, R., et al. (2021). Contribution of rare homozygous and compound heterozygous VPS13C missense mutations to dementia with Lewy bodies and Parkinson's disease. Acta Neuropathol. Commun. *9*, 25. https://doi.org/10.1186/s40478-021-01121-w.

62. Kobayashi, R., Naruse, H., Koyama, S., Kawakatsu, S., Hayashi, H., Ishiura, H., Mitsui, J., Ohta, Y., Toda, T., Tsuji, S., et al. (2020). Familial dementia with Lewy bodies with VPS13C mutations. Parkinsonism Relat. Disord. *81*, 31–33. https://doi.org/10.1016/j.parkreldis.2020.10.008.

63. Lesage, S., Drouet, V., Majounie, E., Deramecourt, V., Jacoupy, M., Nicolas, A., Cormier-Dequaire, F., Hassoun, S.M., Pujol, C., Ciura, S., et al. (2016). Loss of VPS13C function in autosomal-recessive parkinsonism causes mitochondrial dysfunction and increases PINK1/Parkin-dependent mitophagy. Am. J. Hum. Genet. *98*, 500–513. https://doi.org/10.1016/j.ajhg.2016.01.014.

64. Koh, K., Ishiura, H., Shimazaki, H., Tsutsumiuchi, M., Ichinose, Y., Nan, H., Hamada, S., Ohtsuka, T., Tsuji, S., and Takiyama, Y. (2020). VPS13D-related disorders presenting as a pure and complicated form of hereditary spastic paraplegia. Mol. Genet. Genomic Med. *8*, e1108. https://doi.org/10.1002/mgg3.1108.

65. Seong, E., Insolera, R., Dulovic, M., Kamsteeg, E.-J., Trinh, J., Brüggemann, N., Sandford, E., Li, S., Ozel, A.B., Li, J.Z., et al. (2018). Mutations in VPS13D lead to a new recessive ataxia with spasticity and mitochondrial defects. Ann. Neurol. *83*, 1075–1088. https://doi.org/10.1002/ana.25220.

66. Gauthier, J., Meijer, I.A., Lessel, D., Mencacci, N.E., Krainc, D., Hempel, M., Tsiakas, K., Prokisch, H., Rossignol, E., Helm, M.H., et al. (2018). Recessive mutations in VPS13D cause childhood onset movement disorders. Ann. Neurol. *83*, 1089–1095. https://doi.org/10.1002/ana.25204.

67. Chua, J.P., Bedi, K., Paulsen, M.T., Ljungman, M., Tank, E.M.H., Kim, E.S., McBride, J.P., Colón-Mercado, J.M., Ward, M.E., Weisman, L.S., et al. (2022). Myotubularin-related phosphatase 5 is a critical determinant of autophagy in neurons. Curr. Biol. *32*, 2581-2595.e6. https://doi.org/10.1016/j.cub.2022.04.053.

68. Weskamp, K., Tank, E.M., Miguez, R., McBride, J.P., Gómez, N.B., White, M., Lin, Z., Gonzalez, C.M., Serio, A., Sreedharan, J., et al. (2020). Shortened TDP43 isoforms upregulated by neuronal hyperactivity drive TDP43 pathology in ALS. J. Clin. Invest. *130*, 1139–1155. https://doi.org/10.1172/JCI130988.

69. Fernandopulle, M.S., Prestil, R., Grunseich, C., Wang, C., Gan, L., and Ward, M.E. (2018). Transcription factor-mediated differentiation of human iPSCs into neurons: Rapid differentiation of iPSCs into neurons. Curr. Protoc. Cell Biol. *79*, e51. https://doi.org/10.1002/cpcb.51.

70. Lam, R.S., Töpfer, F.M., Wood, P.G., Busskamp, V., and Bamberg, E. (2017). Functional maturation of human stem cell-derived neurons in long-term cultures. PLoS One *12*, e0169506. https://doi.org/10.1371/journal.pone.0169506.

71. Busskamp, V., Lewis, N.E., Guye, P., Ng, A.H.M., Shipman, S.L., Byrne, S.M., Sanjana, N.E., Murn, J., Li, Y., Li, S., et al. (2014). Rapid neurogenesis through transcriptional activation in human stem cells. Mol. Syst. Biol. *10*, 760. https://doi.org/10.15252/msb.20145508.

72. Liu, J., Heinsen, H., Grinberg, L.T., Alho, E., Amaro, E., Jr, Pasqualucci, C.A., Rüb, U., den Dunnen, W., Arzberger, T., Schmitz, C., et al. (2018). Subcortical neurodegeneration in chorea: Similarities and differences between chorea-acanthocytosis and Huntington's disease. Parkinsonism Relat. Disord. *49*, 54–59. https://doi.org/10.1016/j.parkreldis.2018.01.009.

73. Mente, K., Kim, S.A., Grunseich, C., Hefti, M.M., Crary, J.F., Danek, A., Karp, B.I., and Walker, R.H. (2017). Hippocampal sclerosis and mesial temporal lobe epilepsy in chorea-acanthocytosis: a case with clinical, pathologic and genetic evaluation. Neuropathol. Appl. Neurobiol. *43*, 542–546. https://doi.org/10.1111/nan.12403.

74. Miki, Y., Nishie, M., Ichiba, M., Nakamura, M., Mori, F., Ogawa, M., Kaimori, M., Sano, A., and Wakabayashi, K. (2010). Chorea-acanthocytosis with upper motor neuron degeneration and 3419_3420 delCA and 3970_3973 delAGTC VPS13A mutations. Acta Neuropathol. *119*, 271–273. https://doi.org/10.1007/s00401-009-0617-x.

75. Glineburg, M.R., Yildirim, E., Gomez, N., Rodriguez, G., Pak, J., Li, X., Altheim, C., Waksmacki, J., McInerney, G.M., Barmada, S.J., et al. (2024). Stress granule formation helps to mitigate neurodegeneration. Nucleic Acids Res. *52*, 9745–9759. https://doi.org/10.1093/nar/gkae655.

76. Dykstra, M.M., Weskamp, K., Gómez, N.B., Waksmacki, J., Tank, E., Glineburg, M.R., Snyder, A., Pinarbasi, E., Bekier, M., Li, X., et al. (2025). TDP43 autoregulation gives rise to dominant negative isoforms that are tightly controlled by transcriptional and post-translational mechanisms. Cell Rep. *44*, 115113. https://doi.org/10.1016/j.celrep.2024.115113.

77. Flores, B.N., Li, X., Malik, A.M., Martinez, J., Beg, A.A., and Barmada, S.J. (2019). An intramolecular salt bridge linking TDP43 RNA binding, protein stability, and TDP43-dependent neurodegeneration. Cell Rep. *27*, 1133-1150.e8. https://doi.org/10.1016/j.celrep.2019.03.093.

78. Barmada, S.J., Ju, S., Arjun, A., Batarse, A., Archbold, H.C., Peisach, D., Li, X., Zhang, Y., Tank, E.M.H., Qiu, H., et al. (2015). Amelioration of toxicity in neuronal models of amyotrophic lateral sclerosis by hUPF1. Proc. Natl. Acad. Sci. U. S. A. *112*, 7821–7826. https://doi.org/10.1073/pnas.1509744112.

79. Barmada, S.J., Serio, A., Arjun, A., Bilican, B., Daub, A., Ando, D.M., Tsvetkov, A., Pleiss, M., Li, X., Peisach, D., et al. (2014). Autophagy induction enhances TDP43 turnover and survival in neuronal ALS models. Nat. Chem. Biol. *10*, 677–685. https://doi.org/10.1038/nchembio.1563.

80. Maltby, C.J., Krans, A., Grudzien, S.J., Palacios, Y., Muiños, J., Suárez, A., Asher, M., Willey, S., Van Deynze, K., Mumm, C., et al. (2024). AAGGG repeat expansions trigger RFC1-independent synaptic dysregulation in human CANVAS neurons. Sci. Adv. *10*, eadn2321. https://doi.org/10.1126/sciadv.adn2321.

81. Barmada, S.J., Skibinski, G., Korb, E., Rao, E.J., Wu, J.Y., and Finkbeiner, S. (2010). Cytoplasmic mislocalization of TDP-43 is toxic to neurons and enhanced by a mutation associated with familial amyotrophic lateral sclerosis. J. Neurosci. *30*, 639–649. https://doi.org/10.1523/JNEUROSCI.4988-09.2010.

82. Weskamp, K., Safren, N., Miguez, R., and Barmada, S. (2019). Monitoring neuronal survival via longitudinal fluorescence microscopy. J. Vis. Exp., 10.3791/59036. https://doi.org/10.3791/59036.

83. Malik, A.M., Miguez, R.A., Li, X., Ho, Y.-S., Feldman, E.L., and Barmada, S.J. (2018). Matrin 3-dependent neurotoxicity is modified by nucleic acid binding and nucleocytoplasmic localization. Elife *7*, e35977. https://doi.org/10.7554/eLife.35977.

84. Archbold, H.C., Jackson, K.L., Arora, A., Weskamp, K., Tank, E.M.-H., Li, X., Miguez, R., Dayton, R.D., Tamir, S., Klein, R.L., et al. (2018). TDP43 nuclear export and neurodegeneration in models of amyotrophic lateral sclerosis and frontotemporal dementia. Sci. Rep. *8*, 4606. https://doi.org/10.1038/s41598-018-22858-w.

85. Abati, E., Manini, A., Velardo, D., Del Bo, R., Napoli, L., Rizzo, F., Moggio, M., Bresolin, N., Bellone, E., Bassi, M.T., et al. (2022). Clinical and genetic features of a cohort of patients with MFN2-related neuropathy. Sci. Rep. *12*, 6181. https://doi.org/10.1038/s41598-022-10220-0.

86. McMillan, M., Gomez, N., Hsieh, C., Bekier, M., Li, X., Miguez, R., Tank, E.M.H., and Barmada, S.J. (2023). RNA methylation influences TDP43 binding and disease pathogenesis in models of amyotrophic lateral sclerosis and frontotemporal dementia. Mol. Cell *83*, 219-236.e7. https://doi.org/10.1016/j.molcel.2022.12.019.

87. Ran, F.A., Hsu, P.D., Wright, J., Agarwala, V., Scott, D.A., and Zhang, F. (2013). Genome engineering using the CRISPR-Cas9 system. Nat. Protoc. *8*, 2281–2308. https://doi.org/10.1038/nprot.2013.143.

88. Wiesinger, C., Kunze, M., Regelsberger, G., Forss-Petter, S., and Berger, J. (2013). Impaired very long-chain acyl-CoA β-oxidation in human X-linked adrenoleukodystrophy fibroblasts is a direct consequence of ABCD1 transporter dysfunction. J. Biol. Chem. *288*, 19269–19279. https://doi.org/10.1074/jbc.M112.445445.

89. Chen, Z.-P., Xu, D., Wang, L., Mao, Y.-X., Li, Y., Cheng, M.-T., Zhou, C.-Z., Hou, W.-T., and Chen, Y. (2022). Structural basis of substrate recognition and translocation by human very long-chain fatty acid transporter ABCD1. Nat. Commun. *13*, 3299. https://doi.org/10.1038/s41467-022-30974-5.

90. Duplan, L., Bernard, N., Casseron, W., Dudley, K., Thouvenot, E., Honnorat, J., Rogemond, V., De Bovis, B., Aebischer, P., Marin, P., et al. (2010). Collapsin response mediator protein 4a (CRMP4a) is upregulated in motoneurons of mutant SOD1 mice and can trigger motoneuron axonal degeneration and cell death. J. Neurosci. *30*, 785–796. https://doi.org/10.1523/JNEUROSCI.5411-09.2010.

91. Nagai, J., Kitamura, Y., Owada, K., Yamashita, N., Takei, K., Goshima, Y., and Ohshima, T. (2015). Crmp4 deletion promotes recovery from spinal cord injury by

neuroprotection and limited scar formation. Sci. Rep. *5*, 8269. https://doi.org/10.1038/srep08269.

92. Girouard, M.-P., Simas, T., Hua, L., Morquette, B., Khazaei, M.R., Unsain, N., Johnstone, A.D., Rambaldi, I., Sanz, R.L., Di Raddo, M.-E., et al. (2020). Collapsin response mediator protein 4 (CRMP4) facilitates Wallerian degeneration and axon regeneration following sciatic nerve injury. eNeuro *7*, ENEURO.0479-19.2020. https://doi.org/10.1523/ENEURO.0479-19.2020.

93. Asahina, R., Takahashi, M., Takano, H., Yao, R., Abe, M., Goshima, Y., and Ohshima, T. (2024). The role of CRMP4 in LPS-induced neuroinflammation. Brain Res. *1841*, 149094. https://doi.org/10.1016/j.brainres.2024.149094.

94. Park, J.-S., Hollingsworth, N.M., and Neiman, A.M. (2021). Genetic dissection of Vps13 regulation in yeast using disease mutations from human orthologs. Int. J. Mol. Sci. *22*, 6200. https://doi.org/10.3390/ijms22126200.

95. Cong, L., Ran, F.A., Cox, D., Lin, S., Barretto, R., Habib, N., Hsu, P.D., Wu, X., Jiang, W., Marraffini, L.A., et al. (2013). Multiplex genome engineering using CRISPR/Cas systems. Science *339*, 819–823. https://doi.org/10.1126/science.1231143.

96. Park, J.-S., and Neiman, A.M. (2012). VPS13 regulates membrane morphogenesis during sporulation in Saccharomyces cerevisiae. J. Cell Sci. *125*, 3004–3011. https://doi.org/10.1242/jcs.105114.

97. Samaranayake, H.S., Cowan, A.E., and Klobutcher, L.A. (2011). Vacuolar protein sorting protein 13A, TtVPS13A, localizes to the tetrahymena thermophila phagosome membrane and is required for efficient phagocytosis. Eukaryot. Cell *10*, 1207–1218. https://doi.org/10.1128/EC.05089-11.

98. Zhang, Q., and Wang, Y. (2007). Homeodomain-interacting protein kinase-2 (HIPK2) phosphorylates HMGA1a at Ser-35, Thr-52, and Thr-77 and modulates its DNA binding affinity. J. Proteome Res. *6*, 4711–4719. https://doi.org/10.1021/pr700571d.

99. Piekielko, A., Drung, A., Rogalla, P., Schwanbeck, R., Heyduk, T., Gerharz, M., Bullerdiek, J., and Wiśniewski, J.R. (2001). Distinct organization of DNA complexes of various HMGI/Y family proteins and their modulation upon mitotic phosphorylation. J. Biol. Chem. *276*, 1984–1992. https://doi.org/10.1074/jbc.M004065200.

100. Watanabe, M., Ni, S., Lindenberger, A.L., Cho, J., Tinch, S.L., and Kennedy, M.A. (2013). Characterization of the stoichiometry of HMGA1/DNA complexes. Open Biochem. J. *7*, 73–81. https://doi.org/10.2174/1874091X01307010073.

101. Colombo, D.F., Burger, L., Baubec, T., and Schübeler, D. (2017). Binding of high mobility group A proteins to the mammalian genome occurs as a function of AT-content. PLoS Genet. *13*, e1007102. https://doi.org/10.1371/journal.pgen.1007102.

102. Zou, Y., Webb, K., Perna, A.D., Zhang, Q., Clarke, S., and Wang, Y. (2007). A mass spectrometric study on the in vitro methylation of HMGA1a and HMGA1b proteins by PRMTs: methylation specificity, the effect of binding to AT-rich duplex DNA, and the effect of C-terminal phosphorylation. Biochemistry *46*, 7896–7906. https://doi.org/10.1021/bi6024897.

103. Sakimoto, H., Nakamura, M., Nagata, O., Yokoyama, I., and Sano, A. (2016). Phenotypic abnormalities in a chorea-acanthocytosis mouse model are modulated by strain background. Biochem. Biophys. Res. Commun. *472*, 118–124. https://doi.org/10.1016/j.bbrc.2016.02.077.

104. Zhang, X.Q., and Li, L. (2021). Biological function and clinical value of VPS13A in pan-cancer based on bioinformatics analysis. Int. J. Gen. Med. *14*, 6825–6838. https://doi.org/10.2147/IJGM.S330256.

105. Glaß, H., Pal, A., Reinhardt, P., Sterneckert, J., Wegner, F., Storch, A., and Hermann, A. (2018). Defective mitochondrial and lysosomal trafficking in chorea-acanthocytosis is independent of Src-kinase signaling. Mol. Cell. Neurosci. 92, 137–148. https://doi.org/10.1016/j.mcn.2018.08.002.

106. Amos, C., Xu, P., and De Camilli, P. (2023). Erythroid differentiation dependent interaction of VPS13A with XK at the plasma membrane of K562 cells. Contact (Thousand Oaks.) *6*, 25152564231215132. https://doi.org/10.1177/25152564231215133.

107. Guillén-Samander, A., Wu, Y., Pineda, S.S., García, F.J., Eisen, J.N., Leonzino, M., Ugur, B., Kellis, M., Heiman, M., and De Camilli, P. (2022). A partnership between the lipid scramblase XK and the lipid transfer protein VPS13A at the plasma membrane. Proc. Natl. Acad. Sci. U. S. A. *119*, e2205425119. https://doi.org/10.1073/pnas.2205425119.

108. Foti, D., Iuliano, R., Chiefari, E., and Brunetti, A. (2003). A nucleoprotein complex containing Sp1, C/EBP beta, and HMGI-Y controls human insulin receptor gene transcription. Mol. Cell. Biol. *23*, 2720–2732. https://doi.org/10.1128/MCB.23.8.2720-2732.2003.

109. Chiefari, E., Foti, D.P., Sgarra, R., Pegoraro, S., Arcidiacono, B., Brunetti, F.S., Greco, M., Manfioletti, G., and Brunetti, A. (2018). Transcriptional regulation of glucose metabolism: The emerging role of the HMGA1 chromatin factor. Front. Endocrinol. (Lausanne) 9, 357. https://doi.org/10.3389/fendo.2018.00357.

110. Aiello, A., Pandini, G., Sarfstein, R., Werner, H., Manfioletti, G., Vigneri, R., and Belfiore, A. (2010). HMGA1 protein is a positive regulator of the insulin-like growth factor-I receptor gene. Eur. J. Cancer *46*, 1919–1926. https://doi.org/10.1016/j.ejca.2010.02.050.

111. Hermann, A., and Walker, R.H. (2015). Diagnosis and treatment of chorea syndromes. Curr. Neurol. Neurosci. Rep. *15*, 514. https://doi.org/10.1007/s11910-014-0514-0.

112. Al-Asmi, A., Jansen, A.C., Badhwar, A., Dubeau, F., Tampieri, D., Shustik, C., Mercho, S., Savard, G., Dobson-Stone, C., Monaco, A.P., et al. (2005). Familial temporal lobe epilepsy as a presenting feature of choreoacanthocytosis. Epilepsia *46*, 1256–1263. https://doi.org/10.1111/j.1528-1167.2005.65804.x.

113. Richter, J.E., Jr, Vadlamudi, C., Macklin, S.K., Samreen, A., Helmi, H., Broderick, D., Mohammad, A.N., Hines, S.L., VanGerpen, J.A., Atwal, P.S., et al. (2020). Characterization of a pathogenic variant in the ABCD1 gene through protein molecular modeling. Case Rep. Genet. *2020*, 3256539. https://doi.org/10.1155/2020/3256539.

114. Xiong, C., Jia, L.-N., Xiong, W.-X., Wu, X.-T., Xiong, L.-L., Wang, T.-H., Zhou, D., Hong, Z., Liu, Z., and Tang, L. (2023). Structural insights into substrate recognition and translocation of human peroxisomal ABC transporter ALDP. Signal Transduct. Target. Ther. *8*, 74. https://doi.org/10.1038/s41392-022-01280-9.

115. Guo, H., and Xia, B. (2016). Collapsin response mediator protein 4 isoforms (CRMP4a and CRMP4b) have opposite effects on cell proliferation, migration, and invasion in gastric cancer. BMC Cancer *16*, 565. https://doi.org/10.1186/s12885-016-2593-6.

116. Hiroshima, Y., Nakamura, F., Miyamoto, H., Mori, R., Taniguchi, K., Matsuyama, R., Akiyama, H., Tanaka, K., Ichikawa, Y., Kato, S., et al. (2013). Collapsin response mediator protein 4 expression is associated with liver metastasis and poor survival in pancreatic cancer. Ann. Surg. Oncol. 20 Suppl *3*, S369-78. https://doi.org/10.1245/s10434-012-2491-3.

117. Zhou, W., Xie, P., Pang, M., Yang, B., Fang, Y., Shu, T., Liu, C., Wang, X., Zhang, L., Li, S., et al. (2015). Upregulation of CRMP4, a new prostate cancer metastasis suppressor gene, inhibits tumor growth in a nude mouse intratibial injection model. Int. J. Oncol. *46*, 290–298. https://doi.org/10.3892/ijo.2014.2705.

118. Miller, B.H., Zeier, Z., Xi, L., Lanz, T.A., Deng, S., Strathmann, J., Willoughby, D., Kenny, P.J., Elsworth, J.D., Lawrence, M.S., et al. (2012). MicroRNA-132 dysregulation in schizophrenia has implications for both neurodevelopment and

adult brain function. Proc. Natl. Acad. Sci. U. S. A. *109*, 3125–3130. https://doi.org/10.1073/pnas.1113793109.

119. Boulan, B., Ravanello, C., Peyrel, A., Bosc, C., Delphin, C., Appaix, F., Denarier, E., Kraut, A., Jacquier-Sarlin, M., Fournier, A., et al. (2021). CRMP4-mediated fornix development involves Semaphorin-3E signaling pathway. Elife *10*, e70361. https://doi.org/10.7554/eLife.70361.

120. Tsutiya, A., Nakano, Y., Hansen-Kiss, E., Kelly, B., Nishihara, M., Goshima, Y., Corsmeier, D., White, P., Herman, G.E., and Ohtani-Kaneko, R. (2017). Human CRMP4 mutation and disrupted Crmp4 expression in mice are associated with ASD characteristics and sexual dimorphism. Sci. Rep. *7*, 16812. https://doi.org/10.1038/s41598-017-16782-8.

121. Blasco, H., Bernard-Marissal, N., Vourc'h, P., Guettard, Y.O., Sunyach, C., Augereau, O., Khederchah, J., Mouzat, K., Antar, C., Gordon, P.H., et al. (2013). A rare motor neuron deleterious missense mutation in the DPYSL3 (CRMP4) gene is associated with ALS. Hum. Mutat. *34*, 953–960. https://doi.org/10.1002/humu.22329.

122. Maimon, R., Ankol, L., Gradus Pery, T., Altman, T., Ionescu, A., Weissova, R., Ostrovsky, M., Tank, E., Alexandra, G., Shelestovich, N., et al. (2021). A CRMP4-dependent retrograde axon-to-soma death signal in amyotrophic lateral sclerosis. EMBO J. *40*, e107586. https://doi.org/10.15252/embj.2020107586.

123. Tonouchi, A., Nagai, J., Togashi, K., Goshima, Y., and Ohshima, T. (2016). Loss of collapsin response mediator protein 4 suppresses dopaminergic neuron death in an 1-methyl-4-phenyl-1,2,3,6-tetrahydropyridine-induced mouse model of Parkinson's disease. J. Neurochem. *137*, 795–805. https://doi.org/10.1111/jnc.13617.

124. Li, W., Goshima, Y., and Ohshima, T. (2020). Loss of collapsin response mediator protein 4 attenuates 6-hydroxydopamine-induced impairments in a mouse model of Parkinson's disease. Neurochem. Res. *45*, 2286–2301. https://doi.org/10.1007/s11064-020-03086-z.

125. Quach, T.T., Moutal, A., Khanna, R., Deems, N.P., Duchemin, A.-M., and Barrientos, R.M. (2020). Collapsin response mediator proteins: Novel targets for Alzheimer's disease. J. Alzheimers. Dis. *77*, 949–960. https://doi.org/10.3233/JAD-200721.

126. Cole, A.R., Knebel, A., Morrice, N.A., Robertson, L.A., Irving, A.J., Connolly, C.N., and Sutherland, C. (2004). GSK-3 phosphorylation of the Alzheimer epitope within collapsin response mediator proteins regulates axon elongation in primary

neurons. J. Biol. Chem. *279*, 50176–50180. https://doi.org/10.1074/jbc.C400412200.

127. Cole, A.R., Causeret, F., Yadirgi, G., Hastie, C.J., McLauchlan, H., McManus, E.J., Hernández, F., Eickholt, B.J., Nikolic, M., and Sutherland, C. (2006). Distinct priming kinases contribute to differential regulation of collapsin response mediator proteins by glycogen synthase kinase-3 in vivo. J. Biol. Chem. *281*, 16591–16598. https://doi.org/10.1074/jbc.M513344200.

128. Chiefari, E., Nevolo, M.T., Arcidiacono, B., Maurizio, E., Nocera, A., Iiritano, S., Sgarra, R., Possidente, K., Palmieri, C., Paonessa, F., et al. (2012). HMGA1 is a novel downstream nuclear target of the insulin receptor signaling pathway. Sci. Rep. *2*, 251. https://doi.org/10.1038/srep00251.

129. Thanos, D., and Maniatis, T. (1995). Virus induction of human IFN beta gene expression requires the assembly of an enhanceosome. Cell *83*, 1091–1100. https://doi.org/10.1016/0092-8674(95)90136-1.

130. Hill, D.A., Pedulla, M.L., and Reeves, R. (1999). Directional binding of HMG-I(Y) on four-way junction DNA and the molecular basis for competitive binding with HMG-1 and histone H1. Nucleic Acids Res. *27*, 2135–2144. https://doi.org/10.1093/nar/27.10.2135.

131. Gorbounov, M., Carleton, N.M., Asch-Kendrick, R.J., Xian, L., Rooper, L., Chia, L., Cimino-Mathews, A., Cope, L., Meeker, A., Stearns, V., et al. (2020). High mobility group A1 (HMGA1) protein and gene expression correlate with ER-negativity and poor outcomes in breast cancer. Breast Cancer Res. Treat. *179*, 25–35. https://doi.org/10.1007/s10549-019-05419-1.

132. Zanin, R., Pegoraro, S., Ros, G., Ciani, Y., Piazza, S., Bossi, F., Bulla, R., Zennaro, C., Tonon, F., Lazarevic, D., et al. (2019). HMGA1 promotes breast cancer angiogenesis supporting the stability, nuclear localization and transcriptional activity of FOXM1. J. Exp. Clin. Cancer Res. *38*, 313. https://doi.org/10.1186/s13046-019-1307-8.

133. Puca, F., Colamaio, M., Federico, A., Gemei, M., Tosti, N., Bastos, A.U., Del Vecchio, L., Pece, S., Battista, S., and Fusco, A. (2014). HMGA1 silencing restores normal stem cell characteristics in colon cancer stem cells by increasing p53 levels. Oncotarget *5*, 3234–3245. https://doi.org/10.18632/oncotarget.1914.

134. Puca, F., Tosti, N., Federico, A., Kuzay, Y., Pepe, A., Morlando, S., Savarese, T., D'Alessio, F., Colamaio, M., Sarnataro, D., et al. (2019). HMGA1 negatively regulates NUMB expression at transcriptional and post transcriptional level in glioblastoma stem cells. Cell Cycle *18*, 1446–1457. https://doi.org/10.1080/15384101.2019.1618541.

135. Kim, D.K., Seo, E.J., Choi, E.J., Lee, S.I., Kwon, Y.W., Jang, I.H., Kim, S.-C., Kim, K.-H., Suh, D.-S., Seong-Jang, K., et al. (2016). Crucial role of HMGA1 in the self-renewal and drug resistance of ovarian cancer stem cells. Exp. Mol. Med. *48*, e255. https://doi.org/10.1038/emm.2016.73.

136. Liu, X., Zhou, Z., Wang, Y., Zhu, K., Deng, W., Li, Y., Zhou, X., Chen, L., Li, Y., Xie, A., et al. (2020). Downregulation of HMGA1 mediates autophagy and inhibits migration and invasion in bladder cancer via miRNA-221/TP53INP1/p-ERK axis. Front. Oncol. *10*, 589. https://doi.org/10.3389/fonc.2020.00589.

137. Conte, A., Paladino, S., Bianco, G., Fasano, D., Gerlini, R., Tornincasa, M., Renna, M., Fusco, A., Tramontano, D., and Pierantoni, G.M. (2017). High mobility group A1 protein modulates autophagy in cancer cells. Cell Death Differ. *24*, 1948–1962. https://doi.org/10.1038/cdd.2017.117.

138. Olan, I., Ando-Kuri, M., Parry, A.J., Handa, T., Schoenfelder, S., Fraser, P., Ohkawa, Y., Kimura, H., Narita, M., and Narita, M. (2024). HMGA1 orchestrates chromatin compartmentalization and sequesters genes into 3D networks coordinating senescence heterogeneity. Nat. Commun. *15*, 6891. https://doi.org/10.1038/s41467-024-51153-8.

139. Li, G., Luo, W., Wang, B., Qian, C., Ye, Y., Li, Y., and Zhang, S. (2020). HMGA1 induction of miR-103/107 forms a negative feedback loop to regulate autophagy in MPTP model of Parkinson's disease. Front. Cell. Neurosci. *14*, 620020. https://doi.org/10.3389/fncel.2020.620020.

140. Zhong, C., Zhang, Q., Bao, H., Li, Y., and Nie, C. (2024). Hsa_circ_0054220 upregulates HMGA1 by the competitive RNA pattern to promote neural impairment in MPTP model of Parkinson's disease. Appl. Biochem. Biotechnol. *196*, 4008–4023. https://doi.org/10.1007/s12010-023-04740-2.

141. Xu, D., Fan, W., Fu, B., and Nie, H. (2025). HMGA1 regulates IRS2 to promote inflammatory responses and oxidative stress injury in MPP+-induced cells. Cell Biochem. Biophys. *83*, 783–792. https://doi.org/10.1007/s12013-024-01510-7.

142. Manabe, T., Ohe, K., Katayama, T., Matsuzaki, S., Yanagita, T., Okuda, H., Bando, Y., Imaizumi, K., Reeves, R., Tohyama, M., et al. (2007). HMGA1a: sequence-specific RNA-binding factor causing sporadic Alzheimer's disease-linked exon skipping of presenilin-2 pre-mRNA. Genes Cells *12*, 1179–1191. https://doi.org/10.1111/j.1365-2443.2007.01123.x.

143. Mirabelli, M., Chiefari, E., Arcidiacono, B., Salatino, A., Pascarella, A., Morelli, M., Credendino, S.C., Brunetti, F.S., Di Vito, A., Greco, A., et al. (2025). HMGA1 deficiency: a pathogenic link between tau pathology and insulin resistance. EBioMedicine *115*, 105700. https://doi.org/10.1016/j.ebiom.2025.105700.

144. Manabe, T., Katayama, T., Sato, N., Gomi, F., Hitomi, J., Yanagita, T., Kudo, T., Honda, A., Mori, Y., Matsuzaki, S., et al. (2003). Induced HMGA1a expression causes aberrant splicing of Presenilin-2 pre-mRNA in sporadic Alzheimer's disease. Cell Death Differ. *10*, 698–708. https://doi.org/10.1038/sj.cdd.4401221.

145. Wang, R., Yang, Y., Wang, H., He, Y., and Li, C. (2020). MiR-29c protects against inflammation and apoptosis in Parkinson's disease model in vivo and in vitro by targeting SP1. Clin. Exp. Pharmacol. Physiol. *47*, 372–382. https://doi.org/10.1111/1440-1681.13212.

146. Cai, Y., Zhang, M.-M., Wang, M., Jiang, Z.-H., and Tan, Z.-G. (2022). Bone marrow-derived mesenchymal stem cell-derived exosomes containing Gli1 alleviate microglial activation and neuronal apoptosis in vitro and in a mouse Parkinson disease model by direct inhibition of Sp1 signaling. J. Neuropathol. Exp. Neurol. *81*, 522–534. https://doi.org/10.1093/jnen/nlac037.

147. Han, Y.-P., Liu, Z.-J., Bao, H.-H., Wang, Q., and Su, L.-L. (2022). MiR-126-5p targets SP1 to inhibit the progression of Parkinson's disease. Eur. Neurol. *85*, 235–244. https://doi.org/10.1159/000521525.

148. Cao, Y., Tan, X., Lu, Q., Huang, K., Tang, X., and He, Z. (2021). MiR-590-3 and SP1 promote neuronal apoptosis in patients with Alzheimer's disease via AMPK signaling pathway. Contrast Media Mol. Imaging *2021*, 6010362. https://doi.org/10.1155/2021/6010362.

149. Li, R., Song, B., Xu, L., Zheng, J., Pan, W., Cai, F., Wang, J., Wu, Y., and Song, W. (2023). Regulation of USP25 by SP1 associates with amyloidogenesis. J. Alzheimers. Dis. *92*, 1459–1472. https://doi.org/10.3233/JAD-221184.

150. Gong, K., Zhou, S., Xiao, L., Xu, M., Zhou, Y., Lu, K., Yu, X., Zhu, J., Liu, C., and Zhu, Q. (2025). Danggui Shaoyao San ameliorates Alzheimer's disease by regulating lipid metabolism and inhibiting neuronal ferroptosis through the AMPK/Sp1/ACSL4 signaling pathway. Front. Pharmacol. *16*, 1588375. https://doi.org/10.3389/fphar.2025.1588375.

151. Citron, B.A., Saykally, J.N., Cao, C., Dennis, J.S., Runfeldt, M., and Arendash, G.W. (2015). Transcription factor Sp1 inhibition, memory, and cytokines in a mouse model of Alzheimer's disease. Am. J. Neurodegener. Dis. *4*, 40–48.

152. Zhu, Z.-Y., Liu, Y.-D., Gong, Y., Jin, W., Topchiy, E., Turdi, S., Gao, Y.-F., Culver, B., Wang, S.-Y., Ge, W., et al. (2022). Mitochondrial aldehyde dehydrogenase (ALDH2) rescues cardiac contractile dysfunction in an APP/PS1 murine model of Alzheimer's disease via inhibition of ACSL4-dependent ferroptosis. Acta Pharmacol. Sin. *43*, 39–49. https://doi.org/10.1038/s41401-021-00635-2.

153. Chen-Plotkin, A.S., Sadri-Vakili, G., Yohrling, G.J., Braveman, M.W., Benn, C.L., Glajch, K.E., DiRocco, D.P., Farrell, L.A., Krainc, D., Gines, S., et al. (2006). Decreased association of the transcription factor Sp1 with genes downregulated in Huntington's disease. Neurobiol. Dis. *22*, 233–241. https://doi.org/10.1016/j.nbd.2005.11.001.

154. Li, S.-H., Cheng, A.L., Zhou, H., Lam, S., Rao, M., Li, H., and Li, X.-J. (2002). Interaction of Huntington disease protein with transcriptional activator Sp1. Mol. Cell. Biol. *22*, 1277–1287. https://doi.org/10.1128/MCB.22.5.1277-1287.2002.

155. Guida, N., Sanguigno, L., Mascolo, L., Calabrese, L., Serani, A., Molinaro, P., Lau, C.G., Annunziato, L., and Formisano, L. (2021). The transcriptional complex Sp1/KMT2A by up-regulating Restrictive Element 1 Silencing Transcription factor accelerates methylmercury-induced cell death in motor neuron-like NSC34 cells overexpressing SOD1-G93A. Front. Neurosci. *15*, 771580. https://doi.org/10.3389/fnins.2021.771580.

156. García-Morales, V., Rodríguez-Bey, G., Gómez-Pérez, L., Domínguez-Vías, G., González-Forero, D., Portillo, F., Campos-Caro, A., Gento-Caro, Á., Issaoui, N., Soler, R.M., et al. (2019). Sp1-regulated expression of p11 contributes to motor neuron degeneration by membrane insertion of TASK1. Nat. Commun. *10*, 3784. https://doi.org/10.1038/s41467-019-11637-4.

157. Jeong, J.-K., and Park, S.-Y. (2012). Transcriptional regulation of specific protein 1 (SP1) by hypoxia-inducible factor 1 alpha (HIF-1α) leads to PRNP expression and neuroprotection from toxic prion peptide. Biochem. Biophys. Res. Commun. *429*, 93–98. https://doi.org/10.1016/j.bbrc.2012.10.086.

158. Ren, Y., Zhang, H., and Jiang, P. (2018). MicroRNA-382 inhibits cell growth and migration in colorectal cancer by targeting SP1. Biol. Res. *51*, 51. https://doi.org/10.1186/s40659-018-0200-9.

159. Wu, D., Sun, J.K.-L., and Chow, K.H.-M. (2024). Neuronal cell cycle reentry events in the aging brain are more prevalent in neurodegeneration and lead to cellular senescence. PLoS Biol. *22*, e3002559. https://doi.org/10.1371/journal.pbio.3002559.

160. Kruman, I.I., Wersto, R.P., Cardozo-Pelaez, F., Smilenov, L., Chan, S.L., Chrest, F.J., Emokpae, R., Jr, Gorospe, M., and Mattson, M.P. (2004). Cell cycle activation linked to neuronal cell death initiated by DNA damage. Neuron *41*, 549–561. https://doi.org/10.1016/s0896-6273(04)00017-0.

161. McShea, A., Wahl, A.F., and Smith, M.A. (1999). Re-entry into the cell cycle: a mechanism for neurodegeneration in Alzheimer disease. Med. Hypotheses *52*, 525–527. https://doi.org/10.1054/mehy.1997.0680.

162. Martin, M. (2011). Cutadapt removes adapter sequences from high-throughput sequencing reads. EMBnet.journal *17*, 10–12. https://doi.org/10.14806/EJ.17.1.200.

163. Wingett, S.W., and Andrews, S. (2018). FastQ Screen: A tool for multi-genome mapping and quality control. F1000Res. *7*, 1338. https://doi.org/10.12688/f1000research.15931.2.

164. Babraham Bioinformatics - FastQC A Quality Control tool for High Throughput Sequence Data https://www.bioinformatics.babraham.ac.uk/projects/fastqc/.

165. Kim, D., Langmead, B., and Salzberg, S.L. (2015). HISAT: a fast spliced aligner with low memory requirements. Nat. Methods *12*, 357–360. https://doi.org/10.1038/nmeth.3317.

166. DePristo, M.A., Banks, E., Poplin, R., Garimella, K.V., Maguire, J.R., Hartl, C., Philippakis, A.A., del Angel, G., Rivas, M.A., Hanna, M., et al. (2011). A framework for variation discovery and genotyping using next-generation DNA sequencing data. Nat. Genet. *43*, 491–498. https://doi.org/10.1038/ng.806.

167. Wang, K., Li, M., and Hakonarson, H. (2010). ANNOVAR: functional annotation of genetic variants from high-throughput sequencing data. Nucleic Acids Res. *38*, e164. https://doi.org/10.1093/nar/gkq603.

168. Pfaffl, M.W. (2001). A new mathematical model for relative quantification in real-time RT-PCR. Nucleic Acids Res. *29*, e45. https://doi.org/10.1093/nar/29.9.e45.

169. Dobin, A., Davis, C.A., Schlesinger, F., Drenkow, J., Zaleski, C., Jha, S., Batut, P., Chaisson, M., and Gingeras, T.R. (2013). STAR: ultrafast universal RNA-seq aligner. Bioinformatics *29*, 15–21. https://doi.org/10.1093/bioinformatics/bts635.

170. Li, B., and Dewey, C.N. (2011). RSEM: accurate transcript quantification from RNA-Seq data with or without a reference genome. BMC Bioinformatics *12*, 323. https://doi.org/10.1186/1471-2105-12-323.

171. Ewels, P., Magnusson, M., Lundin, S., and Käller, M. (2016). MultiQC: summarize analysis results for multiple tools and samples in a single report. Bioinformatics *32*, 3047–3048. https://doi.org/10.1093/bioinformatics/btw354.

172. Love, M.I., Huber, W., and Anders, S. (2014). Moderated estimation of fold change and dispersion for RNA-seq data with DESeq2. Genome Biol. *15*, 550. https://doi.org/10.1186/s13059-014-0550-8.

173. McAlister, G.C., Nusinow, D.P., Jedrychowski, M.P., Wühr, M., Huttlin, E.L., Erickson, B.K., Rad, R., Haas, W., and Gygi, S.P. (2014). MultiNotch MS3 enables accurate, sensitive, and multiplexed detection of differential expression across

cancer cell line proteomes. Anal. Chem. *86*, 7150–7158. https://doi.org/10.1021/ac502040v.

174. Sharkey, L.M., Safren, N., Pithadia, A.S., Gerson, J.E., Dulchavsky, M., Fischer, S., Patel, R., Lantis, G., Ashraf, N., Kim, J.H., et al. (2018). Mutant UBQLN2 promotes toxicity by modulating intrinsic self-assembly. Proc. Natl. Acad. Sci. U. S. A. *115*, E10495–E10504. https://doi.org/10.1073/pnas.1810522115.

175. Linsley, J.W., Shah, K., Castello, N., Chan, M., Haddad, D., Doric, Z., Wang, S., Leks, W., Mancini, J., Oza, V., et al. (2021). Genetically encoded cell-death indicators (GEDI) to detect an early irreversible commitment to neurodegeneration. Nat. Commun. *12*, 5284. https://doi.org/10.1038/s41467-021-25549-9.

176. Parker, S.S., Moutal, A., Cai, S., Chandrasekaran, S., Roman, M.R., Koshy, A.A., Khanna, R., Zinsmaier, K.E., and Mouneimne, G. (2018). High fidelity cryopreservation and recovery of primary rodent cortical neurons. eNeuro *5*, ENEURO.0135-18.2018. https://doi.org/10.1523/ENEURO.0135-18.2018.

177. Schindelin, J., Arganda-Carreras, I., Frise, E., Kaynig, V., Longair, M., Pietzsch, T., Preibisch, S., Rueden, C., Saalfeld, S., Schmid, B., et al. (2012). Fiji: an open-source platform for biological-image analysis. Nat. Methods *9*, 676–682. https://doi.org/10.1038/nmeth.2019.

178. von Mering, C., Huynen, M., Jaeggi, D., Schmidt, S., Bork, P., and Snel, B. (2003). STRING: a database of predicted functional associations between proteins. Nucleic Acids Res. *31*, 258–261. https://doi.org/10.1093/nar/gkg034.

179. Franceschini, A., Szklarczyk, D., Frankild, S., Kuhn, M., Simonovic, M., Roth, A., Lin, J., Minguez, P., Bork, P., von Mering, C., et al. (2013). STRING v9.1: protein-protein interaction networks, with increased coverage and integration. Nucleic Acids Res. *41*, D808-15. https://doi.org/10.1093/nar/gks1094.

180. Wang, M., Zhao, Y., and Zhang, B. (2015). Efficient test and visualization of multi-set intersections. Sci. Rep. *5*, 16923. https://doi.org/10.1038/srep16923.

Figures

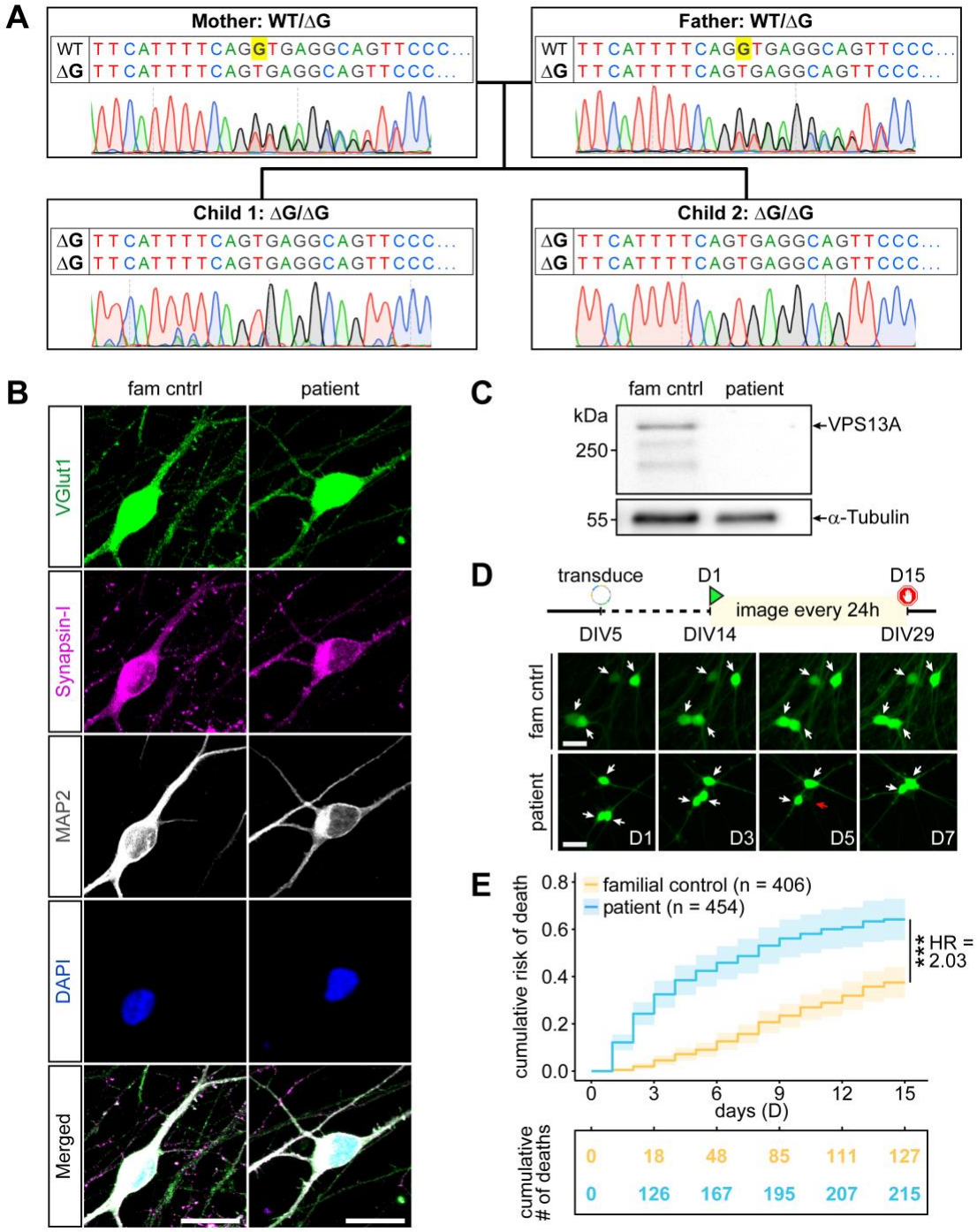


Figure 2.1 Human iNeurons derived from VPS13A disease patients show increased toxicity compared to familial controls.

(**A**) Sequencing chromatograms showing a single nucleotide deletion (ΔG; yellow box) in both offspring. (**B**) Representative images of familial control (fam cntrl) and VPS13A disease (patient)

iNeurons at DIV14 immunostained for VGlut1 (green), synapsin-I (magenta), MAP2 (gray), and Hoechst (blue). Scale bars: 20µm. (**C**) Representative immunoblot of lysate from DIV14 fam cntrl and patient iNeurons probed with an anti-VPS13A antibody. α-Tubulin was used as a loading control. (**D**) Timeline and representative images for neuronal survival experiments. Individual iNeurons (white arrows) were tracked until their time of death (red arrows). Scale bars: 20µm. (**E**) Cumulative hazard plot and cumulative number of deaths in patient (n=454) and fam cntrl (n=406) iNeurons. Results were pooled and stratified from 3 biological replicates; n=number of iNeurons/condition. HR=2.03, ***p=3.18×10^{-10}, Cox proportional hazards analysis.

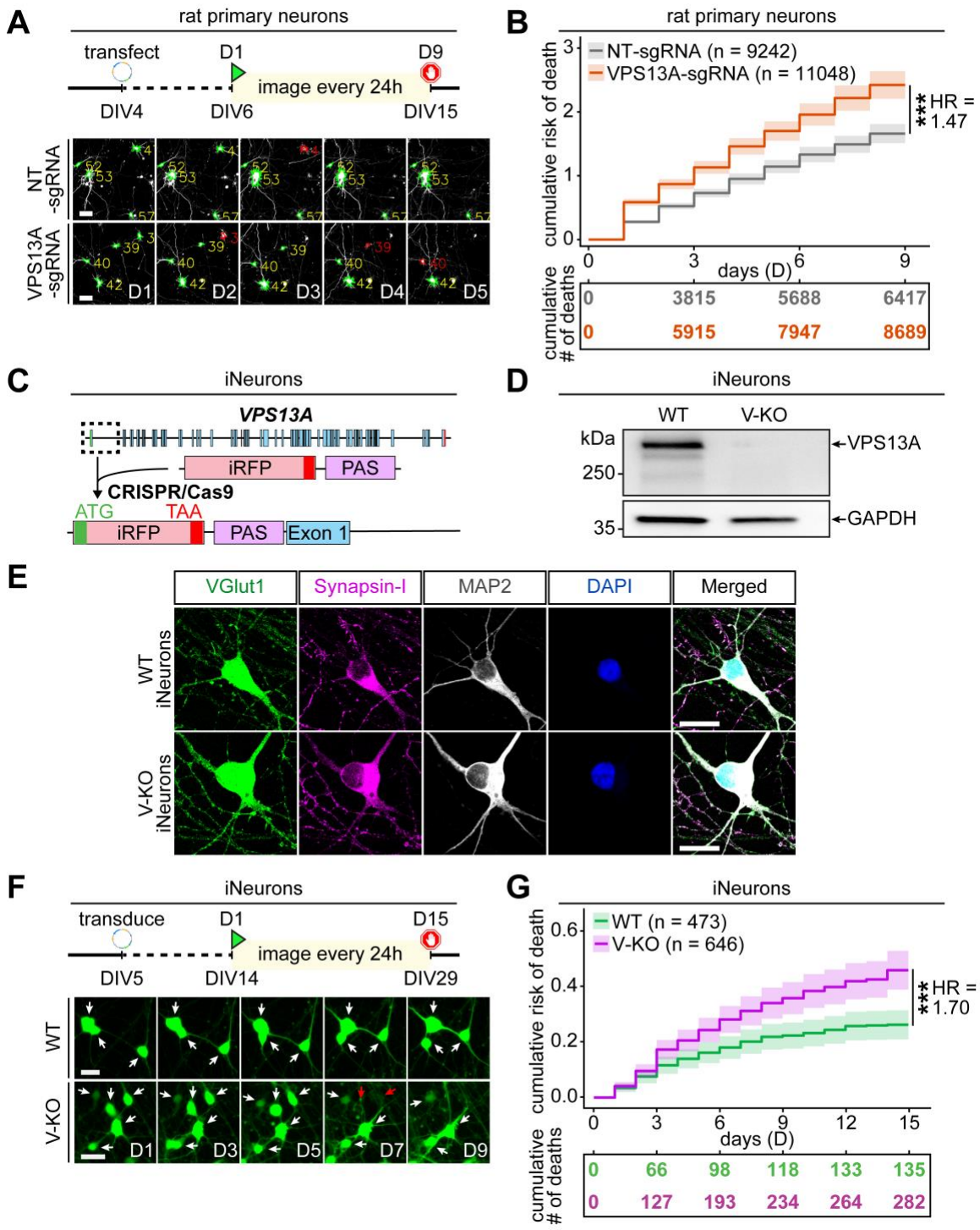


Figure 2.2 VPS13A is necessary for neuronal survival.

(**A**) Timeline and representative images for rat cortical neuron survival experiments. Neurons (yellow) were tracked until time of death (red). Scale bars: 40μm. (**B**) Cumulative hazard plot and cumulative number of deaths in rat neurons expressing VPS13A-sgRNA (n=11,048) and NT-

sgRNA (n=9,242). HR=1.47, ***p<$2x10^{-16}$, Cox proportional hazards analysis. (**C**) Schematic of gene trap strategy to generate V-KO iNeurons. iRFP, infrared fluorescent protein. ATG, start codon. TAA, stop codon. PAS, poly(A) signal. (**D**) Representative immunoblot of lysate from DIV14 isogenic control (WT) and V-KO iNeurons probed with antibodies against VPS13A and GAPDH. (**E**) Representative images of WT and V-KO iNeurons at DIV14 immunostained for VGlut1 (green), synapsin-I (magenta), MAP2 (gray), and Hoechst (blue). Scale bars: 20μm. (**F**) Timeline and representative images for WT and V-KO iNeuron survival experiments. Individual iNeurons (white arrows) were tracked until their time of death (red arrows). Scale bars: 20 μm. (**G**) Cumulative hazard plot and cumulative number of deaths in V-KO (n=646) and WT (n=473) iNeurons. HR=1.7035, ***p=$3.74x10^{-7}$, Cox proportional hazards analysis. Results in (**B**) and (**G**) were pooled and stratified from 3 biological replicates each; n=neurons/condition.

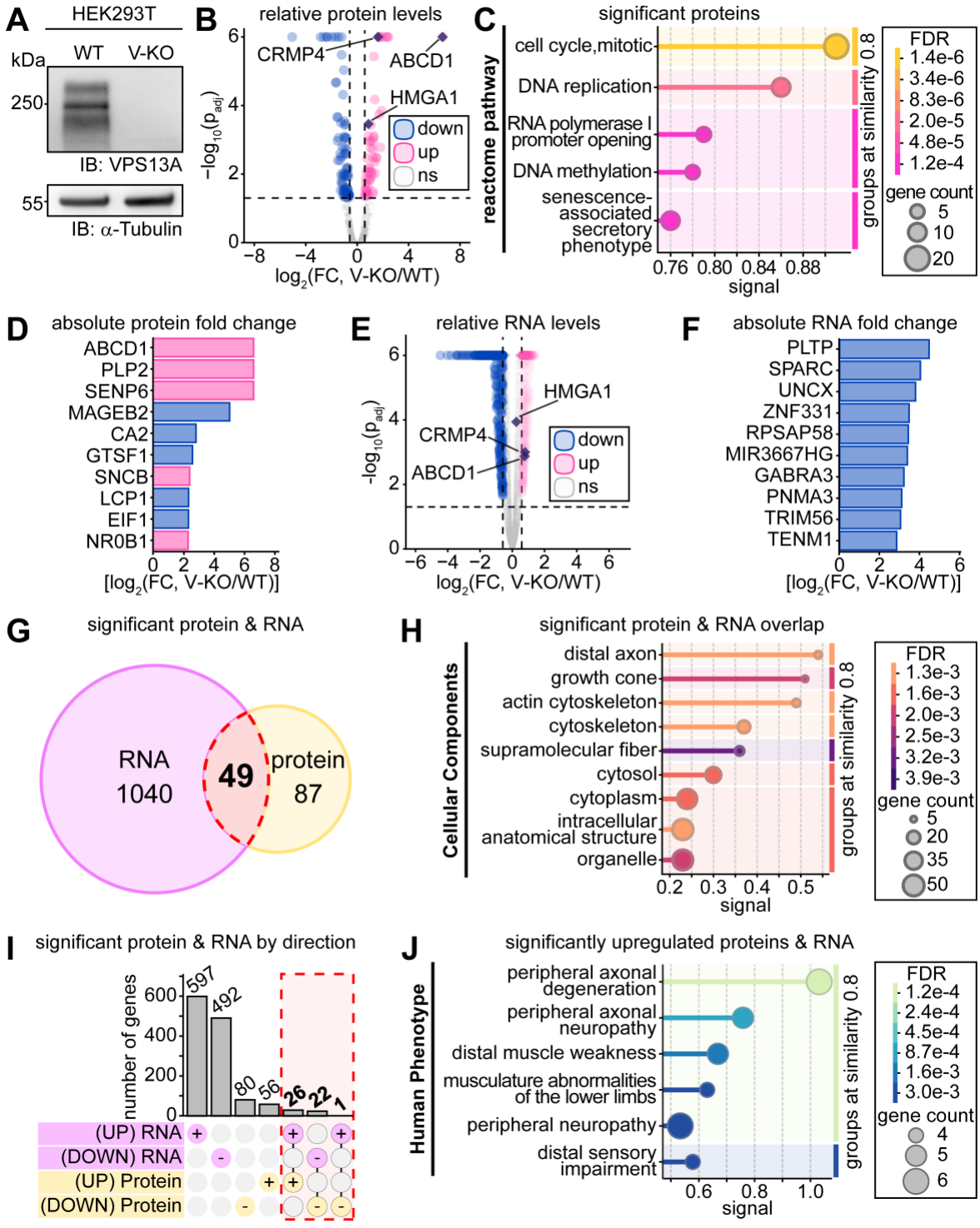


Figure 2.3 VPS13A-deficient HEK293T cells demonstrate concordant changes at both the RNA and protein levels.

(**A**) Representative immunoblot of lysate from V-KO and unmodified (WT) HEK293T cells probed with antibodies against VPS13A and GAPDH. (**B**) Volcano plot of differentially expressed proteins

in V-KO compared to WT (V-KO/WT) HEK293T cells. Dashed lines represent cutoffs for adjusted significance ($p_{adj.}$<0.05; horizontal line, FDR) and magnitude (FC>1.5). Blue=downregulated (n=80); pink=upregulated (n=56); grey=non-significant (ns, n=5110). n=3 biological replicates. (**C**) Reactome Pathway analysis of differentially expressed (non-directional) proteins (n=136) in V-KO/WT from (**B**). (**D**) Bar plot of top 10 differentially expressed proteins in V-KO/WT from (**B**), ordered by descending [FC]. (**E**) Volcano plot of differentially expressed transcripts in V-KO compared to WT HEK293T cells. Dashed lines represent cutoffs for significance adjusted ($p_{adj.}$<0.05; horizontal line, FDR) and magnitude (FC>1.5). Blue=downregulated (n=492); pink=upregulated (n=597); grey=ns (n=14,554). n=3 biological replicates. (**F**) Bar plot of top 10 differentially expressed transcripts in V-KO/WT from (**E**) ordered by descending [FC]. (**G**) Euler plot showing overlap (n=49, $p=2.43x10^{-30}$, super exact test) of differentially expressed proteins and transcripts in V-KO compared to WT HEK293T cells. (**H**) Cellular Component GO analysis for the overlapping set of differentially expressed (non-directional) proteins and transcripts (n=49) in V-KO/WT from (**G**). (**I**) UpSet plot showing directional (+ upregulated, – downregulated) interactions between differentially expressed proteins and transcripts in V-KO compared to WT HEK293T cells. Numbers above bars=number of intersecting proteins/transcripts. Red box highlights intersections containing protein and RNA by direction. (**J**) Human Phenotype (Monarch) analysis for the overlapping set of upregulated proteins and transcripts (n=26) in V-KO/WT from (**I**). Ontology analyses in (**C**), (**H**), and (**J**) sorted by signal≥0.01 using similarity≥0.8, strength≥0.01, and FDR≤0.05.

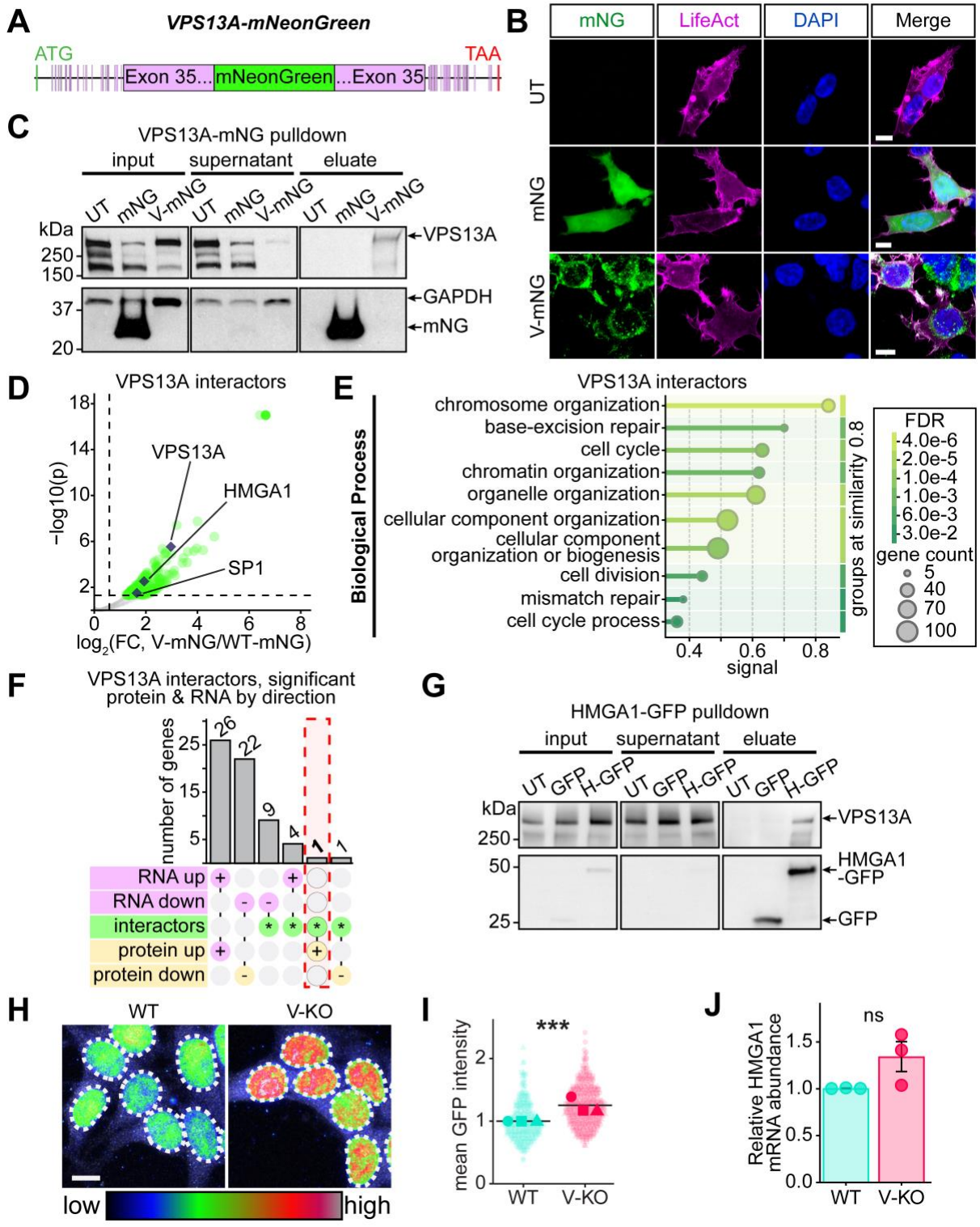


Figure 2.4 VPS13A interacts with HMGA1 in HEK293T cells.

(**A**) Schematic of mNeonGreen (mNG) labeling of endogenous VPS13A (V-mNG) in HEK293T cells. (**B**) Representative images of live untransfected (UT), V-mNG, and mNG transfected (mNG) cells labeled with LifeAct (magenta, actin) and Hoechst (blue, nucleus). Scale bars: 20μm. (**C**) Representative immunoblot from UT, V-mNG, and mNG HEK293T cells after mNG immunoprecipitation. Input, supernatant, and eluate were probed with antibodies against VPS13A, mNG, and GAPDH. (**D**) Volcano plot of proteins enriched by V-mNG compared to mNG (V-mNG/mNG) HEK293T cells following mNG immunoprecipitation. Dashed lines represent cutoffs for significance ($p<0.05$, horizontal line) and magnitude (FC>1.5). Green=significant (n=211, VPS13A interactors); grey=non-significant (n=2,944, ns). n=3 biological replicates. (**E**) Biological Process GO analysis for VPS13A interactors (sorted by signal≥0.01 using similarity≥0.8, strength≥0.01, and FDR≤0.05). (**F**) UpSet plot showing intersections among differentially expressed proteins and transcripts (in V-KO compared to isogenic control (WT) HEK293T cells), and VPS13A interactors (in V-mNG compared to mNG HEK293T cells). Numbers above bars=number of intersecting proteins/transcripts. Red box highlights the single factor (HMGA1) upregulated at the protein level (in V-KO/WT) that also interacts with VPS13A. (**G**) Representative immunoblot from un-transfected (UT), GFP transfected (GFP), and HMGA1-GFP transfected HEK293T cells after GFP co-immunoprecipitation. Input, supernatant, and elute were probed with antibodies against VPS13A, GFP, and α-tubulin. (**H**) Representative images of WT and V-KO HEK293T cells immunostained for HMGA1 (heatmap), β-Actin (gray), and Hoechst (dashed outlines). Scale bars: 10μm. (**I**) Quantification of whole cell mean HMGA1 immunoreactivity in (**H**), normalized to WT mean for each replicate. Data from 3 biological replicates (n=51-140 cells/condition/replicate). ***$p<2x10^{-16}$ (unpaired t-test with Welch's correction). Black lines=mean HMGA1 immunoreactivity for combined replicates. (**J**) qRT-PCR of HMGA1/GAPDH mRNA levels from WT and V-KO HEK293T cells, displayed as mean ± SEM normalized to WT for each replicate. Data from 3 technical replicates/3 biological replicates. $p>0.05$ (ns, unpaired t-test with Welch's correction).

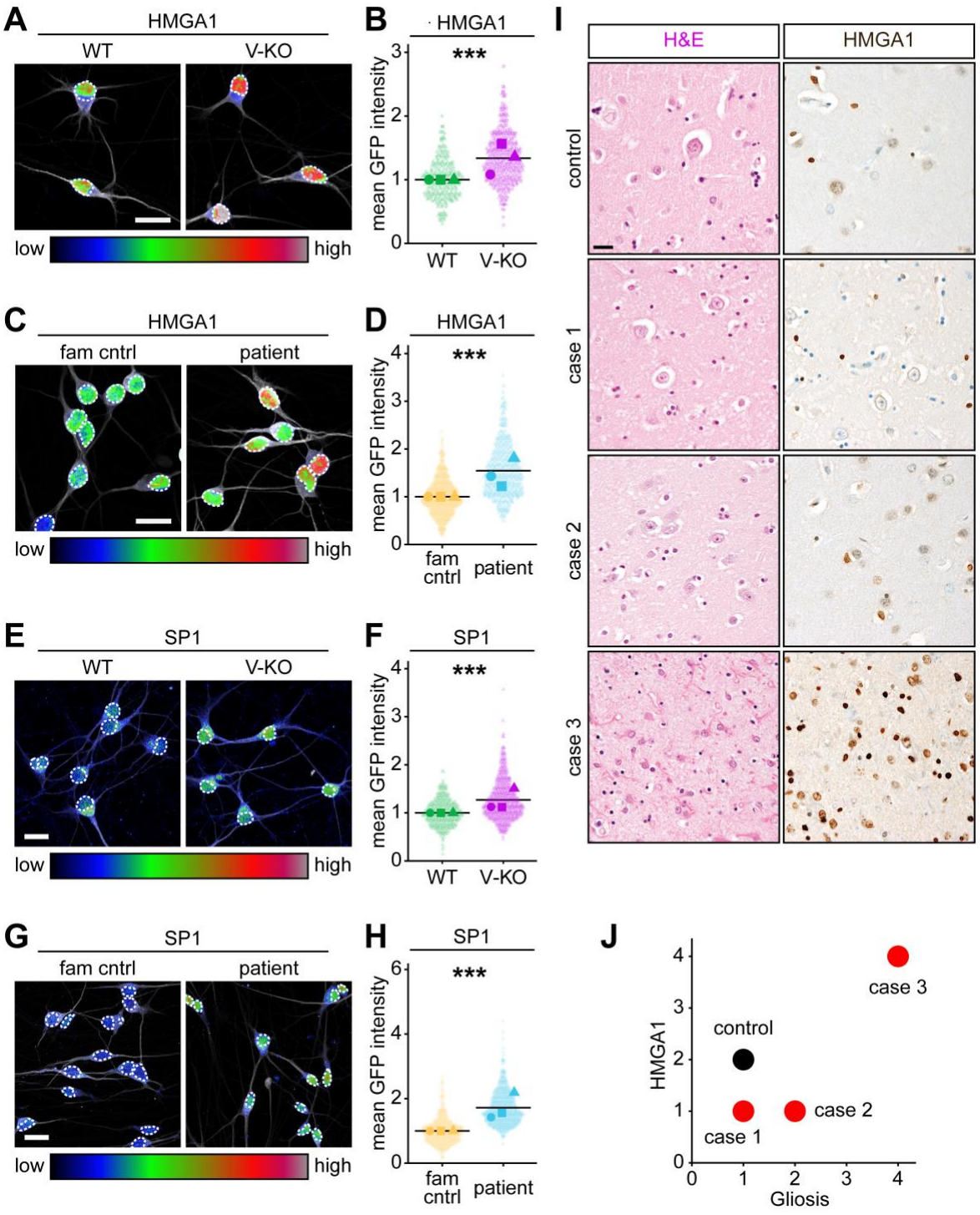


Figure 2.5 HMGA1 is upregulated in VPS13A KO and VPS13A disease iNeurons compared to respective controls.

(**A**) WT and V-KO iNeurons immunostained for HMGA1 (heatmap), MAP2 (gray), and Hoechst (dashed outlines). (**B**) Quantification of HMGA1 immunoreactivity in (**A**), normalized to WT mean for each replicate (n=62–176, cells/condition/replicate). ***$p<2x10^{-16}$. (**C**) Familial control (fam cntrl) and VPS13A disease patient (patient) iNeurons immunostained for HMGA1 (heatmap), MAP2 (gray), and Hoechst (dashed outline). (**D**) Quantification of HMGA1 immunoreactivity in (**C**), normalized to fam cntrl mean for each replicate (n=108–277, cells/ condition/replicate). ***$p<2x10^{-16}$. (**E**) WT and V-KO iNeurons immunostained for SP1 (heatmap), MAP2 (gray), and Hoechst (dashed outline). (**F**) Quantification of SP1 immunoreactivity in (**E**), normalized to WT mean for each replicate (n=73–195, cells /condition/replicate). ***$p<2x10^{-16}$. (**G**) Fam cntrl and patient iNeurons immunostained for SP1 (heatmap), MAP2 (gray), and Hoechst (dashed outline). (**H**) Quantification of SP1 immunoreactivity in (**G**), normalized to fam cntrl mean for each replicate (n=170–213, cells/condition/replicate). Data from 3 biological replicates was used for quantification in (**B**), (**D**), (**F**), and (**H**), and black lines represent mean HMGA1/SP1 immunoreactivity for combined replicates. p-values in (**B**), (**D**), (**F**), and (**H**), were calculated using unpaired t-test with Welch's correction. (**I**) Hematoxylin and eosin (H&E) and HMGA1 immunostaining of putamen from one control and three VPS13A disease cases. (**J**) Relationship between gliosis score (0–4, assessed by H&E) and HMGA1 staining intensity (scored 0–4) in control (black) and patient cases (red). Scale bars in **A**, **C**, **E**, **G**, and **I**: 20µm.

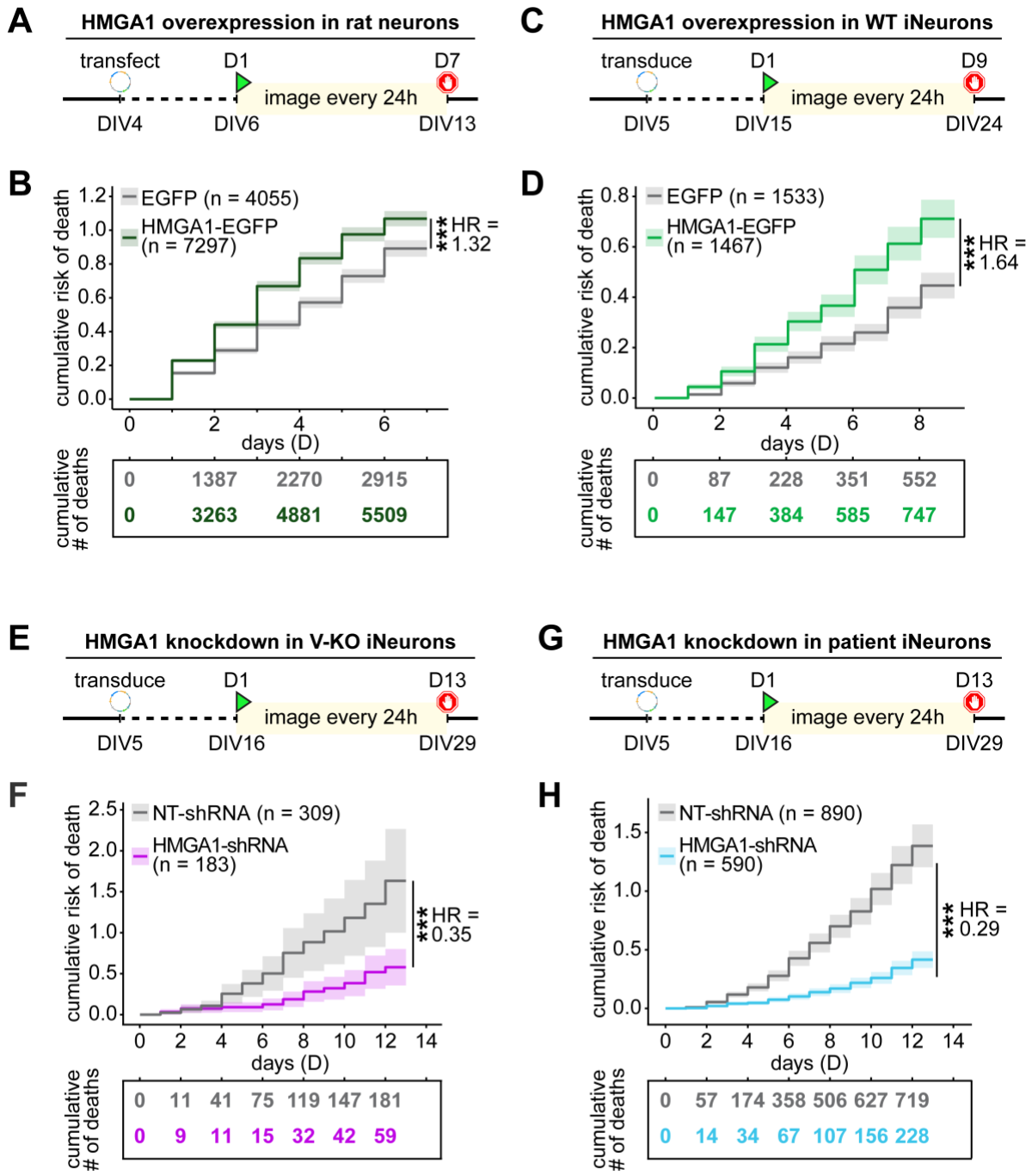
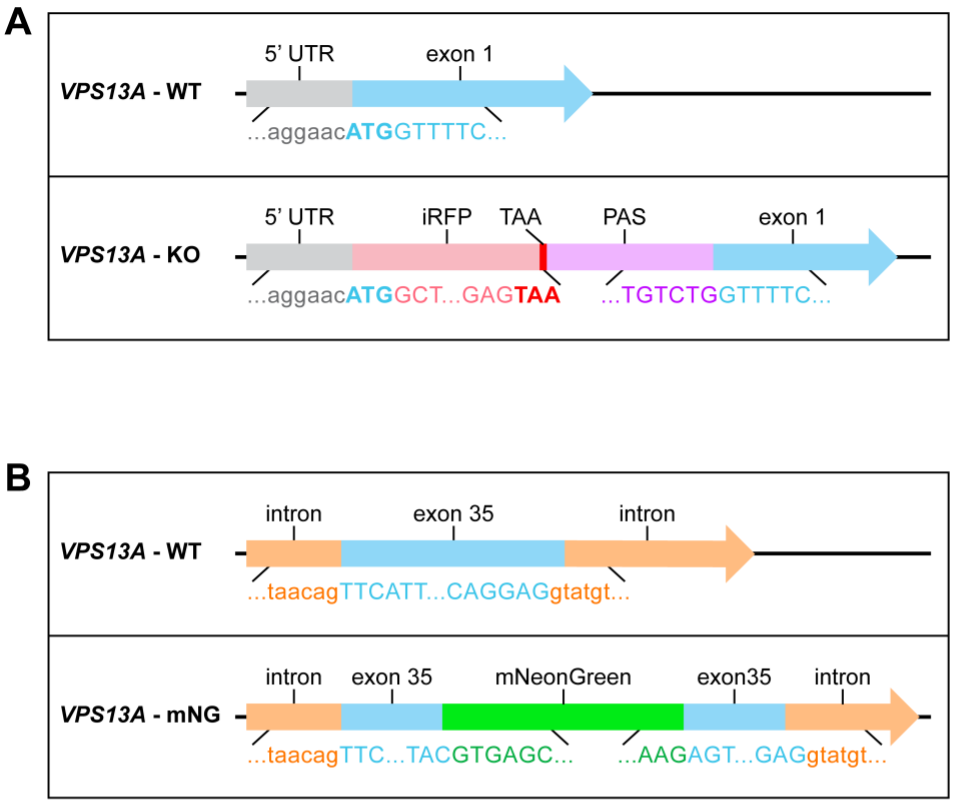


Figure 2.6 HMGA1 is both necessary and sufficient for neurotoxicity.

(**A**) Timeline for rat primary cortical neuron survival experiments. (**B**) Cumulative hazard plot and cumulative number of deaths in rat primary cortical neurons expressing EGFP (n=4055) and HMGA1-EGFP (n=7297). HR=1.32, ***$p<2x10^{-16}$, Cox proportional hazards analysis. (**C**) Timeline for control (WT) iNeuron survival experiments. (**D**) Cumulative hazard plot and cumulative number of deaths in WT iNeurons expressing EGFP (n=1533) and HMGA1-GFP (n=1467). HR=1.64, ***$p<2x10^{-16}$, Cox proportional hazards analysis. (**E**) Timeline for VPS13A knockout (V-KO) iNeuron survival experiments. (**F**) Cumulative hazard plot and cumulative number of deaths in V-KO iNeurons expressing HMGA1-shRNA (n=183) and NT-shRNA (n=309). HR=0.35, ***$p<1.68x10^{-10}$, Cox proportional hazards analysis. (**G**) Timeline for VPS13A disease patient (patient) iNeuron survival experiments. (**H**) Cumulative hazard plot and cumulative number of deaths in patient iNeurons expressing HMGA1-shRNA (n=590) and NT-shRNA (n=890). HR=0.29, ***$p<2x10^{-16}$, Cox proportional hazards analysis. Results in **B**, **D**, **F**, and **H** pooled and stratified from 3 biological replicates each, with n=number of neurons/condition.

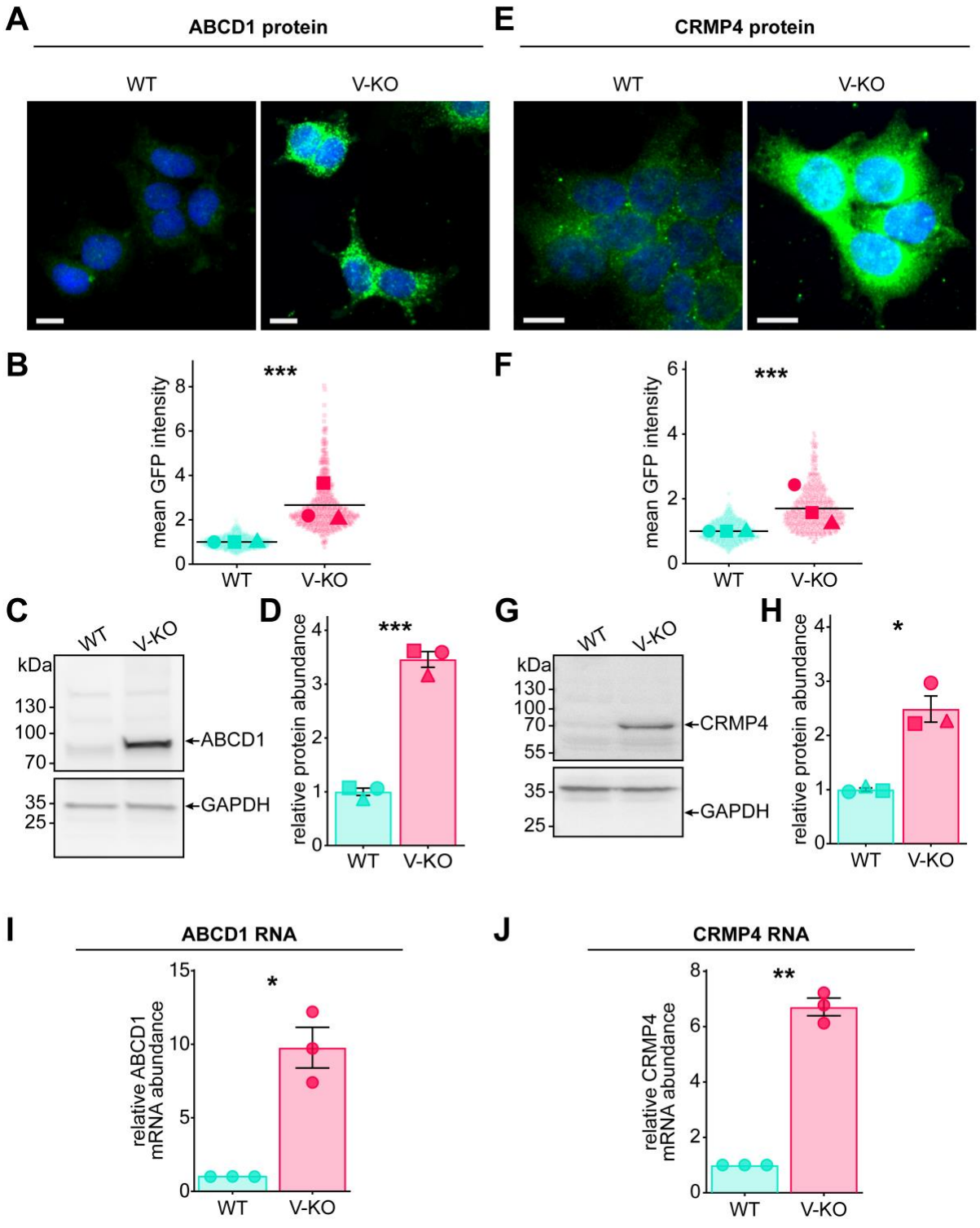
Supplemental figures



Supplemental Figure S2.1 Validation of VPS13A constructs using Sanger sequencing.

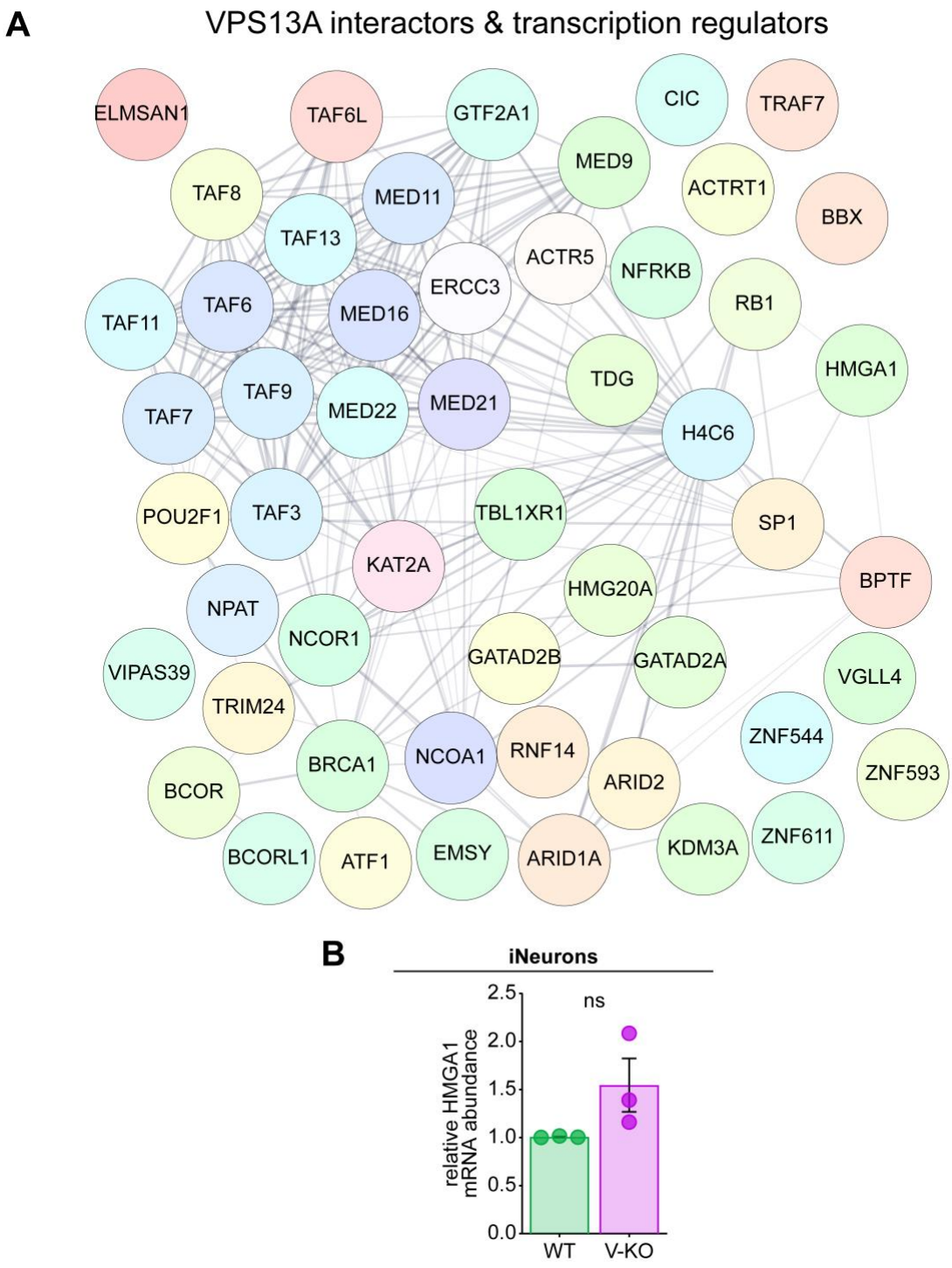
(**A**) Schematic of Sanger sequencing results confirm that the first coding exon of *VPS13A* (blue) was replaced by an open reading frame encoding the far-red fluorescent protein (iRFP; pink), a

stop codon (TAA; red), followed by a strong polyadenylation signal (PAS; purple) to eliminate endogenous VPS13A in otherwise healthy control HEK293T cells. (*VPS13A*-WT = primer 1831 (VPS13A 5' UTR FW) CGGAGCCGGTGAACCG); (*VPS13A*-KO (V-KO) = primer 1831 (VPS13A 5' UTR FW) CGGAGCCGGTGAACCG, primer 2266 (iRFP 3' FW) GCAGATCGGCGTGATGGAAG). (**B**) Sanger sequencing results confirm that the mNeonGreen (mNG; green) coding sequence was inserted in frame of *VPS13A* exon 35 in healthy control HEK293T cells. (*VPS13A*-WT = primer 2258 (VPS13A upstream E35 FW) TGGTGTGGTAGAGGATTGAAACA); (*VPS13A*-mNG = primer 2264 (mNG 3' FW) GAAGAACCAGCCGATGTACG).



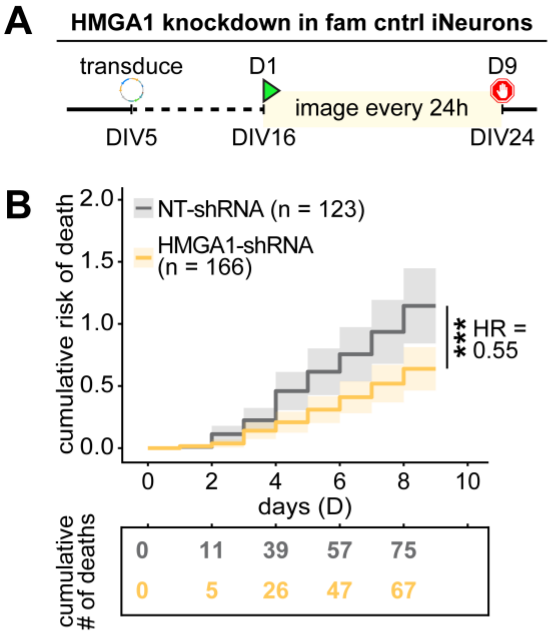
Supplemental Figure S2.2 ABCD1 and CRMP4 display elevated protein and RNA levels in VPS13A KO HEK293T cells.

(**A**) Representative images of WT and V-KO HEK293T cells immunostained for ABCD1 (green) and Hoechst (blue). Scale bars: 30 μm. (**B**) Quantification of whole cell mean ABCD1 immunoreactivity in (**A**), normalized to WT mean for each replicate. Data from 3 biological replicates (n=100–150 cells/replicate/condition). ***p<0.001 (unpaired t-test with Welch's correction). Black lines=mean ABCD1 immunoreactivity for combined replicates. (**C**) Representative immunoblot of lysate from V-KO and WT HEK293T cells probed with an anti-ABCD1 antibody. GAPDH was blotted as a loading control. (**D**) Quantification of ABCD1/GAPDH in (**C**), normalized to WT for each replicate. Data from 3 biological replicates. ***p=0.0008 (unpaired t-test with Welch's correction). Black lines=standard error of the mean for combined replicates. (**E**) Representative images of WT and V-KO HEK293T cells immunostained for CRMP4 (green) and Hoechst (blue) Scale bars: 30 μm. (**F**) Quantification of whole cell mean CRMP4 immunoreactivity in (**E**), normalized to WT mean for each replicate. Data from 3 biological replicates (n=100-150 cells/replicate/condition). ***p<0.001 (unpaired t-test with Welch's correction). Black lines=mean CRMP4 immunoreactivity for combined replicates. (**G**) Representative immunoblot of lysate from V-KO and WT HEK293T cells probed with an anti-CRMP4 antibody. GAPDH was blotted as a loading control. (**H**) Quantification of CRMP4/GAPDH in (**G**), normalized to WT for each replicate. Data from 3 biological replicates. *p=0.0240 (unpaired t-test with Welch's correction). Black lines=standard error of the mean for combined replicates. (**I**) qRT-PCR for *ABCD1/GAPDH* mRNA, normalized to WT for each replicate, from WT and V-KO HEK293T cells, displayed as mean ± SEM. Data from 3 technical replicates/3 biological replicates. *p=0.0240 (unpaired t-test with Welch's correction). (**J**) qRT-PCR for *CRMP4/GAPDH* mRNA normalized to WT for each replicate, from WT and V-KO HEK293T cells, displayed as mean ± SEM. Data from 3 technical replicates/3 biological replicates. **p=0.0031 (unpaired t-test with Welch's correction).



Supplemental Figure S2.3 Enrichment for transcriptional regulators among VPS13A interacting proteins in HEK293T cells.

(**A**) STRING network diagram of VPS13A interactors categorized by the Uniprot keyword 'Transcription Regulation' (n=52; KW-0805). (**B**) qRT-PCR of *HMGA1/GAPDH* mRNA levels, normalized to control (WT) for each replicate, from WT and VPS13A knockout (V-KO) iNeurons, displayed as mean±SEM. Data from 3 technical replicates/3 biological replicates. ns, p=0.1921 (unpaired t-test with Welch's correction).



Supplemental Figure S2.4 Knockdown of HMGA1 is sufficient to rescue neurotoxicity in familial control iNeurons.

(**A**) Timeline for familial control (fam cntrl) iNeuron survival experiments. (**B**) Cumulative hazard plot and cumulative number of deaths in fam cntrl iNeurons expressing HMGA1-shRNA (n=166) and NT-shRNA (n=123). HR=0.55, ***p=4x10^{-4}, Cox proportional hazards analysis. Results in (**B**) pooled and stratified from 2 biological replicates each, with n=number of neurons/condition.

Chapter 3 VPS13A Loss Does Not Disrupt Selective Autophagy in HEK293T Cells

Abstract

VPS13A disease, formerly called chorea acanthocytosis, is an autosomal recessive neurodegenerative disorder caused by loss of function mutations in the gene encoding vacuolar protein sorting factor 13A (VPS13A), resulting in near-complete loss of the protein. VPS13A belongs to the highly conserved VPS13 family of lipid transfer proteins that form elongated bridge-like structures capable of transporting phospholipids between organelle membranes and are enriched at membrane contact sites (MCSs). In yeast and other lower eukaryotes, VPS13 homologs are required for phagophore expansion and have been implicated in bulk and selective autophagy pathways. VPS13 proteins also share sequence and structural homology with the autophagy protein ATG2, suggesting a potential role for human VPS13A in autophagy. Studies in mammalian systems have linked VPS13A loss to altered autophagy-related markers, although phenotypes vary across models. Despite strong evidence that VPS13A localizes to endoplasmic reticulum (ER) and mitochondrial MCSs and contributes to organelle homeostasis, its role in organelle-selective-autophagy in human cells remains unknown. To address this, we analyzed VPS13A knockout (KO) human embryonic kidney (HEK) 293T cells using biochemical assays for ER phagy and mitophagy, together with quantitative mass-spectrometry-based proteomics to assess selective autophagic flux and organelle-associated protein abundance. VPS13A KO cells exhibited normal ER phagic and mitophagic flux, and proteomic analyses revealed no major alterations in ER, mitochondrial, or autophagy-related proteins. These findings indicate that VPS13A is not required for ER phagy or mitophagy in HEK293T cells and suggest that previously reported autophagy phenotypes may reflect indirect effects or cell-type-specific roles.

3.1 Introduction

3.1.1 Macroautophagy

Macroautophagy (sometimes called bulk autophagy), hereafter referred to as autophagy, is a conserved and tightly regulated catabolic pathway in which double-membrane vesicles called autophagosomes enclose damaged or excess cytoplasmic components, or even entire organelles, and deliver them to lysosomes for degradation and recycling[1–4]. When cells experience stress or nutrient deprivation, signaling pathways activate the Unc-51 like kinase 1 (ULK1) kinase complex (Atg1 complex in yeast) to initiate autophagy[5–7]. Activated ULK1 then recruits and stimulates the class III PI3-kinase (PI3K) complex I (PI3KC3-C1), which generates phosphatidylinositol-3-phosphate (PI3P) at specialized endoplasmic reticulum (ER)–associated subdomains called omegasomes[5–7]. Local enrichment of PI3P at omegasomes promotes the recruitment of PI3P-binding proteins, including the ATG2–ATG18 complex and WIPI proteins, that initiate the formation of the curved, cup-shaped double membrane called a phagophore (also known as an isolation membrane), in a process called nucleation[7–13].

Phagophore elongation and expansion require the coordinated action of several additional components, including ATG9-containing vesicles and two ubiquitin-like (UBL) conjugation systems: the ATG12–ATG5–ATG16L1 complex and the LC3-phosphatidylethanolamine (PE) lipidation system[7,14–23]. These conjugation cascades result in lipidated LC3 (LC3-II), which embeds into the phagophore membrane and, together with other factors, promotes membrane curvature, cargo recruitment, and growth of the phagophore[21,23,24]. Once the phagophore has fully enclosed the cytoplasmic cargo, the Endosomal Sorting Complex Required for Transport (ESCRT) machinery and other proteins mediate the closing of the membrane edges to form an autophagosome[25,26].

Autophagosomes then move along microtubules to late endosomes and lysosomes, where RAB7, a small GTPase that regulates late endosome and lysosome trafficking, the HOPS complex, a multi-subunit tethering complex that promotes membrane docking and fusion, and SNARE proteins, a family of membrane-anchored proteins that drive vesicle fusion through formation of trans-SNARE complexes, mediate tethering and fusion[26–28]. This fusion produces an acidic autolysosome in which hydrolytic enzymes break down the sequestered cargo into amino acids, fatty acids, sugars, and

other fundamental building blocks, which cells then export back into the cytosol where they can be reused[2–4,29–31].

A cell's ability to dynamically and effectively modify the rate of autophagy, measured as autophagic flux, is essential for maintaining cellular homeostasis[2,29,32]. Dysregulation of autophagy has been implicated in numerous conditions, including neurodegenerative diseases[4,30,31,33–37], neurodevelopmental disorders[38–40], autoimmune and infectious diseases[41–43], cancers[44–47], and metabolic syndromes[48]. Although many core autophagy proteins and mechanistic steps have been identified, important questions remain regarding how cells source and organize phagophore membrane components, how they regulate membrane expansion, and how disruption of specific autophagy components contributes to human disease.

3.1.2 Selective autophagy

Although autophagy was initially considered a largely nonselective, bulk degradation pathway, it is now well established that it can operate with a high degree of selectivity, targeting specific proteins, protein aggregates, or entire organelles for degradation and recycling[4,49,50]. These selective autophagy pathways rely on receptors that recognize specific cargo or organelle membranes and recruit components of the autophagic machinery to ensure selective removal[49,50]. While less is known about the regulatory mechanisms governing selective autophagy compared to bulk autophagy, these pathways play a critical role in maintaining organelle function and preventing the accumulation of damaged cellular components[4,50].

3.1.3 Mitophagy

Mitophagy, a mitochondria-specific form of selective autophagy, is a process by which cells identify, sequester, degrade, and recycle dysfunctional or excess mitochondrial components to maintain mitochondrial quality and metabolic homeostasis[51–54]. In mammalian cells, the primary mitophagy pathway operates through the PTEN induced putative kinase 1 (PINK1) and the E3 ubiquitin ligase Parkin signaling cascade, hereafter referred to as PINK1-Parkin-mediated mitophagy[54,55].

Healthy mitochondria maintain a negative membrane potential ($\Delta\Psi_m$) that allows PINK1, which anchors at the outer mitochondrial membrane (OMM), to undergo

continuous import into the inner mitochondrial membrane (IMM), where proteases such as presenilin associated rhomboid like protein (PARL) cleave it. This process results in translocation of PINK1 back into the cytosol and maintains low basal levels of full-length PINK1[55–59]. When mitochondria lose membrane potential, PINK1 import is blocked, leading to its accumulation and dimerization on the OMM. This accumulation promotes PINK1 activation through autotransphosphorylation[54,55,58–61]. Activated PINK1 phosphorylates multiple OMM substrates as well as cytosolic Parkin, priming Parkin for recruitment to damaged mitochondria[54,55,59–66]. Upon recruitment to the OMM, Parkin rapidly polyubiquitinates numerous OMM proteins, generating polyubiquitin chains that serve as signals for adaptor proteins. These adaptors bind and further phosphorylate the polyubiquitin chains, amplifying the mitophagy signal and promoting selective recruitment of LC3-positive phagophores to degrade the damaged mitochondria[53,55,62,67].

3.1.3.1 Mitofusin 2 (Mfn2) and mitophagy

Mitofusin 2 (Mfn2) is an OMM-localized GTPase that regulates mitochondrial outer membrane fusion and maintains specialized membrane contact sites (MCSs) between the OMM and the endoplasmic reticulum, known as mitochondria-associated membranes (MAMs)[68–71]. In addition to these functions, Mfn2 plays a key role in regulating PINK1-Parkin-mediated mitophagy[62,63,71–74]. Following mitochondrial depolarization, PINK1 accumulates and activates on the OMM and directly phosphorylates Mfn2, which increases its binding affinity for cytosolic Parkin and facilitates Parkin recruitment to the OMM[60,62,63,71]. After recruitment, Parkin ubiquitinates multiple OMM proteins, including Mfn2, generating a strong polyubiquitin signal that triggers downstream steps leading to degradation of damaged mitochondria, including degradation of Mfn2[65,66,71]. Loss of Mfn2 impairs Parkin recruitment to depolarized mitochondria and reduces ubiquitination of OMM proteins, thereby decreasing mitophagic flux and demonstrating that Mfn2 functions as a critical regulator of mitophagy[71,72,75].

Because PINK1-Parkin-mediated mitophagy rapidly ubiquitinates and degrades Mfn2, changes in Mfn2 protein levels serve as a reliable readout of mitophagic flux[62,71,76]. In contrast, other mitophagy-associated proteins, including PINK1 and Parkin, often display variable expression patterns that do not correlate consistently with mitophagic flux, making them less reliable markers of mitophagy[54,56,59,65]. Measurement of Mfn2

protein abundance therefore provides insight into both basal mitophagy and cellular responses to stimuli that induce or inhibit mitophagy across multiple conditions[62,71,72,74].

Defects in mitophagy have been reported in multiple human diseases, including neurodegenerative disorders[51,77–80], cardiomyopathies[74,81], metabolic syndromes[82,83], and cancer[64,67,84]. Impaired mitophagic flux leads to accumulation of damaged mitochondria, with cascading consequences for cellular health[76,85,86]. Mfn2-dependent mitophagy is particularly relevant in Charcot-Marie-Tooth disease type 2A (CMT2A), a hereditary axonal neurodegenerative disorder characterized by distal muscle weakness, sensory loss, and progressive peripheral nerve degeneration[73,81]. Autosomal dominant mutations in *MFN2* represent the most common cause of CMT2A and are associated with impaired mitochondrial fusion, altered MAM organization, and disrupted mitophagic flux, highlighting the importance of Mfn2 in maintaining neuronal mitochondrial health and axonal integrity[73,81,87,88].

3.1.4 Reticulophagy (ER-phagy)

The selective turnover of the ER via autophagy (also known as reticulophagy or ER-phagy) is critical for maintaining ER protein quality control and overall cellular homeostasis[89,90]. Receptor-mediated ER-phagy, hereafter called ER-phagy, relies on a subset of proteins that selectively recognize damaged or unused ER substrates and act as signals to recruit adaptor proteins and core autophagy machinery components that sequester and degrade that portion of the ER[89–92].

To enable this process, most ER-phagy receptors contain a transmembrane domain and an LC3-interaction region (LIR), that enables their interaction with members of the LC3/GABARAP protein family on autophagosomes[90,91]. To date, studies have identified eight of these transmembrane receptors, including three reticulon-like hairpin domain (RHD)-containing proteins, RETREG1 (also known as FAM134B)[93–97], RETREG2 (also known as FAM134A)[98,99], and RETREG3 (also known as FAM134C)[97,98,100,101], SEC62[102–104], reticulon-3 like protein (RTN3L)[105–107], cell cycle progression 1 (CCPG1)[108–112], atlastin GTPase 3 (ATL3)[113–115], and testis expressed 264 (TEX264)[111,112,116–120]. These receptors localize to different ER regions, respond to specific stimuli, and have additional distinct protein domains, allowing multiple, and sometimes overlapping, ER-phagy pathways within a cell[97,98,101,112,114].

3.1.4.1 ER-phagy receptor TEX264

Among these ER-phagy receptors, TEX264 is a highly abundant single-pass transmembrane protein that is ubiquitously expressed throughout the ER and mediates a large percentage of ER-phagy following nutrient starvation[111,112,116,118,120]. Depletion or loss of TEX264 impairs ER-phagy flux and leads to the accumulation of ER and ER-associated proteins[111,116]. Additionally, TEX264 itself is degraded via ER-phagy, and various studies find that TEX264 associates with multiple markers of early autophagosome formation at the ER, which eventually fuse with lysosomes for degradation, thereby suggesting that TEX264 levels can be used as a readout of ER-phagy flux[111,112,116].

Impaired ER-phagy and ER-phagy receptors are link to a range of human diseases, including hereditary sensory neuropathies associated with mutations in *FAM134B*[121–123], neurodegenerative diseases[90,99,112,124,125], and cancers[119,126–128]. In these diseases, defective ER-phagy may impair the removal of misfolded proteins, resulting in their accumulation and aggregation that can compromise ER function and overall cell survival[89,90,98,124].

3.1.5 VPS13 proteins and autophagy

VPS13A is a peripheral membrane protein that localizes to organelles including, but not limited to, the ER[129,130], mitochondria[129–132], endosomes and lysosomes[131–133], and the plasma membrane[134–138]. Additionally, proteins in the VPS13 family tend to concentrate at organelle MCSs[139–156], where two or more distinct organelles come into close contact with each other to facilitate various functions such as lipid transfer and organelle remodeling[157,158]. Although prior work has implicated VPS13A in mitochondrial and ER homeostasis[129–132,159–163], many questions remain about its specific mechanistic function at these organelles.

3.1.5.1 VPS13 proteins in lower eukaryotic organisms in autophagy pathways

The N- and C-terminal regions of VPS13 proteins share strong sequence and structural homology with the autophagy-related protein ATG2 (ATG2A and ATG2B in humans)[11–13,15,16,148,157,164–169], raising the possibility that VPS13 proteins may participate in autophagy. In yeast, Vps13 has been implicated in multiple autophagy-related

processes. Yeast mutants lacking Vps13 (Vps13Δ) show defects in multivesicular body (MVB)–vacuole (the yeast equivalent of lysosomes) fusion[145,170] and impaired macroautophagy[171]. Although some studies report elevated basal mitophagy and reduced mitophagic flux during starvation in Vps13Δ strains[139], other studies do not support a mitophagy defect[171]. Yeast Vps13Δ cells also show impaired ER-phagy[144,171], defective nucleophagy172, a selective autophagy pathway in which portions of the nucleus are delivered to the vacuole for degradation, and reduced pexophagy, a type of selective autophagy involving peroxisomes[171].

Evidence from other lower eukaryotic organisms further supports an autophagy-related role for VPS13 homologs. In *Dictyostelium discoideum*, mutants lacking the VPS13 homolog–TipC, exhibit reduced autophagosome formation and diminished autophagic flux under both basal and starvation conditions[165]. Likewise, in *Drosophila melanogaster*, loss of the VPS13 ortholog leads to accumulation of ubiquitylated proteins and the p62 homolog Ref(2)P, which also form aggregates throughout the central nervous system. Expression of human VPS13A only partially rescues these phenotypes[173]. Collectively, these findings suggest that VPS13 homologs contribute to autophagy or autophagy-related degradation pathways in lower eukaryotic organisms.

3.1.5.2 VPS13A in autophagy pathways

Recent studies in mammalian cell lines and tissues from individuals with VPS13A disease have reported that loss of VPS13A is associated with accumulation of autophagic markers, such as ULK1[163,174], ATG5 and ATG7[174,175], p62[131,163,174–176], LAMP1[131,133,163,175], LAMP2[133,175], LC3[131,163,165,174,175], RAB7A[131,133], and ubiquitin[174,176], as well as potential deficits in autophagic flux[165,175]. However, these phenotypes vary across cell types, experimental conditions, and between individual patients, leaving open the question of whether autophagic deficits arise directly from loss of VPS13A or instead reflect downstream, potentially compensatory, responses to broader cellular stress. While a handful of studies have shown that loss of VPS13 homologs in yeast and other lower eukaryotic organisms is associated with impaired organelle-specific autophagy pathways, including nucleophagy[172], ER-phagy[144,171], mitophagy[139], and pexophagy[171], studies have not yet explored these pathways for human VPS13A. In addition, localization and functional data linking VPS13A to mitochondria and the ER motivated the studies

described in this chapter. Thus, determining whether VPS13A plays a direct mechanistic role in ER-phagy or mitophagy is essential for clarifying whether organelle-specific autophagy defects contribute to the cellular pathology of VPS13A disease.

3.2 Results

3.2.1 Loss of VPS13A does not lead to accumulation of autophagy markers in HEK293T cells

We utilized the VPS13A knockout (V-KO) human embryonic kidney (HEK) 293T cells described in **Chapter 2** of this thesis. Briefly, a gene-trap strategy was used to replace the first coding exon of *VPS13A* with an open reading frame encoding the far-red fluorescent protein (iRFP), followed by a stop codon (TAA) and a strong polyadenylation signal (PAS) (**Fig. 2.2C**, **Fig. 2.3A**, and **Sup. Fig. S2.1A**). Because prior studies have reported elevated levels of autophagy-related proteins in VPS13A-deficient cells and tissues[131,133,163,174–176], we examined basal protein levels of several autophagy markers by immunoblotting. We observed no significant differences in levels of the lysosome-associated membrane proteins LAMP1 or LAMP2 between control and V-KO cells (**Figs. 3.1A–B**). LAMP1 and LAMP2 are major structural components of the lysosomal membrane and contribute to lysosomal integrity, fusion competency, and autophagosome–lysosome fusion[177–179]. Likewise, levels of LC3-I and LC3-II were unchanged in V-KO cells (**Fig. 3.1C**). CHMP2B, a component of the ESCRT-III complex required for autophagosome maturation[180–182], also showed no significant difference between genotypes (**Fig. 3.1D**). Together, these data suggest that VPS13A loss does not alter basal levels of several key proteins involved in lysosomal function, autophagosome maturation, or macroautophagy under basal conditions.

3.2.2 VPS13A deficiency does not alter ER-phagy or mitophagy flux in HEK293T cells

Previous studies in yeast and other lower eukaryotic organisms reported roles for VPS13 homologs in several organelle-specific autophagy pathways, including mitophagy[139], ER-phagy[144,171], pexophagy[171], and nucleophagy[172]. Although human VPS13A has not been functionally linked to any of these selective pathways, its localization to the ER[129,130] and mitochondria[129–132]-associated membranes, together with

data suggesting that it contributes to organelle integrity[129–132,159–163], led me to hypothesize that VPS13A loss might alter ER or mitochondrial turnover through ER-phagy and/or mitophagy. To first assess whether basal ER-phagy markers changed, we examined basal levels of atlastin-3 (ATL3), an ER-resident GTPase that functions as an ER-phagy receptor and undergoes degradation during ER-phagy[107,113,115,183]. ATL3 levels did not differ between V-KO and WT HEK293T cells (**Fig. 3.2A**). Given that basal receptor levels may not fully recapitulate autophagy activity, we next evaluated ER-phagy flux in response to inducing and/or blocking agents. Treatment with the mTORC1 inhibitor Torin 1 (Torin), which induces ER-phagy[97,100], reduced levels of the ER-phagy receptor TEX264[111,112,116–120] to a similar extent in both WT and V-KO cells. Likewise, treatment with the vesicular ATPase inhibitor Bafilomycin A1 (BafA1)[97,100] led to comparable TEX264 accumulation in both cell lines (**Fig. 3.2B**). We then assessed mitophagy by examining Mfn2, a mitochondrial fusion protein that undergoes ubiquitination and degradation during PINK1-Parkin-mediated mitophagy[62,63,79]. CCCP treatment reduced Mfn2 levels similarly in WT and V-KO cells[55,79], indicating comparable mitophagy induction in both lines (**Fig. 3.2C**). V-KO cells showed a mild but statistically significant elevation of Mfn2 after BafA1 treatment, although the magnitude of this difference was small.

Collectively, these data show that VPS13A knockout HEK293T cells do not exhibit detectable deficits in ER-phagy or mitophagy under either basal or experimentally manipulated conditions.

3.2.3 VPS13A deficiency does not result in broad changes to autophagy-associated protein abundance

To complement our targeted assays of ER-phagy and mitophagy, we examined whether VPS13A loss broadly alters ER-, mitochondrial-, or autophagy-related protein abundance using the tandem mass tag mass spectrometry (TMT-MS) dataset generated in **Chapter 2**. This unbiased proteomic approach enabled us to compare global protein expression patterns between WT and V-KO HEK293T cells. Although this analysis identified selective differences in a small number of ER- or mitochondrial-associated proteins, we did not observe consistent or pathway-related trends that would denote widespread deficits in ER or mitochondrial maintenance, turnover, or membrane integrity

(**Fig. 2.3A**). Likewise, we did not detect significant changes in abundance or consistent trends in the levels of core autophagy machinery, autophagy receptors, or proteins involved in autophagosome maturation (**Fig. 2.3B**). In line with the assays described above, these data indicate that VPS13A loss does not result in broad alterations to the ER or mitochondrial proteome, nor does it impact basal levels of autophagy-related proteins.

3.3 Discussion

In this chapter, we examined whether VPS13A plays a direct role in macroautophagy, receptor mediated ER-phagy, or mitophagy in human cells. Using the V-KO HEK293T cells described in **Chapter 2**, we first asked whether loss of VPS13A is sufficient to alter basal levels of several core autophagy proteins. Contrary to previous reports in other model systems[131,133,163,165,174,175], we did not observe accumulation of LAMP1, LAMP2, LC3, or CHMP2B in VPS13A deficient cells under baseline conditions.

We then evaluated organelle selective autophagy pathways more directly. V-KO cells showed normal abundance of the ER-phagy receptor–ATL3 under unstimulated conditions, and ER-phagy activation and suppression caused comparable changes in levels of the major ER-phagy receptor TEX264. Similarly, induction of mitophagy via CCCP led to comparable reductions in Mfn2 in both cell lines, with a small but significant increase in Mfn2 levels in V-KO cells compared to WT cells following autophagy inhibition. Finally, unbiased quantitative proteomic analysis revealed limited alterations among ER, mitochondrial, and autophagy related proteins in V-KO cells, but collectively these findings did not point to significant disruptions in autophagy pathways. Together, these data show that VPS13A loss does not produce strong autophagy phenotypes in HEK293T cells.

Although our findings are not consistent with other reports of macroautophagy and organelle selective autophagy impairments in VPS13 deficient models[131,133,139,145,163,165,170–172,174–176], one possibility is that a mechanistic role for VPS13A in autophagy is highly context dependent. Autophagy flux, selective autophagy receptor expression, organelle contact site composition, and organelle organization and

function vary dramatically across cell types and tissues[39,184–187]. For example, non dividing cells such as neurons rely heavily on selective autophagy pathways for organelle quality control and long term cellular survival[39,187], whereas other cell types such as HEK293T cells, which divide continuously, often display higher metabolic activity and greater tolerance to cellular stress[185,186].

It is also important to consider the potential contribution of functional redundancy between VPS13A and other bridge like lipid transfer proteins, particularly ATG2A and ATG2B[15,146,166,167], as well as the other human VPS13 paralogs VPS13B, VPS13C, and VPS13D[156,164,188]. While yeast encode a single VPS13 homolog, other VPS13 paralogs or lipid transfer proteins in human cells may compensate for certain VPS13A functions in a cell type specific manner.

Another possibility is that previously reported autophagy deficits in VPS13A deficient models reflect secondary or downstream responses rather than primary disruptions in autophagy machinery. As outlined in **Chapter 1**, evidence suggests that VPS13A contributes to mitochondrial homeostasis[130], cytoskeletal organization[161,162,189–192], and lipid transfer at multiple membrane contact sites[148,193]. Defects in any of these processes may increase susceptibility to cellular stress and indirectly elevate autophagy related markers.

Finally, experimental differences in autophagy induction or inhibition protocols, flux assays, or antibody usage may contribute to discrepancies across studies. This variability is particularly evident in reports describing VPS13A localization, which sometimes differ across experimental systems[130,171,194].

3.3.1 Limitations and future directions

While our findings did not reveal autophagy deficits in V-KO HEK293T cells, our methodology relied on immunoblot based assays and basal state proteomics. These techniques capture only a subset of potential autophagy pathway alterations and do not directly test autophagic flux. Live cell cargo trackers or tandem fluorescent autophagy reporters can help capture dynamic differences.

Future studies should investigate macro and organelle selective autophagy pathways in more disease relevant models such as V-KO iPSC derived neurons and patient derived cells utilized in **Chapter 2**. Combining these neuronal models with live

autophagic flux reporters can help determine whether deficits in these pathways contribute to neuropathology in VPS13A disease.

References

1. Ravikumar, B., Futter, M., Jahreiss, L., Korolchuk, V.I., Lichtenberg, M., Luo, S., Massey, D.C.O., Menzies, F.M., Narayanan, U., Renna, M., et al. (2009). Mammalian macroautophagy at a glance. J. Cell Sci. 122, 1707-1711. https://doi.org/10.1242/jcs.031773.

2. Yang, Z., and Klionsky, D.J. (2010). Eaten alive: a history of macroautophagy. Nat. Cell Biol. 12, 814–822. https://doi.org/10.1038/ncb0910-814.

3. Chew, L.H., and Yip, C.K. (2014). Structural biology of the macroautophagy machinery. Front. Biol. 9, 18–34. https://doi.org/10.1007/s11515-014-1293-3.

4. Fleming, A., Bourdenx, M., Fujimaki, M., Karabiyik, C., Krause, G.J., Lopez, A., Martín-Segura, A., Puri, C., Scrivo, A., Skidmore, J., et al. (2022). The different autophagy degradation pathways and neurodegeneration. Neuron 110, 935–966. https://doi.org/10.1016/j.neuron.2022.01.017.

5. Axe, E.L., Walker, S.A., Manifava, M., Chandra, P., Roderick, H.L., Habermann, A., Griffiths, G., and Ktistakis, N.T. (2008). Autophagosome formation from membrane compartments enriched in phosphatidylinositol 3-phosphate and dynamically connected to the endoplasmic reticulum. J. Cell Biol. 182, 685–701. https://doi.org/10.1083/jcb.200803137.

6. Karanasios, E., Stapleton, E., Manifava, M., Kaizuka, T., Mizushima, N., Walker, S.A., and Ktistakis, N.T. (2013). Dynamic association of the ULK1 complex with omegasomes during autophagy induction. J. Cell Sci. 126, 5224–5238. https://doi.org/10.1242/jcs.132415.

7. Karanasios, E., Walker, S.A., Okkenhaug, H., Manifava, M., Hummel, E., Zimmermann, H., Ahmed, Q., Domart, M.-C., Collinson, L., and Ktistakis, N.T. (2016). Autophagy initiation by ULK complex assembly on ER tubulovesicular regions marked by ATG9 vesicles. Nat. Commun. 7, 12420. https://doi.org/10.1038/ncomms12420.

8. Coutts, A.S., and La Thangue, N.B. (2015). Actin nucleation by WH2 domains at the autophagosome. Nature communications 6. https://doi.org/10.1038/ncomms8888.

9. Nascimbeni, A.C., Codogno, P., and Morel, E. (2017). Local detection of PtdIns3P at autophagosome biogenesis membrane platforms. Autophagy 13, 1602–1612. https://doi.org/10.1080/15548627.2017.1341465.

10. Otomo, T., and Maeda, S. (2019). ATG2A transfers lipids between membranes in vitro. Autophagy 15, 2031–2032. https://doi.org/10.1080/15548627.2019.1659622.

11. Tamura, N., Nishimura, T., Sakamaki, Y., Koyama-Honda, I., Yamamoto, H., and Mizushima, N. (2017). Differential requirement for ATG2A domains for localization to autophagic membranes and lipid droplets. FEBS Lett. 591, 3819–3830. https://doi.org/10.1002/1873-3468.12901.

12. Valverde, D.P., Yu, S., Boggavarapu, V., Kumar, N., Lees, J.A., Walz, T., Reinisch, K.M., and Melia, T.J. (2019). ATG2 transports lipids to promote autophagosome biogenesis. J. Cell Biol. 218, 1787–1798. https://doi.org/10.1083/jcb.201811139.

13. Osawa, T., Kotani, T., Kawaoka, T., Hirata, E., Suzuki, K., Nakatogawa, H., Ohsumi, Y., and Noda, N.N. (2019). Atg2 mediates direct lipid transfer between membranes for autophagosome formation. Nat. Struct. Mol. Biol. 26, 281–288. https://doi.org/10.1038/s41594-019-0203-4.

14. Vargas Duarte, P., and Reggiori, F. (2023). The organization and function of the phagophore-ER membrane contact sites. Contact (Thousand Oaks.) 6, 25152564231183896. https://doi.org/10.1177/25152564231183898.

15. van Vliet, A.R., Jefferies, H.B.J., Faull, P.A., Chadwick, J., Ibrahim, F., Skehel, M.J., and Tooze, S.A. (2024). Exploring the ATG9A interactome uncovers interaction with VPS13A. J. Cell Sci. 137, jcs261081. https://doi.org/10.1242/jcs.261081.

16. Gómez-Sánchez, R., Rose, J., Guimarães, R., Mari, M., Papinski, D., Rieter, E., Geerts, W.J., Hardenberg, R., Kraft, C., Ungermann, C., et al. (2018). Atg9 establishes Atg2-dependent contact sites between the endoplasmic reticulum and phagophores. J. Cell Biol. 217, 2743–2763. https://doi.org/10.1083/jcb.201710116.

17. Choi, J., Jang, H., Xuan, Z., and Park, D. (2024). Emerging roles of ATG9/ATG9A in autophagy: implications for cell and neurobiology. Autophagy 20, 2373–2387. https://doi.org/10.1080/15548627.2024.2384349.

18. Zhang, W., Ji, C., Li, X., He, T., Jiang, W., Liu, Y., Wu, M., Zhao, Y., Chen, X., Wang, X., et al. (2025). Autophagy-independent role of ATG9A vesicles as carriers for galectin-9 secretion. Nat. Commun. 16, 4259. https://doi.org/10.1038/s41467-025-59605-5.

19. Holzer, E., Martens, S., and Tulli, S. (2024). The role of ATG9 vesicles in autophagosome biogenesis. J. Mol. Biol. 436, 168489. https://doi.org/10.1016/j.jmb.2024.168489.

20. van Vliet, A.R., Chiduza, G.N., Maslen, S.L., Pye, V.E., Joshi, D., De Tito, S., Jefferies, H.B.J., Christodoulou, E., Roustan, C., Punch, E., et al. (2022). ATG9A and ATG2A form a heteromeric complex essential for autophagosome formation. Mol. Cell 82, 4324-4339.e8. https://doi.org/10.1016/j.molcel.2022.10.017.

21. Fujita, N., Itoh, T., Omori, H., Fukuda, M., Noda, T., and Yoshimori, T. (2008). The Atg16L complex specifies the site of LC3 lipidation for membrane biogenesis in autophagy. Mol. Biol. Cell 19, 2092–2100. https://doi.org/10.1091/mbc.e07-12-1257.

22. Lystad, A.H., Carlsson, S.R., and Simonsen, A. (2019). Toward the function of mammalian ATG12-ATG5-ATG16L1 complex in autophagy and related processes. Autophagy 15, 1485–1486. https://doi.org/10.1080/15548627.2019.1618100.

23. Iriondo, M.N., Etxaniz, A., Varela, Y.R., Ballesteros, U., Lázaro, M., Valle, M., Fracchiolla, D., Martens, S., Montes, L.R., Goñi, F.M., et al. (2023). Effect of ATG12-ATG5-ATG16L1 autophagy E3-like complex on the ability of LC3/GABARAP proteins to induce vesicle tethering and fusion. Cell. Mol. Life Sci. 80, 56. https://doi.org/10.1007/s00018-023-04704-z.

24. Runwal, G., Stamatakou, E., Siddiqi, F.H., Puri, C., Zhu, Y., and Rubinsztein, D.C. (2019). LC3-positive structures are prominent in autophagy-deficient cells. Sci. Rep. 9, 10147. https://doi.org/10.1038/s41598-019-46657-z.

25. Knorr, R.L., Lipowsky, R., and Dimova, R. (2015). Autophagosome closure requires membrane scission. Autophagy 11, 2134–2137. https://doi.org/10.1080/15548627.2015.1091552.

26. Kraft, C., and Reggiori, F. (2024). Phagophore closure, autophagosome maturation and autophagosome fusion during macroautophagy in the yeast Saccharomyces cerevisiae. FEBS Lett. 598, 73–83. https://doi.org/10.1002/1873-3468.14720.

27. Zhao, Y.G., and Zhang, H. (2019). Autophagosome maturation: An epic journey from the ER to lysosomes. J. Cell Biol. 218, 757–770. https://doi.org/10.1083/jcb.201810099.

28. Ganesan, D., and Cai, Q. (2021). Understanding amphisomes. Biochem. J. 478, 1959–1976. https://doi.org/10.1042/BCJ20200917.

29. Mauvezin, C., Nagy, P., Juhász, G., and Neufeld, T.P. (2015). Autophagosome-lysosome fusion is independent of V-ATPase-mediated acidification. Nat. Commun. 6, 7007. https://doi.org/10.1038/ncomms8007.

30. Lo, C.H., and Zeng, J. (2023). Defective lysosomal acidification: a new prognostic marker and therapeutic target for neurodegenerative diseases. Transl. Neurodegener. 12, 29. https://doi.org/10.1186/s40035-023-00362-0.

31. Lee, J.-H., Yu, W.H., Kumar, A., Lee, S., Mohan, P.S., Peterhoff, C.M., Wolfe, D.M., Martinez-Vicente, M., Massey, A.C., Sovak, G., et al. (2010). Lysosomal proteolysis and autophagy require presenilin 1 and are disrupted by Alzheimer-

related PS1 mutations. Cell 141, 1146–1158. https://doi.org/10.1016/j.cell.2010.05.008.

32. Safren, N., Tank, E.M., Malik, A.M., Chua, J.P., Santoro, N., and Barmada, S.J. (2021). Development of a specific live-cell assay for native autophagic flux. J. Biol. Chem. 297, 101003. https://doi.org/10.1016/j.jbc.2021.101003.

33. Yousefi, P., Ghadirian, S., Mobedi, M., Jafarzadeh, M., Alirezaei, A., Gholami, A., and Tabibzadeh, A. (2025). Autophagy related genes polymorphisms in Parkinson's Disease; A systematic review of literature. Clin. Park. Relat. Disord. 12, 100312. https://doi.org/10.1016/j.prdoa.2025.100312.

34. Metzger, S., Saukko, M., Van Che, H., Tong, L., Puder, Y., Riess, O., and Nguyen, H.P. (2010). Age at onset in Huntington's disease is modified by the autophagy pathway: implication of the V471A polymorphism in Atg7. Hum. Genet. 128, 453–459. https://doi.org/10.1007/s00439-010-0873-9.

35. Komatsu, M., Wang, Q.J., Holstein, G.R., Friedrich, V.L., Jr, Iwata, J.-I., Kominami, E., Chait, B.T., Tanaka, K., and Yue, Z. (2007). Essential role for autophagy protein Atg7 in the maintenance of axonal homeostasis and the prevention of axonal degeneration. Proc. Natl. Acad. Sci. U. S. A. 104, 14489–14494. https://doi.org/10.1073/pnas.0701311104.

36. Youn, J., Lee, S.-B., Lee, H.S., Yang, H.O., Park, J., Kim, J.S., Oh, E., Park, S., and Jang, W. (2018). Cerebrospinal fluid levels of autophagy-related proteins represent potentially novel biomarkers of early-stage Parkinson's disease. Sci. Rep. 8, 16866. https://doi.org/10.1038/s41598-018-35376-6.

37. Baldo, B., Soylu, R., and Petersén, A. (2013). Maintenance of basal levels of autophagy in Huntington's disease mouse models displaying metabolic dysfunction. PLoS One 8, e83050. https://doi.org/10.1371/journal.pone.0083050.

38. Deng, Z., Zhou, X., Lu, J.-H., and Yue, Z. (2021). Autophagy deficiency in neurodevelopmental disorders. Cell Biosci. 11, 214. https://doi.org/10.1186/s13578-021-00726-x.

39. Lieberman, O.J., Frier, M.D., McGuirt, A.F., Griffey, C.J., Rafikian, E., Yang, M., Yamamoto, A., Borgkvist, A., Santini, E., and Sulzer, D. (2020). Cell-type-specific regulation of neuronal intrinsic excitability by macroautophagy. Elife 9. https://doi.org/10.7554/eLife.50843.

40. Collier, J.J., Guissart, C., Oláhová, M., Sasorith, S., Piron-Prunier, F., Suomi, F., Zhang, D., Martinez-Lopez, N., Leboucq, N., Bahr, A., et al. (2021). Developmental consequences of defective ATG7-mediated autophagy in humans. N. Engl. J. Med. 384, 2406–2417. https://doi.org/10.1056/NEJMoa1915722.

41. Cadwell, K., Liu, J.Y., Brown, S.L., Miyoshi, H., Loh, J., Lennerz, J.K., Kishi, C., Kc, W., Carrero, J.A., Hunt, S., et al. (2008). A key role for autophagy and the autophagy gene Atg16l1 in mouse and human intestinal Paneth cells. Nature 456, 259–263. https://doi.org/10.1038/nature07416.

42. Kabat, A.M., Harrison, O.J., Riffelmacher, T., Moghaddam, A.E., Pearson, C.F., Laing, A., Abeler-Dörner, L., Forman, S.P., Grencis, R.K., Sattentau, Q., et al. (2016). The autophagy gene Atg16l1 differentially regulates Treg and TH2 cells to control intestinal inflammation. Elife 5, e12444. https://doi.org/10.7554/eLife.12444.

43. Conway, K.L., Kuballa, P., Song, J.-H., Patel, K.K., Castoreno, A.B., Yilmaz, O.H., Jijon, H.B., Zhang, M., Aldrich, L.N., Villablanca, E.J., et al. (2013). Atg16l1 is required for autophagy in intestinal epithelial cells and protection of mice from Salmonella infection. Gastroenterology 145, 1347–1357. https://doi.org/10.1053/j.gastro.2013.08.035.

44. Conte, A., Paladino, S., Bianco, G., Fasano, D., Gerlini, R., Tornincasa, M., Renna, M., Fusco, A., Tramontano, D., and Pierantoni, G.M. (2017). High mobility group A1 protein modulates autophagy in cancer cells. Cell Death Differ. 24, 1948–1962. https://doi.org/10.1038/cdd.2017.117.

45. Liu, X., Zhou, Z., Wang, Y., Zhu, K., Deng, W., Li, Y., Zhou, X., Chen, L., Li, Y., Xie, A., et al. (2020). Downregulation of HMGA1 mediates autophagy and inhibits migration and invasion in bladder cancer via miRNA-221/TP53INP1/p-ERK axis. Front. Oncol. 10, 589. https://doi.org/10.3389/fonc.2020.00589.

46. Takamura, A., Komatsu, M., Hara, T., Sakamoto, A., Kishi, C., Waguri, S., Eishi, Y., Hino, O., Tanaka, K., and Mizushima, N. (2011). Autophagy-deficient mice develop multiple liver tumors. Genes Dev. 25, 795–800. https://doi.org/10.1101/gad.2016211.

47. Cho, K.J., Shin, S.Y., Moon, H., Kim, B.K., and Ro, S.W. (2021). Knockdown of Atg7 suppresses Tumorigenesis in a murine model of liver cancer. Transl. Oncol. 14, 101158. https://doi.org/10.1016/j.tranon.2021.101158.

48. Menikdiwela, K.R., Ramalingam, L., Rasha, F., Wang, S., Dufour, J.M., Kalupahana, N.S., Sunahara, K.K.S., Martins, J.O., and Moustaid-Moussa, N. (2020). Autophagy in metabolic syndrome: breaking the wheel by targeting the renin-angiotensin system. Cell Death Dis. 11, 87. https://doi.org/10.1038/s41419-020-2275-9.

49. Li, W., He, P., Huang, Y., Li, Y.-F., Lu, J., Li, M., Kurihara, H., Luo, Z., Meng, T., Onishi, M., et al. (2021). Selective autophagy of intracellular organelles: recent

research advances. Theranostics 11, 222–256. https://doi.org/10.7150/thno.49860.

50. Yao, R.-Q., Ren, C., Xia, Z.-F., and Yao, Y.-M. (2021). Organelle-specific autophagy in inflammatory diseases: a potential therapeutic target underlying the quality control of multiple organelles. Autophagy 17, 385–401. https://doi.org/10.1080/15548627.2020.1725377.

51. Chen, B., Wang, Q., Wang, Y., Liu, Q., Chen, W., Mao, H., Li, J., Liu, Q., and Zhou, X. (2025). Mitochondrial quality control in neurodegenerative diseases: from molecular mechanisms to natural product therapies. Front. Physiol. 16, 1695681. https://doi.org/10.3389/fphys.2025.1695681.

52. Zhao, H., Zhang, Y., Ren, Y., and Wang, W. (2024). PINK1/Parkin-mediated mitophagy ameliorates mitochondrial dysfunction in lacrimal gland acinar cells during aging. Invest. Ophthalmol. Vis. Sci. 65, 12. https://doi.org/10.1167/iovs.65.13.12.

53. Lin, Q., Li, S., Jiang, N., Shao, X., Zhang, M., Jin, H., Zhang, Z., Shen, J., Zhou, Y., Zhou, W., et al. (2019). PINK1-parkin pathway of mitophagy protects against contrast-induced acute kidney injury via decreasing mitochondrial ROS and NLRP3 inflammasome activation. Redox Biol. 26, 101254. https://doi.org/10.1016/j.redox.2019.101254.

54. Lazarou, M., Sliter, D.A., Kane, L.A., Sarraf, S.A., Wang, C., Burman, J.L., Sideris, D.P., Fogel, A.I., and Youle, R.J. (2015). The ubiquitin kinase PINK1 recruits autophagy receptors to induce mitophagy. Nature 524, 309–314. https://doi.org/10.1038/nature14893.

55. Yan, C., Gong, L., Chen, L., Xu, M., Abou-Hamdan, H., Tang, M., Désaubry, L., and Song, Z. (2020). PHB2 (prohibitin 2) promotes PINK1-PRKN/Parkin-dependent mitophagy by the PARL-PGAM5-PINK1 axis. Autophagy 16, 419–434. https://doi.org/10.1080/15548627.2019.1628520.

56. Jin, S.M., Lazarou, M., Wang, C., Kane, L.A., Narendra, D.P., and Youle, R.J. (2010). Mitochondrial membrane potential regulates PINK1 import and proteolytic destabilization by PARL. J. Cell Biol. 191, 933–942. https://doi.org/10.1083/jcb.201008084.

57. Sekine, S., and Youle, R.J. (2018). PINK1 import regulation; a fine system to convey mitochondrial stress to the cytosol. BMC Biol. 16, 2. https://doi.org/10.1186/s12915-017-0470-7.

58. Becker, D., Richter, J., Tocilescu, M.A., Przedborski, S., and Voos, W. (2012). Pink1 kinase and its membrane potential (Deltaψ)-dependent cleavage product

both localize to outer mitochondrial membrane by unique targeting mode. J. Biol. Chem. 287, 22969–22987. https://doi.org/10.1074/jbc.M112.365700.

59. Greene, A.W., Grenier, K., Aguileta, M.A., Muise, S., Farazifard, R., Haque, M.E., McBride, H.M., Park, D.S., and Fon, E.A. (2012). Mitochondrial processing peptidase regulates PINK1 processing, import and Parkin recruitment. EMBO Rep. 13, 378–385. https://doi.org/10.1038/embor.2012.14.

60. Kondapalli, C., Kazlauskaite, A., Zhang, N., Woodroof, H.I., Campbell, D.G., Gourlay, R., Burchell, L., Walden, H., Macartney, T.J., Deak, M., et al. (2012). PINK1 is activated by mitochondrial membrane potential depolarization and stimulates Parkin E3 ligase activity by phosphorylating Serine 65. Open Biol. 2, 120080. https://doi.org/10.1098/rsob.120080.

61. Okatsu, K., Uno, M., Koyano, F., Go, E., Kimura, M., Oka, T., Tanaka, K., and Matsuda, N. (2013). A dimeric PINK1-containing complex on depolarized mitochondria stimulates Parkin recruitment. J. Biol. Chem. 288, 36372–36384. https://doi.org/10.1074/jbc.M113.509653.

62. Chen, Y., and Dorn, G.W., 2nd (2013). PINK1-phosphorylated mitofusin 2 is a Parkin receptor for culling damaged mitochondria. Science 340, 471–475. https://doi.org/10.1126/science.1231031.

63. Li, J., Dang, X., Franco, A., and Dorn, G.W., 2nd (2022). Reciprocal regulation of mitofusin 2-mediated mitophagy and mitochondrial fusion by different PINK1 phosphorylation events. Front. Cell Dev. Biol. 10, 868465. https://doi.org/10.3389/fcell.2022.868465.

64. Yao, N., Wang, C., Hu, N., Li, Y., Liu, M., Lei, Y., Chen, M., Chen, L., Chen, C., Lan, P., et al. (2019). Inhibition of PINK1/Parkin-dependent mitophagy sensitizes multidrug-resistant cancer cells to B5G1, a new betulinic acid analog. Cell Death Dis. 10, 232. https://doi.org/10.1038/s41419-019-1470-z.

65. Kane, L.A., Lazarou, M., Fogel, A.I., Li, Y., Yamano, K., Sarraf, S.A., Banerjee, S., and Youle, R.J. (2014). PINK1 phosphorylates ubiquitin to activate Parkin E3 ubiquitin ligase activity. J. Cell Biol. 205, 143–153. https://doi.org/10.1083/jcb.201402104.

66. Heo, J.-M., Ordureau, A., Paulo, J.A., Rinehart, J., and Harper, J.W. (2015). The PINK1-PARKIN mitochondrial ubiquitylation pathway drives a program of OPTN/NDP52 recruitment and TBK1 activation to promote mitophagy. Mol. Cell 60, 7–20. https://doi.org/10.1016/j.molcel.2015.08.016.

67. Villa, E., Proïcs, E., Rubio-Patiño, C., Obba, S., Zunino, B., Bossowski, J.P., Rozier, R.M., Chiche, J., Mondragón, L., Riley, J.S., et al. (2017). Parkin-

independent mitophagy controls chemotherapeutic response in cancer cells. Cell Rep. 20, 2846–2859. https://doi.org/10.1016/j.celrep.2017.08.087.

68. Filadi, R., Greotti, E., Turacchio, G., Luini, A., Pozzan, T., and Pizzo, P. (2015). Mitofusin 2 ablation increases endoplasmic reticulum-mitochondria coupling. Proc. Natl. Acad. Sci. U. S. A. 112, E2174-81. https://doi.org/10.1073/pnas.1504880112.

69. Gottschalk, B., Koshenov, Z., Bachkoenig, O.A., Rost, R., Malli, R., and Graier, W.F. (2022). MFN2 mediates ER-mitochondrial coupling during ER stress through specialized stable contact sites. Front. Cell Dev. Biol. 10, 918691. https://doi.org/10.3389/fcell.2022.918691.

70. Chen, H., Detmer, S.A., Ewald, A.J., Griffin, E.E., Fraser, S.E., and Chan, D.C. (2003). Mitofusins Mfn1 and Mfn2 coordinately regulate mitochondrial fusion and are essential for embryonic development. J. Cell Biol. 160, 189–200. https://doi.org/10.1083/jcb.200211046.

71. McLelland, G.-L., Goiran, T., Yi, W., Dorval, G., Chen, C.X., Lauinger, N.D., Krahn, A.I., Valimehr, S., Rakovic, A., Rouiller, I., et al. (2018). Mfn2 ubiquitination by PINK1/parkin gates the p97-dependent release of ER from mitochondria to drive mitophagy. Elife 7. https://doi.org/10.7554/eLife.32866.

72. Sebastián, D., Sorianello, E., Segalés, J., Irazoki, A., Ruiz-Bonilla, V., Sala, D., Planet, E., Berenguer-Llergo, A., Muñoz, J.P., Sánchez-Feutrie, M., et al. (2016). Mfn2 deficiency links age-related sarcopenia and impaired autophagy to activation of an adaptive mitophagy pathway. EMBO J. 35, 1677–1693. https://doi.org/10.15252/embj.201593084.

73. Abati, E., Manini, A., Velardo, D., Del Bo, R., Napoli, L., Rizzo, F., Moggio, M., Bresolin, N., Bellone, E., Bassi, M.T., et al. (2022). Clinical and genetic features of a cohort of patients with MFN2-related neuropathy. Sci. Rep. 12, 6181. https://doi.org/10.1038/s41598-022-10220-0.

74. Xiong, W., Ma, Z., An, D., Liu, Z., Cai, W., Bai, Y., Zhan, Q., Lai, W., Zeng, Q., Ren, H., et al. (2019). Mitofusin 2 participates in mitophagy and mitochondrial fusion against angiotensin II-induced cardiomyocyte injury. Front. Physiol. 10, 411. https://doi.org/10.3389/fphys.2019.00411.

75. Ding, Y., Gao, H., Zhao, L., Wang, X., and Zheng, M. (2015). Mitofusin 2-deficiency suppresses cell proliferation through disturbance of autophagy. PLoS One 10, e0121328. https://doi.org/10.1371/journal.pone.0121328.

76. Tanaka, A., Cleland, M.M., Xu, S., Narendra, D.P., Suen, D.-F., Karbowski, M., and Youle, R.J. (2010). Proteasome and p97 mediate mitophagy and degradation of mitofusins induced by Parkin. J. Cell Biol. 191, 1367–1380. https://doi.org/10.1083/jcb.201007013.

77. Vaillant-Beuchot, L., Mary, A., Pardossi-Piquard, R., Bourgeois, A., Lauritzen, I., Eysert, F., Kinoshita, P.F., Cazareth, J., Badot, C., Fragaki, K., et al. (2021). Accumulation of amyloid precursor protein C-terminal fragments triggers mitochondrial structure, function, and mitophagy defects in Alzheimer's disease models and human brains. Acta Neuropathol. 141, 39–65. https://doi.org/10.1007/s00401-020-02234-7.

78. Ma, K.Y., Fokkens, M.R., Reggiori, F., Mari, M., and Verbeek, D.S. (2021). Parkinson's disease-associated VPS35 mutant reduces mitochondrial membrane potential and impairs PINK1/Parkin-mediated mitophagy. Transl. Neurodegener. 10, 19. https://doi.org/10.1186/s40035-021-00243-4.

79. Benischke, A.-S., Vasanth, S., Miyai, T., Katikireddy, K.R., White, T., Chen, Y., Halilovic, A., Price, M., Price, F., Jr, Liton, P.B., et al. (2017). Activation of mitophagy leads to decline in Mfn2 and loss of mitochondrial mass in Fuchs endothelial corneal dystrophy. Sci. Rep. 7, 6656. https://doi.org/10.1038/s41598-017-06523-2.

80. Lesage, S., Drouet, V., Majounie, E., Deramecourt, V., Jacoupy, M., Nicolas, A., Cormier-Dequaire, F., Hassoun, S.M., Pujol, C., Ciura, S., et al. (2016). Loss of VPS13C function in autosomal-recessive parkinsonism causes mitochondrial dysfunction and increases PINK1/Parkin-dependent mitophagy. Am. J. Hum. Genet. 98, 500–513. https://doi.org/10.1016/j.ajhg.2016.01.014.

81. Franco, A., Li, J., Kelly, D.P., Hershberger, R.E., Marian, A.J., Lewis, R.M., Song, M., Dang, X., Schmidt, A.D., Mathyer, M.E., et al. (2023). A human mitofusin 2 mutation can cause mitophagic cardiomyopathy. Elife 12. https://doi.org/10.7554/eLife.84235.

82. Chen, W., Zhao, H., and Li, Y. (2023). Mitochondrial dynamics in health and disease: mechanisms and potential targets. Signal Transduct. Target. Ther. 8, 333. https://doi.org/10.1038/s41392-023-01547-9.

83. Seillier, M., Pouyet, L., N'Guessan, P., Nollet, M., Capo, F., Guillaumond, F., Peyta, L., Dumas, J.-F., Varrault, A., Bertrand, G., et al. (2015). Defects in mitophagy promote redox-driven metabolic syndrome in the absence of TP53INP1. EMBO Mol. Med. 7, 802–818. https://doi.org/10.15252/emmm.201404318.

84. Zou, J., Yue, F., Li, W., Song, K., Jiang, X., Yi, J., and Liu, L. (2014). Autophagy inhibitor LRPPRC suppresses mitophagy through interaction with mitophagy initiator Parkin. PLoS One 9, e94903. https://doi.org/10.1371/journal.pone.0094903.

85. Mauro-Lizcano, M., Esteban-Martínez, L., Seco, E., Serrano-Puebla, A., Garcia-Ledo, L., Figueiredo-Pereira, C., Vieira, H.L.A., and Boya, P. (2015). New method to assess mitophagy flux by flow cytometry. Autophagy 11, 833–843. https://doi.org/10.1080/15548627.2015.1034403.

86. Twig, G., Elorza, A., Molina, A.J.A., Mohamed, H., Wikstrom, J.D., Walzer, G., Stiles, L., Haigh, S.E., Katz, S., Las, G., et al. (2008). Fission and selective fusion govern mitochondrial segregation and elimination by autophagy. EMBO J. 27, 433–446. https://doi.org/10.1038/sj.emboj.7601963.

87. Rizzo, F., Ronchi, D., Salani, S., Nizzardo, M., Fortunato, F., Bordoni, A., Stuppia, G., Del Bo, R., Piga, D., Fato, R., et al. (2016). Selective mitochondrial depletion, apoptosis resistance, and increased mitophagy in human Charcot-Marie-Tooth 2A motor neurons. Hum. Mol. Genet. 25, 4266–4281. https://doi.org/10.1093/hmg/ddw258.

88. Zhou, Y., Carmona, S., Muhammad, A.K.M.G., Bell, S., Landeros, J., Vazquez, M., Ho, R., Franco, A., Lu, B., Dorn, G.W., 2nd, et al. (2019). Restoring mitofusin balance prevents axonal degeneration in a Charcot-Marie-Tooth type 2A model. J. Clin. Invest. 129, 1756–1771. https://doi.org/10.1172/JCI124194.

89. Ferro-Novick, S., Reggiori, F., and Brodsky, J.L. (2021). ER-phagy, ER homeostasis, and ER quality control: Implications for disease. Trends Biochem. Sci. 46, 630–639. https://doi.org/10.1016/j.tibs.2020.12.013.

90. Hübner, C.A., and Dikic, I. (2020). ER-phagy and human diseases. Cell Death Differ. 27, 833–842. https://doi.org/10.1038/s41418-019-0444-0.

91. Stephani, M., Picchianti, L., Gajic, A., Beveridge, R., Skarwan, E., Sanchez de Medina Hernandez, V., Mohseni, A., Clavel, M., Zeng, Y., Naumann, C., et al. (2020). A cross-kingdom conserved ER-phagy receptor maintains endoplasmic reticulum homeostasis during stress. Elife 9, e58396. https://doi.org/10.7554/elife.58396.

92. Liang, J.R., Lingeman, E., Luong, T., Ahmed, S., Muhar, M., Nguyen, T., Olzmann, J.A., and Corn, J.E. (2020). A genome-wide ER-phagy screen highlights key roles of mitochondrial metabolism and ER-resident UFMylation. Cell 180, 1160-1177.e20. https://doi.org/10.1016/j.cell.2020.02.017.

93. Khaminets, A., Heinrich, T., Mari, M., Grumati, P., Huebner, A.K., Akutsu, M., Liebmann, L., Stolz, A., Nietzsche, S., Koch, N., et al. (2015). Regulation of endoplasmic reticulum turnover by selective autophagy. Nature 522, 354–358. https://doi.org/10.1038/nature14498.

94. Liao, Y., Duan, B., Zhang, Y., Zhang, X., and Xia, B. (2019). Excessive ER-phagy mediated by the autophagy receptor FAM134B results in ER stress, the unfolded

protein response, and cell death in HeLa cells. J. Biol. Chem. 294, 20009–20023. https://doi.org/10.1074/jbc.RA119.008709.

95. Jiang, X., Wang, X., Ding, X., Du, M., Li, B., Weng, X., Zhang, J., Li, L., Tian, R., Zhu, Q., et al. (2020). FAM134B oligomerization drives endoplasmic reticulum membrane scission for ER-phagy. EMBO J. 39, e102608. https://doi.org/10.15252/embj.2019102608.

96. De Leonibus, C., Maddaluno, M., Ferriero, R., Besio, R., Cinque, L., Lim, P.J., Palma, A., De Cegli, R., Gagliotta, S., Montefusco, S., et al. (2024). Sestrin2 drives ER-phagy in response to protein misfolding. Dev. Cell 59, 2035-2052.e10. https://doi.org/10.1016/j.devcel.2024.07.004.

97. Berkane, R., Ho-Xuan, H., Glogger, M., Sanz-Martinez, P., Brunello, L., Glaesner, T., Kuncha, S.K., Holzhüter, K., Cano-Franco, S., Buonomo, V., et al. (2023). The function of ER-phagy receptors is regulated through phosphorylation-dependent ubiquitination pathways. Nat. Commun. 14, 8364. https://doi.org/10.1038/s41467-023-44101-5.

98. Reggio, A., Buonomo, V., Berkane, R., Bhaskara, R.M., Tellechea, M., Peluso, I., Polishchuk, E., Di Lorenzo, G., Cirillo, C., Esposito, M., et al. (2021). Role of FAM134 paralogues in endoplasmic reticulum remodeling, ER-phagy, and Collagen quality control. EMBO Rep. 22, e52289. https://doi.org/10.15252/embr.202052289.

99. Lim, J.R., Chae, C.W., Yoon, J.H., Cho, J.H., Park, J.Y., Han, S.J., Chang, H.S., Kim, S.Y., Kim, H.J., Jung, Y.H., et al. (2025). Recovery of FAM134A-mediated ER-phagy through BRD4 inhibition alleviates ethanol-induced neurodegeneration. Int. J. Biol. Sci. 21, 5167–5184. https://doi.org/10.7150/ijbs.116673.

100. Di Lorenzo, G., Iavarone, F., Maddaluno, M., Plata-Gómez, A.B., Aureli, S., Quezada Meza, C.P., Cinque, L., Palma, A., Reggio, A., Cirillo, C., et al. (2022). Phosphorylation of FAM134C by CK2 controls starvation-induced ER-phagy. Sci. Adv. 8, eabo1215. https://doi.org/10.1126/sciadv.abo1215.

101. Kumar, D., Lak, B., Suntio, T., Vihinen, H., Belevich, I., Viita, T., Xiaonan, L., Vartiainen, A., Vartiainen, M., Varjosalo, M., et al. (2021). RTN4B interacting protein FAM134C promotes ER membrane curvature and has a functional role in autophagy. Mol. Biol. Cell 32, 1158–1170. https://doi.org/10.1091/mbc.E20-06-0409.

102. Fumagalli, F., Noack, J., Bergmann, T.J., Cebollero, E., Pisoni, G.B., Fasana, E., Fregno, I., Galli, C., Loi, M., Soldà, T., et al. (2016). Translocon component Sec62 acts in endoplasmic reticulum turnover during stress recovery. Nat. Cell Biol. 18, 1173–1184. https://doi.org/10.1038/ncb3423.

103. Wu, J., Zhang, Z., Teng, Z., Abdullah, S.W., Sun, S., and Guo, H. (2021). Sec62 regulates endoplasmic reticulum stress and autophagy balance to affect foot-and-mouth disease virus replication. Front. Cell. Infect. Microbiol. 11, 707107. https://doi.org/10.3389/fcimb.2021.707107.

104. Chen, Z., Cheng, J., Zhou, Q., Wu, L.-L., Chen, J.-W., Duan, X.-N., Yan, J.-L., Cao, J.-G., Xia, X.-D., Li, L.-F., et al. (2025). SEC62-dependent ER-phagy contributes to apelin-13/APJ-induced monocyte-vascular endothelial cell adhesion in atherosclerosis pathogenesis. Acta Pharmacol. Sin. 46, 1652–1663. https://doi.org/10.1038/s41401-024-01471-w.

105. Grumati, P., Morozzi, G., Hölper, S., Mari, M., Harwardt, M.-L.I., Yan, R., Müller, S., Reggiori, F., Heilemann, M., and Dikic, I. (2017). Full length RTN3 regulates turnover of tubular endoplasmic reticulum via selective autophagy. Elife 6. https://doi.org/10.7554/eLife.25555.

106. Chidambaram, R., Kumar, K., Parashar, S., Ramachandran, G., Chen, S., and Ferro-Novick, S. (2024). PINK1 controls RTN3L-mediated ER autophagy by regulating peripheral tubule junctions. J. Cell Biol. 223. https://doi.org/10.1083/jcb.202407193.

107. Kumar, K., Chidambaram, R., Parashar, S., and Ferro-Novick, S. (2024). RTN3L and CALCOCO1 function in parallel to maintain proteostasis in the endoplasmic reticulum. Autophagy 20, 2067–2075. https://doi.org/10.1080/15548627.2024.2353502.

108. Chino, H., Ishii, S., Mizushima, N., and Itakura, E. (2023). Cargo-interacting regions (CIR) of CCPG1 capture ER luminal cargos for reticulophagy. Autophagy Rep. 2, 2213560. https://doi.org/10.1080/27694127.2023.2213560.

109. Ishii, S., Chino, H., Ode, K.L., Kurikawa, Y., Ueda, H.R., Matsuura, A., Mizushima, N., and Itakura, E. (2023). CCPG1 recognizes endoplasmic reticulum luminal proteins for selective ER-phagy. Mol. Biol. Cell 34, ar29. https://doi.org/10.1091/mbc.E22-09-0432.

110. Smith, M.D., Harley, M.E., Kemp, A.J., Wills, J., Lee, M., Arends, M., von Kriegsheim, A., Behrends, C., and Wilkinson, S. (2018). CCPG1 is a non-canonical autophagy cargo receptor essential for ER-phagy and pancreatic ER proteostasis. Dev. Cell 44, 217-232.e11. https://doi.org/10.1016/j.devcel.2017.11.024.

111. Chino, H., Hatta, T., Natsume, T., and Mizushima, N. (2019). Intrinsically disordered protein TEX264 mediates ER-phagy. Mol. Cell 74, 909-921.e6. https://doi.org/10.1016/j.molcel.2019.03.033.

112. Hoyer, M.J., Capitanio, C., Smith, I.R., Paoli, J.C., Bieber, A., Jiang, Y., Paulo, J.A., Gonzalez-Lozano, M.A., Baumeister, W., Wilfling, F., et al. (2024).

Combinatorial selective ER-phagy remodels the ER during neurogenesis. Nat. Cell Biol. 26, 378–392. https://doi.org/10.1038/s41556-024-01356-4.

113. Chen, Q., Xiao, Y., Chai, P., Zheng, P., Teng, J., and Chen, J. (2019). ATL3 is a tubular ER-phagy receptor for GABARAP-mediated selective autophagy. Curr. Biol. 29, 846-855.e6. https://doi.org/10.1016/j.cub.2019.01.041.

114. Tan, X., Cai, K., Li, J., Yuan, Z., Chen, R., Xiao, H., Xu, C., Hu, B., Qin, Y., and Ding, B. (2023). Coronavirus subverts ER-phagy by hijacking FAM134B and ATL3 into p62 condensates to facilitate viral replication. Cell Rep. 42, 112286. https://doi.org/10.1016/j.celrep.2023.112286.

115. Liang, J.R., Lingeman, E., Ahmed, S., and Corn, J.E. (2018). Atlastins remodel the endoplasmic reticulum for selective autophagy. J. Cell Biol. 217, 3354–3367. https://doi.org/10.1083/jcb.201804185.

116. An, H., Ordureau, A., Paulo, J.A., Shoemaker, C.J., Denic, V., and Harper, J.W. (2019). TEX264 is an endoplasmic reticulum-resident ATG8-interacting protein critical for ER remodeling during nutrient stress. Mol. Cell 74, 891-908.e10. https://doi.org/10.1016/j.molcel.2019.03.034.

117. Yan, M., Wang, Z., Xia, T., Jin, S., Liu, Y., Hu, H., and Chang, Q. (2021). Enhancement of TEX264-mediated ER-phagy contributes to the therapeutic effect of glycycoumarin against APA hepatotoxicity in mice. Biomedicines 9, 939. https://doi.org/10.3390/biomedicines9080939.

118. Chino, H., Yamasaki, A., Ode, K.L., Ueda, H.R., Noda, N.N., and Mizushima, N. (2022). Phosphorylation by casein kinase 2 enhances the interaction between ER-phagy receptor TEX264 and ATG8 proteins. EMBO Rep. 23, e54801. https://doi.org/10.15252/embr.202254801.

119. Lascaux, P., Hoslett, G., Tribble, S., Trugenberger, C., Antičević, I., Otten, C., Torrecilla, I., Koukouravas, S., Zhao, Y., Yang, H., et al. (2024). TEX264 drives selective autophagy of DNA lesions to promote DNA repair and cell survival. Cell 187, 5698-5718.e26. https://doi.org/10.1016/j.cell.2024.08.020.

120. Johnson, C.J., Tiwaa, A., Parihar, A., Antonio, E., Lorenz, B.D., Kudallur, R., Ramonett, A., Coon, A., Sarkar, M.K., Gudjonsson, J.E., et al. (2025). The endoplasmic reticulum autophagy receptor TEX264 drives epidermal differentiation and is dysregulated in Darier disease. bioRxivorg. https://doi.org/10.1101/2025.08.05.668774.

121. Park, G.-Y., Jang, D.-H., Lee, D.-W., Jang, J.-H., and Joo, J. (2019). Hereditary sensory and autonomic neuropathy 2B caused by a novel RETREG1 mutation (c.765dupT) and paternal uniparental isodisomy of chromosome 5. Front. Genet. 10, 1085. https://doi.org/10.3389/fgene.2019.01085.

122. Falcão de Campos, C., Vidailhet, M., Toutain, A., de Becdelièvre, A., Funalot, B., Bonello-Palot, N., and Stojkovic, T. (2019). Hereditary sensory autonomic neuropathy type II: Report of two novel mutations in the FAM134B gene. J. Peripher. Nerv. Syst. 24, 354–358. https://doi.org/10.1111/jns.12352.

123. Murphy, S.M., Davidson, G.L., Brandner, S., Houlden, H., and Reilly, M.M. (2012). Mutation in FAM134B causing severe hereditary sensory neuropathy. J. Neurol. Neurosurg. Psychiatry 83, 119–120. https://doi.org/10.1136/jnnp.2010.228965.

124. Wang, Z., Huang, J., Yang, S.-P., and Weaver, D.F. (2022). Anti-inflammatory anthranilate analogue enhances autophagy through mTOR and promotes ER-turnover through TEX264 during Alzheimer-associated neuroinflammation. ACS Chem. Neurosci. 13, 406–422. https://doi.org/10.1021/acschemneuro.1c00818.

125. Kim, D.Y., Shin, J.Y., Lee, J.E., Kim, H.N., Chung, S.J., Yoo, H.S., Kim, S.J., Cho, H.J., Lee, E.-J., Nam, S.J., et al. (2023). A selective ER-phagy exerts neuroprotective effects via modulation of α-synuclein clearance in parkinsonian models. Proc. Natl. Acad. Sci. U. S. A. 120, e2221929120. https://doi.org/10.1073/pnas.2221929120.

126. Chipurupalli, S., Ganesan, R., Martini, G., Mele, L., Reggio, A., Esposito, M., Kannan, E., Namasivayam, V., Grumati, P., Desiderio, V., et al. (2022). Cancer cells adapt FAM134B/BiP mediated ER-phagy to survive hypoxic stress. Cell Death Dis. 13, 357. https://doi.org/10.1038/s41419-022-04813-w.

127. Gössl, F.J., Polo, P., Helmprobst, F., Menzenbach, A., Visekruna, A., Gress, T.M., Adhikary, T., and Lauth, M. (2025). ER-phagy mediates the anti-tumoral synergism between HDAC inhibition and chemotherapy. Cell Commun. Signal. 23, 202. https://doi.org/10.1186/s12964-025-02198-9.

128. Zhou, H., Wang, K., Wang, M., Zhao, W., Zhang, C., Cai, M., Qiu, Y., Zhang, T., Shao, R., and Zhao, W. (2022). ER-phagy in the occurrence and development of cancer. Biomedicines 10, 707. https://doi.org/10.3390/biomedicines10030707.

129. Kumar, N., Leonzino, M., Hancock-Cerutti, W., Horenkamp, F.A., Li, P., Lees, J.A., Wheeler, H., Reinisch, K.M., and De Camilli, P. (2018). VPS13A and VPS13C are lipid transport proteins differentially localized at ER contact sites. J. Cell Biol. 217, 3625–3639. https://doi.org/10.1083/jcb.201807019.

130. Yeshaw, W.M., van der Zwaag, M., Pinto, F., Lahaye, L.L., Faber, A.I., Gómez-Sánchez, R., Dolga, A.M., Poland, C., Monaco, A.P., van IJzendoorn, S.C., et al. (2019). Human VPS13A is associated with multiple organelles and influences mitochondrial morphology and lipid droplet motility. Elife 8, e43561. https://doi.org/10.7554/eLife.43561.

131. Muñoz-Braceras, S., Tornero-Écija, A.R., Vincent, O., and Escalante, R. (2019). VPS13A is closely associated with mitochondria and is required for efficient lysosomal degradation. Dis. Model. Mech. 12, dmm036681. https://doi.org/10.1242/dmm.036681.

132. Tornero-Écija, A., Zapata-Del-Baño, A., Antón-Esteban, L., Vincent, O., and Escalante, R. (2023). The association of lipid transfer protein VPS13A with endosomes is mediated by sorting nexin SNX5. Life Sci. Alliance 6, e202201852. https://doi.org/10.26508/lsa.202201852.

133. Tornero-Écija, A.R., Navas, M.A., Muñoz-Braceras, S., Vincent, O., and Escalante, R. (2023). Effect of rapamycin on lysosomal accumulation in a CRISPR/Cas9-based cellular model of VPS13A deficiency. J. Cell. Mol. Med. 27, 1557–1564. https://doi.org/10.1111/jcmm.17768.

134. Park, J.-S., and Neiman, A.M. (2020). XK is a partner for VPS13A: a molecular link between Chorea-Acanthocytosis and McLeod Syndrome. Mol. Biol. Cell 31, 2425–2436. https://doi.org/10.1091/mbc.E19-08-0439-T.

135. Guillén-Samander, A., Wu, Y., Pineda, S.S., García, F.J., Eisen, J.N., Leonzino, M., Ugur, B., Kellis, M., Heiman, M., and De Camilli, P. (2022). A partnership between the lipid scramblase XK and the lipid transfer protein VPS13A at the plasma membrane. Proc. Natl. Acad. Sci. U. S. A. 119, e2205425119. https://doi.org/10.1073/pnas.2205425119.

136. Park, J.-S., Hu, Y., Hollingsworth, N.M., Miltenberger-Miltenyi, G., and Neiman, A.M. (2022). Interaction between VPS13A and the XK scramblase is important for VPS13A function in humans. J. Cell Sci. 135, jcs260227. https://doi.org/10.1242/jcs.260227.

137. Ryoden, Y., Segawa, K., and Nagata, S. (2022). Requirement of Xk and Vps13a for the P2X7-mediated phospholipid scrambling and cell lysis in mouse T cells. Proc. Natl. Acad. Sci. U. S. A. 119, e2119286119. https://doi.org/10.1073/pnas.2119286119.

138. Nishizawa, Y., Sakimoto, H., Nagata, O., Sasaki, N., Urata, Y., Arai, K., Hiwatashi, H., Yokoyama, I., Kishida, S., Sano, A., et al. (2025). Chorein deficiency promotes ferroptosis. FEBS Open Bio 15, 58–68. https://doi.org/10.1002/2211-5463.13870.

139. Park, J.-S., Thorsness, M.K., Policastro, R., McGoldrick, L.L., Hollingsworth, N.M., Thorsness, P.E., and Neiman, A.M. (2016). Yeast Vps13 promotes mitochondrial function and is localized at membrane contact sites. Mol. Biol. Cell 27, 2435–2449. https://doi.org/10.1091/mbc.E16-02-0112.

140. Lang, A.B., John Peter, A.T., Walter, P., and Kornmann, B. (2015). ER-mitochondrial junctions can be bypassed by dominant mutations in the endosomal protein Vps13. J. Cell Biol. 210, 883–890. https://doi.org/10.1083/jcb.201502105.

141. John Peter, A.T., Herrmann, B., Antunes, D., Rapaport, D., Dimmer, K.S., and Kornmann, B. (2017). Vps13-Mcp1 interact at vacuole-mitochondria interfaces and bypass ER-mitochondria contact sites. J. Cell Biol. 216, 3219–3229. https://doi.org/10.1083/jcb.201610055.

142. Bean, B.D.M., Dziurdzik, S.K., Kolehmainen, K.L., Fowler, C.M.S., Kwong, W.K., Grad, L.I., Davey, M., Schluter, C., and Conibear, E. (2018). Competitive organelle-specific adaptors recruit Vps13 to membrane contact sites. J. Cell Biol. 217, 3593–3607. https://doi.org/10.1083/jcb.201804111.

143. Yuan, W., Akşit, A., de Boer, R., Krikken, A.M., and van der Klei, I.J. (2022). Yeast Vps13 is crucial for peroxisome expansion in cells with reduced peroxisome-ER contact sites. Front. Cell Dev. Biol. 10, 842285. https://doi.org/10.3389/fcell.2022.842285.

144. Chen, S., Mari, M., Parashar, S., Liu, D., Cui, Y., Reggiori, F., Novick, P.J., and Ferro-Novick, S. (2020). Vps13 is required for the packaging of the ER into autophagosomes during ER-phagy. Proc. Natl. Acad. Sci. U. S. A. 117, 18530–18539. https://doi.org/10.1073/pnas.2008923117.

145. Suzuki, S.W., West, M., Zhang, Y., Fan, J.S., Roberts, R.T., Odorizzi, G., and Emr, S.D. (2024). A role for Vps13-mediated lipid transfer at the ER-endosome contact site in ESCRT-mediated sorting. J. Cell Biol. 223, e202307094. https://doi.org/10.1083/jcb.202307094.

146. Dabrowski, R., Tulli, S., and Graef, M. (2023). Parallel phospholipid transfer by Vps13 and Atg2 determines autophagosome biogenesis dynamics. J. Cell Biol. 222, e202211039. https://doi.org/10.1083/jcb.202211039.

147. Nakamura, N., and Hirose, S. (2008). Regulation of mitochondrial morphology by USP30, a deubiquitinating enzyme present in the mitochondrial outer membrane. Mol. Biol. Cell 19, 1903–1911. https://doi.org/10.1091/mbc.e07-11-1103.

148. Rzepnikowska, W., Flis, K., Kaminska, J., Grynberg, M., Urbanek, A., Ayscough, K.R., and Zoladek, T. (2017). Amino acid substitution equivalent to human chorea-acanthocytosis I2771R in yeast Vps13 protein affects its binding to phosphatidylinositol 3-phosphate. Hum. Mol. Genet. 26, 1497–1510. https://doi.org/10.1093/hmg/ddx054.

149. Kolakowski, D., Rzepnikowska, W., Kaniak-Golik, A., Zoladek, T., and Kaminska, J. (2021). The GTPase Arf1 is a determinant of yeast Vps13 localization to the

Golgi apparatus. Int. J. Mol. Sci. 22, 12274. https://doi.org/10.3390/ijms222212274.

150. Park, J.-S., and Neiman, A.M. (2012). VPS13 regulates membrane morphogenesis during sporulation in Saccharomyces cerevisiae. J. Cell Sci. 125, 3004–3011. https://doi.org/10.1242/jcs.105114.

151. Park, J.-S., Okumura, Y., Tachikawa, H., and Neiman, A.M. (2013). SPO71 encodes a developmental stage-specific partner for Vps13 in Saccharomyces cerevisiae. Eukaryot. Cell 12, 1530–1537. https://doi.org/10.1128/EC.00239-13.

152. Guillén-Samander, A., Leonzino, M., Hanna, M.G., Tang, N., Shen, H., and De Camilli, P. (2021). VPS13D bridges the ER to mitochondria and peroxisomes via Miro. J. Cell Biol. 220, e202010004. https://doi.org/10.1083/jcb.202010004.

153. Du, Y., Fan, X., Song, C., Chang, W., Xiong, J., Deng, L., and Ji, W.-K. (2024). Sec23IP recruits VPS13B/COH1 to ER exit site-Golgi interface for tubular ERGIC formation. J. Cell Biol. 223. https://doi.org/10.1083/jcb.202402083.

154. Ugur, B., Schueder, F., Shin, J., Hanna, M.G., Wu, Y., Leonzino, M., Su, M., McAdow, A.R., Wilson, C., Postlethwait, J., et al. (2024). VPS13B is localized at the interface between Golgi cisternae and is a functional partner of FAM177A1. J. Cell Biol. 223, e202311189. https://doi.org/10.1083/jcb.202311189.

155. Du, Y., Hu, X., Chang, W., Deng, L., Ji, W.-K., and Xiong, J. (2023). A possible role of VPS13B in the formation of Golgi-lipid droplet contacts associating with the ER. Contact (Thousand Oaks.) 6, 25152564231195720. https://doi.org/10.1177/25152564231195718.

156. Dall'Armellina, F., Stagi, M., and Swan, L.E. (2023). In silico modeling human VPS13 proteins associated with donor and target membranes suggests lipid transfer mechanisms. Proteins 91, 439–455. https://doi.org/10.1002/prot.26446.

157. Lees, J.A., and Reinisch, K.M. (2020). Inter-organelle lipid transfer: a channel model for Vps13 and chorein-N motif proteins. Curr. Opin. Cell Biol. 65, 66–71. https://doi.org/10.1016/j.ceb.2020.02.008.

158. Henne, W.M. (2016). Organelle remodeling at membrane contact sites. J. Struct. Biol. 196, 15–19. https://doi.org/10.1016/j.jsb.2016.05.003.

159. Glaß, H., Pal, A., Reinhardt, P., Sterneckert, J., Wegner, F., Storch, A., and Hermann, A. (2018). Defective mitochondrial and lysosomal trafficking in chorea-acanthocytosis is independent of Src-kinase signaling. Mol. Cell. Neurosci. 92, 137–148. https://doi.org/10.1016/j.mcn.2018.08.002.

160. Glaß, H., Neumann, P., Pal, A., Reinhardt, P., Storch, A., Sterneckert, J., and Hermann, A. (2020). Combined dendritic and axonal deterioration are responsible

for motoneuronopathy in patient-derived neuronal cell models of chorea-acanthocytosis. Int. J. Mol. Sci. 21, 1797. https://doi.org/10.3390/ijms21051797.

161. Föller, M., Hermann, A., Gu, S., Alesutan, I., Qadri, S.M., Borst, O., Schmidt, E.-M., Schiele, F., vom Hagen, J.M., Saft, C., et al. (2012). Chorein-sensitive polymerization of cortical actin and suicidal cell death in chorea-acanthocytosis. FASEB J. 26, 1526–1534. https://doi.org/10.1096/fj.11-198317.

162. Honisch, S., Yu, W., Liu, G., Alesutan, I., Towhid, S.T., Tsapara, A., Schleicher, S., Handgretinger, R., Stournaras, C., and Lang, F. (2015). Chorein addiction in VPS13A overexpressing rhabdomyosarcoma cells. Oncotarget 6, 10309–10319. https://doi.org/10.18632/oncotarget.3582.

163. Lupo, F., Tibaldi, E., Matte, A., Sharma, A.K., Brunati, A.M., Alper, S.L., Zancanaro, C., Benati, D., Siciliano, A., Bertoldi, M., et al. (2016). A new molecular link between defective autophagy and erythroid abnormalities in chorea-acanthocytosis. Blood 128, 2976–2987. https://doi.org/10.1182/blood-2016-07-727321.

164. Leterme, S., Bastien, O., Aiese Cigliano, R., Amato, A., and Michaud, M. (2023). Phylogenetic and structural analyses of VPS13 proteins in Archaeplastida reveal their complex evolutionary history in Viridiplantae. Contact (Thousand Oaks.) 6, 25152564231211976. https://doi.org/10.1177/25152564231211976.

165. Muñoz-Braceras, S., Calvo, R., and Escalante, R. (2015). TipC and the chorea-acanthocytosis protein VPS13A regulate autophagy in Dictyostelium and human HeLa cells. Autophagy 11, 918–927. https://doi.org/10.1080/15548627.2015.1034413.

166. Levine, T.P. (2019). Remote homology searches identify bacterial homologues of eukaryotic lipid transfer proteins, including Chorein-N domains in TamB and AsmA and Mdm31p. BMC Mol. Cell Biol. 20, 43. https://doi.org/10.1186/s12860-019-0226-z.

167. Levine, T.P. (2022). Sequence analysis and structural predictions of lipid transfer bridges in the repeating beta groove (RBG) superfamily reveal past and present domain variations affecting form, function and interactions of VPS13, ATG2, SHIP164, hobbit and tweek. Contact (Thousand Oaks.) 5, 251525642211343. https://doi.org/10.1177/25152564221134328.

168. McEwan, D.G., and Ryan, K.M. (2022). ATG2 and VPS13 proteins: molecular highways transporting lipids to drive membrane expansion and organelle communication. FEBS J. 289, 7113–7127. https://doi.org/10.1111/febs.16280.

169. Ugur, B., Hancock-Cerutti, W., Leonzino, M., and De Camilli, P. (2020). Role of VPS13, a protein with similarity to ATG2, in physiology and disease. Curr. Opin. Genet. Dev. 65, 61–68. https://doi.org/10.1016/j.gde.2020.05.027.

170. De, M., Oleskie, A.N., Ayyash, M., Dutta, S., Mancour, L., Abazeed, M.E., Brace, E.J., Skiniotis, G., and Fuller, R.S. (2017). The Vps13p-Cdc31p complex is directly required for TGN late endosome transport and TGN homotypic fusion. J. Cell Biol. 216, 425–439. https://doi.org/10.1083/jcb.201606078.

171. Lei, Y., Wen, X., and Klionsky, D.J. (2022). Vps13 is required for efficient autophagy in Saccharomyces cerevisiae. Contact (Thousand Oaks.) 5, 251525642211363. https://doi.org/10.1177/25152564221136388.

172. Takuma, T., and Ushimaru, T. (2025). The bridge-like lipid transfer protein Vps13 are required for NVJ integrity and nucleophagy. Biochem. Biophys. Res. Commun. 791, 152932. https://doi.org/10.1016/j.bbrc.2025.152932.

173. Vonk, J.J., Yeshaw, W.M., Pinto, F., Faber, A.I.E., Lahaye, L.L., Kanon, B., van der Zwaag, M., Velayos-Baeza, A., Freire, R., van IJzendoorn, S.C., et al. (2017). Drosophila Vps13 is required for protein homeostasis in the brain. PLoS One 12, e0170106. https://doi.org/10.1371/journal.pone.0170106.

174. Peikert, K., Federti, E., Matte, A., Constantin, G., Pietronigro, E.C., Fabene, P.F., Defilippi, P., Turco, E., Del Gallo, F., Pucci, P., et al. (2021). Therapeutic targeting of Lyn kinase to treat chorea-acanthocytosis. Acta Neuropathol. Commun. 9, 81. https://doi.org/10.1186/s40478-021-01181-y.

175. Riccardi, V., Viscomi, C.F., Sandri, M., D'Alessandro, A., Dzieciatkowska, M., Stephenson, D., Federti, E., Hermann, A., Salviati, L., Siciliano, A., et al. (2025). Premature skeletal muscle aging in VPS13A deficiency relates to impaired autophagy. Acta Neuropathol. Commun. 13, 83. https://doi.org/10.1186/s40478-025-01997-y.

176. Ditzel, R.M., Jr, Walker, R.H., Nirenberg, M.J., Tetlow, A.M., Farrell, K., Lind-Watson, K.J., Thorn, E.L., Dangoor, D.K., Gordon, R., De Sanctis, C., et al. (2023). An autopsy series of seven cases of VPS13A disease (chorea-acanthocytosis). Mov. Disord. 38, 2163–2172. https://doi.org/10.1002/mds.29589.

177. Eskelinen, E.-L., Schmidt, C.K., Neu, S., Willenborg, M., Fuertes, G., Salvador, N., Tanaka, Y., Lüllmann-Rauch, R., Hartmann, D., Heeren, J., et al. (2004). Disturbed cholesterol traffic but normal proteolytic function in LAMP-1/LAMP-2 double-deficient fibroblasts. Mol. Biol. Cell 15, 3132–3145. https://doi.org/10.1091/mbc.E04-02-0103.

178. Cheng, X.-T., Xie, Y.-X., Zhou, B., Huang, N., Farfel-Becker, T., and Sheng, Z.-H. (2018). Revisiting LAMP1 as a marker for degradative autophagy-lysosomal

organelles in the nervous system. Autophagy 14, 1472–1474. https://doi.org/10.1080/15548627.2018.1482147.

179. Terasawa, K., Tomabechi, Y., Ikeda, M., Ehara, H., Kukimoto-Niino, M., Wakiyama, M., Podyma-Inoue, K.A., Rajapakshe, A.R., Watabe, T., Shirouzu, M., et al. (2016). Lysosome-associated membrane proteins-1 and -2 (LAMP-1 and LAMP-2) assemble via distinct modes. Biochem. Biophys. Res. Commun. 479, 489–495. https://doi.org/10.1016/j.bbrc.2016.09.093.

180. Lee, J.-A., Beigneux, A., Ahmad, S.T., Young, S.G., and Gao, F.-B. (2007). ESCRT-III dysfunction causes autophagosome accumulation and neurodegeneration. Curr. Biol. 17, 1561–1567. https://doi.org/10.1016/j.cub.2007.07.029.

181. Lee, J.-A., and Gao, F.-B. (2009). Inhibition of autophagy induction delays neuronal cell loss caused by dysfunctional ESCRT-III in frontotemporal dementia. J. Neurosci. 29, 8506–8511. https://doi.org/10.1523/JNEUROSCI.0924-09.2009.

182. Deng, X., Sun, X., Yue, W., Duan, Y., Hu, R., Zhang, K., Ni, J., Cui, J., Wang, Q., Chen, Y., et al. (2022). CHMP2B regulates TDP-43 phosphorylation and cytotoxicity independent of autophagy via CK1. J. Cell Biol. 221. https://doi.org/10.1083/jcb.202103033.

183. Liu, N., Zhao, H., Zhao, Y.G., Hu, J., and Zhang, H. (2021). Atlastin 2/3 regulate ER targeting of the ULK1 complex to initiate autophagy. J. Cell Biol. 220. https://doi.org/10.1083/jcb.202012091.

184. Liénard, C., Pintart, A., and Bomont, P. (2024). Neuronal autophagy: Regulations and implications in health and disease. Cells 13, 103. https://doi.org/10.3390/cells13010103.

185. Musiwaro, P., Smith, M., Manifava, M., Walker, S.A., and Ktistakis, N.T. (2013). Characteristics and requirements of basal autophagy in HEK 293 cells. Autophagy 9, 1407–1417. https://doi.org/10.4161/auto.25455.

186. Salvatore, S.V., Ilagan, M.X.G., Shu, H., Lambert, P.M., Benz, A., Qian, M., Covey, D.F., Zorumski, C.F., and Mennerick, S. (2024). Neuroactive steroid effects on autophagy in a human embryonic kidney 293 (HEK) cell model. Sci Rep 14. https://doi.org/10.1038/s41598-024-51582-x.

187. Valencia, M., Kim, S.R., Jang, Y., and Lee, S.H. (2021). Neuronal Autophagy: Characteristic Features and Roles in Neuronal Pathophysiology. Biomol Ther (Seoul) 29, 605–614. https://doi.org/10.4062/biomolther.2021.012.

188. Velayos-Baeza, A., Vettori, A., Copley, R.R., Dobson-Stone, C., and Monaco, A.P. (2004). Analysis of the human VPS13 gene family. Genomics 84, 536–549. https://doi.org/10.1016/j.ygeno.2004.04.012.

189. Alesutan, I., Seifert, J., Pakladok, T., Rheinlaender, J., Lebedeva, A., Towhid, S.T., Stournaras, C., Voelkl, J., Schäffer, T.E., and Lang, F. (2013). Chorein sensitivity of actin polymerization, cell shape and mechanical stiffness of vascular endothelial cells. Cell. Physiol. Biochem. 32, 728–742. https://doi.org/10.1159/000354475.

190. Shiokawa, N., Nakamura, M., Sameshima, M., Deguchi, A., Hayashi, T., Sasaki, N., and Sano, A. (2013). Chorein, the protein responsible for chorea-acanthocytosis, interacts with β-adducin and β-actin. Biochem. Biophys. Res. Commun. 441, 96–101. https://doi.org/10.1016/j.bbrc.2013.10.011.

191. Honisch, S., Gu, S., Vom Hagen, J.M., Alkahtani, S., Al Kahtane, A.A., Tsapara, A., Hermann, A., Storch, A., Schöls, L., Lang, F., et al. (2015). Chorein sensitive arrangement of cytoskeletal architecture. Cell. Physiol. Biochem. 37, 399–408. https://doi.org/10.1159/000430363.

192. Soczewka, P., Kolakowski, D., Smaczynska-de Rooij, I., Rzepnikowska, W., Ayscough, K.R., Kaminska, J., and Zoladek, T. (2019). Yeast-model-based study identified myosin- and calcium-dependent calmodulin signalling as a potential target for drug intervention in chorea-acanthocytosis. Dis. Model. Mech. 12, dmm036830. https://doi.org/10.1242/dmm.036830.

193. Kolakowski, D., Kaminska, J., and Zoladek, T. (2020). The binding of the APT1 domains to phosphoinositides is regulated by metal ions in vitro. Biochim. Biophys. Acta Biomembr. 1862, 183349. https://doi.org/10.1016/j.bbamem.2020.183349.

194. García-García, E., Ramón-Lainez, A., Conde-Berriozabal, S., Del Toro, D., Escaramis, G., Giralt, A., Masana, M., Alberch, J., and Rodríguez, M.J. (2023). VPS13A knockdown impairs corticostriatal synaptic plasticity and locomotor behavior in a new mouse model of chorea-acanthocytosis. Neurobiol. Dis. 187, 106292. https://doi.org/10.1016/j.nbd.2023.106292.

Figures

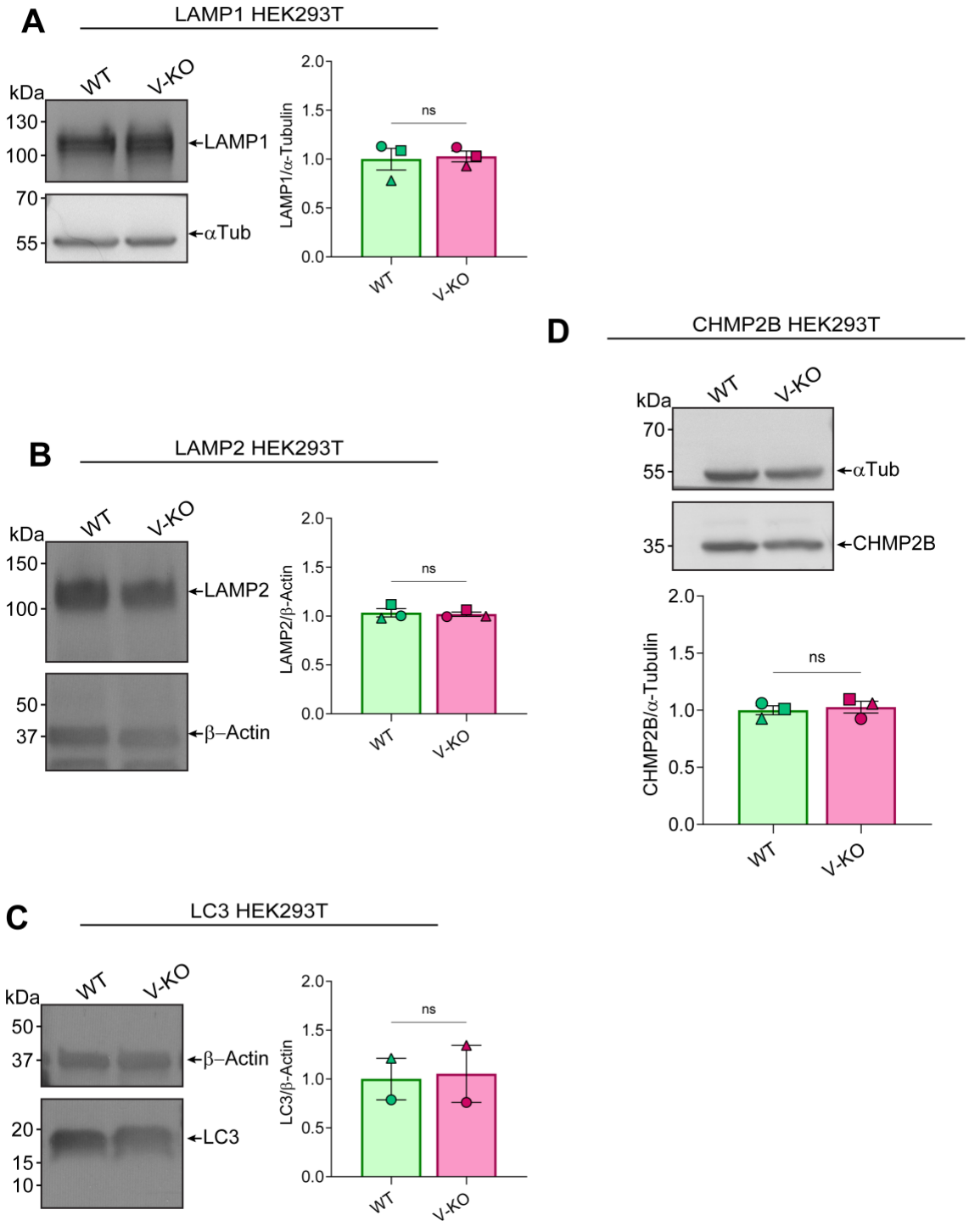


Figure 3.1 VPS13A KO HEK293T cells do not show significant differences in basal levels of autophagy markers.

Representative immunoblots and quantification of lysate from control (WT) and VPS13A knockout (V-KO) HEK293T cells probed for autophagy-related proteins: (**A**) glycosylated (mature) lysosome-associated membrane protein 1 (LAMP1) and (**B**) LAMP2, (**C**) the autophagosome marker microtubule-associated protein 1 light chain 3 (LC3), and (**D**) a core component of the ESCRT-III complex, charged multivesicular body protein 2B (CHMP2B). Alpha-tubulin (α-Tub) and beta-actin (β-actin) were blotted as loading controls. Quantification of LAMP1/α-Tub in (**A**), LAMP2/β-actin in (**B**), LC3/β-actin in (**C**), and CHMP2B/α-Tub in (**D**) were normalized to WT for each replicate. Data from 2–3 biological replicates. ns = non-significant. Unpaired Student's t-test. Black lines represent standard error of the mean for combined replicates.

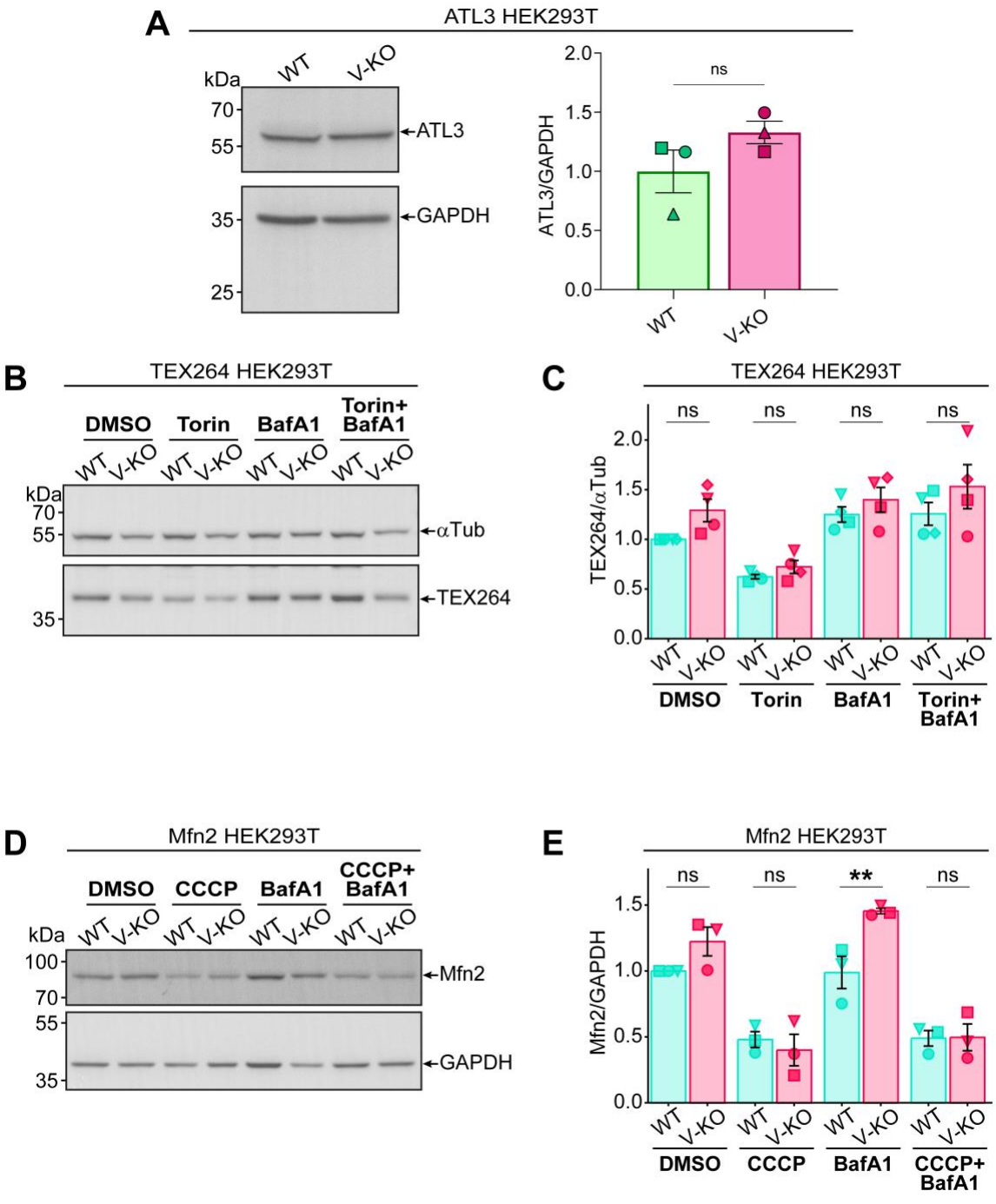


Figure 3.2 VPS13A KO HEK293T cells do not show significant differences in ER-phagy or mitophagy.

(**A**) Representative immunoblot and quantification of lysate from WT and V-KO HEK293T cells probed for Atlastin-3 (ATL3), an ER-phagy receptor and macroautophagy protein. GAPDH was blotted as a loading control. Quantification of ATL3/GAPDH in (**A**) was normalized to WT for each replicate from a total of 3 biological replicates. ns=non-significant. Unpaired Students t-test. Black lines=standard error of the mean for combined replicates. (**B**) Representative immunoblot of lysate from WT and V-KO HEK293T cells collected following 4h treatment with DMSO, 250 nM Torin-1 (Torin; an mTORC1 inhibitor and ER-phagy inducing agent), 1 μM Bafilomycin A1 (BafA1; a vacuolar H^+-ATPase selective inhibitor that disrupts acidification of organelles and is an autophagy blocking agent), or both 250 nM Torin-1 + 1 μM Bafilomycin A1 probed for testis expressed protein 264 (TEX264), a major ER-phagy receptor. Alpha-Tubulin (α-Tub) was blotted as a loading control. (**C**) Quantification of TEX264/α-Tub in (**B**), normalized to WT-DMSO for each replicate. Data from 4 biological replicates. ns=non-significant (ordinary two-way ANOVA with Tukey's post comparisons test with a single pooled variance). Black lines=standard error of the mean for combined replicates. (**D**) Representative immunoblot of lysate from WT and V-KO HEK293T cells collected following 4 h treatment with DMSO, 20 μM carbonyl cyanide m-chlorophenyl hydrazone (CCCP; a protonophore and uncoupler of oxidative phosphorylation that causes the depolarization of mitochondria and functions as a mitophagy inducing agent), 1 μM BafA1, or both 20 μM CCCP + 1 μM BafA1 probed for mitofusin-2 (Mfn2), a mitochondrial membrane protein involved in mitophagy. Glyceraldehyde-3-phosphate dehydrogenase (GAPDH) was blotted as a loading control. (**E**) Quantification of Mfn2/GAPDH in (**D**), normalized to WT-DMSO for each replicate. Data from 3 biological replicates. ns=non-significant, **p=0.0015 (ordinary two-way ANOVA with Tukey's post comparisons test with a single pooled variance). Black lines = standard error of the mean for combined replicates.

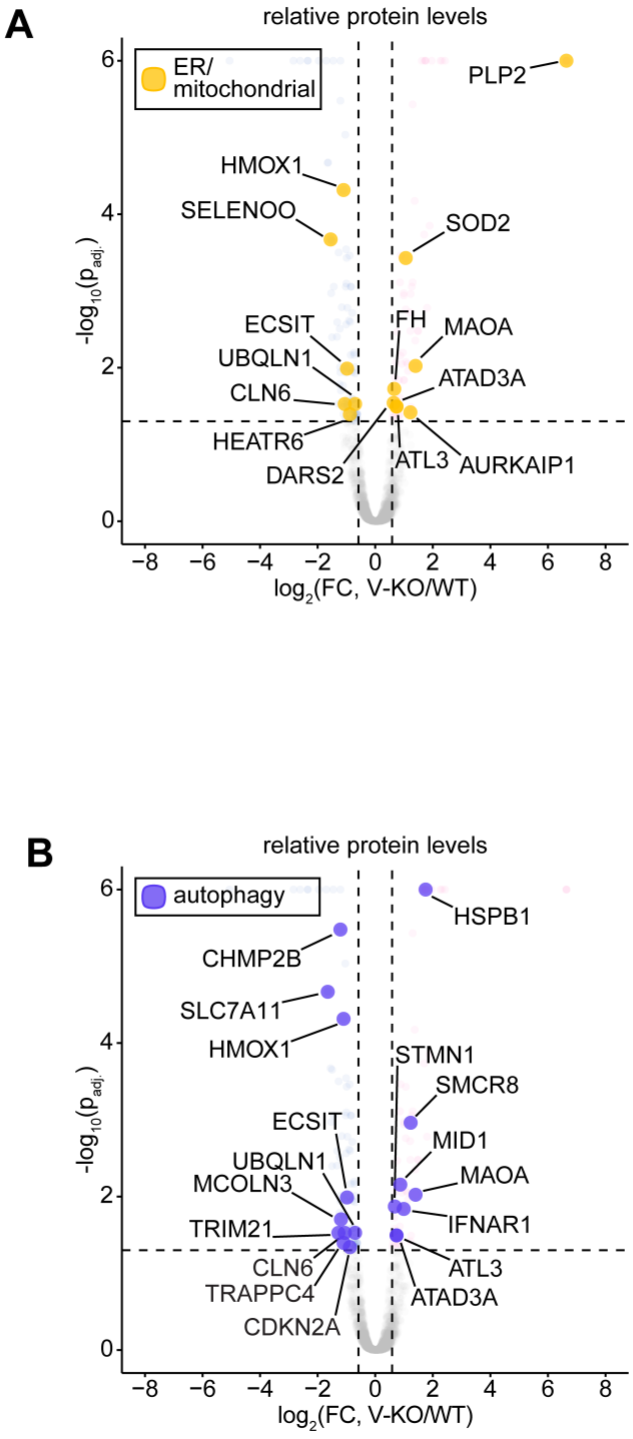


Figure 3.3 VPS13A KO HEK293T cells do not show widespread alterations in ER-, mitochondrial-, or autophagy related proteins via global proteomic analysis.

(**A**) Volcano plot of differentially expressed proteins in V-KO compared to WT HEK293T cells. Dashed lines represent cutoffs for significance ($p_{adj.}$<0.05; horizontal line, FDR) and magnitude (fold change (FC)>1.5). Yellow=significant ER or mitochondrial proteins (n=14). (**B**) Purple=significant autophagy related proteins (n=18). n=3 biological replicates.

Chapter 4 Discussion

VPS13A disease is a rare, autosomal-recessive neurodegenerative disorder caused by loss-of-function mutations in *vacuolar protein sorting factor 13 A* (*VPS13A*), a large bridge-like lipid-transfer protein enriched at multiple organelle contact sites. Although neurons show a unique vulnerability to VPS13A loss, the molecular mechanisms driving neurodegeneration, as well as the substantial clinical variability among affected individuals, remain poorly defined. **Chapter 1** outlines the clinical neuropathological features of VPS13A disease and summarizes current knowledge of VPS13A structure and proposed molecular functions. In **Chapter 2**, I demonstrate that VPS13A is essential for neuronal survival, uncover a potential link between VPS13A in transcriptional regulation, identify the chromatin architectural protein HMGA1 as a VPS13A interactor, and show that HMGA1 upregulation is both necessary and sufficient for survival in VPS13A-deficient neurons. In **Chapter 3**, I show that receptor-mediated ER-phagy and PINK1-Parkin mitophagy are not impaired in VPS13A deficient HEK293T cells, indicating that selective autophagy pathways are not broadly impaired by VPS13A loss. Despite these findings and prior work in the field, significant knowledge gaps remain. This chapter will discuss open questions, mechanistic hypotheses, and potential strategies for advancing our understanding of VPS13A biology and disease.

4.1 Establishing VPS13A disease relevant models

A central goal of this dissertation was to establish experimental systems that model VPS13A disease and enable mechanistic investigations of *VPS13A* function. Because VPS13A disease is extremely rare, clinically heterogeneous, and most commonly associated with progressive neuronal loss and neuroinflammation, for which neuropathological data remains limited[1–3], generating physiologically relevant human cellular models is critical for understanding how *VPS13A* loss leads to neurodegeneration. In **Chapter 2**, I developed and utilized several complementary cellular models, including VPS13A disease patient-derived iPSCs differentiated into neurons (iNeurons), VPS13A knock out (V-KO) iNeurons, rodent primary neurons, V-KO HEK293T cells, and endogenously tagged VPS13A (V-mNG) HEK293T cells, to investigate VPS13A-dependent mechanisms across neuronal and non-neuronal contexts. Collectively, these approaches provided evidence that VPS13A is essential for neuronal survival, revealed transcriptional dysregulation as an unexpected consequence of VPS13A loss, and identified HMGA1 as a candidate VPS13A interactor and mediator of neurotoxicity in VPS13A deficient cells. To begin establishing physiologically relevant human models of VPS13A disease, this work first focused on patient-derived induced pluripotent stem cell–based neuronal systems.

4.1.1 VPS13A disease patient-derived iNeurons and their limitations

VPS13A disease is caused by over 70 known pathogenic homozygous or compound heterozygous mutations that result in undetectable levels of VPS13A, but the mechanisms linking protein loss to the vulnerability of neuronal loss remain unclear[1,4–8]. In **Chapter 1**, we reprogrammed fibroblasts collected from an individual with VPS13A disease and from one of their heterozygous parents, who served as a familial control, to generate human induced pluripotent stem cells (iPSCs). We then differentiated these iPSCs into forebrain-like excitatory neurons (iNeurons). Using longitudinal fluorescence-based survival analysis, we found that patient-derived iNeurons exhibited a significantly higher risk of death, recapitulating the selective neuronal vulnerability associated with VPS13A disease. Together, these neurons represent one of the first human neuronal models of VPS13A disease and provide a platform for investigating molecular changes and physiologically relevant pathways that contribute to neuronal death.

4.1.2 Complementary VPS13A KO models

While patient-derived cell models can provide disease relevant insight, they can vary significantly due to factors such as individual mutations, differences in genetic backgrounds, and the lived experiences of individuals who donated their tissue, all of which can confound interpretation of findings[9–11]. To bypass such potential individual variability, we utilized two gene editing approaches: acute CRISPR/Cas9-mediated V-KO in wild-type (WT) rat primary neurons and gene-trap based V-KO in isogenic human iPSCs. Both systems corroborated our findings that VPS13A deficiency causes a marked increase in the risk of neuronal death, thereby supporting the hypothesis that VPS13A is required for neuronal survival. While these two V-KO strategies provide us with systems to investigate mechanisms that contribute to neuronal death in VPS13A disease, they also come with significant limitations that need to be considered during interpretation.

In our first model we selectively disrupted *VPS13A* in rat primary cortical neurons (rat neurons) by modifying a previously published CRISPR/Cas9 gene targeting system[12,13]. Briefly, we transfected rat neurons with vectors encoding single-guide (sg)RNAs targeting the rat *VPS13A* locus (VPS13A-sgRNA) together with Cas9 nuclease and EGFP. Although this approach enables us to assess VPS13A loss in a neuronal model, it produces a mixed cell culture in which only a fraction of neurons take up the constructs, contributing to heterogeneous KO efficiency and variable degrees of *VPS13A* disruption across individual cells[14]. In this system these factors are strongly dependent on the target gene, target copy number, sgRNA efficacy, and cell-specific transcriptional activity[14]. Further complicating this system is the fact that transfection itself introduces cellular stress and certain subpopulations of cells may have elevated transcriptional efficiency[15]. Finally, although the use of rodent neurons to study VPS13A provides a higher-throughput model, it does not capture human-specific aspects of VPS13A biology[16,17].

In our second model, we modified a CRISPR/Cas9 gene trap strategy[12,18] to KO *VPS13A* in isogenic human iPSCs by replacing the first coding exon of *VPS13A* with a cassette encoding infrared fluorescent protein (iRFP), followed by a stop codon (TAA) and a strong polyadenylation signal (PAS). While this provides a stable VPS13A KO human cell line, it also has its own limitations. Several studies have shown that Cas9 can

bind to unintended genomic sites and induce off-target cleavage, which can confound interpretation[19–21]. Additionally, while this strategy controls for the broad spectrum of pathogenic mutations that lead to VPS13A disease, it can obscure potential mutation-specific and patient-specific modifiers that may influence disease severity, pathway engagement, or compensatory responses. Finally, while both the patient derived and V-KO iNeurons provide us with disease relevant neuronal models, it is important to keep in mind that there are many key differences between iPSC-derived neurons compared to adult human neurons such as morphology, physiology, and gene expression differences, raising the possibility that some VPS13A-dependent phenotypes may be a result of methodological differences[9–11,22].

Future studies that incorporate multiple patient-derived iPSC lines representing diverse VPS13A mutations, alongside isogenic knockout and rescue approaches, may help disentangle mutation-specific effects from consequences of complete *VPS13A* loss. Comparative analyses across neuronal subtypes, maturation states, and stress conditions may further clarify which VPS13A-dependent pathways are required for neuronal survival broadly versus those selectively engaged in vulnerable neuronal populations. Together, these complementary knockout models underscore the need for additional experimental systems, such as genetically tractable human cell lines, that enable precise and scalable interrogation of VPS13A function while minimizing variability and technical constraints.

4.1.3 VPS13A KO HEK293T cells as a system for investigating mechanistic functions

Because neurons are non-dividing cells and therefore limit the feasibility of high-throughput assays, we utilized the same gene trap strategy detailed above to generate V-KO HEK293T cells as a system for mechanistic investigation. Although HEK293T cells are widely used in research because they offer advantages such as high transfection efficiency, rapid division rates, and low maintenance[23], as fundamentally epithelial cells, they lack neuronal specialization and therefore may not be able to recapitulate pathways that are cell-type dependent[24]. Using these cells, we found that V-KO was associated with pronounced transcriptional and proteomic changes, suggesting that VPS13A may function in transcriptional regulation. However, it remains possible that these changes

reflect compensatory or stress-induced responses specific to dividing non-neuronal cells rather than mechanisms that directly drive neuronal vulnerability. Together, these findings establish V-KO HEK293T cells as a tractable system for dissecting specific molecular pathways and candidate effectors downstream of VPS13A loss, which are explored in the following mechanistic sections.

4.2 ABCD1 and peroxisomal function

As described in **Chapter 2**, we used unbiased quantitative proteomics to identify pathways and proteins altered by VPS13A loss. One of the most significantly affected proteins was ATP-binding cassette subfamily D member 1 (ABCD1), also known as adrenoleukodystrophy protein (ALDP), a peroxisomal membrane transporter required for shuttling very long-chain fatty acids (VLCFAs) from the cytosol into peroxisomes, where they undergo β-oxidation and recycling[25–29]. Pathogenic mutations in ABCD1 cause X-linked adrenoleukodystrophy (X-ALD), a severe metabolic disease characterized by progressive central nervous system demyelination and adrenal insufficiency[25,28,29]. In VPS13A KO cells, ABCD1 was markedly upregulated at both the protein and RNA levels, consistent with transcriptional rather than post-translational dysregulation. Given that peroxisomes regulate VLCFA metabolism and cellular responses to oxidative stress[26], these findings raise the possibility that VPS13A loss may disrupt peroxisomal homeostasis and trigger compensatory changes in peroxisomal lipid transport machinery.

A key remaining question is whether the observed upregulation of ABCD1 reflects an underlying impairment in peroxisomal function, such as reduced efficiency in VLCFA import or β-oxidation, or instead represents a broader transcriptional stress response as proposed in **Chapter 2**. This distinction is important for our understanding of the disease, as peroxisomal dysfunction, even if modest, could potentially exacerbate lipid imbalance and oxidative stress in neurons, which have high energetic demands and are post-mitotic. Accordingly, it will be critical to directly investigate peroxisomal function in VPS13A-deficient models rather than inferring peroxisomal involvement from ABCD1 upregulation alone.

Support for a potential link between VPS13A and peroxisomal pathways comes from studies of other VPS13 family members. VPS13D and VPS13C have been observed

at mitochondrial-peroxisome membrane contact sites (MCSs)[30–33], and yeast Vps13 localizes to ER-peroxisome MCSs where it can influence pexophagy, a peroxisome-specific autophagy pathway[34]. Although direct evidence for a peroxisomal role of VPS13A remains limited, V-KO mice exhibit activation of the oxidative-stress–responsive transcription factor called nuclear factor erythroid 2-related factor 2 (NRF2), consistent with redox imbalance. Together, these findings raise the possibility that VPS13A contributes to peroxisome-ER or peroxisome-mitochondria communication, and that its loss may drive compensatory remodeling of peroxisomal lipid handling pathways, including ABCD1 upregulation.

Future experiments could test these possibilities by manipulating ABCD1 levels in control and VPS13A KO iNeurons and assessing whether this alters peroxisomal function or neuronal survival phenotypes. In parallel, direct assays of peroxisomal function, including quantification of VLCFA species, measurement of peroxisomal β-oxidation capacity, assessment of peroxisome abundance and morphology, evaluation of matrix protein import, and analysis of peroxisome-associated oxidative stress markers such as ROS and NRF2 activation, would help determine whether VPS13A loss results in direct peroxisomal dysfunction. Conversely, preserved peroxisomal function would suggest that ABCD1 upregulation reflects a broader transcriptional response to VPS13A loss rather than a peroxisome-limiting defect in neurons.

Beyond peroxisomal pathways, our proteomic analyses identified significant changes in proteins involved in cytoskeletal regulation, prompting further investigation of these pathways.

4.3 CRMP4 and cytoskeletal pathways in VPS13A disease

CRMP4, or dihydropyrimidinase-related protein 3 (DPYSL3/TUC-4), is a member of a family of cytosolic phosphoproteins that regulate cytoskeletal dynamics[35]. In **Chapter 2**, we identified consistent elevations in both CRMP4 protein and RNA levels in V-KO HEK293T cells, suggesting that VPS13A loss may influence cytoskeletal organization. CRMP4 has been implicated in various biological and disease processes, including multiple cancer types[36–38], autism spectrum disorder[39,40], and several neurodegenerative diseases such as amyotrophic lateral sclerosis (ALS)[41–43], Parkinson's disease (PD)[44–46],

and Alzheimer's disease (AD)[45,47–49]. As outlined in **Chapter 1**, previous studies also link VPS13A to cytoskeletal organization and actin dynamics, raising the possibility that VPS13A and CRMP4 may participate in shared pathways regulating cellular structure.

CRMP4 encodes two major isoforms generated by alternative splicing: a short isoform (CRMP4s/CRMP4a) and a long isoform (CRMP4L/CRMP4b), the latter containing an additional ~100 amino acids at the N-terminus. These isoforms bind distinct protein partners and often exert opposing effects on cellular processes[36,47]. During neurodevelopment, CRMP4 isoforms differentially regulate neurite elongation and branching, growth cone collapse, and actin-dependent cytoskeletal remodeling[35,47,50–53]. In mature cells, the isoforms also have distinct functions in inflammation, scarring, neuronal and axonal regeneration after injury, cell cycle progression, migration, invasion, adhesion, and cell death[36–38,41–45,50,53–57]. Importantly, CRMP4 function is further modulated by phosphorylation, as binding interactions and downstream effects vary depending on isoform-specific phosphorylation states (pCRMP4) and cell type[47,48,50,52,56]. Additionally, studies suggest that CRMP4 isoforms localize to distinct subcellular regions, even within the same cell, and play distinct roles in the central nervous system (CNS) compared to the peripheral nervous system (PNS)[55]. Following injury, the CRMP4L isoform can be cleaved at its C-terminus to generate a truncated form (tCRMP4), which has a different expression pattern and distinct functions compared to CRMP4L and CRMP4s[51,55,56,58].

Together, these findings suggest that VPS13A loss may influence cytoskeletal dynamics through pathways involving CRMP4, potentially in an isoform- and phosphorylation-dependent manner. However, additional studies are needed to directly test this hypothesis and to define how altered CRMP4 signaling contributes to cellular dysfunction in VPS13A-associated disease. One approach to address this question is to assess cytoskeletal dynamics in V-KO neurons using live-cell imaging strategies. For example, iNeurons could be transduced with EGFP or EGFP-tagged end-binding protein 3 (EB3), a microtubule plus-end tracking protein that selectively binds growing microtubules and promotes their stabilization during neurite outgrowth and dendritic development[35]. We could then use live-cell fluorescence microscopy to quantify neurite length, branching complexity, growth cone dynamics, and spine density in V-KO or

patient-derived iNeurons compared to their respective controls. If *VPS13A* loss results in altered EB3 dynamics, reduced neurite complexity, or impaired microtubule growth, this would provide functional evidence that cytoskeletal regulation is disrupted downstream of VPS13A deficiency, complementing the proteomic and transcriptional changes identified in **Chapter 2**. Conversely, if gross neurite morphology appears preserved despite VPS13A loss, this could suggest that cytoskeletal defects are context-dependent or represent a subtle, downstream outcome. It could also imply that cytoskeletal defects emerge preferentially under stress or during neuronal maturation, potentially consistent with the typical degenerative nature of VPS13A-associated neurodegeneration discussed in **Chapter 1**.

Furthermore, correlating these phenotypes with CRMP4 expression levels, isoform balance, or phosphorylation state could help determine whether CRMP4 acts as a direct mediator of cytoskeletal dysfunction or instead represents a compensatory response to broader disruptions in lipid homeostasis and organelle function.

Extending these analyses beyond neuronal systems may also provide critical insight into the hematologic manifestations of VPS13A disease, particularly acanthocytosis. Red blood cells (RBCs) rely on a highly specialized actin–spectrin cytoskeleton to maintain membrane stability, surface area, and deformability, and disruption of this network is a well-established cause of abnormal RBC morphology[59–66]. Given the emerging link between VPS13A loss and altered cytoskeletal signaling[62,64,66], future studies could examine whether CRMP4 expression, isoform composition, or phosphorylation state is altered in erythroid progenitors or patient-derived RBCs. In parallel, biophysical assays measuring RBC deformability, membrane fragility, and cytoskeletal organization could be used to determine whether VPS13A deficiency produces quantifiable mechanical defects consistent with acanthocyte formation.

Collectively, the proposed experiments will test whether disrupted lipid–cytoskeleton coordination represents a common downstream consequence of VPS13A loss across diverse cell types, and whether this mechanism can unify neuronal dysfunction and abnormal RBC morphology in VPS13A disease.

In addition to cytoskeletal regulators, our proteomic analyses identified alterations in proteins involved in intracellular calcium signaling, prompting investigation of carbonic anhydrase 8 (CA8).

4.4 Carbonic anhydrase 8

Carbonic anhydrase 8 (CA8) and HMGA1 were the only two proteins that both emerged as candidate VPS13A interactors in our V-mNG pull-down mass spectrometry screen and were significantly altered at the protein level in V-KO HEK293T cells. While this dissertation focused primarily on HMGA1, CA8 represents a compelling candidate for future investigation. Despite its name, CA8 lacks carbonic anhydrase enzymatic activity and instead functions primarily in neurons, where it binds the inositol trisphosphate receptor type 1 (IP3R1)[67,68]. By inhibiting IP3 binding to IP3R1, CA8 directly regulates IP3-mediated calcium release from the endoplasmic reticulum (ER), thereby modulating intracellular calcium signaling dynamics[67]. Pathogenic mutations in CA8 cause cerebellar ataxia, impaired intellectual development, and disequilibrium syndrome-3 (CAMRQ3)[69,70], a neurodevelopmental disorder characterized by degeneration of the cerebellum, brainstem, and spinal cord. Beyond neurodevelopmental disease, altered CA8 expression has been reported in several cancers, including colorectal cancer, lung cancer, and osteosarcoma[67], suggesting broader roles in regulating cell survival and signaling pathways. Additional studies demonstrate that CA8 influences apoptosis, cell proliferation and migration, responses to metabolic stress, and calcium-dependent signaling, and that it is highly enriched in cerebellar Purkinje cells[68].

These observations align with our proteomic findings indicating coordinated downregulation of multiple calcium signaling–related proteins in V-KO cells, including calmodulin. As discussed in **Chapter 1**, ER–mitochondrial MCSs play a central role in calcium exchange between organelles and are sensitive to changes in intracellular calcium levels[71–73]. In addition, binding of the VPS13A APT1 domain to phosphoinositides such as PI3P and PI5P is calcium-dependent[74], further linking VPS13A function to calcium-regulated membrane processes. Consistent with these observations, VPS13A patient-derived iNeurons exhibit impaired store-operated calcium entry (SOCE) and

reduced expression of ORAI1, the calcium release–activated calcium channel protein, phenotypes that correlate with increased neuronal apoptosis[75–77].

Together, these findings support a model in which VPS13A loss disrupts neuronal calcium homeostasis and raise the possibility that CA8 downregulation contributes directly to this defect. To determine whether CA8 is a significant contributor to neurodegeneration in VPS13A disease, future studies could manipulate CA8 expression in V-KO iNeurons and assess calcium handling, ER calcium release, and SOCE dynamics using live-cell calcium imaging approaches. If restoring CA8 levels rescues calcium signaling defects or reduces apoptosis in VPS13A-deficient neurons, this would support a mechanistic role for CA8 downstream of VPS13A loss. Conversely, if CA8 knockdown in control neurons phenocopies calcium dysregulation and cell death observed in V-KO models, this could suggest that CA8 loss is sufficient to drive key aspects of neuronal vulnerability. Together, these experiments would clarify whether CA8 functions as a causal mediator of calcium dysregulation in VPS13A disease or instead reflects a downstream consequence of broader disruptions in lipid transfer and organelle communication.

While CA8 represents a strong candidate for future investigation, our analyses prioritized HMGA1 for deeper mechanistic study, given its consistent regulation across models and its known roles in transcriptional control.

4.5 HMGA1 and VPS13A

4.5.1 Identification of HMGA1 as a VPS13A-related protein

In **Chapter 2**, we found that High Mobility Group AT-hook 1 (HMGA1) was the only VPS13A interactor that showed significant upregulation at the protein level following VPS13A knockout, despite no corresponding change in HMGA1 transcript levels. This discordance suggests that VPS13A may regulate HMGA1 through post-transcriptional mechanisms, including altered protein stability or turnover, rather than through compensatory changes in gene expression. These observations position HMGA1 as a candidate downstream effector of VPS13A loss and motivate deeper investigation into how VPS13A regulates nuclear protein homeostasis.

4.5.2 Molecular properties of HMGA1 and implications for transcriptional control

To understand how VPS13A might influence HMGA1 protein abundance and function, it is important to first consider the molecular properties of HMGA1 itself. Although HMGA1 is not considered a classical transcription factor, it functions as an architectural chromatin regulator that binds to and remodels DNA structure[78–83]. HMGA1 produces two major isoforms, HMGA1a (HMGI) and HMGA1b (HMGY), generated through alternative splicing and sharing high sequence similarity. Both isoforms contain three AT-hook DNA-binding domains and have a negatively charged acidic C-terminal tail that undergoes phosphorylation[81,84,85]. The charge difference between the AT hook domain and the acidic carboxyl tail alters DNA conformation, thereby altering recruitment of transcription factors and other regulators to specific transcriptional regulatory regions[78,79,85–87]. Further complicating the interactions between HMGA1 and DNA is the observation that HMGA1 is a substrate of most protein kinases, and that post-translational modifications of the protein, including phosphorylation, methylation, acetylation, ubiquitylation, and SUMOylation at different domains and sites, can alter HMGA1's affinity to DNA in diverse ways[79,81,86,88]. Together, these features suggest that modest changes in HMGA1 abundance, localization, or modification state could have disproportionately large effects on transcriptional programs.

4.5.3 HMGA1 dysregulation across disease contexts

Given these molecular features, dysregulation of HMGA1 has the potential to exert broad effects across diverse biological contexts. Historically, HMGA1 has been most extensively studied in cancer biology, where it promotes tumorigenesis in a wide range of malignancies including glioma, breast, pancreatic, thyroid, colorectal, bladder, and other cancers[78,79,86,89–95]. More recent studies, however, suggest that HMGA1 may also be involved in various non-cancer diseases. Dysregulation of HMGA1 has been associated with insulin resistance in type 2 diabetes[88,96,97], aberrant tau accumulation in AD[98–101], autophagy defects in PD[102–104], apoptosis, cell cycle progression, cellular senescence, and altered cell adhesion[96,98–104]. Although its precise role in these processes and diseases has yet to be fully defined, studies suggest that HMGA1 may induce many of these changes at the transcriptional level[78,93]. The breadth of these downstream effects highlights how dysregulation of a single architectural chromatin

regulator could plausibly contribute to the wide spectrum of neurological and systemic symptoms observed in VPS13A disease patients.

4.5.4 HMGA1 transcript variability and genetic background effects

Consistent with the variability of HMGA1 regulation across disease contexts, we observed only slightly elevated, but not significantly different, levels of *HMGA1* RNA between V-KO and otherwise isogenic control (WT) iNeurons. However, in contrast to both V-KO HEK293T cells and isogenic V-KO iNeurons, we observed significantly reduced levels of *HMGA1* RNA in VPS13A patient iNeurons compared to familial controls. Because these patient and familial control lines are not isogenic, this difference may reflect effects of genetic background, upstream HMGA1 regulatory pathways, or isoform-specific autoregulation, rather than a direct consequence of VPS13A loss. This discrepancy underscores the complexity of HMGA1 transcriptional regulation and highlights the need for additional studies to define how VPS13A status, genetic background, and cellular context intersect to influence HMGA1 expression.

Future studies should test the contribution of genetic background by expanding to multiple patient and control iPSC lines and comparing both the magnitude and variability in HMGA1 expression across lines. Parallel use of primer sets targeting distinct HMGA1 isoforms or regions of the transcript could help determine whether observed differences reflect isoform-specific regulation rather than global transcriptional changes. If HMGA1 expression varies across genetic backgrounds or depends on primer placement and isoform detection, this could suggest that the observed RNA differences reflect background-dependent or isoform-specific regulatory effects rather than a direct effect of VPS13A loss. In contrast, consistent HMGA1 measurements across primer sets and across multiple patient and control lines could support a model in which VPS13A deficiency more directly influences HMGA1 expression.

4.5.5 HMGA1 protein accumulation and neuropathology

Despite this variability at the RNA level, we consistently saw HMGA1 protein upregulation in both V-KO and patient iNeurons using immunofluorescence. As explained in **Chapter 2**, we were unable to detect HMGA1 protein by western blot analysis, likely due to limitations in antibody sensitivity and specificity. Interestingly, post-mortem

analysis of tissue from VPS13A patients showed a potential correlation between HMGA1 intensity in the putamen and astrogliosis in the basal ganglia, a neuropathological feature often seen VPS13A disease. Although preliminary and limited by the small number of available samples, this observation suggests that HMGA1 upregulation may track with neuroinflammatory severity and neuropathology.

Future studies incorporating larger patient cohorts should include quantitative immunohistochemistry across multiple basal ganglia regions, particularly the caudate nucleus and putamen, as well as additional vulnerable regions such as the hippocampus. These analyses should incorporate blinded scoring of astrogliosis and microgliosis markers and systemic correlation of regional HMGA1 abundance with neuropathologic severity measures to validate this potential link. Such studies could clarify whether HMGA1 accumulation is merely associated with neuroinflammatory pathology or reflects a mechanistically relevant contributor to regional neuronal vulnerability.

4.5.6 HMGA1-SP1 axis and transcriptional network remodeling

In addition to its role in remodeling chromatin structure, HMGA1 can also modulate gene expression by interacting directly with other transcriptional regulators[78,82,91,97]. One such protein is specificity protein 1 (SP1), a transcription factor that binds GC-rich sequences in promoters to activate or repress genes involved in apoptosis[105–112], cell growth[107,113,114], cell cycle[106,113,115], and autophagy[105,116–118]. Like HMGA1, SP1 functions in a highly context- and cell type-specific manner and is regulated through multiple post-translational modifications including phosphorylation, acetylation, SUMOylation, ubiquitination, and glycosylation[111,119,120]. SP1 has been implicated in a wide range of cancers, including gastric, colorectal, prostate, pancreatic, and ovarian tumors[91,106,113], as well as in neurodegenerative diseases including AD[105,108,121–123], HD[124,125], PD[109,110,112], ALS[126,127], and prion disease[128], although its precise mechanistic roles remain unresolved.

In our VPS13A-deficient models, we observed increased SP1 protein levels in both V-KO and patient derived iNeurons, parallelling HMGA1 protein upregulation. Because SP1 has been identified in prior studies as a downstream transcriptional target of HMGA1[82,91,97], this increase is consistent with, but does not directly demonstrate, HMGA1-dependent regulation of SP1 in this context. Together, these findings support the

hypothesis that VPS13A deficiency perturbs the abundance or stability of multiple transcriptional regulators, potentially through pathways involving HMGA1, leading to broader remodeling of transcriptional regulatory networks with downstream consequences for neuronal gene expression and function. Future studies could disentangle these relationships by selectively manipulating HMGA1 or SP1 levels and assessing effects on shared transcriptional targets and neuronal survival.

However, interpreting HMGA1–SP1 relationships remains inherently complex, as HMGA1 can either enhance or suppress SP1 DNA binding in a context-dependent manner, and reciprocal regulation has also been reported, with SP1 modulating HMGA1 expression in certain settings[82,91,97]. These bidirectional and condition-specific interactions suggest the existence of regulatory feedback loops, and disease states such as cancer can further reshape these dynamics, complicating efforts to infer causal relationships between HMGA1 and SP1 from correlative changes alone.

4.5.7 HMGA1 as a functional mediator of neurodegeneration

Together with our findings indicating a role for HMGA1 in neuronal survival, and the observed correlation between HMGA1 accumulation and basal ganglia astrogliosis in VPS13A patient post-mortem tissue, these data suggest that HMGA1 may contribute to neurodegeneration and neuroinflammation in VPS13A disease. Rather than reflecting a passive marker of pathology, HMGA1 upregulation could represent an active contributor to disease-relevant cellular stress responses. Functional significance can be tested by HMGA1 gain- and loss-of-function experiments in VPS13A-deficient and control iNeurons, followed by assessment of neuronal survival, cellular stress pathways, and inflammatory signaling, as well as rescue experiments to determine whether reducing HMGA1 levels mitigates VPS13A-dependent neuronal vulnerability. Defining dose–response relationships between HMGA1 levels and neuronal viability could further clarify thresholds at which HMGA1 transitions from adaptive to pathogenic.

4.5.8 VPS13A-HMGA1 spatial organization and nuclear homeostasis

Because VPS13A is a cytoplasmic protein and HMGA1 is primarily nuclear, a central question is whether these proteins interact directly and, if so, where this interaction occurs. Our V-mNG pull-down data provide biochemical evidence for an association

between VPS13A and HMGA1, although the subcellular context of this interaction remains unresolved. One possibility is that VPS13A, which localizes to the ER, also associates with the nuclear envelope, a membrane domain continuous with the ER that directly surrounds the nucleus. Consistent with this idea, several studies have shown VPS13A puncta at perinuclear ER regions[129–133], and in yeast, Vps13 localizes to the nuclear–ER–vacuole junction (NVJ)[134–136]. Together, these observations place VPS13A in close proximity to the nuclear compartment, raising the possibility that VPS13A-HMGA1 interactions occur at or near ER–nuclear envelope contact sites rather than within the nucleoplasm itself.

Additionally, HMGA1 is a highly dynamic protein that can relocalize from the nucleus to the cytoplasm under specific cellular conditions and has also been reported to localize to mitochondria, where it can influence mitochondrial DNA regulation[137,138]. These observations indicate that HMGA1 trafficking is regulated and context dependent, rather than strictly nuclear. Although the mechanisms governing HMGA1 subcellular redistribution remain unclear, this raises the possibility that VPS13A influences HMGA1 localization indirectly by regulating membrane-associated trafficking or retention at organelle interfaces. In this model, loss of VPS13A could alter the balance between nuclear, cytoplasmic, and organelle-associated pools of HMGA1, thereby contributing to its accumulation or mislocalization in VPS13A-deficient cells.

Another potential mechanism through which VPS13A loss may influence HMGA1 involves nuclear remodeling and degradation pathways. In yeast, the NVJ serves as a platform for micro-autophagy of the nucleus, known as micronucleophagy, in which the vacuole engulfs portions of the nucleus and nucleolar proteins into intravacuolar vesicles for degradation[139]. Activation of micronucleophagy via rapamycin leads to pronounced Vps13 recruitment to the NVJ, while Vps13 mutants show markedly reduced nucleophagic flux[140]. In humans, nucleophagy is essential for neuronal health and maintains genome stability by degrading damaged DNA, nuclear buds, and other dysfunctional or unnecessary nuclear structures[139]. Although neither HMGA1 nor VPS13A has been directly linked to nucleophagy in mammalian neurons, these findings suggest that VPS13 family proteins can support nuclear autophagic processes by supplying membrane material required for nuclear sequestration. Loss of VPS13A could

therefore impair nuclear quality-control pathways, leading to inefficient clearance of nuclear components and accumulation of nuclear proteins such as HMGA1.

This hypothesis could be tested by measuring nucleophagic flux in VPS13A-deficient neurons using a nuclear-targeted Rosella reporter (n-Rosella), which enables relative detection of nuclear material delivery to acidic lysosomal compartments[141]. Nucleophagic flux could be assessed under basal conditions and following induction with rapamycin or other cellular stressors, in the presence or absence of lysosomal inhibitors such as bafilomycin A1 along with immunolabeling for lysosomal markers (for example, LAMP1). Rescue experiments assessing whether VPS13A re-expression restores n-Rosella flux would further clarify whether VPS13A is required for efficient nuclear clearance.

Together, these approaches could determine whether VPS13A supports nuclear quality-control pathways and whether impaired nuclear clearance contributes to HMGA1 accumulation and transcriptional dysregulation.

4.5.9 A working model for VPS13A–HMGA1 interactions

The data presented here support a model in which HMGA1 acts as a downstream effector of VPS13A loss, linking VPS13A deficiency to disrupted nuclear homeostasis and transcriptional regulation (**Fig. 4.1**). Across cell lines, HMGA1 protein accumulation occurs despite variable transcript levels, suggesting that post-transcriptional regulation, altered protein turnover, or impaired nuclear quality-control pathways could contribute to this phenotype. The parallel dysregulation of additional transcriptional regulators, including SP1, supports a model in which VPS13A loss may broadly reshape transcriptional networks rather than targeting isolated genes. Together, this framework suggests that defects in nuclear membrane dynamics and nuclear clearance could couple VPS13A loss to maladaptive transcriptional programs, neuroinflammation, and neuronal vulnerability in VPS13A disease.

4.6 Conclusions

Pathogenic loss-of-function mutations in *VPS13A* underlie VPS13A disease, yet the physiological functions of VPS13A and the mechanisms underlying selective neuronal vulnerability remain poorly defined. Although VPS13A has been characterized primarily

as a bridge-like lipid-transfer protein at organelle membrane contact sites, the work presented in this dissertation reveals previously unknown roles for VPS13A in neuronal survival, cytoskeletal regulation, and transcriptional homeostasis, while also clarifying cellular processes that are not disrupted by its absence. It is my hope that future studies will build on these insights to elucidate the precise molecular functions of VPS13A and support the development of targeted therapeutic strategies for VPS13A disease.

References

1. Peikert, K., Dobson-Stone, C., Rampoldi, L., Miltenberger-Miltenyi, G., Neiman, A., De Camilli, P., Hermann, A., Walker, R.H., Monaco, A.P., and Danek, A. (1993). VPS13A disease. In GeneReviews(®) (University of Washington, Seattle).

2. Walker, R.H., Peikert, K., Jung, H.H., Hermann, A., and Danek, A. (2023). Neuroacanthocytosis syndromes: The clinical perspective. Contact (Thousand Oaks.) 6, 25152564231210340. https://doi.org/10.1177/25152564231210339.

3. Ditzel, R.M., Jr, Walker, R.H., Nirenberg, M.J., Tetlow, A.M., Farrell, K., Lind-Watson, K.J., Thorn, E.L., Dangoor, D.K., Gordon, R., De Sanctis, C., et al. (2023). An autopsy series of seven cases of VPS13A disease (chorea-acanthocytosis). Mov. Disord. 38, 2163–2172. https://doi.org/10.1002/mds.29589.

4. Ueno, S., Maruki, Y., Nakamura, M., Tomemori, Y., Kamae, K., Tanabe, H., Yamashita, Y., Matsuda, S., Kaneko, S., and Sano, A. (2001). The gene encoding a newly discovered protein, chorein, is mutated in chorea-acanthocytosis. Nat. Genet. 28, 121–122. https://doi.org/10.1038/88825.

5. Velayos-Baeza, A., Vettori, A., Copley, R.R., Dobson-Stone, C., and Monaco, A.P. (2004). Analysis of the human VPS13 gene family. Genomics 84, 536–549. https://doi.org/10.1016/j.ygeno.2004.04.012.

6. Dobson-Stone, C., Velayos-Baeza, A., Filippone, L.A., Westbury, S., Storch, A., Erdmann, T., Wroe, S.J., Leenders, K.L., Lang, A.E., Dotti, M.T., et al. (2004). Chorein detection for the diagnosis of chorea-acanthocytosis. Ann. Neurol. 56, 299–302. https://doi.org/10.1002/ana.20200.

7. Rampoldi, L., Dobson-Stone, C., Rubio, J.P., Danek, A., Chalmers, R.M., Wood, N.W., Verellen, C., Ferrer, X., Malandrini, A., Fabrizi, G.M., et al. (2001). A conserved sorting-associated protein is mutant in chorea-acanthocytosis. Nat. Genet. 28, 119–120. https://doi.org/10.1038/88821.

8. Dobson-Stone, C., Danek, A., Rampoldi, L., Hardie, R.J., Chalmers, R.M., Wood, N.W., Bohlega, S., Dotti, M.T., Federico, A., Shizuka, M., et al. (2002). Mutational spectrum of the CHAC gene in patients with chorea-acanthocytosis. Eur. J. Hum. Genet. 10, 773–781. https://doi.org/10.1038/sj.ejhg.5200866.

9. Workman, M.J., Lim, R.G., Wu, J., Frank, A., Ornelas, L., Panther, L., Galvez, E., Perez, D., Meepe, I., Lei, S., et al. (2023). Large-scale differentiation of iPSC-derived motor neurons from ALS and control subjects. Neuron 111, 1191-1204.e5. https://doi.org/10.1016/j.neuron.2023.01.010.

10. Heinzelmann, E., Piraino, F., Costa, M., Roch, A., Norkin, M., Garnier, V., Homicsko, K., and Brandenberg, N. (2024). iPSC-derived and Patient-Derived

Organoids: Applications and challenges in scalability and reproducibility as pre-clinical models. Curr. Res. Toxicol. 7, 100197. https://doi.org/10.1016/j.crtox.2024.100197.

11. Marchetto, M.C., Brennand, K.J., Boyer, L.F., and Gage, F.H. (2011). Induced pluripotent stem cells (iPSCs) and neurological disease modeling: progress and promises. Hum. Mol. Genet. 20, R109-15. https://doi.org/10.1093/hmg/ddr336.

12. Cong, L., Ran, F.A., Cox, D., Lin, S., Barretto, R., Habib, N., Hsu, P.D., Wu, X., Jiang, W., Marraffini, L.A., et al. (2013). Multiplex genome engineering using CRISPR/Cas systems. Science 339, 819–823. https://doi.org/10.1126/science.1231143.

13. Weskamp, K., Safren, N., Miguez, R., and Barmada, S. (2019). Monitoring neuronal survival via longitudinal fluorescence microscopy. J. Vis. Exp., 10.3791/59036. https://doi.org/10.3791/59036.

14. Yuen, G., Khan, F.J., Gao, S., Stommel, J.M., Batchelor, E., Wu, X., and Luo, J. (2017). CRISPR/Cas9-mediated gene knockout is insensitive to target copy number but is dependent on guide RNA potency and Cas9/sgRNA threshold expression level. Nucleic Acids Res. 45, 12039–12053. https://doi.org/10.1093/nar/gkx843.

15. Chakrabarti, A.M., Henser-Brownhill, T., Monserrat, J., Poetsch, A.R., Luscombe, N.M., and Scaffidi, P. (2019). Target-specific precision of CRISPR-mediated genome editing. Mol. Cell 73, 699-713.e6. https://doi.org/10.1016/j.molcel.2018.11.031.

16. Leterme, S., Bastien, O., Aiese Cigliano, R., Amato, A., and Michaud, M. (2023). Phylogenetic and structural analyses of VPS13 proteins in Archaeplastida reveal their complex evolutionary history in Viridiplantae. Contact (Thousand Oaks.) 6, 25152564231211976. https://doi.org/10.1177/25152564231211976.

17. Leterme, S., and Michaud, M. (2025). Standardization of VPS13 proteins description in Viridiplantae to facilitate their characterization. New Phytol. 248, 1123–1125. https://doi.org/10.1111/nph.70558.

18. Ran, F.A., Hsu, P.D., Wright, J., Agarwala, V., Scott, D.A., and Zhang, F. (2013). Genome engineering using the CRISPR-Cas9 system. Nat. Protoc. 8, 2281–2308. https://doi.org/10.1038/nprot.2013.143.

19. Alkan, F., Wenzel, A., Anthon, C., Havgaard, J.H., and Gorodkin, J. (2018). CRISPR-Cas9 off-targeting assessment with nucleic acid duplex energy parameters. Genome Biol. 19, 177. https://doi.org/10.1186/s13059-018-1534-x.

20. Fu, Y., Foden, J.A., Khayter, C., Maeder, M.L., Reyon, D., Joung, J.K., and Sander, J.D. (2013). High-frequency off-target mutagenesis induced by CRISPR-

Cas nucleases in human cells. Nat. Biotechnol. 31, 822–826. https://doi.org/10.1038/nbt.2623.

21. Singh, D., Sternberg, S.H., Fei, J., Doudna, J.A., and Ha, T. (2016). Real-time observation of DNA recognition and rejection by the RNA-guided endonuclease Cas9. Nat. Commun. 7, 12778. https://doi.org/10.1038/ncomms12778.

22. Kang, S., Chen, X., Gong, S., Yu, P., Yau, S., Su, Z., Zhou, L., Yu, J., Pan, G., and Shi, L. (2017). Characteristic analyses of a neural differentiation model from iPSC-derived neuron according to morphology, physiology, and global gene expression pattern. Sci. Rep. 7, 12233. https://doi.org/10.1038/s41598-017-12452-x.

23. Tan, E., Chin, C.S.H., Lim, Z.F.S., and Ng, S.K. (2021). HEK293 cell line as a platform to produce recombinant proteins and viral vectors. Front. Bioeng. Biotechnol. 9, 796991. https://doi.org/10.3389/fbioe.2021.796991.

24. Sapeta-Nowińska, M., Sołtys, K., Gębczak, K., Barg, E., and Młynarz, P. (2025). Resistance of HEK-293 and COS-7 cell lines to oxidative stress as a model of metabolic response. Acta Biochim. Pol. 72, 14164. https://doi.org/10.3389/abp.2025.14164.

25. Xiong, C., Jia, L.-N., Xiong, W.-X., Wu, X.-T., Xiong, L.-L., Wang, T.-H., Zhou, D., Hong, Z., Liu, Z., and Tang, L. (2023). Structural insights into substrate recognition and translocation of human peroxisomal ABC transporter ALDP. Signal Transduct. Target. Ther. 8, 74. https://doi.org/10.1038/s41392-022-01280-9.

26. Chen, Z.-P., Xu, D., Wang, L., Mao, Y.-X., Li, Y., Cheng, M.-T., Zhou, C.-Z., Hou, W.-T., and Chen, Y. (2022). Structural basis of substrate recognition and translocation by human very long-chain fatty acid transporter ABCD1. Nat. Commun. 13, 3299. https://doi.org/10.1038/s41467-022-30974-5.

27. Jia, Y., Zhang, Y., Wang, W., Lei, J., Ying, Z., and Yang, G. (2022). Structural and functional insights of the human peroxisomal ABC transporter ALDP. Elife 11, e75039. https://doi.org/10.7554/eLife.75039.

28. Wiesinger, C., Kunze, M., Regelsberger, G., Forss-Petter, S., and Berger, J. (2013). Impaired very long-chain acyl-CoA β-oxidation in human X-linked adrenoleukodystrophy fibroblasts is a direct consequence of ABCD1 transporter dysfunction. J. Biol. Chem. 288, 19269–19279. https://doi.org/10.1074/jbc.M112.445445.

29. Richter, J.E., Jr, Vadlamudi, C., Macklin, S.K., Samreen, A., Helmi, H., Broderick, D., Mohammad, A.N., Hines, S.L., VanGerpen, J.A., Atwal, P.S., et al. (2020). Characterization of a pathogenic variant in the ABCD1 gene through protein molecular modeling. Case Rep. Genet. 2020, 3256539. https://doi.org/10.1155/2020/3256539.

30. Federti, E., Matte, A., Riccardi, V., Peikert, K., Alper, S.L., Danek, A., Walker, R.H., Siciliano, A., Iatcenko, I., Hermann, A., et al. (2021). Adaptative up-regulation of PRX2 and PRX5 expression characterizes brain from a mouse model of chorea-acanthocytosis. Antioxidants (Basel) 11, 76. https://doi.org/10.3390/antiox11010076.

31. Nishizawa, Y., Sakimoto, H., Nagata, O., Sasaki, N., Urata, Y., Arai, K., Hiwatashi, H., Yokoyama, I., Kishida, S., Sano, A., et al. (2025). Chorein deficiency promotes ferroptosis. FEBS Open Bio 15, 58–68. https://doi.org/10.1002/2211-5463.13870.

32. Guillén-Samander, A., Leonzino, M., Hanna, M.G., Tang, N., Shen, H., and De Camilli, P. (2021). VPS13D bridges the ER to mitochondria and peroxisomes via Miro. J. Cell Biol. 220, e202010004. https://doi.org/10.1083/jcb.202010004.

33. Wang, X., Xu, P., Bentley-DeSousa, A., Hancock-Cerutti, W., Cai, S., Johnson, B.T., Tonelli, F., Shao, L., Talaia, G., Alessi, D.R., et al. (2025). The bridge-like lipid transport protein VPS13C/PARK23 mediates ER-lysosome contacts following lysosome damage. Nat. Cell Biol. 27, 776–789. https://doi.org/10.1038/s41556-025-01653-6.

34. Yao, R.-Q., Ren, C., Xia, Z.-F., and Yao, Y.-M. (2021). Organelle-specific autophagy in inflammatory diseases: a potential therapeutic target underlying the quality control of multiple organelles. Autophagy 17, 385–401. https://doi.org/10.1080/15548627.2020.1725377.

35. Khazaei, M.R., Girouard, M.-P., Alchini, R., Ong Tone, S., Shimada, T., Bechstedt, S., Cowan, M., Guillet, D., Wiseman, P.W., Brouhard, G., et al. (2014). Collapsin response mediator protein 4 regulates growth cone dynamics through the actin and microtubule cytoskeleton. J. Biol. Chem. 289, 30133–30143. https://doi.org/10.1074/jbc.M114.570440.

36. Guo, H., and Xia, B. (2016). Collapsin response mediator protein 4 isoforms (CRMP4a and CRMP4b) have opposite effects on cell proliferation, migration, and invasion in gastric cancer. BMC Cancer 16, 565. https://doi.org/10.1186/s12885-016-2593-6.

37. Hiroshima, Y., Nakamura, F., Miyamoto, H., Mori, R., Taniguchi, K., Matsuyama, R., Akiyama, H., Tanaka, K., Ichikawa, Y., Kato, S., et al. (2013). Collapsin response mediator protein 4 expression is associated with liver metastasis and poor survival in pancreatic cancer. Ann. Surg. Oncol. 20 Suppl 3, S369-78. https://doi.org/10.1245/s10434-012-2491-3.

38. Zhou, W., Xie, P., Pang, M., Yang, B., Fang, Y., Shu, T., Liu, C., Wang, X., Zhang, L., Li, S., et al. (2015). Upregulation of CRMP4, a new prostate cancer metastasis

suppressor gene, inhibits tumor growth in a nude mouse intratibial injection model. Int. J. Oncol. 46, 290–298. https://doi.org/10.3892/ijo.2014.2705.

39. Miller, B.H., Zeier, Z., Xi, L., Lanz, T.A., Deng, S., Strathmann, J., Willoughby, D., Kenny, P.J., Elsworth, J.D., Lawrence, M.S., et al. (2012). MicroRNA-132 dysregulation in schizophrenia has implications for both neurodevelopment and adult brain function. Proc. Natl. Acad. Sci. U. S. A. 109, 3125–3130. https://doi.org/10.1073/pnas.1113793109.

40. Tsutiya, A., Nakano, Y., Hansen-Kiss, E., Kelly, B., Nishihara, M., Goshima, Y., Corsmeier, D., White, P., Herman, G.E., and Ohtani-Kaneko, R. (2017). Human CRMP4 mutation and disrupted Crmp4 expression in mice are associated with ASD characteristics and sexual dimorphism. Sci. Rep. 7, 16812. https://doi.org/10.1038/s41598-017-16782-8.

41. Maimon, R., Ankol, L., Gradus Pery, T., Altman, T., Ionescu, A., Weissova, R., Ostrovsky, M., Tank, E., Alexandra, G., Shelestovich, N., et al. (2021). A CRMP4-dependent retrograde axon-to-soma death signal in amyotrophic lateral sclerosis. EMBO J. 40, e107586. https://doi.org/10.15252/embj.2020107586.

42. Blasco, H., Bernard-Marissal, N., Vourc'h, P., Guettard, Y.O., Sunyach, C., Augereau, O., Khederchah, J., Mouzat, K., Antar, C., Gordon, P.H., et al. (2013). A rare motor neuron deleterious missense mutation in the DPYSL3 (CRMP4) gene is associated with ALS. Hum. Mutat. 34, 953–960. https://doi.org/10.1002/humu.22329.

43. Duplan, L., Bernard, N., Casseron, W., Dudley, K., Thouvenot, E., Honnorat, J., Rogemond, V., De Bovis, B., Aebischer, P., Marin, P., et al. (2010). Collapsin response mediator protein 4a (CRMP4a) is upregulated in motoneurons of mutant SOD1 mice and can trigger motoneuron axonal degeneration and cell death. J. Neurosci. 30, 785–796. https://doi.org/10.1523/JNEUROSCI.5411-09.2010.

44. Tonouchi, A., Nagai, J., Togashi, K., Goshima, Y., and Ohshima, T. (2016). Loss of collapsin response mediator protein 4 suppresses dopaminergic neuron death in an 1-methyl-4-phenyl-1,2,3,6-tetrahydropyridine-induced mouse model of Parkinson's disease. J. Neurochem. 137, 795–805. https://doi.org/10.1111/jnc.13617.

45. Asahina, R., Takahashi, M., Takano, H., Yao, R., Abe, M., Goshima, Y., and Ohshima, T. (2024). The role of CRMP4 in LPS-induced neuroinflammation. Brain Res. 1841, 149094. https://doi.org/10.1016/j.brainres.2024.149094.

46. Li, W., Goshima, Y., and Ohshima, T. (2020). Loss of collapsin response mediator protein 4 attenuates 6-hydroxydopamine-induced impairments in a mouse model

of Parkinson's disease. Neurochem. Res. 45, 2286–2301. https://doi.org/10.1007/s11064-020-03086-z.

47. Cole, A.R., Causeret, F., Yadirgi, G., Hastie, C.J., McLauchlan, H., McManus, E.J., Hernández, F., Eickholt, B.J., Nikolic, M., and Sutherland, C. (2006). Distinct priming kinases contribute to differential regulation of collapsin response mediator proteins by glycogen synthase kinase-3 in vivo. J. Biol. Chem. 281, 16591–16598. https://doi.org/10.1074/jbc.M513344200.

48. Cole, A.R., Knebel, A., Morrice, N.A., Robertson, L.A., Irving, A.J., Connolly, C.N., and Sutherland, C. (2004). GSK-3 phosphorylation of the Alzheimer epitope within collapsin response mediator proteins regulates axon elongation in primary neurons. J. Biol. Chem. 279, 50176–50180. https://doi.org/10.1074/jbc.C400412200.

49. Auvergnon, N., Reibel, S., Touret, M., Honnorat, J., Baron, T., Giraudon, P., and Bencsik, A. (2009). Altered expression of CRMPs in the brain of bovine spongiform encephalopathy-infected mice during disease progression. Brain Res. 1261, 1–6. https://doi.org/10.1016/j.brainres.2009.01.006.

50. Nagai, J., Takaya, R., Piao, W., Goshima, Y., and Ohshima, T. (2016). Deletion of Crmp4 attenuates CSPG-induced inhibition of axonal growth and induces nociceptive recovery after spinal cord injury. Mol. Cell. Neurosci. 74, 42–48. https://doi.org/10.1016/j.mcn.2016.03.006.

51. Cha, C., Zhang, J., Ji, Z., Tan, M., Li, S., Wu, F., Chen, K., Gong, S., Guo, G., and Lin, H. (2016). CRMP4 regulates dendritic growth and maturation via the interaction with actin cytoskeleton in cultured hippocampal neurons. Brain Res. Bull. 124, 286–294. https://doi.org/10.1016/j.brainresbull.2016.06.008.

52. Boulan, B., Ravanello, C., Peyrel, A., Bosc, C., Delphin, C., Appaix, F., Denarier, E., Kraut, A., Jacquier-Sarlin, M., Fournier, A., et al. (2021). CRMP4-mediated fornix development involves Semaphorin-3E signaling pathway. Elife 10, e70361. https://doi.org/10.7554/eLife.70361.

53. Alabed, Y.Z., Pool, M., Ong Tone, S., and Fournier, A.E. (2007). Identification of CRMP4 as a convergent regulator of axon outgrowth inhibition. J. Neurosci. 27, 1702–1711. https://doi.org/10.1523/JNEUROSCI.5055-06.2007.

54. Nagai, J., Goshima, Y., and Ohshima, T. (2012). CRMP4 mediates MAG-induced inhibition of axonal outgrowth and protection against Vincristine-induced axonal degeneration. Neurosci. Lett. 519, 56–61. https://doi.org/10.1016/j.neulet.2012.05.020.

55. Girouard, M.-P., Simas, T., Hua, L., Morquette, B., Khazaei, M.R., Unsain, N., Johnstone, A.D., Rambaldi, I., Sanz, R.L., Di Raddo, M.-E., et al. (2020). Collapsin

response mediator protein 4 (CRMP4) facilitates Wallerian degeneration and axon regeneration following sciatic nerve injury. eNeuro 7, ENEURO.0479-19.2020. https://doi.org/10.1523/ENEURO.0479-19.2020.

56. Nagai, J., Kitamura, Y., Owada, K., Yamashita, N., Takei, K., Goshima, Y., and Ohshima, T. (2015). Crmp4 deletion promotes recovery from spinal cord injury by neuroprotection and limited scar formation. Sci. Rep. 5, 8269. https://doi.org/10.1038/srep08269.

57. Rosslenbroich, V., Dai, L., Baader, S.L., Noegel, A.A., Gieselmann, V., and Kappler, J. (2005). Collapsin response mediator protein-4 regulates F-actin bundling. Exp. Cell Res. 310, 434–444. https://doi.org/10.1016/j.yexcr.2005.08.005.

58. Tan, M., Cha, C., Ye, Y., Zhang, J., Li, S., Wu, F., Gong, S., and Guo, G. (2015). CRMP4 and CRMP2 interact to coordinate cytoskeleton dynamics, regulating growth cone development and axon elongation. Neural Plast. 2015, 947423. https://doi.org/10.1155/2015/947423.

59. Li, N., Chen, S., Xu, K., He, M.-T., Dong, M.-Q., Zhang, Q.C., and Gao, N. (2023). Structural basis of membrane skeleton organization in red blood cells. Cell 186, 1912-1929.e18. https://doi.org/10.1016/j.cell.2023.03.017.

60. Salomao, M., Zhang, X., Yang, Y., Lee, S., Hartwig, J.H., Chasis, J.A., Mohandas, N., and An, X. (2008). Protein 4.1R-dependent multiprotein complex: new insights into the structural organization of the red blood cell membrane. Proc. Natl. Acad. Sci. U. S. A. 105, 8026–8031. https://doi.org/10.1073/pnas.0803225105.

61. Olivieri, O., De Franceschi, L., Bordin, L., Manfredi, M., Miraglia del Giudice, E., Perrotta, S., De Vivo, M., Guarini, P., and Corrocher, R. (1997). Increased membrane protein phosphorylation and anion transport activity in chorea-acanthocytosis. Haematologica 82, 648–653.

62. Cloos, A.-S., Ghodsi, M., Stommen, A., Recktenwald, S.M., Kaestner, L., Danek, A., Spranger, A., Hermann, A., Peikert, K., and Tyteca, D. (2025). Red blood cell lipid distribution in the pathophysiology and laboratory evaluation of chorea-acanthocytosis and McLeod syndrome patients. Front. Physiol. 16, 1543812. https://doi.org/10.3389/fphys.2025.1543812.

63. Terada, N., Fujii, Y., Ueda, H., Kato, Y., Baba, T., Hayashi, R., and Ohno, S. (1999). Ultrastructural changes of erythrocyte membrane skeletons in chorea-acanthocytosis and McLeod syndrome revealed by the quick-freezing and deep-etching method. Acta Haematol. 101, 25–31. https://doi.org/10.1159/000040917.

64. Reichel, F., Kräter, M., Peikert, K., Glaß, H., Rosendahl, P., Herbig, M., Rivera Prieto, A., Kihm, A., Bosman, G., Kaestner, L., et al. (2022). Changes in blood cell

deformability in Chorea-Acanthocytosis and effects of treatment with dasatinib or lithium. Front. Physiol. 13, 852946. https://doi.org/10.3389/fphys.2022.852946.

65. De Franceschi, L., Scardoni, G., Tomelleri, C., Danek, A., Walker, R.H., Jung, H.H., Bader, B., Mazzucco, S., Dotti, M.T., Siciliano, A., et al. (2012). Computational identification of phospho-tyrosine sub-networks related to acanthocyte generation in neuroacanthocytosis. PLoS One 7, e31015. https://doi.org/10.1371/journal.pone.0031015.

66. De Franceschi, L., Tomelleri, C., Matte, A., Brunati, A.M., Bovee-Geurts, P.H., Bertoldi, M., Lasonder, E., Tibaldi, E., Danek, A., Walker, R.H., et al. (2011). Erythrocyte membrane changes of chorea-acanthocytosis are the result of altered Lyn kinase activity. Blood 118, 5652–5663. https://doi.org/10.1182/blood-2011-05-355339.

67. Shimobayashi, E., and Kapfhammer, J.P. (2018). Calcium signaling, PKC gamma, IP3R1 and CAR8 link spinocerebellar ataxias and Purkinje cell dendritic development. Curr. Neuropharmacol. 16, 151–159. https://doi.org/10.2174/1570159X15666170529104000.

68. Aspatwar, A., Tolvanen, M.E.E., Ortutay, C., and Parkkila, S. (2010). Carbonic anhydrase related protein VIII and its role in neurodegeneration and cancer. Curr. Pharm. Des. 16, 3264–3276. https://doi.org/10.2174/138161210793429823.

69. Richmond, C.M., Leventer, R., Ryan, M.M., and Delatycki, M.B. (2020). Cerebellar ataxia with normal intellect associated with a homozygous truncating variant in CA8. Clin. Genet. 97, 516–520. https://doi.org/10.1111/cge.13666.

70. Kaiyrzhanov, R., Ortigoza-Escobar, J.D., Stringer, B.W., Ganieva, M., Gowda, V.K., Srinivasan, V.M., Macaya, A., Laner, A., Onbool, E., Al-Shammari, R., et al. (2024). Clinical and molecular spectrum of autosomal recessive CA8-related cerebellar ataxia. Mov. Disord. 39, 983–995. https://doi.org/10.1002/mds.29754.

71. Osellame, L.D., Blacker, T.S., and Duchen, M.R. (2012). Cellular and molecular mechanisms of mitochondrial function. Best Pract. Res. Clin. Endocrinol. Metab. 26, 711–723. https://doi.org/10.1016/j.beem.2012.05.003.

72. Yeshaw, W.M., van der Zwaag, M., Pinto, F., Lahaye, L.L., Faber, A.I., Gómez-Sánchez, R., Dolga, A.M., Poland, C., Monaco, A.P., van IJzendoorn, S.C., et al. (2019). Human VPS13A is associated with multiple organelles and influences mitochondrial morphology and lipid droplet motility. Elife 8, e43561. https://doi.org/10.7554/eLife.43561.

73. Yan, C., Gong, L., Chen, L., Xu, M., Abou-Hamdan, H., Tang, M., Désaubry, L., and Song, Z. (2020). PHB2 (prohibitin 2) promotes PINK1-PRKN/Parkin-

dependent mitophagy by the PARL-PGAM5-PINK1 axis. Autophagy 16, 419–434. https://doi.org/10.1080/15548627.2019.1628520.

74. Kolakowski, D., Kaminska, J., and Zoladek, T. (2020). The binding of the APT1 domains to phosphoinositides is regulated by metal ions in vitro. Biochim. Biophys. Acta Biomembr. 1862, 183349. https://doi.org/10.1016/j.bbamem.2020.183349.

75. Yu, W., Honisch, S., Schmidt, S., Yan, J., Schmid, E., Alkahtani, S., AlKahtane, A.A., Alarifi, S., Stournaras, C., and Lang, F. (2016). Chorein sensitive Orai1 expression and store operated Ca2+ entry in rhabdomyosarcoma cells. Cell. Physiol. Biochem. 40, 1141–1152. https://doi.org/10.1159/000453168.

76. Silva-Rojas, R., Laporte, J., and Böhm, J. (2020). STIM1/ORAI1 loss-of-function and gain-of-function mutations inversely impact on SOCE and calcium homeostasis and cause multi-systemic mirror diseases. Front. Physiol. 11, 604941. https://doi.org/10.3389/fphys.2020.604941.

77. Pelzl, L., Hauser, S., Elsir, B., Sukkar, B., Sahu, I., Singh, Y., Höflinger, P., Bissinger, R., Jemaà, M., Stournaras, C., et al. (2017). Lithium sensitive ORAI1 expression, store operated Ca2+ entry and suicidal death of neurons in chorea-Acanthocytosis. Sci. Rep. 7, 6457. https://doi.org/10.1038/s41598-017-06451-1.

78. Conte, A., Paladino, S., Bianco, G., Fasano, D., Gerlini, R., Tornincasa, M., Renna, M., Fusco, A., Tramontano, D., and Pierantoni, G.M. (2017). High mobility group A1 protein modulates autophagy in cancer cells. Cell Death Differ. 24, 1948–1962. https://doi.org/10.1038/cdd.2017.117.

79. Watanabe, M., Ni, S., Lindenberger, A.L., Cho, J., Tinch, S.L., and Kennedy, M.A. (2013). Characterization of the stoichiometry of HMGA1/DNA complexes. Open Biochem. J. 7, 73–81. https://doi.org/10.2174/1874091X01307010073.

80. Hill, D.A., Pedulla, M.L., and Reeves, R. (1999). Directional binding of HMG-I(Y) on four-way junction DNA and the molecular basis for competitive binding with HMG-1 and histone H1. Nucleic Acids Res. 27, 2135–2144. https://doi.org/10.1093/nar/27.10.2135.

81. Zou, Y., Webb, K., Perna, A.D., Zhang, Q., Clarke, S., and Wang, Y. (2007). A mass spectrometric study on the in vitro methylation of HMGA1a and HMGA1b proteins by PRMTs: methylation specificity, the effect of binding to AT-rich duplex DNA, and the effect of C-terminal phosphorylation. Biochemistry 46, 7896–7906. https://doi.org/10.1021/bi6024897.

82. Foti, D., Iuliano, R., Chiefari, E., and Brunetti, A. (2003). A nucleoprotein complex containing Sp1, C/EBP beta, and HMGI-Y controls human insulin receptor gene transcription. Mol. Cell. Biol. 23, 2720–2732. https://doi.org/10.1128/MCB.23.8.2720-2732.2003.

83. Thanos, D., and Maniatis, T. (1995). Virus induction of human IFN beta gene expression requires the assembly of an enhanceosome. Cell 83, 1091–1100. https://doi.org/10.1016/0092-8674(95)90136-1.

84. Wei, T., Liu, H., Chu, B., Blasco, P., Liu, Z., Tian, R., Li, D.X., and Li, X. (2021). Phosphorylation-regulated HMGA1a-P53 interaction unveils the function of HMGA1a acidic tail phosphorylations via synthetic proteins. Cell Chem. Biol. 28, 722-732.e8. https://doi.org/10.1016/j.chembiol.2021.01.007.

85. Zhang, Q., and Wang, Y. (2007). Homeodomain-interacting protein kinase-2 (HIPK2) phosphorylates HMGA1a at Ser-35, Thr-52, and Thr-77 and modulates its DNA binding affinity. J. Proteome Res. 6, 4711–4719. https://doi.org/10.1021/pr700571d.

86. Puca, F., Tosti, N., Federico, A., Kuzay, Y., Pepe, A., Morlando, S., Savarese, T., D'Alessio, F., Colamaio, M., Sarnataro, D., et al. (2019). HMGA1 negatively regulates NUMB expression at transcriptional and post transcriptional level in glioblastoma stem cells. Cell Cycle 18, 1446–1457. https://doi.org/10.1080/15384101.2019.1618541.

87. Colombo, D.F., Burger, L., Baubec, T., and Schübeler, D. (2017). Binding of high mobility group A proteins to the mammalian genome occurs as a function of AT-content. PLoS Genet. 13, e1007102. https://doi.org/10.1371/journal.pgen.1007102.

88. Chiefari, E., Nevolo, M.T., Arcidiacono, B., Maurizio, E., Nocera, A., Iiritano, S., Sgarra, R., Possidente, K., Palmieri, C., Paonessa, F., et al. (2012). HMGA1 is a novel downstream nuclear target of the insulin receptor signaling pathway. Sci. Rep. 2, 251. https://doi.org/10.1038/srep00251.

89. Olan, I., Ando-Kuri, M., Parry, A.J., Handa, T., Schoenfelder, S., Fraser, P., Ohkawa, Y., Kimura, H., Narita, M., and Narita, M. (2024). HMGA1 orchestrates chromatin compartmentalization and sequesters genes into 3D networks coordinating senescence heterogeneity. Nat. Commun. 15, 6891. https://doi.org/10.1038/s41467-024-51153-8.

90. Zanin, R., Pegoraro, S., Ros, G., Ciani, Y., Piazza, S., Bossi, F., Bulla, R., Zennaro, C., Tonon, F., Lazarevic, D., et al. (2019). HMGA1 promotes breast cancer angiogenesis supporting the stability, nuclear localization and transcriptional activity of FOXM1. J. Exp. Clin. Cancer Res. 38, 313. https://doi.org/10.1186/s13046-019-1307-8.

91. Aiello, A., Pandini, G., Sarfstein, R., Werner, H., Manfioletti, G., Vigneri, R., and Belfiore, A. (2010). HMGA1 protein is a positive regulator of the insulin-like growth

factor-I receptor gene. Eur. J. Cancer 46, 1919–1926. https://doi.org/10.1016/j.ejca.2010.02.050.

92. Kim, D.K., Seo, E.J., Choi, E.J., Lee, S.I., Kwon, Y.W., Jang, I.H., Kim, S.-C., Kim, K.-H., Suh, D.-S., Seong-Jang, K., et al. (2016). Crucial role of HMGA1 in the self-renewal and drug resistance of ovarian cancer stem cells. Exp. Mol. Med. 48, e255. https://doi.org/10.1038/emm.2016.73.

93. Puca, F., Colamaio, M., Federico, A., Gemei, M., Tosti, N., Bastos, A.U., Del Vecchio, L., Pece, S., Battista, S., and Fusco, A. (2014). HMGA1 silencing restores normal stem cell characteristics in colon cancer stem cells by increasing p53 levels. Oncotarget 5, 3234–3245. https://doi.org/10.18632/oncotarget.1914.

94. Gorbounov, M., Carleton, N.M., Asch-Kendrick, R.J., Xian, L., Rooper, L., Chia, L., Cimino-Mathews, A., Cope, L., Meeker, A., Stearns, V., et al. (2020). High mobility group A1 (HMGA1) protein and gene expression correlate with ER-negativity and poor outcomes in breast cancer. Breast Cancer Res. Treat. 179, 25–35. https://doi.org/10.1007/s10549-019-05419-1.

95. Liu, X., Zhou, Z., Wang, Y., Zhu, K., Deng, W., Li, Y., Zhou, X., Chen, L., Li, Y., Xie, A., et al. (2020). Downregulation of HMGA1 mediates autophagy and inhibits migration and invasion in bladder cancer via miRNA-221/TP53INP1/p-ERK axis. Front. Oncol. 10, 589. https://doi.org/10.3389/fonc.2020.00589.

96. Mirabelli, M., Chiefari, E., Arcidiacono, B., Salatino, A., Pascarella, A., Morelli, M., Credendino, S.C., Brunetti, F.S., Di Vito, A., Greco, A., et al. (2025). HMGA1 deficiency: a pathogenic link between tau pathology and insulin resistance. EBioMedicine 115, 105700. https://doi.org/10.1016/j.ebiom.2025.105700.

97. Chiefari, E., Foti, D.P., Sgarra, R., Pegoraro, S., Arcidiacono, B., Brunetti, F.S., Greco, M., Manfioletti, G., and Brunetti, A. (2018). Transcriptional regulation of glucose metabolism: The emerging role of the HMGA1 chromatin factor. Front. Endocrinol. (Lausanne) 9, 357. https://doi.org/10.3389/fendo.2018.00357.

98. Ebrahimifar, A., Ahmadi, S., Rostamzadeh, J., and Rahimi, K. (2025). Vanadyl sulfate restores memory impairment in streptozotocin-induced rat model of sporadic alzheimer's disease by repressing FoxO1 gene expression. Sci. Rep. 15, 27293. https://doi.org/10.1038/s41598-025-12426-4.

99. Manabe, T., Katayama, T., Sato, N., Gomi, F., Hitomi, J., Yanagita, T., Kudo, T., Honda, A., Mori, Y., Matsuzaki, S., et al. (2003). Induced HMGA1a expression causes aberrant splicing of Presenilin-2 pre-mRNA in sporadic Alzheimer's disease. Cell Death Differ. 10, 698–708. https://doi.org/10.1038/sj.cdd.4401221.

100. Ohe, K., and Mayeda, A. (2010). HMGA1a trapping of U1 snRNP at an authentic 5' splice site induces aberrant exon skipping in sporadic Alzheimer's disease. Mol. Cell. Biol. 30, 2220–2228. https://doi.org/10.1128/MCB.00114-10.

101. Manabe, T., Ohe, K., Katayama, T., Matsuzaki, S., Yanagita, T., Okuda, H., Bando, Y., Imaizumi, K., Reeves, R., Tohyama, M., et al. (2007). HMGA1a: sequence-specific RNA-binding factor causing sporadic Alzheimer's disease-linked exon skipping of presenilin-2 pre-mRNA. Genes Cells 12, 1179–1191. https://doi.org/10.1111/j.1365-2443.2007.01123.x.

102. Zhong, C., Zhang, Q., Bao, H., Li, Y., and Nie, C. (2024). Hsa_circ_0054220 upregulates HMGA1 by the competitive RNA pattern to promote neural impairment in MPTP model of Parkinson's disease. Appl. Biochem. Biotechnol. 196, 4008–4023. https://doi.org/10.1007/s12010-023-04740-2.

103. Xu, D., Fan, W., Fu, B., and Nie, H. (2025). HMGA1 regulates IRS2 to promote inflammatory responses and oxidative stress injury in MPP+-induced cells. Cell Biochem. Biophys. 83, 783–792. https://doi.org/10.1007/s12013-024-01510-7.

104. Li, G., Luo, W., Wang, B., Qian, C., Ye, Y., Li, Y., and Zhang, S. (2020). HMGA1 induction of miR-103/107 forms a negative feedback loop to regulate autophagy in MPTP model of Parkinson's disease. Front. Cell. Neurosci. 14, 620020. https://doi.org/10.3389/fncel.2020.620020.

105. Cao, Y., Tan, X., Lu, Q., Huang, K., Tang, X., and He, Z. (2021). MiR-590-3 and SP1 promote neuronal apoptosis in patients with Alzheimer's disease via AMPK signaling pathway. Contrast Media Mol. Imaging 2021, 6010362. https://doi.org/10.1155/2021/6010362.

106. Waby, J.S., Chirakkal, H., Yu, C., Griffiths, G.J., Benson, R.S.P., Bingle, C.D., and Corfe, B.M. (2010). Sp1 acetylation is associated with loss of DNA binding at promoters associated with cell cycle arrest and cell death in a colon cell line. Mol. Cancer 9, 275. https://doi.org/10.1186/1476-4598-9-275.

107. Chen, H., Li, M., Zhang, Y., Song, M., Que, Y., Wang, J., Sun, F., Zhu, J., Huang, J., Liu, J., et al. (2025). AURKB inhibition induces rhabdomyosarcoma apoptosis and ferroptosis through NPM1/SP1/ACSL5 axis. JCI Insight 10, e182429. https://doi.org/10.1172/jci.insight.182429.

108. Zhu, Z.-Y., Liu, Y.-D., Gong, Y., Jin, W., Topchiy, E., Turdi, S., Gao, Y.-F., Culver, B., Wang, S.-Y., Ge, W., et al. (2022). Mitochondrial aldehyde dehydrogenase (ALDH2) rescues cardiac contractile dysfunction in an APP/PS1 murine model of Alzheimer's disease via inhibition of ACSL4-dependent ferroptosis. Acta Pharmacol. Sin. 43, 39–49. https://doi.org/10.1038/s41401-021-00635-2.

109. Wang, R., Yang, Y., Wang, H., He, Y., and Li, C. (2020). MiR-29c protects against inflammation and apoptosis in Parkinson's disease model in vivo and in vitro by targeting SP1. Clin. Exp. Pharmacol. Physiol. 47, 372–382. https://doi.org/10.1111/1440-1681.13212.

110. Cai, Y., Zhang, M.-M., Wang, M., Jiang, Z.-H., and Tan, Z.-G. (2022). Bone marrow-derived mesenchymal stem cell-derived exosomes containing Gli1 alleviate microglial activation and neuronal apoptosis in vitro and in a mouse Parkinson disease model by direct inhibition of Sp1 signaling. J. Neuropathol. Exp. Neurol. 81, 522–534. https://doi.org/10.1093/jnen/nlac037.

111. Torabi, B., Flashner, S., Beishline, K., Sowash, A., Donovan, K., Bassett, G., and Azizkhan-Clifford, J. (2018). Caspase cleavage of transcription factor Sp1 enhances apoptosis. Apoptosis 23, 65–78. https://doi.org/10.1007/s10495-017-1437-4.

112. Han, Y.-P., Liu, Z.-J., Bao, H.-H., Wang, Q., and Su, L.-L. (2022). MiR-126-5p targets SP1 to inhibit the progression of Parkinson's disease. Eur. Neurol. 85, 235–244. https://doi.org/10.1159/000521525.

113. Ren, Y., Zhang, H., and Jiang, P. (2018). MicroRNA-382 inhibits cell growth and migration in colorectal cancer by targeting SP1. Biol. Res. 51, 51. https://doi.org/10.1186/s40659-018-0200-9.

114. Kaminska, J., Rzepnikowska, W., Polak, A., Flis, K., Soczewka, P., Bala, K., Sienko, M., Grynberg, M., Kaliszewski, P., Urbanek, A., et al. (2016). Phosphatidylinositol-3-phosphate regulates response of cells to proteotoxic stress. Int. J. Biochem. Cell Biol. 79, 494–504. https://doi.org/10.1016/j.biocel.2016.08.007.

115. Yin, B.-K., Lázaro, D., and Wang, Z.-Q. (2023). TRRAP-mediated acetylation on Sp1 regulates adult neurogenesis. Comput. Struct. Biotechnol. J. 21, 472–484. https://doi.org/10.1016/j.csbj.2022.12.024.

116. Huang, C., Chen, Y., Lai, B., Chen, Y.-X., Xu, C.-Y., and Liu, Y.-F. (2021). Overexpression of SP1 restores autophagy to alleviate acute renal injury induced by ischemia-reperfusion through the miR-205/PTEN/Akt pathway. J. Inflamm. (Lond.) 18, 7. https://doi.org/10.1186/s12950-021-00270-y.

117. Kim, J.-E., Ko, A.-R., Hyun, H.-W., Min, S.-J., and Kang, T.-C. (2018). P2RX7-MAPK1/2-SP1 axis inhibits MTOR independent HSPB1-mediated astroglial autophagy. Cell Death Dis. 9, 546. https://doi.org/10.1038/s41419-018-0586-x.

118. Zhuang, M., Zhu, S., Su, L., Liu, L., Ji, M., Dai, C., Liu, J., Zhang, W., and Pu, H. (2024). PKCδ modulates SP1 mediated mitochondrial autophagy to exacerbate

diacetylmorphine-induced ferroptosis in neurons. Int. Immunopharmacol. 143, 113468. https://doi.org/10.1016/j.intimp.2024.113468.

119. Hasegawa, Y., and Struhl, K. (2021). Different SP1 binding dynamics at individual genomic loci in human cells. Proc. Natl. Acad. Sci. U. S. A. 118, e2113579118. https://doi.org/10.1073/pnas.2113579118.

120. Gong, L., Ji, W.-K., Hu, X.-H., Hu, W.-F., Tang, X.-C., Huang, Z.-X., Li, L., Liu, M., Xiang, S.-H., Wu, E., et al. (2014). Sumoylation differentially regulates Sp1 to control cell differentiation. Proc. Natl. Acad. Sci. U. S. A. 111, 5574–5579. https://doi.org/10.1073/pnas.1315034111.

121. Li, R., Song, B., Xu, L., Zheng, J., Pan, W., Cai, F., Wang, J., Wu, Y., and Song, W. (2023). Regulation of USP25 by SP1 associates with amyloidogenesis. J. Alzheimers. Dis. 92, 1459–1472. https://doi.org/10.3233/JAD-221184.

122. Gong, K., Zhou, S., Xiao, L., Xu, M., Zhou, Y., Lu, K., Yu, X., Zhu, J., Liu, C., and Zhu, Q. (2025). Danggui Shaoyao San ameliorates Alzheimer's disease by regulating lipid metabolism and inhibiting neuronal ferroptosis through the AMPK/Sp1/ACSL4 signaling pathway. Front. Pharmacol. 16, 1588375. https://doi.org/10.3389/fphar.2025.1588375.

123. Citron, B.A., Saykally, J.N., Cao, C., Dennis, J.S., Runfeldt, M., and Arendash, G.W. (2015). Transcription factor Sp1 inhibition, memory, and cytokines in a mouse model of Alzheimer's disease. Am. J. Neurodegener. Dis. 4, 40–48.

124. Li, S.-H., Cheng, A.L., Zhou, H., Lam, S., Rao, M., Li, H., and Li, X.-J. (2002). Interaction of Huntington disease protein with transcriptional activator Sp1. Mol. Cell. Biol. 22, 1277–1287. https://doi.org/10.1128/MCB.22.5.1277-1287.2002.

125. Chen-Plotkin, A.S., Sadri-Vakili, G., Yohrling, G.J., Braveman, M.W., Benn, C.L., Glajch, K.E., DiRocco, D.P., Farrell, L.A., Krainc, D., Gines, S., et al. (2006). Decreased association of the transcription factor Sp1 with genes downregulated in Huntington's disease. Neurobiol. Dis. 22, 233–241. https://doi.org/10.1016/j.nbd.2005.11.001.

126. Guida, N., Sanguigno, L., Mascolo, L., Calabrese, L., Serani, A., Molinaro, P., Lau, C.G., Annunziato, L., and Formisano, L. (2021). The transcriptional complex Sp1/KMT2A by up-regulating Restrictive Element 1 Silencing Transcription factor accelerates methylmercury-induced cell death in motor neuron-like NSC34 cells overexpressing SOD1-G93A. Front. Neurosci. 15, 771580. https://doi.org/10.3389/fnins.2021.771580.

127. García-Morales, V., Rodríguez-Bey, G., Gómez-Pérez, L., Domínguez-Vías, G., González-Forero, D., Portillo, F., Campos-Caro, A., Gento-Caro, Á., Issaoui, N., Soler, R.M., et al. (2019). Sp1-regulated expression of p11 contributes to motor

neuron degeneration by membrane insertion of TASK1. Nat. Commun. 10, 3784. https://doi.org/10.1038/s41467-019-11637-4.

128. Jeong, J.-K., and Park, S.-Y. (2012). Transcriptional regulation of specific protein 1 (SP1) by hypoxia-inducible factor 1 alpha (HIF-1α) leads to PRNP expression and neuroprotection from toxic prion peptide. Biochem. Biophys. Res. Commun. 429, 93–98. https://doi.org/10.1016/j.bbrc.2012.10.086.

129. Kurano, Y., Nakamura, M., Ichiba, M., Matsuda, M., Mizuno, E., Kato, M., Agemura, A., Izumo, S., and Sano, A. (2007). In vivo distribution and localization of chorein. Biochem. Biophys. Res. Commun. 353, 431–435. https://doi.org/10.1016/j.bbrc.2006.12.059.

130. Park, J.-S., and Neiman, A.M. (2020). XK is a partner for VPS13A: a molecular link between Chorea-Acanthocytosis and McLeod Syndrome. Mol. Biol. Cell 31, 2425–2436. https://doi.org/10.1091/mbc.E19-08-0439-T.

131. Hayashi, T., Kishida, M., Nishizawa, Y., Iijima, M., Koriyama, C., Nakamura, M., Sano, A., and Kishida, S. (2012). Subcellular localization and putative role of VPS13A/chorein in dopaminergic neuronal cells. Biochem. Biophys. Res. Commun. 419, 511–516. https://doi.org/10.1016/j.bbrc.2012.02.047.

132. Muñoz-Braceras, S., Calvo, R., and Escalante, R. (2015). TipC and the chorea-acanthocytosis protein VPS13A regulate autophagy in Dictyostelium and human HeLa cells. Autophagy 11, 918–927. https://doi.org/10.1080/15548627.2015.1034413.

133. García-García, E., Chaparro-Cabanillas, N., Coll-Manzano, A., Carreras-Caballé, M., Giralt, A., Del Toro, D., Alberch, J., Masana, M., and Rodríguez, M.J. (2021). Unraveling the spatiotemporal distribution of VPS13A in the mouse brain. Int. J. Mol. Sci. 22, 13018. https://doi.org/10.3390/ijms222313018.

134. Leonzino, M., Reinisch, K.M., and De Camilli, P. (2021). Insights into VPS13 properties and function reveal a new mechanism of eukaryotic lipid transport. Biochim. Biophys. Acta Mol. Cell Biol. Lipids 1866, 159003. https://doi.org/10.1016/j.bbalip.2021.159003.

135. Park, J.-S., Thorsness, M.K., Policastro, R., McGoldrick, L.L., Hollingsworth, N.M., Thorsness, P.E., and Neiman, A.M. (2016). Yeast Vps13 promotes mitochondrial function and is localized at membrane contact sites. Mol. Biol. Cell 27, 2435–2449. https://doi.org/10.1091/mbc.E16-02-0112.

136. Lang, A.B., John Peter, A.T., Walter, P., and Kornmann, B. (2015). ER-mitochondrial junctions can be bypassed by dominant mutations in the endosomal protein Vps13. J. Cell Biol. 210, 883–890. https://doi.org/10.1083/jcb.201502105.

137. Dement, G.A., Treff, N.R., Magnuson, N.S., Franceschi, V., and Reeves, R. (2005). Dynamic mitochondrial localization of nuclear transcription factor HMGA1. Exp. Cell Res. 307, 388–401. https://doi.org/10.1016/j.yexcr.2005.04.004.

138. Dement, G.A., Maloney, S.C., and Reeves, R. (2007). Nuclear HMGA1 nonhistone chromatin proteins directly influence mitochondrial transcription, maintenance, and function. Exp. Cell Res. 313, 77–87. https://doi.org/10.1016/j.yexcr.2006.09.014.

139. Papandreou, M.-E., Konstantinidis, G., and Tavernarakis, N. (2023). Nucleophagy delays aging and preserves germline immortality. Nat. Aging 3, 34–46. https://doi.org/10.1038/s43587-022-00327-4.

140. Takuma, T., and Ushimaru, T. (2025). The bridge-like lipid transfer protein Vps13 are required for NVJ integrity and nucleophagy. Biochem. Biophys. Res. Commun. 791, 152932. https://doi.org/10.1016/j.bbrc.2025.152932.

141. Mijaljica, D., Prescott, M., and Devenish, R.J. (2011). A fluorescence microscopy assay for monitoring mitophagy in the yeast Saccharomyces cerevisiae. J. Vis. Exp., 2779. https://doi.org/10.3791/2779.

Figures

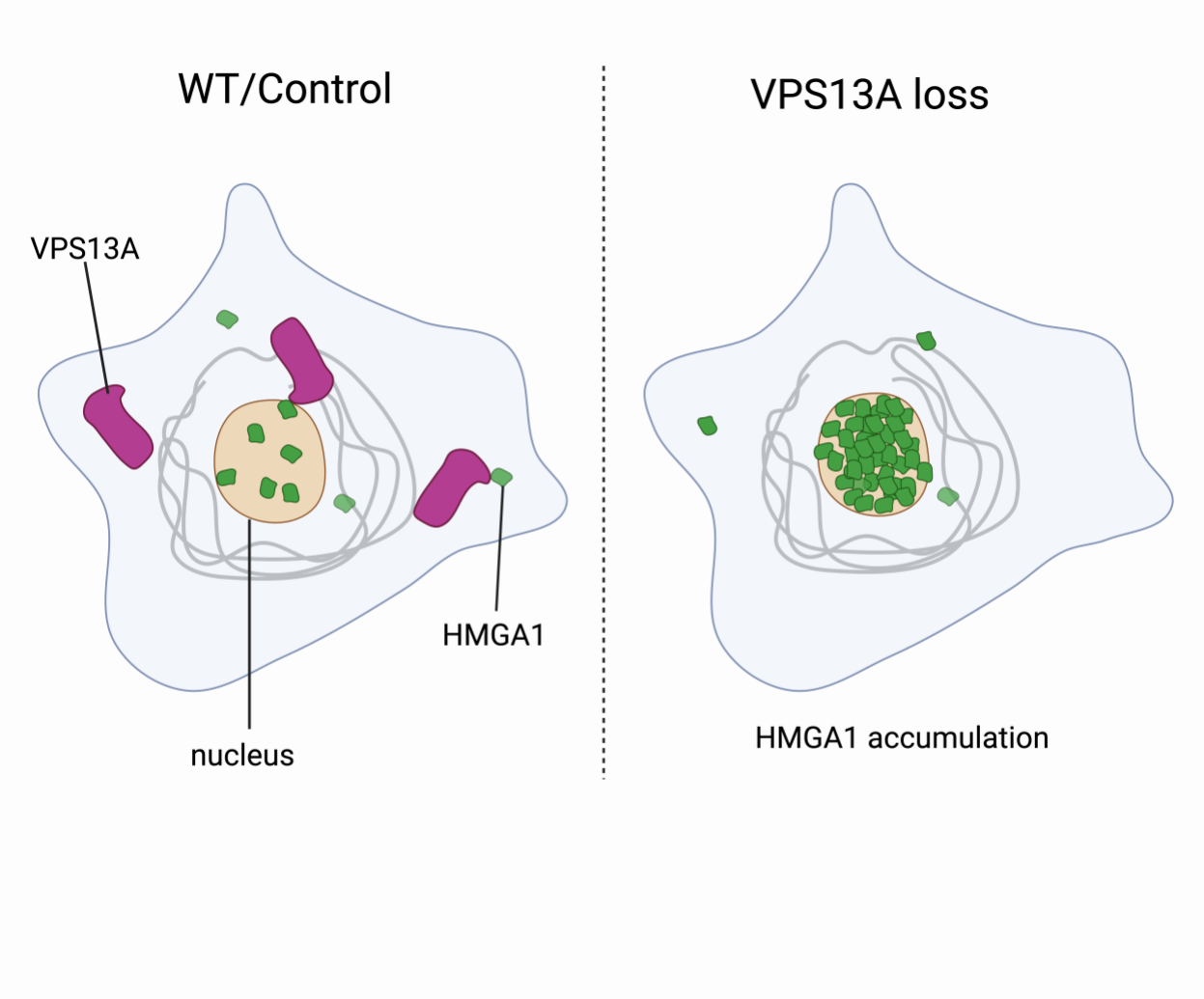


Figure 4.1 Accumulation of HMGA1 protein in VPS13A-deficient cells

In WT/control cells, VPS13A is cytoplasmic and HMGA1 exhibits low-level nuclear localization. In contrast, VPS13A deficiency is associated with marked HMGA1 accumulation, particularly within the nucleus.